

# **Understanding the role of Apoptosis Inhibitor 5 (Api5) in breast cancer**

A thesis Submitted in partial fulfilment of the requirements

Of the degree of

Doctor of Philosophy

By

Abhijith K

Reg. No. 20163438



**INDIAN INSTITUTE OF SCIENCE EDUCATION AND RESEARCH**

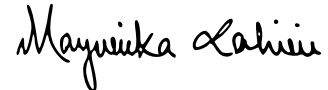
**PUNE**

**2021**

# CERTIFICATE

Certified that the work incorporated in the thesis entitled "**Understanding the role of Apoptosis Inhibitor 5 (Api5) in breast cancer**" submitted by **Abhijith K** was carried out by the candidate, under my supervision. The work presented here or any part of it has not been included in any other thesis submitted previously for the award of any degree or diploma from any other University or institution.

Date: 09 December 2021



**Dr. Mayurika Lahiri**

Associate Professor

Biology Division, IISER Pune

# DECLARATION

I declare that this written submission represents my idea in my own words and where others' ideas have been included; I have adequately cited and referenced the original sources. I also declare that I have adhered to all principles of academic honesty and integrity and have not misrepresented or fabricated or falsified any idea/data/fact/source in my submission. I understand that violation of the above will be cause for disciplinary action by the Institute and can also evoke penal action from the sources which have thus not been properly cited or from whom proper permission has not been taken when needed.

Date: 9<sup>th</sup> December 2021

A handwritten signature in blue ink, appearing to read 'Abhijith K', is written on a light-colored background.

Abhijith K  
20163438

## Acknowledgements

My life at IISER has been through various phases, which includes mostly fun, happiness, and adventure, while there were also times when I needed support. I am incredibly thankful to every single person who came through my life during these last five years and before, as they all have contributed directly or indirectly to my journey till now.

First, I would like to thank my family, especially my mother (**Beena Mohan**), grandmother (**Sujatha Mohan**) and my wife (**M Vandana**), without whom I may not have even thought of taking this path in my life. They have constantly been holding my back till now. They have provided all the care and love that have provided the strength to me to move ahead. Special thanks to all my other family members, especially my cousins (**Pavithra** and **Pruthu**), Aunt (**Chithra**) and in-laws (**Madhusudhanan Nair**, **Bindu** and **Achu**) for their enthusiasm and motivation.

Further, I would like to acknowledge my PI, **Mayurika Lahiri**. she has helped me improve my scientific temperament and mould a better researcher out of me. As a PI, she has provided all the support and guidance during my time in her lab. Also, she has constantly encouraged me to take new steps, provided the freedom to think on my own, introduce new directions to the project, and develop my scientific and soft skills. I sincerely thank her for all the help and support that she provided.

I thank my RAC members, **Dr Sorab Dalal**, ACTREC, Mumbai and **Dr Richa Rikhy**, IISER Pune, for their valuable suggestions and guidance throughout my project. Also, I would like to thank **Dr Santosh Dixit**, who played a significant role in helping us with patient samples related work and the *in-silico* studies. I thank **Dr T.S. Sridhar**, SJRI, Bangalore, and his lab members, especially **Dr Jyothi Prabhu**, for teaching me IHC and TCGA analyses. Special thanks to **Dr Madhura**, CTCR, Pune, for her help with IHC analysis.

I also wish to thank **Dr Sabarinathan Radhakrishanan**, NCBS Bangalore and his student **Faseela E.E** (who is also and past Lahiri lab member) for helping me with eh *in silico* studies that I could not have carried out without them. I am also grateful to **Dr Nagaraj Balasubramanian**, IISER Pune and **Dr Anjan Banerjee**, IISER Pune, for allowing me to use their microscopy and other instruments, which were critical for the studies that I carried out.



I would like to take this opportunity to thank **CSIR** and **IISER** for providing me with the fellowship. Special thanks to IISER for infrastructure and facilities.

When I joined Mayurika's lab, **Rintu** was the first friend I got, and she still stays as a very close friend that I got from IISER. She has constantly helped me learn, understand, and improve during the last 5 years and has been there with me to solve varieties of problems that we encountered. I would like to thank her for her support during my PhD journey. Her husband, **Virender**, has also been an important person in my stay at IISER. He has helped me improve myself scientifically as well as personally. My heartfelt thanks to him for all the help.

I thank all the present and previous Lahiri lab members, especially **Ashiq, Libi** and **Vaishali**, who have taught me most of the techniques in the lab. They all have also played a major role in teaching and guiding me through various troubles I faced during my project and life. Special thanks to **Dr Rupa**, who has been the go-to person for any doubts and help that I required during my scientific journey in IISER. I would like to thank **Aishwarya**, who have also been a good colleague and helped with her suggestions during the project. I sincerely thank all the other lab members, **Kezia, Faseela, Vishakha, Debiprasad, Gautami, Radhika, Benchamin, Nikki, Madhu, Snehal, Anisha, Kshitija, Rose, Thathagath, Suraj, Shrunal, Abhilash, Sonali, Jhanvi** and **Sudheeksha**, for their support and suggestions. It was all these people who made the lab a happy and memorable place.

I also wish to thank my other friends at IISER Pune, including **Bhavin, Sneha, Jisha, Ketakee, Sarang, Manesh** and **Neelay**, for creating a pleasant environment during my stay at IISER Pune. Special thanks to all my other friends, especially **Vineeth, Nithin, Nimal, Ashish, Sarath** and **Vimal**, for their unconditional support and care.

I also wish to thank my previous teachers from the school, college and previous labs, including **Dr Devyani Haldar, Dr Santanu Kumar Ghosh, Dr Jayashree G, Dr Shobha V N, Dr Sanjay Pal, Dr Nandita Mishra, Dr Nidheesh** and all other teaching and non-teaching staffs who had paved the base for my scientific enthusiasm and supported me for pursuing this path.

My sincere thanks to **National Facility for Gene Function in Health and Disease (NFGFHD)** and its members for helping me with the animal-related studies. Special

thanks to various facilities and the respective person in-charge at IISER Pune, including **Amit** (Perkin Elmer- IISER CoE), **Saurabh** (BD-IISER Pune FACS facility), and **Vijay and Santosh** (IISER Pune Microscopy facility). These people have made my life easier by helping with these specific facilities. I would also like to thank the Bio-admin staff, **Piyush, Kalpesh, Hariprasad, Sachin, Sandeep, Mahesh, Sandeep Mrinalini, Rupali** and **Shabnam**, for taking care of all the paperwork, formalities, general requirement, instrument handling training and repairs without which it wouldn't have been easy for completing my PhD work. Special thanks to the academic office staff, **Tushar**, and **Sayalee** for helping with the timely disbursement of the fellowship.

I would like to take this opportunity to also thank every person who has come through my life as he/she have played a role in moulding me to who I am today and possibly who I will be in the future.

And above all, I am thankful to the "The Almighty" for His blessings. His act of mercy kept me healthy and safe throughout this journey.

# Synopsis

**Title: - Understanding the role of Apoptosis Inhibitor 5 (Api5) in breast cancer**

Name of student: **Abhijith K**

Rolle Number: - 20163438

Name of thesis advisor: - Dr Mayurika Lahiri

Date of Registration: - 1<sup>st</sup> August 2016

Indian Institute of Science Education and Research (IISER), Pune, India

## Introduction

The breast is an organ made of glandular epithelium, and it produces Milk in response to the hormonal signalling (Javed and Lteif, 2013). Breast development begins from the early days of embryogenesis, which then continues after the individual attains puberty. Further, a continuous cycle of hormonal signalling regulates the gland functionally and morphologically (Macias and Hinck, 2012). The signalling activates cell proliferation and cell death in a spatiotemporal manner. A delicate balance between cell growth and cell death, majorly through apoptosis, maintains homeostasis and, thereby, proper breast development (Sternlicht, 2006). Bcl2 family proteins such as Bim and Bcl2 constitute a significant class of apoptosis regulators. During breast development, Bim mediated apoptosis is responsible for lumen clearance in ducts and acini (Mailleux et al., 2008; Mailleux et al., 2007). Milk is secreted to these hollow regions, which is then carried to the nipple.

Deregulation in the signalling cascades often causes uncontrolled cell growth and reduced cell death leading to malignancies. Apoptosis inhibition mediated by upregulation of anti-apoptotic proteins and downregulation of pro-apoptotic proteins is reported in different cancers, including the breast cancer (Plati et al., 2011). Apoptosis Inhibitor 5 (Api5) is an anti-apoptotic protein that is reported as a possible oncogene (Basset et al., 2017).

Api5 regulates apoptosis by inhibiting E2F1 transcriptional activity, preventing caspase-2 activation and activating Bim degradation (Imre et al., 2017; Morris et al., 2006; Noh et al., 2014). Recent evidence from the lab also shows that Api5 may be

involved in cell cycle regulation (Sharma and Lahiri, 2021). These results suggest that Api5 can be a regulator of both cell death and cell proliferation. Deregulation of these two events can lead to the development of malignancies.

Interestingly, cancers such as NSCLC, Ovarian cancer and bladder cancer have higher expression of Api5 (Sasaki et al., 2001). Api5 levels are upregulated in tamoxifen resistant breast cancer cells as well. Recent studies show Api5 expression as a factor associated with drug resistance in TNBC breast cancers (Bousquet et al., 2019). Through ER $\alpha$  interaction Api5 could also regulate carcinogenic characteristics in hormone receptor-positive breast cancer cell line (Basset et al., 2017). These studies indicated a significant involvement of Api5 in breast carcinogenesis.

Even though numerous discoveries have identified novel biomarkers and therapeutic targets for better handling breast cancer, it remains the major cause of death due to cancer in women worldwide. GLOBOCAN, 2020 data shows that breast cancer has the highest incidence and mortality rate among all cancers in India. Further studies on identifying novel target genes are needed to support drug regimen development and improve patient survival. Api5 may be a plausible biomarker or target gene for better management of breast cancers. Interestingly there has been recent evidence in using Api5 targeted therapies using peptides that can bind and inhibit Api5 activity in *in vitro* conditions. They also show that this inhibition could enhance chemosensitivity (Bousquet et al., 2019). Thus exploring the importance of Api5 in breast cancer and the molecular signalling associated with Api5 during breast carcinogenesis can be beneficial to cancer management.

Using multiple model systems, including *in silico*, *in vitro* and *in vivo*, we explored the necessity and function of Api5 during breast cancer development and progression. The specific objectives for this study were as follows:

**Objective:**

- 1) To identify whether Api5 overexpression can lead to a transformation of non-tumorigenic breast epithelial cells

Api5 overexpression in MCF10A cells resulted in transformation of the breast epithelial cell line, as observed with altered morphology, polarity and enhanced

proliferation in acinar cultures. Api5 OE also led to reduced apoptosis, elevated migratory potential and partial-EMT like characteristics.

- 2) To identify whether Api5 knockdown can affect the tumorigenic phenotypes of transformed breast cells.

Api5 knockdown in malignant cells reduced their proliferative capacity, migratory potential, and anchorage independent growth. Also, the Api5 knockdown in highly malignant breast cells reduced the *in vivo* tumorigenic potential of the cells.

- 3) To investigate the molecular mechanism behind Api5 mediated breast epithelial cell transformation.

Upon Api5 overexpression in MCF10A cells and culturing them on Matrigel®, it alters multiple signalling cascades during the acinar morphogenesis. During initial days, Api5 OE activated FGF2-Ras/ PDK1-Akt/cMYC signalling which would promote proliferation and EMT. Later the signalling shifts to ERK activation leading Bim degradation and thereby reduced apoptosis and enhanced proliferation.

- 4) Understanding Api5 expression in breast cancer patients using *in silico* analyses

API5 expression were upregulated in breast cancer patient samples and the higher expression predicted poor patient survival. Gene expression-based pathway analysis revealed positive correlation between API5 expression and cellular proliferation and cell membrane components.

- 5) Identifying the expression pattern of Api5 in the Indian Breast Cancer scenario.

Indian breast cancer patients have higher expression of Api5 as compared with adjacent normal tissues. Stage 2 breast cancer patients have Api5 expression than Stage 1.

### **Altered expression of Api5 affects breast carcinogenesis**

MCF10A cells are non-tumorigenic breast epithelial cells (Soule et al., 1990). When they are grown on Matrigel as 3D acinar cultures, it forms growth-arrested acinar structures by Day 16(Debnath and Brugge, 2005). They closely resemble the human mammary gland. MCF10A cells maintain the apicobasal polarity as well the cell-cell

junctions present in *in vivo* conditions(Debnath et al., 2003a). During the morphogenesis, the cells in the lumen that have lost contact with the matrix undergo Bim mediated apoptosis leading to a clear lumen by the end of culture.

Oncogene overexpression in MCF10A cells disrupts these characteristics and alters the morphology of acinar cultures(Debnath et al., 2003b; Partanen et al., 2007). Such transformation events lead to filled lumen, multi lumen, and protrusion-like structures in 3D acinar cultures. We observed a similar phenotype upon Api5 OE, suggesting a possible transformation event. Reduced apoptosis resulted in filled lumen structures, while enhanced proliferation led to the larger size of acini formed. Our further studies identified that Api5 OE could also disrupt apico-basal polarity and cell-cell junctions. Loss of polarity in epithelial cells suggests characteristic changes in the cells such as Epithelial to Mesenchymal Transition (EMT) (Coradini et al., 2011). The cells acquired expression of specific mesenchymal markers. However, some epithelial markers were still expressed, suggesting a partial-EMT state. A partial EMT state is reported to promote cancer progression and is present in several malignant conditions.

MCF10AT1 and MCF10CA1a are isogenic cell lines derived from MCF10A (Dawson et al., 1996; Santner et al., 2001). They exhibited premalignant and malignant characteristics, respectively. MCF10CA1a cells could form tumours in athymic mice when the cells are orthotopically injected (Bessette et al., 2015). 3D cultures of malignant cells lead to spheroid formation, which closely resembles the *in vivo* malignant tissue characteristics. Api5 knockdown in MCF10AT1 and MCF10CA1a resulted in reduced spheroid size in 3D cultures which was attributed to apoptosis and reduced proliferation.

Interestingly, MCF10A cells could grow in an anchorage-independent manner upon Api5 OE, while Api5 KD in MCF10AT1 and MCF10CA1a reduced their growth in anchorage-independent conditions. Api5 expression could also regulate the migratory potential of cells. Api5 OE enhanced single-cell migration while KD negatively affected cell migration in MCF10CA1a. Furthermore, Api5 KD in MCF10CA1a reduced the *in vivo* tumorigenic potential of the cell line.

Negative regulators of apoptosis are found to be upregulated in various cancers. They usually suppress apoptosis and thereby promoting carcinogenesis (LaCasse et

al., 2008; Pluta et al., 2015). Api5, though it is an anti-apoptotic protein, could regulate several cellular events other than apoptosis. Many of these characteristic changes suggested a transformation of the epithelial cell. We also found that Api5 is essential for the maintenance of carcinogenic characteristics in malignant cells.

Our results identify Api5 as a major regulator of various cellular characteristics during breast carcinogenesis. This data sheds light to its role in breast cancer and the functional importance of the protein.

### **Api5 regulates FGF2 signalling leading PDK1-Akt/cMYC and Ras-ERK signalling**

Various signalling cascades regulate breast acinar morphogenesis. However, the specific signalling events associated with different stages during acinar development is not thoroughly studied (Watson and Khaled, 2020). But is known that several known signalling pathways are deregulated in breast cancer. It is known that FGF2, ERK, Akt and Bim plays a significant role during breast acinar development and breast carcinogenesis. Api5 is reported to regulate ERK signalling and thereby regulate Bim levels(Noh et al., 2014). Multiple studies have identified the Api5-FGF2 interaction and its functional importance(Jang et al., 2017; Krejci et al., 2007).

Api5 OE in MCF10A resulted in activation of FGF2 signalling from early days of morphogenesis in 3D cultures. This activation resulted in PDK1 mediated Akt phosphorylation and cMYC activation. Early activation of these signalling could have enhanced proliferation and disturbed the growth of acini. The polarisation of cells could also be negatively affected. cMYC activation is also known to enhance mesenchymal characteristics, thereby promoting EMT. Interestingly, morphometrically we observed all these changes in Api5 OE MCF10A acini.

Furthermore, we found that Api5 OE mediated FGF2 signalling shifted to Ras-ERK mediated Bim degradation in the latter days of morphogenesis. Api5 OE mediated Bim degradation should be the reason for the filled lumen that was observed. FGF2 mediated Ras-ERK signalling could also have provided sustained proliferative capacity in the MCF10A cells.

Our results confirmed that Api5 regulated multiple signalling pathways, resulting in various changes in the acini development and cellular characteristics.

## **Breast cancer patients have upregulated Api5 expression and predict poor survival.**

*In vitro* studies have identified a significant role of Api5 in breast carcinogenesis. However, it is essential to explore the status in breast cancer patients. Currently, multiple databases provide patient sample-based gene expression data. This can be used to identify the expression pattern of candidate genes in cancers. GENT2 and TCGA are databases that provide genomic and clinical data from different cancer populations (Huang et al., 2015; Park et al., 2019). KMplotter is an online tool that can be used to analyse patients' survival chances based on the expression of query genes (Gyorffy et al., 2010).

Using these various tools, we addressed the problem of Api5 expression in breast cancer patients. Both GENT2 and TCGA data confirmed that API5 levels are upregulated in breast cancer tissues. Kmploter data identified that higher API5 expression correlates with poor patient survival. Further studies confirmed that higher API5 expression could signal higher cellular proliferation and alter cell membrane components. The results supported the molecular signalling and characteristic changes that we observed in 3D cultures.

Finally, we also found that Indian breast cancer patients have higher Api5 protein expression than adjacent normal tissues. Also, stage 2 cancer samples show higher expression than stage 1. Thus, our study confirmed that Api5 expression levels are upregulated in breast cancer and can also trigger enhanced proliferation and characteristic changes in breast epithelial cells.

## **Conclusion**

Taken together our studies identified Api5 as a major regulator of breast carcinogenesis. We identified the molecular signalling involved in Api5 mediated transformation of breast epithelial cells and the morphological and characteristic changes that Api5 can regulate during breast carcinogenesis. Studies on patient samples confirmed that our findings have potential for future drug development studies using Api5 as a target or biomarker (Figure 1).



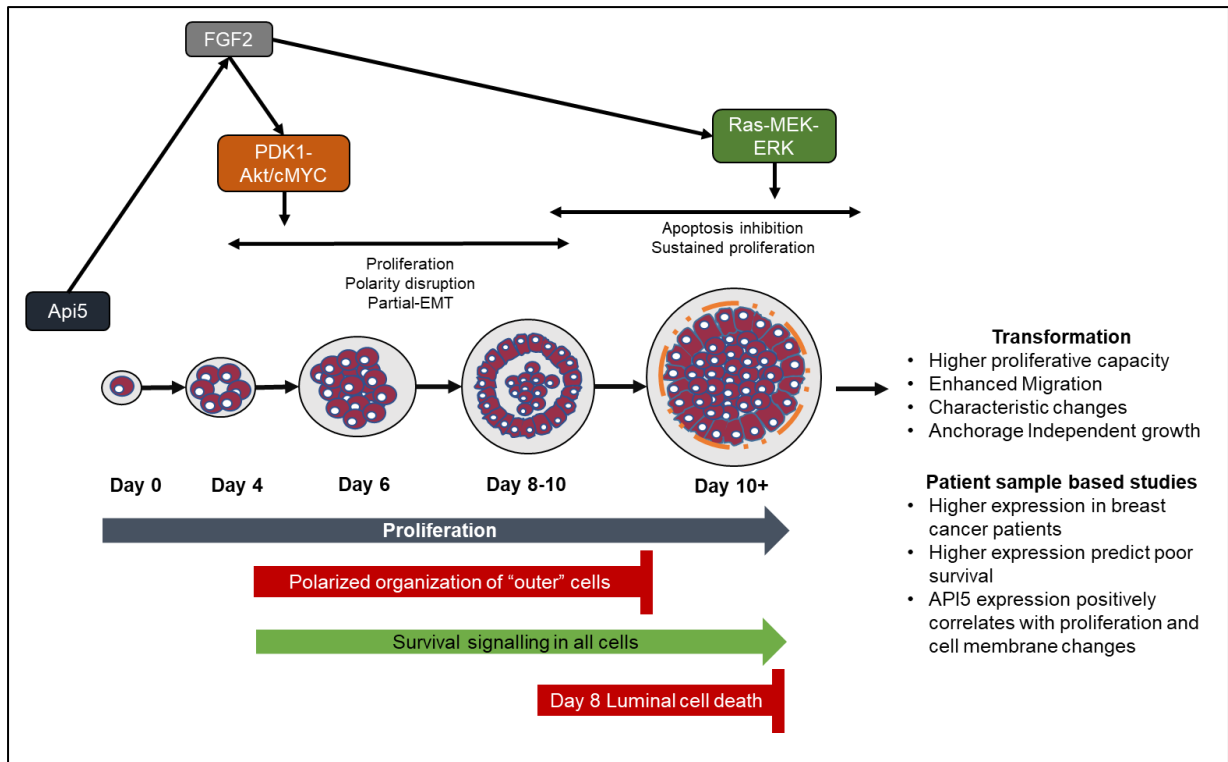


**Figure 1: Schematic summarising the study described in this thesis.**

**Understanding the role of Api5 in breast cancer.** Altered expression of Api5 led to phenotypic and characteristic changes in both epithelial cell line and malignant cell line. Api5 signalled Akt/cMYC and ERK pathways through FGF2 which mediated the transformation of breast epithelial cell during acinar morphogenesis. Patient sample-based studies also confirmed higher expression of Api5 in breast cancer patients.

## **References**

**Basset, C., Bonnet-Magnaval, F., Navarro, M. G., Touriol, C., Courtade, M., Prats, H., Garmy-Susini, B. and Lacazette, E.** (2017). Api5 a new cofactor of estrogen receptor alpha involved in breast cancer outcome. *Oncotarget* **8**, 52511-52526.

**Besette, D. C., Tilch, E., Seidens, T., Quinn, M. C., Wiegman, A. P., Shi, W., Cocciardi, S., McCart-Reed, A., Saunus, J. M., Simpson, P. T. et al.** (2015). Using the MCF10A/MCF10CA1a Breast Cancer Progression Cell Line Model to Investigate the Effect of Active, Mutant Forms of EGFR in Breast Cancer Development and Treatment Using Gefitinib. *PLoS One* **10**, e0125232.

**Bousquet, G., Feugas, J. P., Gu, Y., Leboeuf, C., Bouchtaoui, M. E., Lu, H., Espie, M., Janin, A. and Benedetto, M. D.** (2019). High expression of apoptosis protein (Api-5) in chemoresistant triple-negative breast cancers: an innovative target. *Oncotarget* **10**, 6577-6588.

**Coradini, D., Casarsa, C. and Oriana, S.** (2011). Epithelial cell polarity and tumorigenesis: new perspectives for cancer detection and treatment. *Acta Pharmacol Sin* **32**, 552-64.

**Dawson, P. J., Wolman, S. R., Tait, L., Heppner, G. H. and Miller, F. R.** (1996). MCF10AT: a model for the evolution of cancer from proliferative breast disease. *Am J Pathol* **148**, 313-9.

**Debnath, J. and Brugge, J. S.** (2005). Modelling glandular epithelial cancers in three-dimensional cultures. *Nat Rev Cancer* **5**, 675-88.

**Debnath, J., Muthuswamy, S. K. and Brugge, J. S.** (2003a). Morphogenesis and oncogenesis of MCF-10A mammary epithelial acini grown in three-dimensional basement membrane cultures. *Methods* **30**, 256-68.

**Debnath, J., Walker, S. J. and Brugge, J. S.** (2003b). Akt activation disrupts mammary acinar architecture and enhances proliferation in an mTOR-dependent manner. *J Cell Biol* **163**, 315-26.

**Gyorffy, B., Lanczky, A., Eklund, A. C., Denkert, C., Budczies, J., Li, Q. and Szallasi, Z.** (2010). An online survival analysis tool to rapidly assess the effect of 22,277 genes on breast cancer prognosis using microarray data of 1,809 patients. *Breast Cancer Res Treat* **123**, 725-31.

**Huang, Z., Duan, H. and Li, H.** (2015). Identification of Gene Expression Pattern Related to Breast Cancer Survival Using Integrated TCGA Datasets and Genomic Tools. *Biomed Res Int* **2015**, 878546.

**Imre, G., Berthelet, J., Heering, J., Kehrloesser, S., Melzer, I. M., Lee, B. I., Thiede, B., Dotsch, V. and Rajalingam, K.** (2017). Apoptosis inhibitor 5 is an endogenous inhibitor of caspase-2. *EMBO Rep* **18**, 733-744.

**Jang, H. S., Woo, S. R., Song, K. H., Cho, H., Chay, D. B., Hong, S. O., Lee, H. J., Oh, S. J., Chung, J. Y., Kim, J. H. et al.** (2017). API5 induces cisplatin resistance through FGFR signaling in human cancer cells. *Exp Mol Med* **49**, e374.

**Javed, A. and Lteif, A.** (2013). Development of the human breast. *Semin Plast Surg* **27**, 5-12.

**Krejci, P., Pejchalova, K., Rosenbloom, B. E., Rosenfelt, F. P., Tran, E. L., Laurell, H. and Wilcox, W. R.** (2007). The antiapoptotic protein Api5 and its partner, high molecular weight FGF2, are up-regulated in B cell chronic lymphoid leukemia. *J Leukoc Biol* **82**, 1363-4.

**LaCasse, E. C., Mahoney, D. J., Cheung, H. H., Plenchette, S., Baird, S. and Korneluk, R. G.** (2008). IAP-targeted therapies for cancer. *Oncogene* **27**, 6252-75.

**Macias, H. and Hinck, L.** (2012). Mammary gland development. *Wiley Interdiscip Rev Dev Biol* **1**, 533-57.

**Mailleux, A. A., Overholtzer, M. and Brugge, J. S.** (2008). Lumen formation during mammary epithelial morphogenesis: insights from in vitro and in vivo models. *Cell Cycle* **7**, 57-62.

**Mailleux, A. A., Overholtzer, M., Schmelzle, T., Bouillet, P., Strasser, A. and Brugge, J. S.** (2007). BIM regulates apoptosis during mammary ductal morphogenesis, and its absence reveals alternative cell death mechanisms. *Dev Cell* **12**, 221-34.

**Morris, E. J., Michaud, W. A., Ji, J. Y., Moon, N. S., Rocco, J. W. and Dyson, N. J.** (2006). Functional identification of Api5 as a suppressor of E2F-dependent apoptosis in vivo. *PLoS Genet* **2**, e196.

**Noh, K. H., Kim, S. H., Kim, J. H., Song, K. H., Lee, Y. H., Kang, T. H., Han, H. D., Sood, A. K., Ng, J., Kim, K. et al.** (2014). API5 confers tumoral immune escape through FGF2-dependent cell survival pathway. *Cancer Res* **74**, 3556-66.

**Park, S. J., Yoon, B. H., Kim, S. K. and Kim, S. Y.** (2019). GENT2: an updated gene expression database for normal and tumor tissues. *BMC Med Genomics* **12**, 101.

**Partanen, J. I., Nieminen, A. I., Makela, T. P. and Klefstrom, J.** (2007). Suppression of oncogenic properties of c-Myc by LKB1-controlled epithelial organization. *Proc Natl Acad Sci U S A* **104**, 14694-9.

**Plati, J., Bucur, O. and Khosravi-Far, R.** (2011). Apoptotic cell signaling in cancer progression and therapy. *Integr Biol (Camb)* **3**, 279-96.

**Pluta, P., Jeziorski, A., Cebula-Obrzut, A. P., Wierzbowska, A., Piekarski, J. and Smolewski, P.** (2015). Expression of IAP family proteins and its clinical importance in breast cancer patients. *Neoplasma* **62**, 666-73.

**Santner, S. J., Dawson, P. J., Tait, L., Soule, H. D., Eliason, J., Mohamed, A. N., Wolman, S. R., Heppner, G. H. and Miller, F. R.** (2001). Malignant MCF10CA1 cell lines derived from premalignant human breast epithelial MCF10AT cells. *Breast Cancer Res Treat* **65**, 101-10.

**Sasaki, H., Moriyama, S., Yukiue, H., Kobayashi, Y., Nakashima, Y., Kaji, M., Fukai, I., Kiriya, M., Yamakawa, Y. and Fujii, Y.** (2001). Expression of the antiapoptosis gene, AAC-11, as a prognosis marker in non-small cell lung cancer. *Lung Cancer* **34**, 53-7.

**Sharma, V. K. and Lahiri, M.** (2021). Interplay between p300 and HDAC1 regulate acetylation and stability of Api5 to regulate cell proliferation. *Sci Rep* **11**, 16427.

**Soule, H. D., Maloney, T. M., Wolman, S. R., Peterson, W. D., Jr., Brenz, R., McGrath, C. M., Russo, J., Pauley, R. J., Jones, R. F. and Brooks, S. C.** (1990). Isolation and characterization of a spontaneously immortalized human breast epithelial cell line, MCF-10. *Cancer Res* **50**, 6075-86.

**Sternlicht, M. D.** (2006). Key stages in mammary gland development: the cues that regulate ductal branching morphogenesis. *Breast Cancer Res* **8**, 201.

**Watson, C. J. and Khaled, W. T.** (2020). Mammary development in the embryo and adult: new insights into the journey of morphogenesis and commitment. *Development* **147**.

## List of Publications

1. **Abhijith K**, Debiprasad Panda, Radhika Malaviya, Gautami Gaidhani, and Mayurika Lahiri, Altered expression of Api5 affects breast carcinogenesis by modulating FGF2 signalling. **BioRxiv**, 2021.
2. Chakravarty V, Anandi L, Ashiq KA, **Abhijith K**, Umesh R, Lahiri M. Prolonged Exposure to Platelet Activating Factor Transforms Breast Epithelial Cells. **Front Genet.** 2021 Mar 25; 12:634938.

# Table of Contents

Declaration.....	iii
Acknowledgement.....	iv
Synopsis.....	vii
Table of Contents.....	1
Abbreviations .....	8
Abstract.....	10
Chapter 1: Introduction.....	11
1.1. Tissue Homeostasis .....	12
1.2. Hallmarks of cancer.....	13
1.3. Apoptosis.....	14
1.4. The extrinsic death receptor pathway.....	15
1.5. The Intrinsic Mitochondrial Pathway.....	15
1.6. Apoptosis Inhibitor 5 (Api5).....	18
1.7. Api5 discovery and functions.....	18
1.8. Api5 and Cancer.....	19
1.9. Breast Cancer.....	20
1.10. Significance of 3D breast acinar cultures for transformation studies .....	22
Chapter 2: Materials and Methods .....	26
2.1. Cell lines and culture conditions .....	27
2.2. Chemicals and antibodies.....	27
2.3. Plasmids.....	28
2.4. In-silico analyses .....	29
2.5. Stable cell line preparation .....	30
2.6. 3D 'on-top' culture .....	31
2.7. Immunofluorescence staining.....	31
2.8. Immunoblotting.....	32

2.9. Gelatin Zymography .....	33
2.10. DQ Collagen assay.....	33
2.11. Single Cell Migration.....	34
2.12 Soft Agar Assay .....	34
2.13 Clonogenicity assay.....	34
2.14 <i>In-vivo</i> tumorigenicity assay.....	35
2.15 Immunohistochemistry.....	35
2.16 Statistical analysis .....	37
2.17 Ethics approvals .....	37
Chapter 3: Altered Api5 expression affects breast carcinogenesis .....	38
3.1 Background .....	39
3.2 Results.....	41
3.2.1 Preparation of Api5 OE MCF10A, Api5 KD MCF10AT1 and Api5 KD MCF10CA1a stable cells.....	41
3.2.2 Api5 overexpression resulted in altered morphology of MCF10A acinar cultures. ....	45
3.2.3 Api5 knockdown in MCF10AT1 and MCF10CA1a cells affects their growth in spheroid cultures .....	50
3.2.4 Altered expression of Api5 affects proliferation and apoptosis in 3D cultures .....	52
3.2.5 Api5 overexpression results in disruption of polarity in 3D acinar structures .....	60
3.2.6 Api5 overexpression results in partial-EMT like phenotype.....	67
3.2.7 Api5 knockdown affects EMT marker expression in malignant breast cells	74
3.2.8 Api5 overexpression led to higher migratory potential.....	75
3.2.9 Api5 knockdown reduced colony formation ability of malignant cells ....	81

3.2.10	Api5 overexpression results in anchorage-independent growth of breast epithelial cells.....	83
3.2.11	To investigate whether Api5 overexpression can induce <i>in vivo</i> tumorigenic potential.....	85
3.3	Discussion .....	88
Chapter 4:	Api5 regulates Akt and ERK signalling through FGF2 .....	92
3.1	Background .....	93
4.2	Result .....	94
4.2.1	To investigate the molecular mechanism behind Api5 mediated breast epithelial cell transformation.....	94
4.3	Discussion .....	99
Chapter 5:	Breast cancer patients have upregulated API5 levels which can predicts poor patient survival .....	101
5.1	Background .....	102
5.2	Results.....	103
5.2.1	API5 expression is upregulated in tumour tissues as compared to adjacent normal tissue .....	103
5.2.2	Higher Api5 transcript expression correlates with elevated proliferation and affects cell-cell junction components.....	106
5.2.3	Immunohistochemical analysis of breast cancer samples.....	110
5.3	Discussion .....	112
Chapter 6:	Conclusion and Future Prospective .....	113
Bibliography	.....	120
Appendix	.....	129
Appendix I-	Vector maps .....	129
Appendix II-	Media Composition.....	135
Appendix III:	Buffers for Immunofluorescence: .....	135
Appendix IV-	Buffers for Immunoblotting .....	136



Appendix V: Buffers and staining solution for Gelatin Zymography .....	137
Publications.....	139
Research Articles .....	141

## Table of Figures

Fig 1.1 Hallmarks of cancer.....	13
Fig1.2 Overview of Apoptosis signalling cascade .....	17
Fig 1.3 The schematic representation of Api5 with its domains.....	18
Fig 1.4 Api5 mediated regulation of FGF2 signalling and Bim degradation.....	19
Fig 1.5 Breast cancer statistics in India. ....	21
Fig 1.6 MCF10A cells seeded on Matrigel <sup>®</sup> forms growth-arrested acinar structures by day 16.....	23
Fig 1.7 MCF10A acini resembles human mammary gland acini. ....	24
Fig 1.8 Transformation induced morphological changes in MCF10A 3D cultures. ...	25
Fig 3.1 Api5 OE stable cell line preparation. ....	42
Fig 3.2 FACS sorting of Api5 OE cells.....	43
Fig 3.3 Sorting parameters for selecting Api5 KD MCF10AAT1 and Api5 KD MCF10CA1a cells .....	44
Fig 3.4 MCF10AT1 and MCF10CA1a cells with Api5 knockdown were prepared and sorted using FACS. ....	45
Fig 3.5 Api5 OE results in altered MCF10A acinar morphology. ....	46
Fig 3.6 Api5 OE results in altered size of MCF10A acini. ....	47
Fig 3.7 Api5 OE did not alter nuclear size. ....	47
Fig 3.8 Api5 overexpression leads to the increased number of cells per acini. ....	48
Fig 3.9 MCF10A cells overexpressing Api5 does not form acini with protrusions ....	49
Fig 3.10 Api5 OE resulted in lumen filling of 16-day MCF10A acinar cultures .....	50
Fig 3.11 Api5 KD in MCF10AT1 and MCF10CA1a affects spheroid formation in 3D cultures.....	52
Fig 3.12 Api5 overexpression leads to increased proliferation .....	53
Fig 3.13 Schematic showing apoptosis during acinar morphogenesis .....	54
Fig 3.14 Api5 overexpression results in reduced apoptosis during MCF10A breast acinar morphogenesis.....	54

Fig 3.15 Api5 knockdown results in reduced proliferation of malignant breast cells.	56
Fig 3.16 Api5 KD leads to an increase in apoptosis.	58
Fig 3.17 Api5 KD in malignant cells activates apoptosis through Bax.	59
Fig 3.18 Schematic showing polarity in MCF10A acinar structure	60
Fig 3.19 Api5 overexpression in MCF10A cells disrupted $\alpha$ 6-integrin localisation.	61
Fig 3.20 Api5 OE in MCF10A led to loss of basal polarity marker, Laminin V.	61
Fig 3.21 Api5 OE disrupts apical polarity of MCF10A 3D acinar cultures.	62
Fig 3.22 Api5 overexpression results in dispersal of Golgi	63
Fig 3.23 Api5 overexpression resulted in higher pERM staining	64
Fig 3.24 Api5 overexpression results in variation in levels of cell-cell junction markers.	65
Fig 3.25 Api5 overexpression affects cell-cell junctions	66
Fig 3.26 Api5 overexpression might be resulting in partial EMT like characteristics.	68
Fig 3.27 Api5 OE results in partial-EMT characteristics, which are maintained even after dissociating from 3D culture.	70
Fig 3.28 Api5 overexpression results in higher cytokeratin-8 expressions.	72
Fig 3.29 Api5 overexpression results in altered expression of Desmosomal Armadillo proteins.	73
Fig 3.30 Api5 KD results in altered EMT marker expression.	75
Fig 3.31 Api5 OE affects MMP activity during early days of acinar morphogenesis.	76
Fig 3.32 Api5 KD does not affect MMP2 and MMP9 activity.	77
Fig 3.33 Api5 OE does not induce invasive potential in the epithelial cell line.	78
Fig 3.34 Api5 overexpression increases single-cell migration.	79
Fig 3.35 Api5 KD results in reduced cell migratory potential.	80
Fig 3.36 Api5 KD results in reduced cell migratory potential.	81
Fig 3.37 Api5 knockdown results in reduced proliferation.	82
Fig 3.38 Api5 overexpression induces the ability to grow in an anchorage-independent manner.	83

Fig 3.39 Api5 knockdown results in reduced ability to grow in an anchorage-independent manner. ....	84
Fig 3.40 Api5 OE do not induce <i>in vivo</i> tumorigenic potential in MCF10A cells. ....	85
Fig 3.41 Api5 KD in MCF10CA1a affects tumor growth <i>in vivo</i> . ....	86
Fig 3.42 Api5 knockdown reduces <i>in vivo</i> tumorigenicity potential. ....	87
Fig 3.43 Summary graphics showing the effect of Api5 OE in epithelial cell line and Api5 KD in the malignant breast cell line. ....	91
Fig 4.1 Api5 overexpression results in ERK signalling activation during late days of MCF10A acinar morphogenesis. ....	95
Fig 4.2 Api5 OE results in FGF2 mediated PDK1-Akt signalling. ....	96
Fig 4.3 Api5 KD results down-regulate FGF2-Akt/ ERK signalling ....	97
Fig 4.4 Schematic showing the signalling mechanisms in which Api5 affect breast carcinogenesis. ....	100
Fig 5.1 Api5 transcript levels are upregulated in breast cancer. ....	104
Fig 5.2 Higher Api5 expression suggest poor patient survival. ....	105
Fig 5.4 Results from DAVID analysis with Upregulated gene set as query genes. ....	107
Fig 5.5 Results from DAVID analysis with down-regulated gene set as query genes. ....	107
Fig 5.6 Results from DAVID platform when KEGG pathway terms were selected. ....	108
Fig 5.7 cAMP signalling pathway as shown by KEGG pathway ....	108
Fig 5.8 Results from DAVID platform when KEGG pathway terms were selected after submitting negatively correlated gene list. ....	109
Fig 5.10 Api5 protein expression in Indian breast cancer patients. ....	110
Fig 5.11 Api5 proteins levels are upregulated in tumour tissues of Indian breast cancer patients. ....	111
Fig 6.1 Regulation of breast morphogenesis by Api5. ....	117
Fig 6.2 Alternative signalling pathway in Api5 mediated transformation of breast epithelial cells. ....	119

## Abbreviations

Api5	Apoptosis Inhibitor 5
FGF2	Fibroblast Growth Factor-2
PDK1	3-Phosphoinositide Dependent Protein Kinase -1
TCGA	The Cancer Genome Atlas
GENT2	Gene Expression database of Normal and Tumor tissues 2
NSCLC	Non-Small Cell Lung Cancer
OE	Overexpression
KD	Knockdown
DMEM	Dulbecco's Modified Eagle Medium
FACS	Fluorescence Assisted Cell Sorter
PBS	Phosphate Buffered Saline
IF	Immunofluorescence
EDTA	Ethylenediaminetetraacetic acid
RT	Room Temperature
TBST	Tris Buffered Saline- Tween 20
CTCF	Corrected Total Cell Fluorescence
MTT	2,5-diphenyl-2H-tetrazolium bromide
GC	Growth Constituents
IHC	Immunohistochemistry
ER $\alpha$	Estrogen Receptor alpha
MNU	N-Methyl-N-Nitrosourea
GFP	Green Fluorescent Protein
ERM	Ezrin, Radixin and Moesin
FWHM	Full-Width Half Max
EMT	Full-Width Half Max
GAPDH	Glyceraldehyde Phosphate Dehydrogenase
MMP	Matrix Metalloproteinases
DQ	Dye Quenched
GEO	Gene Expression Omnibus
TNBC	Triple Negative Breast Cancer

DAVID	Database for Annotation, Visualization, and Integrated Discovery
FFPE	Formalin Fixed Paraffin Embedded
PDX	Patient Derived Organoids

## Abstract

The balance between cell death and cell division is essential for the maintenance of homeostasis in multicellular organisms. Apoptosis, or programmed cell death, plays a vital role in the maintenance of this homeostasis and therefore, is a tightly regulated process. Deregulation of apoptosis can lead to cancer. Apoptosis inhibitor 5 (Api5) is an inhibitor of apoptosis. The molecular mechanism underlying the activation and regulation of Api5 is yet to be thoroughly explored. Api5 has been reported to be associated with several cancers, including ovarian, bladder, and lung cancers. Studies suggest that Api5 can be used as a biomarker for ovarian and bladder cancers. However, the role of Api5 in breast cancer, which reports the highest number of deaths due to cancer, remains unclear. My project focuses on investigating the role of Api5 in breast cancer. *In vitro* overexpression studies using 3D breast acinar cultures demonstrated that overexpression of Api5 resulted in the transformation of non-tumorigenic breast epithelial cells with increased proliferation and various phenotypic changes. Api5 knockdown affected the tumorigenic potential and associated phenotypes of breast cancer cells. Mechanistically Api5 was shown to activate FGF2 signalling, possibly leading to PDK1-Akt and ERK pathway activation. Interestingly Api5-FGF2 signalling activates PDK1-Akt/ cMYC axis during the early days of acinar morphogenesis, while activation of ERK signalling occurred during the later days. Together this led to elevated proliferation, migration, anchorage-independent growth, protein synthesis and reduced apoptosis, supporting the malignant growth of Api5 overexpressing cells. *in silico* studies using TCGA and GENT2 database demonstrated that elevated levels of Api5 transcript in breast cancers that was also associated with poor patient survival. This further correlated with histopathological analyses of tumour samples where higher expression of Api5 was observed in breast tumour tissue compared to the adjacent normal tissue, thus suggesting that elevated levels of Api5 might be associated with breast malignancy.

## **Chapter 1: Introduction**



## **1.1. Tissue Homeostasis**

Multicellular organisms need to maintain a steady state for their healthy survival. The proper development and prevention of morphological and characteristic alterations are dependent on this homeostasis. Cell death and cell division are the significant factors involved in maintaining the balance. The regulation sustains throughout the lifespan of the organisms, starting from early development and continues to maintain a healthy state (Cooper and Youle, 2012).

Cell division in a multicellular organism plays a major role in organ development and thus are also tightly regulated. Organs like breasts undergo constant remodelling during the lifetime of a female. Breast development initiates from the early stages of development and stays inactive till puberty. Upon attaining puberty, the hormonal changes reactivate the development and lead to constant remodelling till pregnancy (Russo and Russo, 2004). This growth involves both proliferation and cell death. Further, during pregnancy, the glandular epithelium expands to the fat pad—post lactation, the epithelium is involuted by cell death. Similarly, during the lifespan of a multicellular organism, tissue homeostasis maintains the proper development of the organs and thereby the organism.

Any deviation in the delicate balance between cell death and cell division can lead to disease conditions, including cancer (Gudipaty et al., 2018). Deregulated proliferation can lead to a higher number of cells in the tissue than it should have. Often such transformed cell tends to migrate to the circulatory system and/ or to other organs leading to metastasis. On the other hand, cells that acquire mutations may undergo cell death if the damages are unrepairable. Deviation from tissue homeostasis leading to reduced cell death can lead to survival of such cells sustaining the mutations. This can also drive cancer progression (Kesari et al., 2003).

Hanahan and Weinberg, in 2011, coined the hallmarks of cancer, which are the characteristics that a cell acquires during the transition from a normal cell to a cancer cell. Increased proliferation and decreased cell death are also part of these hallmarks of cancer (Hanahan and Weinberg, 2011).

## 1.2. Hallmarks of cancer

Carcinogenesis is a multi-step process that includes changes in multiple morphological and characteristics changes in a cell. Deregulation of various molecular events can pave the way for carcinogenesis. As discussed earlier, loss of balance in tissue homeostasis can trigger deregulated growth of cells in an organism. The hallmarks of cancer list the possible changes and alterations that a normal cell can acquire during transformation (Fig 1.1). Many of these changes induce enhanced proliferation, such as sustaining proliferative signalling, evading growth suppressors, and enabling replicative immortality. Cancer cells can also alter cell death machinery to support survival. Thus resisting cell death is also identified as an ability that can support carcinogenesis (Hanahan and Weinberg, 2011).

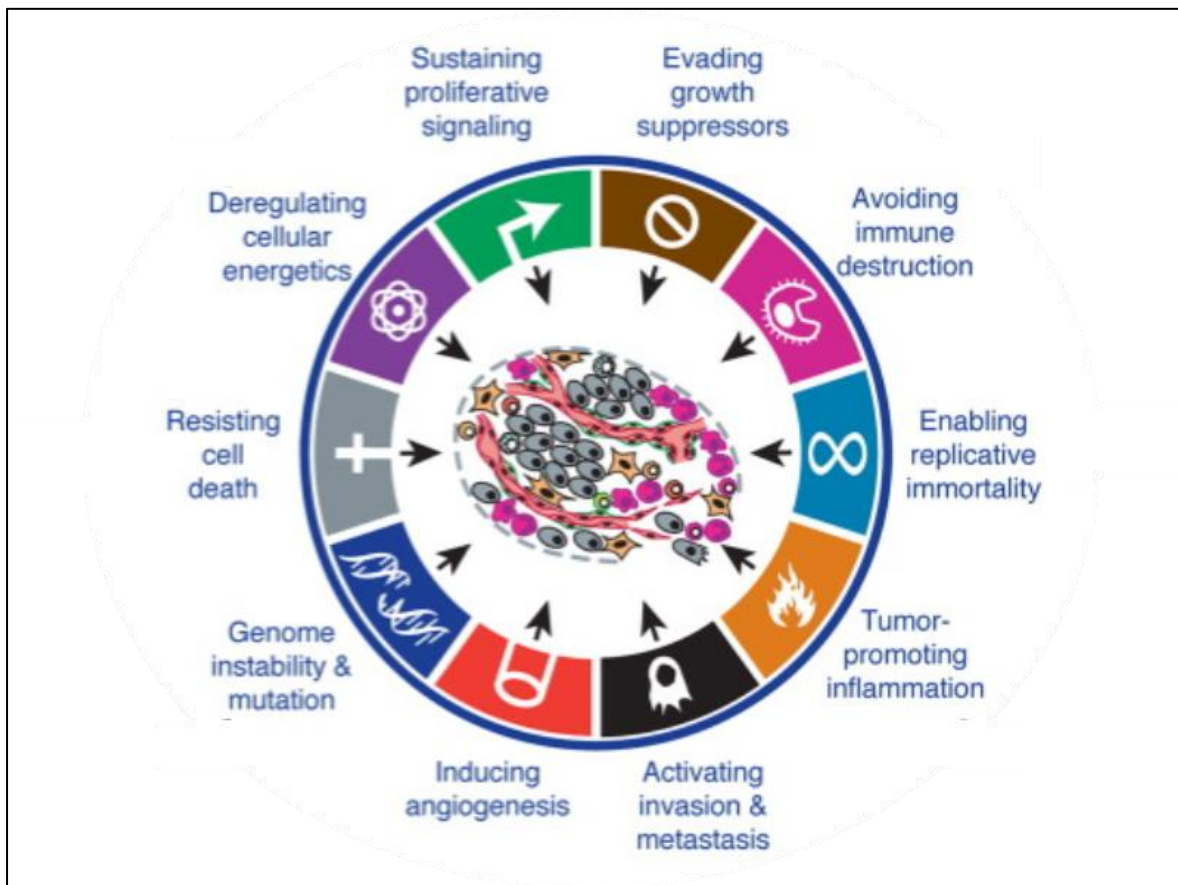


**Fig 1.1** Hallmarks of cancer.

The characteristic changes that a normal cell acquires when a cell transforms. Reproduced from Hanahan and Weinberg Cell 2011.

### 1.3. Apoptosis

Cell death is as vital as cell division, as the balance between the two helps maintain a healthy cell population in a multicellular organism. A disturbance in this balance could lead to catastrophe. As it is essential to maintain the balance, multiple control measures modulate the activity of the two processes. Apoptosis, the programmed cell death, being one of the primary cell death mechanisms, plays an essential role in the development of an organism (Elmore, 2007) and during the later phases of life. It also plays an essential role in maintaining the uniformity of cells in a tissue.

Apoptosis prevents the survival of cells with altered gene expression due to external and damages like radiation, chemicals, and ROS. Maintaining a healthy and proper internal environment in a multicellular organism is important for its healthy survival, and apoptosis does a major part of the work. The term apoptosis means falling off, like leaves falling off. It was first described by Kerr et al. (Kerr et al., 1972), who named it a controlled cell deletion that could play an opposite role to mitosis. The review describes the two major steps during apoptosis, which are breaking up of cellular components and clearing the cleaved products. Later in 1999, Horvitz came up with a much-detailed explanation on the process of apoptosis, which was based on the studies in nematode *C. elegans*. It shows the role of apoptosis in *C. elegans* during the development of the worm, where a set of somatic cells undergo apoptosis at a particular time during the organism's development (Horvitz, 1999). After the initial reports, several studies on apoptosis explained the mechanism and its importance in different clinical conditions.

The main morphological changes that happen in apoptosis were later found to be chromatin condensation and fragmentation of the nucleus. This ends in rounding up of cells and then a reduction in the cell's total volume (Poon et al., 2014). Finally, the cell gets phagocytosed. The pathways that trigger these vary across different situations, but the basic steps remain almost similar.

Along with the changes in the morphology of the cell that is undergoing apoptosis, specific biochemical changes take place, which helps in the apoptosis like the activation of caspases and DNA and protein breakdown (Wong, 2011). Further, there will be changes on the membrane, including the flipping of Phosphatidylserine from the inner membrane to the outer membrane, which will help detect apoptotic cells by macrophages (Hengartner, 2001). This flipping happens in the early stages of

apoptosis. The activated caspases can activate DNAase leading to DNA fragmentation (Larsen and Sorensen, 2017). Even though these biochemical changes are present in cells undergoing apoptosis, any cell showing such phenotype may not necessarily have an apoptosis pathway under process. It can either undergo apoptosis or lead to other cell death pathways. The morphological changes are the main factor to categorize whether the cell death mechanism adapted by the cell is apoptosis (Galluzzi et al., 2007).

Apoptosis signalling majorly gets activated through the extrinsic death receptor pathway or the intrinsic pathway (Fig 1.2). The extrinsic pathway responds to external stimuli for apoptosis activation, while the intrinsic pathway responds to internal stimuli.

#### **1.4. The extrinsic death receptor pathway**

Death receptors that are present on the cell surface when bound with death ligands signals apoptosis through extrinsic death receptor signalling. Type 1 TNF receptor (TNFR1) and Fas (CD95) are the major death receptors that can activate the signalling. These death receptors are activated by binding TNF and Fas ligand, respectively (Hengartner, 2001). The receptor binding to ligand activates the complex and forms a site for adaptor proteins to bind. A Death Inducing Ligand Complex (DISC) is formed when TNF receptor Associated Death Domain (TRADD) and Fas-associated Death Domain (FADD), which are the adaptor proteins, bind to the corresponding death receptor ligand complex (O'Brien et al., 2008; Schneider and Tschopp, 2000). The DISC can activate pro-caspase 8. Activated caspase 8 further downstream activates caspases like caspase 3, caspase 6 and caspase 7, called effector caspases. Caspase 3 leads to activation of DNAase by inactivating inhibitor of caspase-activated DNAase, and along with caspase 7 it is involved in proteolytic activities (Wong, 2011).

#### **1.5. The Intrinsic Mitochondrial Pathway**

As the extrinsic pathway is triggered from outside the cell, intrinsic pathway is activated from inside. The intrinsic pathway is a response to internal stimuli due to stress conditions inside the cell. The internal stimuli can be either genetic damage that cannot be repaired, a high concentration of  $Ca^{2+}$ , or hypoxia (Wong, 2011). Also, it could be understood that this is a mechanism that the cells have developed

to protect the tissue by activating a suicide pathway and not getting converted to a malignant cell that proliferates in an uncontrolled manner. Even though the stimuli are different, the process is quite similar in all the cases, where there is an increased mitochondrial permeability which results in the release of pro-apoptotic molecules like cytochrome c (Danial and Korsmeyer, 2004) to the cytoplasm, which later leads to cell death. The Bcl2 family of proteins functions as a major regulator of this apoptosis signalling (Tsujimoto et al., 1984). The Bcl2 family of proteins are further classified as either anti-apoptotic or pro-apoptotic. The mode of action of these two classes are opposing as the pro-apoptotic proteins like Bax, Bik, and Bim promote the release of cytochrome c to the cytoplasm from mitochondria anti-apoptotic proteins block the release of cytochrome-c to the cytoplasm (Reed, 1997). As one can hypothesize, the correct balance between these two sets would decide the survival of the cells (Dewson et al., 2010) In the case of stress or if the outer mitochondrial membrane breaks the proteins including cytochrome c, Smac, AIF, and endonuclease G will be released to the cytoplasm. Once cytochrome-c reaches the cytoplasm, it binds to Apaf-1, further exposing a domain on which caspase 9 can bind and activate it. This further activates the executioner caspases like caspase 3 (Kroemer et al., 2009).

Both extrinsic and intrinsic pathways activate caspase 3, which is considered the effector caspase as they further promote the cleavage of protein kinases, cytoskeletal proteins, DNA repair proteins, etc. It affects all cellular functions, including cell cycle regulation and signalling pathways. This further leads to the total collapse of the cell (Ghobrial et al., 2005).

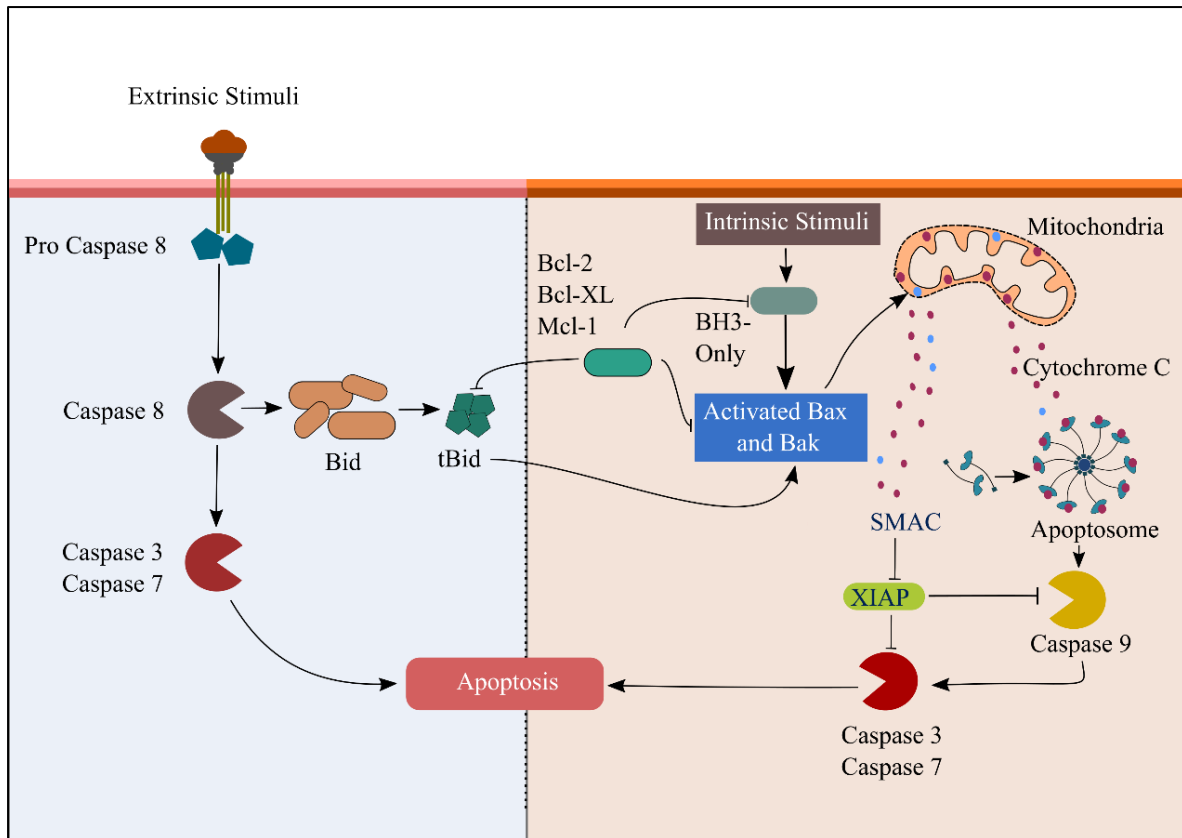


**Fig1.2** Overview of Apoptosis signalling cascade

Other than these two, there is a poorly understood pathway which is the Endoplasmic Reticulum pathway. ER stress leads to  $Ca^{2+}$  release, which can activate caspase 12, which further activates caspase 9, and so caspase 3 leading to (O'Brien et al., 2008). This ER-dependent pathway is found to work with different pathways, one of which, as said above, is caspase 12 dependent the other one is based on Ire1 activation, which reduces Bcl-2, and the balance between proapoptotic and antiapoptotic proteins gets affected, leading to apoptosis (Dewson et al., 2010).

Along with the Bcl2 family of proteins, Inhibitors of Apoptosis Proteins (IAP), Api5, and Par4 (Wei et al., 2008) regulate Apoptosis. IAPs are inhibitors of caspase, which are known to bind the enzyme's active site through the BIR domains (**B**aculovirus **I**AP **R**epeats domains), which are zinc finger domains. The BIR domains can lead to the degradation of active caspase or prevent the substrate from binding to the enzyme(Wei et al., 2008). Every member of the IAP family is structurally similar because of the presence of one to three BIR repeats (LaCasse et al., 2008). Par4 is

a pro-apoptotic molecule that is known to induce apoptosis by different mechanisms. Api5 is an anti-apoptotic protein but not a member of IAPs. The mechanism of Api5 in inhibiting apoptosis is not yet completely elucidated. Multiple studies suggests various ways of apoptosis inhibition by Api5.

### 1.6. Apoptosis Inhibitor 5 (Api5)

Apoptosis Inhibitor 5 (Api5), also known as Aac11 (Anti-apoptotic clone 11)/ MIG 8(Migration Inducing Gene 8) and FIF (FGF2 interacting factor), is a 55kDa protein localised to the nucleus. The protein has a Leucine Zipper Domain (LZD), an LxxLL motif and a Nuclear Localization Signal (NLS)(Han et al., 2012) (Fig 1.3). Even though Api5 has an LZD domain, which is essentially a DNA binding domain, no reports show Api5 interaction with DNA.



**Fig 1.3** The schematic representation of Api5 with its domains.

### 1.7. Api5 discovery and functions

Tewari *et al.* in 1997 screened a cDNA library to identify possible genes that support survival following serum deprivation. They found a colony of cells that overexpressed a cDNA clone from the library, which survived for four months in serum-free conditions. The cDNA was named AAC-11(Tewari et al., 1997). Later in 2006, using *Drosophila* as a model system, Morris *et al.* found that Aac-11 can inhibit E2F1 mediated apoptosis by regulating the transcriptional activity of E2F1 (Morris et al., 2006). Garcia *et al.* in 2013 showed that Api5, a mammalian homolog of Aac-11, may also be involved in the cell cycle. They found that Api5 regulates E2F1 transcriptional activity during G1/S transition as well. Api5 knockdown leads to G1/S cell cycle arrest due to reduced expression of Cyclin E, Cyclin D1, and Cdks(Garcia-Jove Navarro et al., 2013). Later a study by Rigou *et al.* identified Acinus as an interacting partner of Api5. Api5 also prevents caspase-mediated cleavage of Acinus, leading to apoptosis-related DNA fragmentation and chromatin condensation (Rigou et al., 2009). In 2017, Imre *et al.* showed that Caspase 2, which has roles in Apoptosis and autophagy, interacts with the C terminal domain of Api5 through the CARD domain. This also prevents the dimerisation of caspase 2, which is required to activate caspase 2 and caspase 2-mediated apoptosis (Imre et al., 2017).

Noh *et al.* in 2014 identified that Api5 could help in tumoral immune escape of murine cancer cells. They found that Api5 levels upregulate in cells that are resistant to cytosolic T lymphocytes (CTL). They also found that Api5 overexpression in CTL susceptible cell line resulted in immune-resistant cells activating the FGFR1- ERK pathway (Fig 1.4). This pathway leads to phosphorylation of Bim, a pro-apoptotic molecule which thereby results in signalling for Bim degradation (Noh *et al.*, 2014). Even though all these different modes of Apoptosis inhibition by Api5 is known, the molecular mechanism underlying the initiation and regulation of Api5 activity remain unclear.

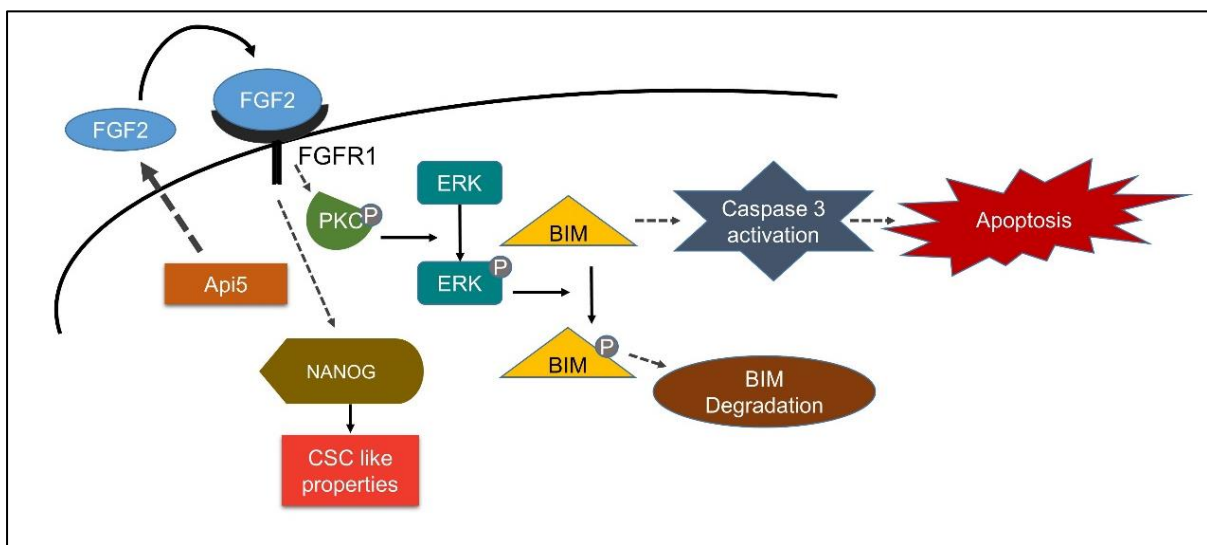


**Fig 1.4** Api5 mediated regulation of FGF2 signalling and Bim degradation.

Adapted from Noh *et al.* Cancer Res. 2014.

### 1.8. Api5 and Cancer

Following the initial studies, Kim *et al.* demonstrated cancer promoting ability of Api5 (Aac11) by overexpression studies. They concluded that Aac11 overexpression could protect human cervical cancer cells from apoptosis (Kim *et al.*, 2000). Later Sasaki *et al.* studied the transcript-level expression of Api5 in patient samples of non-small cell lung cancer (NSCLC) and compared it with the adjacent normal of the cancer tissue. They showed that higher levels of API5 are associated with poor survival of non-small cell lung cancer (NSCLC) patients (Sasaki *et al.*, 2001). Morris and group in 2006 demonstrated that depletion of Api5 in squamous cell carcinoma cells led to increased cell death (Morris *et al.*, 2006). Following the report by Morris



et al., another study in 2007 showed that Api5 and its interacting partner FGF2 were found to be upregulated in B cell chronic lymphoid leukaemia patient samples (Krejci et al., 2007). In 2014 Cho *et al.* showed that Api5 levels are elevated in cervical cancer tissues compared to healthy tissue. Also, Api5 overexpression leads to increased proliferation in cervical cancer cells (Cho et al., 2014). Song *et al.* showed that Api5 could induce cancer stem cell-like properties (Song et al., 2017).

Even though many studies suggest the relation between Api5 and cancer, the function and necessity of Api5 in breast cancer remains unclear.

### **1.9. Breast Cancer**

Breast cancer is one of the leading cause of death among women. According to GLOBOCAN 2020 data, it is the second significant type of cancer affecting people worldwide (Fig 1.5). It is also reported that breast cancer has the highest mortality rate in India (Song et al., 2017). A recent study in 2017 in America shows that 30% of cancer cases in females are breast-related and results in 14% of the total deaths caused by cancer (Siegel et al., 2018)

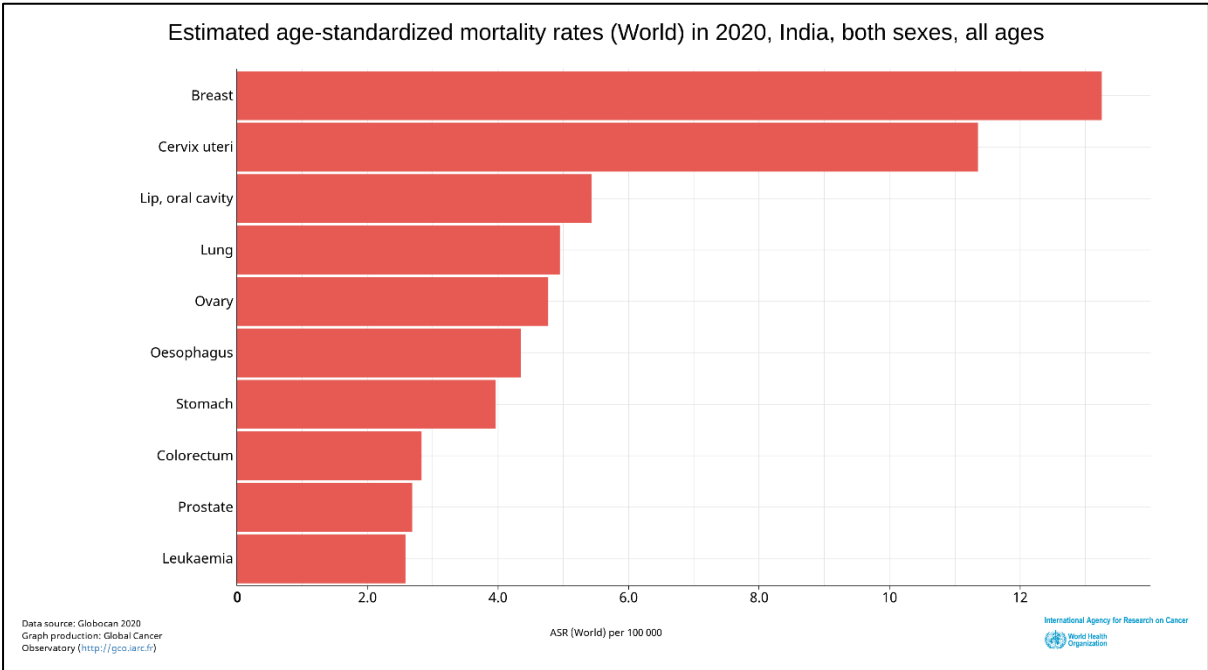
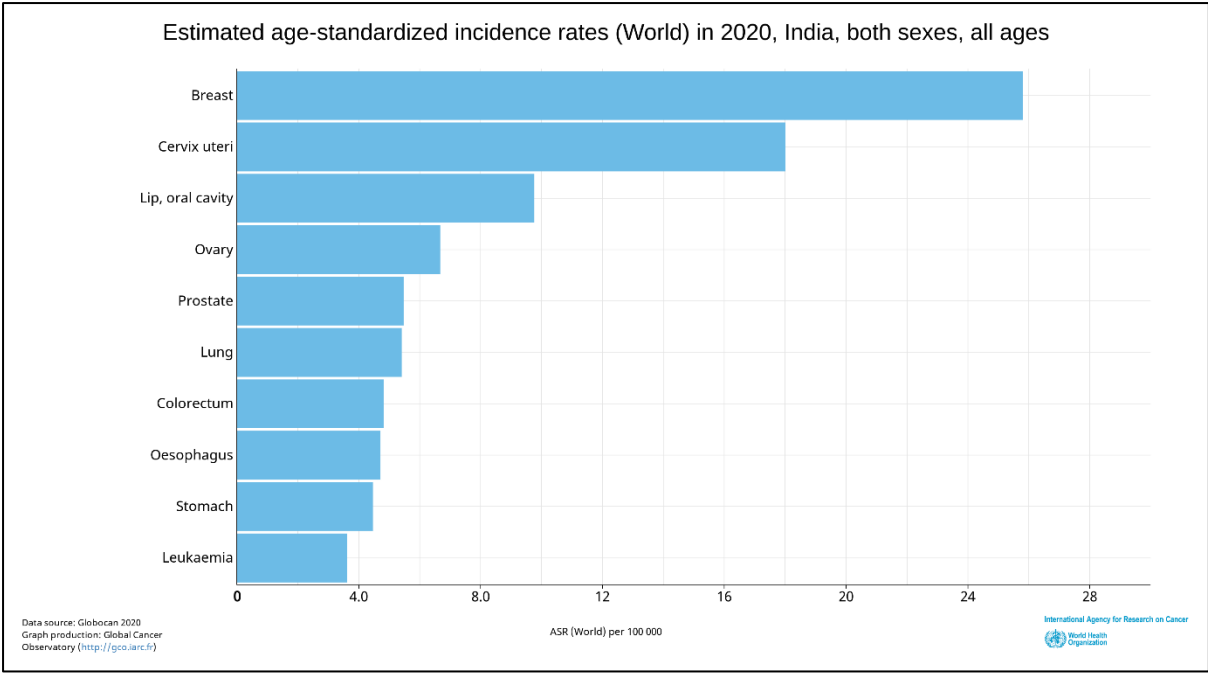


**Fig 1.5 Breast cancer statistics in India.**

Graph showing the incident cases and the number of deaths in India due to different cancers. Breast cancer leads to the highest percentage of incident cases as well as the number of deaths.

Lack of awareness and proper diagnostics are the primary reasons for the increase in breast cancer cases in India, as identifying the same during the early stages will help the patient's better survival. Identifying potential biomarkers will help early

detection of breast cancer and may eventually reduce the high mortality due to breast cancer in India.

#### **1.10. Significance of 3D breast acinar cultures for transformation studies**

Even though traditional 2D monolayer cultures have provided many insights into cancer studies, they could not provide a deeper understanding of the molecular mechanism that triggers tumorigenesis (Edmondson et al., 2014). The monolayer cultures do not recapitulate the three-dimensional morphology of tissues, and the signalling will be different due to the lack of an extracellular matrix. As our studies on Api5 focus on understanding the morphological changes that Api5 overexpression can lead to and understanding the molecular mechanism underlying the same, 3D culture system will be better than 2D cultures for the same (Bissell and Radisky, 2001). To have a better understanding, we will be using three-dimensional acinar cultures using Matrigel<sup>®</sup>. Matrigel<sup>®</sup>, enriched with Laminin, Collagen IV, and entactin, act as a basement membrane matrix for the epithelial cells. Matrigel<sup>®</sup> is the extracellular matrix from the Engelbreth Holm-Swarm mouse sarcoma (Kleinman and Martin, 2005). It also contains heparin sulphate and several growth factors which facilitates the breast epithelial cells to grow as acini. The 3D culture system resembles the *in vivo* model system than 2D regarding the morphology as well as signalling pathways (Schmeichel and Bissell, 2003). MCF10A cells, which are non-tumorigenic breast epithelial cells seeded on top of Matrigel<sup>®</sup> form growth, arrested polarised acinar structures by day 16 (Fig 1.6). The cells that are in the lumen will undergo apoptosis from Day 6 to Day 8 as it does not get signals from the extracellular matrix or the Matrigel<sup>®</sup> (Debnath et al., 2003a).

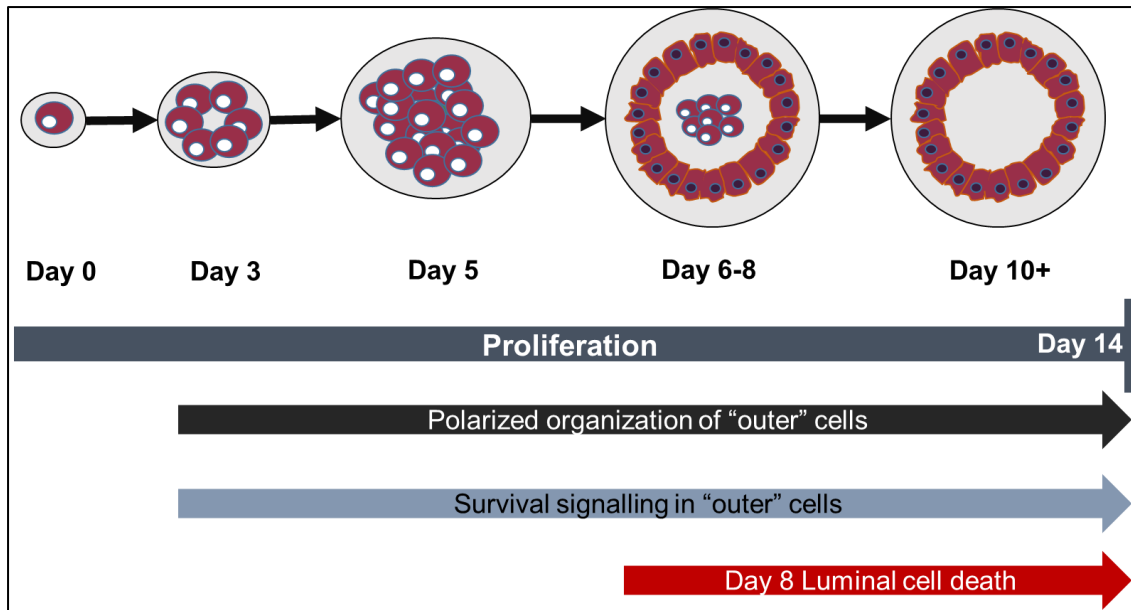


**Fig 1.6** MCF10A cells seeded on Matrigel<sup>®</sup> forms growth-arrested acinar structures by day 16.

Adapted from Debnath *et al.*, *Methods*, 2003.

These acinar structures resemble the mammalian breast acini, the basic functional unit of the Breast. The breast acini have myoepithelial cells lining the luminal cells. These myoepithelial cells support the contraction and relaxation of breast acini. The acini grown on Matrigel<sup>®</sup> lacks myoepithelial cells as it is a monolayer of cells with a hollow lumen (Fig 1.7).

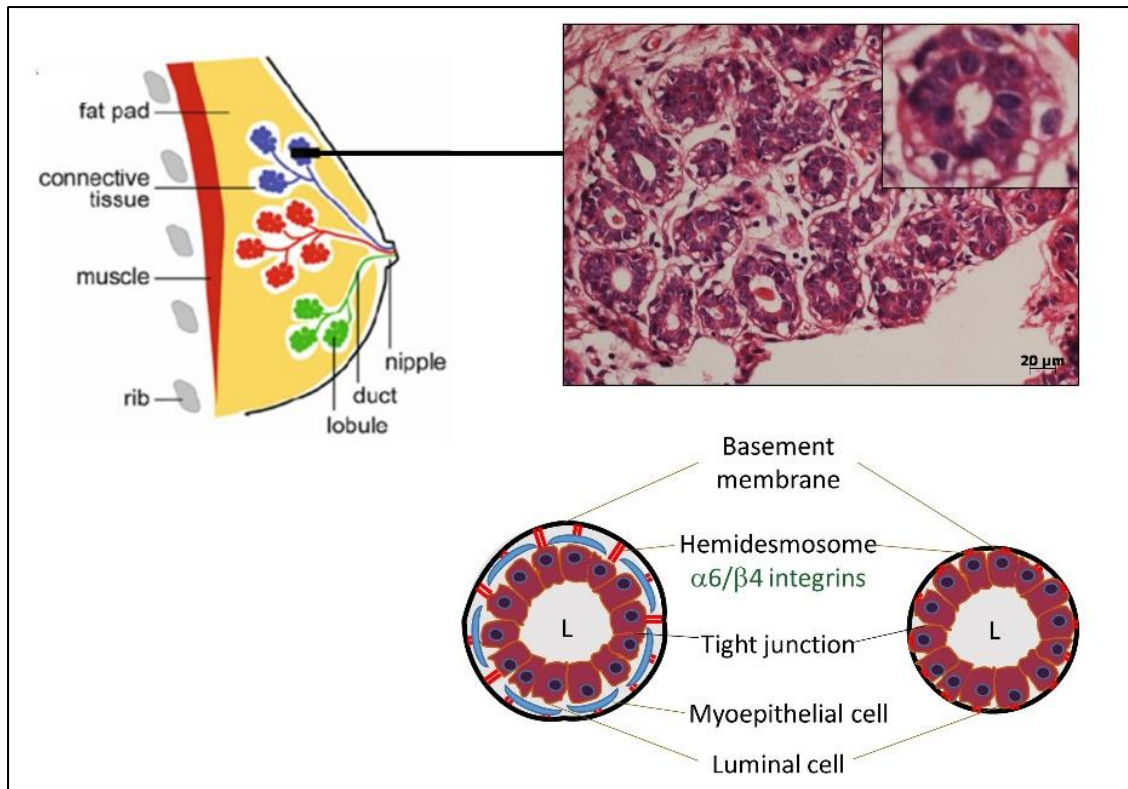


**Fig 1.7** MCF10A acini resembles human mammary gland acini.

The 3D culture resembles the breast acini to a larger extent; it has a similar polarised structure but lacks the myoepithelial cells. Adapted from Vidi *et al.*, *Methods Mol Bio.* 2013.

These structures are found to be disrupted in the case of overexpression of oncogenes in MCF10A cells (Vidi *et al.*, 2013). They lose the polarised structure and often form protrusive structures coming out of acini with partially or entirely filled lumen. Such characteristic changes can be used as a marker suggesting transformation (Fig 1.8) (Debnath *et al.*, 2003a).

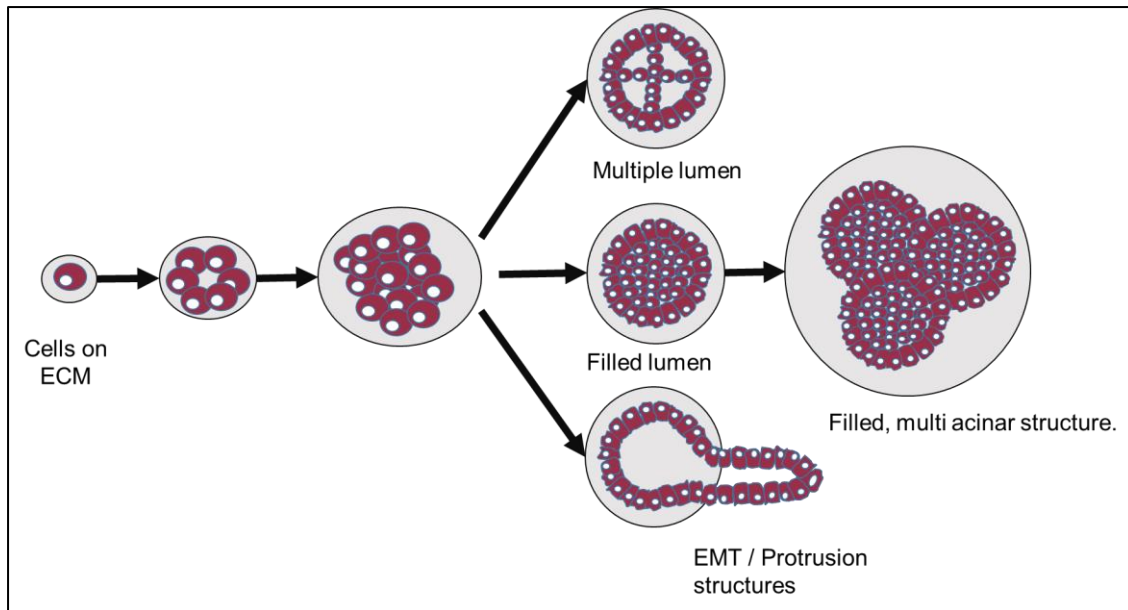


**Fig 1.8** Transformation induced morphological changes in MCF10A 3D cultures. MCF10A 3D cultures provide a reliable model for understanding transformation event in epithelial cell line. Morphometric changes include filled lumen, and protrusion like structures.

## **Chapter 2: Materials and Methods**

## **2.1. Cell lines and culture conditions**

The MCF10A cell line was a generous gift from Prof. Raymond C. Stevens (The Scripps Research Institute, La Jolla, CA), while MCF10AT1 and MCF10CA1a were purchased from ATCC. These cells were grown in DMEM with high glucose and without sodium pyruvate (Invitrogen) containing 5% horse serum (Invitrogen), 20 ng/ml EGF (Sigma-Aldrich), 0.5 µg/ml hydrocortisone (Sigma-Aldrich), 100 ng/ml cholera toxin (Sigma-Aldrich), 10 µg/ml insulin (Sigma-Aldrich) and 100 units/ml penicillin-streptomycin (Invitrogen). Cells were resuspended in high glucose DMEM without sodium pyruvate, containing 20% horse serum and 100 units/ml penicillin-streptomycin (Invitrogen) during passaging. The overlay medium in which the cell suspension was made for seeding (assay medium) contained DMEM without sodium pyruvate, horse serum, hydrocortisone, cholera toxin, insulin, EGF and penicillin-streptomycin. HEK 293T cell line was a generous gift from Dr Jomon Joseph (National Centre for Cell Science, Pune, India). The cells were grown in DMEM with high glucose and sodium pyruvate (Invitrogen) containing 10% foetal bovine serum (Invitrogen), and 100 units/ml penicillin-streptomycin (Invitrogen). Cells were resuspended in the same media for passaging. All cell lines were maintained in 100 mm petri dishes (Corning, Sigma-Aldrich / Nunc, Thermo Fisher Scientific / Eppendorf) at 37°C in a humidified 5% CO<sub>2</sub> incubator (Eppendorf).

## **2.2. Chemicals and antibodies**

Cholera Toxin (C8052), Epidermal Growth Factor (E9644), Hydrocortisone (H0888), Insulin (I1882), Polybrene (H9268), Triton X-100 (T8787), Tris Base (B9754), EDTA (E6758), Na<sub>3</sub>VO<sub>4</sub> (S6508), Protease inhibitor cocktail (P8340) and Poly-L-Lysine (P8920) were purchased from Sigma-Aldrich. Lipofectamine-2000 (11668-500) was purchased from Invitrogen, Thermo Fisher Scientific. Dispase (354235) was purchased from Corning, Sigma-Aldrich. NaF (RM1081) Na<sub>2</sub>HPO<sub>4</sub> (GRM1417), and KH<sub>2</sub>PO<sub>4</sub> (MB050) were purchased from HiMedia. NaCl (15918), Xylene (Q35417), Isopropanol (Q26897), and 30% H<sub>2</sub>O<sub>2</sub> (Q15465) were purchased from Qualigens. 16% paraformaldehyde (AA433689M) was purchased from Alfa Aesar.

Immunofluorescence staining was carried out using Ki67 (Abcam, monoclonal, ab16667), α6-integrin (Merck, monoclonal, MAB1378), Laminin V (Merck, monoclonal, MAB19562), GM130 (Abcam, polyclonal, ab30637), E-cadherin (Abcam, monoclonal, ab1416), Vimentin (Abcam, monoclonal, ab92547), and β-



catenin (Abcam, monoclonal, ab32572). IHC against Api5 was performed using Api5 (Sigma polyclonal, HPA026598). Api5 (Sigma, polyclonal HPA026598 or Abnova, polyclonal, PAB7951), PCNA (Cell signalling, monoclonal, 2586), E-cadherin (BD, monoclonal, 610182), N-cadherin (Abcam, polyclonal, ab18203), GAPDH (Sigma, polyclonal, G9545), Vimentin (Abcam, monoclonal, ab92547), Slug (Cell Signalling, monoclonal, 9585), Twist (Abcam, Polyclonal, ab50581), Fibronectin (BD, monoclonal, 610077),  $\beta$ -catenin (BD, monoclonal, 610153), Cytokeratin 14 (Abcam, monoclonal, ab7800), Cytokeratin 19 (Abcam, monoclonal, ab52625), Bim (Abcam, monoclonal, ab32158), Cleaved Caspase-9 (Abcam, polyclonal, ab2324), pERK 1&2 (Abcam, monoclonal, ab50011), ERK2 (Abcam, monoclonal, ab32081), pMEK1 (Abcam, monoclonal, ab32088), MEK1 (Abcam, monoclonal, ab32091), FGF2 (Millipore, monoclonal, 05-118), pAkt T308 (Cell Signalling, monoclonal, 4056), pAkt S473 (Invitrogen/ Biosource, monoclonal, 44-621G), Akt (Cell Signalling, monoclonal, 9272S), and cMYC (Santacruz, monoclonal, SC-40) were used for the immunoblotting experiments. Peroxidase-conjugated AffiniPure goat anti-mouse (115-035-003) and anti-rabbit(111-035-003), as well as AffiniPure F(ab')<sub>2</sub> fragment goat anti-mouse IgG, F(ab')<sub>2</sub> fragment specific (115-006-006), were obtained from Jackson Immuno Research. Hoechst 33342 (H3570), Hoechst 33258 (H3569), Alexa Fluor® 488 conjugated anti-mouse secondary antibody(A-11029), Alexa Fluor® 488 conjugated anti-rabbit secondary antibody (A-11034), Alexa Fluor® 568 conjugated anti-mouse secondary antibody(A-11004), Alexa Fluor® 568 conjugated anti-rabbit secondary antibody(A-11036), Alexa Fluor® 568 conjugated anti-rat secondary antibody(A-11077), Alexa Fluor® 633 conjugated anti-mouse secondary antibody (A-21052), Alexa Fluor® 633 conjugated anti-rabbit secondary antibody (A-21071), and Alexa Fluor® 568 phalloidin (A-12380) were bought from Invitrogen, Thermo Fisher Scientific.

### **2.3. Plasmids**

CSII-EF-MCS plasmid was a gift from Dr Sourav Banerjee, NBRC, Manesar, India. pCAG-HIVgp and pCMV-VSV-G-RSV-Rev plasmids were purchased from RIKEN BioResource Centre. mVenusC1 was gifted by Jennifer Lippincott-Schwartz, NIH, USA in which Api5 was cloned.

Primers used for Api5 CDS insertion to CSII-EF-MCS vector were: Forward primer: 5'- AAGGAAAAAGCGGCCGCATATGCCGACAGTAGAGGAGCT- 3' and reverse primer: 5'-GCTCTAGATCAGTAGAGTCTTCCCCGAC - 3'.

pMD2.G and pPax2 were generous gift from Dr Manas Kumar Santra, NCCS, Pune, India. pLKO1.EGFP was a generous gift from Dr Sorab Dalal, ACTREC, Mumbai, India.

Primers used for shApi5 insertion to pLKO1 vector were: Forward primer: 5'- CCGGAAGACCTAGAACAGACCTTCACTCGAGTGAAGGTCTGTTCTAGGTCTTTT TTTG - 3' and reverse primer: 5'- AATTCAAAAAAAGACCTAGAACAGACCTTCACTCGAGTGAAGGTCTGTTCTAGG TCTT - 3'.

#### **2.4. In-silico analyses**

The analyses were carried out using gene expression data from various sources. This include GENT2, TCGA and kmplot.

The gene expression data from GENT2 was downloaded by searching for "API5" in the gene symbol search bar in both Gene Profile section and Subtype Profile section. Subtype data as well as normal and tumor tissue expression data were downloaded from the GENT2 website. They were manually sorted and analysed. The plots were drawn using Graphpad Prism (Graph Pad Software, La Jolla, CA, USA). Survival data is downloaded and used as provided by the tool.

TCGA dataset can be accessed using multiple online tools including UCSC Xena browser and cBioportal. We downloaded the data using UCSC Xena browser by selecting the TCGA data (Legacy dataset). Both IlluminaHiSeq and Clinical data were downloaded and merged based on the patient sample ID. Adjacent normal data in breast tissue sample of TCGA can be accessed by sorting the samples with sample ID ending as "11". These data were separated and analysed using Graph Pad prism (Graph Pad Software, La Jolla, CA, USA).

Kaplan-Meier Plotter was used for studying the patient survival data. In the online tool, API5 was searched as a gene symbol. "201687\_s at" dataset, which is also the best probe set, was selected for the studies. Relapse Free Survival plot was generated by using median as cut off and without any further categorisations.

Mutation data were analysed using the TCGAportal online tool. TCGA BRCA was selected as a dataset, and Api5 was given as a gene symbol. The graph is presented as provided by the online tool.

For DAVID pathway analyses, the data were sorted as mentioned in the results. The gene set were submitted a single set of Query genes and *Homo Sapiens* were selected as the organism. Identifier was selected as Official Gene Symbol. Further the gene list was submitted and then Functional Annotation Tool results were selected.

### **2.5. Stable cell line preparation**

HEK293T cells are passaged and seeded at transduction.  $5 \times 10^5$  cells per well in a 6 well plate. Post 16 hours the cells are transfected with  $1 \mu\text{g}$  CSII-EF MCS mCherry Api5 vector having a mCherry-Api5 sequence, along with  $0.5 \mu\text{g}$  pCMV-VSV-G-RSV-Rev and  $1 \mu\text{g}$  pCAG-HIVgp.  $10 \mu\text{l}$  Lipofectamine 2000 and  $240 \mu\text{l}$  Opti-MEM were mixed (Solution A) and allowed to stand at RT for 5 minutes. In the meantime, Opti-MEM and the plasmids were mixed to make a total volume of  $250 \mu\text{l}$  (Solution B). The Solution A and B were mixed and incubated at RT for 20 minutes. During this incubation, cells were preconditioned with Opti-MEM. Post 20 minutes, the mixture is added to the cells and another  $500 \mu\text{l}$  of Opti-MEM was added on top. 24 hours post transfection, DMEM containing 15% horse serum was added to the cells. 48 hours post transfection, the viral particles were collected and filtered through a  $0.45 \mu\text{m}$  filter to remove cell debris.

For transduction, MCF10A cells were plated at  $5 \times 10^5$  cells per well density in a 35mm dish. After 16 hours, the viral particles collected were added on top of the cells, along with  $4 \mu\text{g}$  polybrene. 48 hours post transduction, cells were replenished with fresh media. The transduced cells were sorted using BD FACS Aria (BD Biosciences) to get a pure population with maximum number of transduced cells.

Api5 KD stable cells were generated in MCF10AT1 and MCF10CA1a in a similar manner. The shRNA was cloned in pLKO.1-EGFP vector, and packaging plasmids pMD2.G and pPax2 were used for lentiviral preparation. Cells were then sorted in BD FACS Aria with the aid of the GFP signal.

### **2.6. 3D 'on-top' culture**

3D breast acinar cultures were set up in an 8-well chamber cover glass plates (Nunc Lab-Tek, Thermo Fisher Scientific) or 12-well plates (Eppendorf) using established protocols (Anandi et al., 2017; Anandi et al., 2016; Debnath et al., 2003a). In an 8 well chamber, each well was coated with 55 $\mu$ l growth factor reduced laminin rich extra cellular matrix or Matrigel, and it was allowed to gel at 37°C for 15 minutes. Further the required number of cells were seeded on top with 5ng/mL EGF and Matrigel (2% for MCF10A and 5% for MCF10AT1 and MCF10CA1a). Usually for IF studies, MCF10A cells were seeded at a density of 8 X 10<sup>3</sup> cells/ well. MCF10AT1 and MCF10CA1a cells were seeded at 5 X 10<sup>3</sup> cells/well and 3 X 10<sup>3</sup> cells/well respectively. Cultures were grown in a humidified incubator with 5% CO<sub>2</sub> and maintained at 37°C (Eppendorf). The medium was changed every four days. For lysate collection on different days, higher cell density was seeded for Day 4 and Day 8 at 1 X 10<sup>4</sup> cells/well. MCF10AT1 and MCF10CA1a spheroid cultures were grown for 7 days before collecting for IF or western blotting studies.

For dissociation of acinar culture, Dispase™ (Corning, Sigma-Aldrich) was used. For a 12 well dish 400 $\mu$ l of Dispase was added and after the addition of Dispase™, the culture was incubated for 20 minutes. The dislodged acini were spun down at 900 rpm for 10 minutes, followed by 2 rounds of 1X PBS wash before plating in 12-well petri plates.

### **2.7. Immunofluorescence staining**

3D spheroid cultures were immune-stained with specific antibodies by established protocols (Anandi et al., 2017). After the 16/ 7 days of culture, the cultures were fixed using freshly prepared 4% Paraformaldehyde (in 1X PBS). A 15-minute pre-treatment with PBS-EDTA was done at 4°C when the staining is performed against GM130. After 20 minutes incubation at RT, PFA is removed and washed once with 1X PBS. Further permeabilization was carried out using 0.5% Triton X-100 for 10 minutes at 4°C. With disturbing the Matrigel base, remove the Triton and add glycine containing PBS. Washes of 1X PBS containing glycine were carried out for 2 times at RT for 10 minutes each, followed by 10 minutes wash with 1X PBS. Primary blocking was carried out using 10% (v/v) goat serum prepared in 1X IF buffer for 1 hour at RT. Further secondary blocking with 10% goat serum containing 1% F(ab')<sub>2</sub> fragment goat anti-mouse IgG was carried out for 1 hour. Primary antibody staining

was done using antibody prepared in 10% goat serum at 1:100 dilution. For staining chamber were incubated overnight at 4°C. The next day the chamber is kept at RT for 20 minutes before three washes with 1X IF buffer. Each of the washes are for 20 minutes each at RT. Further secondary antibody prepared at 1:200 dilution (1:100 phalloidin is used when required) in 1X IF containing 10% goat serum. The chambers were incubated at RT for 1 hour (2 hours for MCF10AT1 and MCF10CA1a cells). Following the incubation one wash with 1X IF buffer and 2 washes with 1X PBS were carried out. The nuclei were then counterstained using Hoechst 33258 (0.5µg/ml in 1X PBS) for 10 minutes at RT. After washing with 1X PBS to remove excess stain, the chambers were mounted with SlowFade Gold Antifade solution. For MCF10CA1a and MCF10AT1 spheroid staining, the 1X PBS and 1X IF buffer washes were added with 0.5% Triton X to aid for better penetration of antibodies. Also, for Phospho ERM staining, phosphatase inhibitors 1 mM sodium orthovanadate and 1.5 mM sodium fluoride were added in all steps till primary antibody.

In case of 2D IF, instead of Goat serum, 10% FBS was used and there was no secondary blocking step involved. Also secondary antibody concentration were 1:500. Images were captured using Leica SP8 or Zeiss LSM 710 laser scanning confocal microscope.

## **2.8. Immunoblotting**

Lysates from 2D or 3D cultures were collected in lysis buffer containing 50 mM Tris-HCl, pH 7.4, 0.1% Triton X-100, 5 mM EDTA, 250 mM NaCl, 50 mM NaF, 0.1 mM Na<sub>3</sub>VO<sub>4</sub> and protease inhibitors. Lysates were resolved in required percentage of SDS gel and transferred to PVDF membrane (Millipore). Blocking was performed using 5% skimmed milk (non-fat milk powder) for non phospho proteins. For phosphorylation, 4% BlockAce prepared in 1X TBST were used as a blocking solution. Blocking step can be at RT for 1 hour or 16 hours at 4°C. Following blocking blots were probed with primary antibody for standardised time at RT or 4°C. Following 3 washes with 1X TBST, blots were incubated with secondary antibody conjugated with HRP at 1:10000 dilution prepared in 5% skimmed milk for 1 hour. Blots were then developed after washes with 1X TBST using Immobilon substrate. Blots were then imaged using LAS4000 or Thermo iBright imaging systems. The blot images represented shows all the bands that were captured using the imaging

system. None of the images have been cropped. The entire blots were cut as per experimental requirement and probed for different antibodies.

### **2.9. Gelatin Zymography**

Conditioned media from 3D cultures were collected and stored at  $-80^{\circ}\text{C}$ . On the day of the experiment the media was thawed on ice. Further it was mixed in non-denaturing 6X sample buffer ( $87\mu\text{l}$  with  $13\mu\text{l}$  of media).  $10\mu\text{l}$  from this was loaded on SDS gel containing 0.1% gelatin. Unstained ladder was used for molecular weight comparison. Gel was run at 125volt at  $4^{\circ}\text{C}$  till the dye front runs out. The gel was further incubated in renaturing buffer (2.5 % v/v of Triton X-100 in water) for 30 minutes and this step was repeated. This was followed by washing with water and then incubation in developing buffer (0.5 M Tris-HCl pH-7.8, 2M NaCl, 0.05M  $\text{CaCl}_2$  and 0.2% Brij35) for 30 minutes at RT with gentle shaking. Developing buffer was changed and then the gel was incubated at  $37^{\circ}\text{C}$  for 24 hours. This was again replenished and incubated for 24 hours. The gel was stained in Coomassie blue staining solution (0.1% w/v Coomassie blue (Sigma-Aldrich), 50% v/v Methanol (FisherScientific), 10% v/v Acetic acid (Fisher Scientific and 40% v/v distilled water). The gels were destained using destaining solution (mixture of 50% v/v Methanol, 10% v/v acetic acid and 40% v/v distilled water) to visualize the cleared regions of gelatin against a dark blue background. The gel was then imaged in iBright imaging system.

### **2.10. DQ Collagen assay**

Dissociated cells were seeded on a 24 well plate supplied with required media. MCF10A cells were seeded at  $12 \times 10^3$  cells per well, while MCF10AT1 at  $8 \times 10^3$  cells per well and MCF10AT1 at  $6 \times 10^3$  cells per well. The wells were coated with 1.6mg/ml rat tail Collagen type 1 (neutralized with NaOH) containing  $25\mu\text{g/ml}$  of DQ collagen type 1 (Invitrogen). Post 16 hours of seeding (10 hours for MCF10CA1a), the cells were imaged using Leica SP8 microscope. The nuclei of the cells were stained with Hoechst 33342 for 10 minutes at  $37^{\circ}\text{C}$ . 10 images per well were acquired and at least 100 cells were quantified for fluorescence intensity per cell. Corrected Total Cell Fluorescence (CTCF) were calculated.

### **2.11. Single Cell Migration**

MCF10A cells were seeded at  $8 \times 10^3$  cells per well, while MCF10AT1 at  $5 \times 10^3$  cells per well and MCF10CA1a at  $2.5 \times 10^3$  cells per well in a 48 well dish or 8 well chamber. After 16 hours of incubation in 37°C incubator supplied with 5% CO<sub>2</sub> for MCF10A and MCF10AT1 cells while 10 hours for MCF10CA1a, the cells were stained with Hoechst 33342 (Invitrogen). Media was changed to L15 with growth constituents in order to shift to incubators that do not have CO<sub>2</sub> supply. Cells were then imaged using 20X objective in Leica SP8 confocal microscope or EVOS microscope. Images were taken at every 2 minutes from 10 positions in each well for 3 hours. The data was processed using FastTracks software (DuChez, 2017) and plotted using Graph Pad Prism (Graph Pad Software, La Jolla, CA, USA).

### **2.12 Soft Agar Assay**

1.2% and 0.6% agar were prepared in MilliQ water and sterilised by autoclaving. 2X DMEM was prepared from powder (HiMedia) using Nuclease Free Water. The DMEM were supplemented with 3.7g/L sodium bicarbonate.

Base agar was prepared by dissolving 1.6% agar (pre warmed at 40°C) and 2X DMEM (with 2X GC) mixed in a 1:1 ratio. As soon as it is mixed 1.5ml is added to a well in a 6-well dish. The top layer is made similarly using 0.6% agar, although the 2X DMEM is added with required number of cells before mixing with agar. MCF10A were seeded at  $1.25 \times 10^5$  cells /well, while MCF10AT1 and MCF10CA1a cells were seeded at  $0.8 \times 10^5$  cells /well. 3 hours post seeding 0.75ml of DMEM (with GC) were added on top of the culture. MCF10A were maintained for 21 days with media change on every 3<sup>rd</sup> day, while MCF10AT1 and MCF10CA1a were maintained for 7 days. The cultures were then stained with 0.5mg/ml solution of MTT. After MTT addition cultures were incubated for 1 hour. Images were acquired using the 10X objective of a Nikon phase-contrast microscope. Ten randomly selected fields were imaged, and the colonies were manually counted.

### **2.13 Clonogenicity assay**

Clonogenicity assay was performed by sparsely seeding cells in 6-well plates (Corning) with three replicates for each set. After 7 days of incubation, cells were stained with crystal violet (HiMedia) after fixing with Methanol (4°C for 15 minutes)

and images were captured using HP Scanner after drying the plates. The colonies were manually counted for quantification.

#### **2.14 *In-vivo* tumorigenicity assay**

Dissociated cells cultured and  $6 \times 10^6$  cells were collected, it was mixed with 1:1 diluted Matrigel<sup>®</sup> PBS mixture. The cells were carried to animal house in ice. They were injected to the flanks of athymic mice (Foxnl<sup>nu</sup> / Foxnl<sup>nu</sup>, 6-8 weeks old) using insulin syringes. Mice were kept in controlled environment and monitored for 12 weeks. Tumour size was measured with a vernier calliper. After 12 weeks, mice were sacrificed, and the tumour was dissected out. For MCF10CA1a,  $4 \times 10^6$  cells were injected to the flanks. Tumour area was calculated by multiplying the major and minor axis of the tumour as measured with a vernier calliper

The tumour was then fixed with 10% formaldehyde for 48-72 hours at RT. Further the tissue was processed to dehydration steps by incubating in increasing concentration of iso-propanol. This is carried out from 70% to 100%. Further the tissues were incubated in xylene for 30 minutes, which was replenished once for another 30 minutes. Later the tissues were put in warmed paraffin wax (in liquid state), in which it was incubated for 30 minutes before pouring on to a 60mm dish coated with Vaseline.

#### **2.15 Immunohistochemistry**

Formalin-fixed and paraffin-embedded breast cancer patient samples were collected from Prashanti Cancer Care Mission, Pune. The samples from each patient may contain tumour area, adjacent normal tissue, lymph nodes, and the reduction mammoplasty tissue. Frosted slides were coated with poly-L-Lysine (Sigma). Tissue samples were sectioned using Leica Microtome at 3  $\mu$ m thickness. To deparaffinise the tissue sections, the slides were kept at 62°C for at least 18 hours. Further the slides were washed in Xylene(Fisher scientific) for 15 minutes which was replenished once. The tissues were then rehydrated with decreasing concentration of iso-propanol, and then washing once with dH<sub>2</sub>O. Endogenous peroxidase were blocked by incubating the tissue sample in 3% H<sub>2</sub>O<sub>2</sub> (made from 30% H<sub>2</sub>O<sub>2</sub>, Fisher scientific, by diluting with methanol). Antigen retrieval was carried out using 0.001M EDTA buffer (pH 7.4). Microwave based method was used for antigen retrieval which involves keep the tissues at 800W for 2 minutes, 2-minute cooling at RT, heating



tissue in buffer at 480W for 5 minutes followed by 2 minutes cooling at RT, 2-minute heating at 480W and cooling again at RT for 2 minutes. Finally, the tissues immersed in the buffer were heated for 4 cycles of 2-minute heating at 160W and 2-minute cooling at RT. Post final heating the tissue with the buffer is left at RT for 20 minutes. The tissues were then treated with 3% BSA for blocking nonspecific antibody binding. The tissue samples were then incubated in Api5 antibody prepared in Antibody Diluent (Dako) at 1:2000 dilution. Antibody was incubated for 2 hours at RT. After the incubation, the tissue samples were washed with 1X TBST for 5 minutes. Following which, the tissues were incubated with HRP conjugated secondary antibody (Dako) for 30 minutes at RT. After removing the excess antibody binding with 2 washes of 1X TBST for 5 minutes each, the staining was developed using DAB (Dako). Nuclei are counterstained with 10% haematoxylin prepared in distilled water. After drying the slides were mounted with DPX mountant (Fisher Scientific). Images were acquired in EVOS microscope at 20X objective. For scoring, the slides were observed under a compound microscope at 20X objective. 10 positions in each slides are scored and median value is reported by each person. The score based on staining intensity and percentage positivity ranges from 0 to 3, and the maximum H score is 9. The score distribution is mentioned below.

<b>Percentage positivity</b>	<b>Score</b>	<b>Intensity</b>	<b>Score</b>
0%	0	No staining	0
>0 to 30%	1	Weak	1
>20 to 70%	2	Moderate	2
>70 to 100%	3	Strong	3

Three individuals calculated the scores independently by observing ten different positions on the slide corresponding to the tissue ID. The median value from this observation was plotted on the graph.

H-score for IHC is calculated as follows:

H-Score = Intensity score X Percentage positivity score

## **2.16 Statistical analysis**

Different morphometric parameters were tested for significance using the Mann-Whitney test. Significance test for the *in-silico* data was performed using either Mann-Whitney or Kruskal- Wallis test. The Mann–Whitney U-test was used to analyse the statistical significance of relative Golgi area changes and relative fluorescence intensity in the 3D culture immunostaining. The different parameters for analysing cell migration were tested for significance using the Mann-Whitney test. Statistical analysis for mice tumour area was performed using the 2-way ANOVA followed by Sidak's multiple comparison test.  $P < 0.05$  was considered statistically significant. Graph Pad Prism software (Graph Pad Software, La Jolla, CA, USA) was used to analyse data.

## **2.17 Ethics approvals**

Ethics approval from Institutional Human Ethics Committee (IHEC) was obtained for using patient paraffin embedded tissue blocks in this study (IHEC/Admin/2021/012). Written informed consent was obtained by Prashanti Cancer Care Mission, Pune from all patients, and the study was conducted in accordance with the Declaration of Helsinki, institutional guidelines, and all local, state and national regulations. For preparing Api5 OE MCF10A cells, Api5 KD MCF10AT1 and Api5 KD MCF10CA1a cells Institutional Biosafety Committee (IBSC) clearance was approved by the institute. The *in vivo* tumorigenicity studies were approved by the Institutional Animal Ethics Committee (IAEC) (IAEC/2018\_02/010 and IISER\_Pune/IAEC/2021\_01/06).

## **Chapter 3: Altered Api5 expression affects breast carcinogenesis**

### 3.1 Background

Api5 is an anti-apoptotic protein which was initially discovered as a cDNA that can help in survival of cells during serum deprivation. Api5 is established as a significant regulator of Cell cycle, DNA-damage response and Apoptosis (Garcia-Jove Navarro et al., 2013; Sharma and Lahiri, 2021). Studies were also identified possible involvement of Api5 in malignancies (Basset et al., 2017; Cho et al., 2014; Jang et al., 2017).

Api5, which is known to be upregulated in various cancer and a biomarker for Lung cancer and bladder cancer, could be playing a significant role in breast cancer. In 2005, Jansen et al. showed that Api5 expression is increased in Tamoxifen, a drug that binds to the estrogen receptor, resistant breast carcinomas (Jansen et al., 2005). Also, another study showed that Tocotrienol treatment in breast cancer cell line MCF7 showed a reduction in Api5 levels where Tocotrienol is a Vitamin E family member with several anticancer effects (Ramdas et al., 2011).

Furthermore, Basset *et al.* demonstrated the possible role of Api5 in ER+ breast cancer by its interaction with estrogen receptor alpha (ER $\alpha$ ) using the LxxLL motif. (Basset et al., 2017). Also, they showed that Api5 knockdown could reduce *in vivo* tumorigenicity of breast cancer cell line.

Further, in 2019, Bousquet *et al.* identified that Api5 is highly expressed in chemo resistant triple-negative breast cancers using PDX model-based studies. They have also found that using an anti-Api5 peptide, Api5 inhibition can trigger apoptosis in these cancer cells.

These data suggest that Api5 could be playing a significant role in breast cancer. A recent study in our lab showed that chemical damage induced transformation of non-tumorigenic breast epithelial cells resulted in upregulation of Api5. In this study, MNU, a DNA methylating agent, was used as a DNA damaging agent, and the cells were grown in 3D cultures where they formed acinar structures. Compared to untreated, the treated acini showed phenotypic changes that suggest transformation (Anandi et al., 2017). The increase in levels of Api5 observed during transformation indicate the possibility of Api5 playing a role in the same. Based on these data, we will be investigating the role of Api5 in breast cancer and the possibility of Api5 to be used as a biomarker for breast cancer detection.

For the studies on Api5, we will be using 3D acinar cultures of MCF10A cells overexpressing Api5. Acinar cultures provide a reliable model for analysing the transformation potential of oncogene. They are widely used for identifying and characterising various malignancy associated properties (Anandi et al., 2017; Anandi et al., 2016; Qu et al., 2015). Oncogene induced transformation of MCF10A cells can lead to altered morphology, polarity disruption, EMT characteristics and higher migratory potential (Anandi et al., 2017; Besette et al., 2015; Debnath et al., 2003a; Debnath et al., 2003b).

Using stable overexpression of Api5 in MCF10A, we could identify that Api5 can initiate transformation in breast epithelial cells. We found that Api5 OE resulted in morphological as well as characteristic changes in MCF10A acinar cultures.

## **3.2 Results**

### **3.2.1 Preparation of Api5 OE MCF10A, Api5 KD MCF10AT1 and Api5 KD MCF10CA1a stable cells**

To understand the role of Api5 in breast carcinogenesis, we decided to overexpress Api5 in MCF10A, a non-tumorigenic breast epithelial cell line. Along with the overexpression, we also decided to knock down Api5 in MCF10AT1 and MCF10CA1a, which are isogenic cancer cell lines derived from MCF10A. MCF10AT1 is a premalignant cell line, while MCF10CA1a is a malignant cell line.

For overexpression, we used lentiviral-mediated transduction. Transfection of the plasmids was done in HEK293T to prepare viral particles containing Api5 gene tagged to mCherry fluorescent protein in CSII EF MCS vector. These viruses were transduced to MCF10A. The transduced cells are further sorted based on fluorescence. MCF10A overexpressing only mCherry is kept as control cells (Fig 3.1).

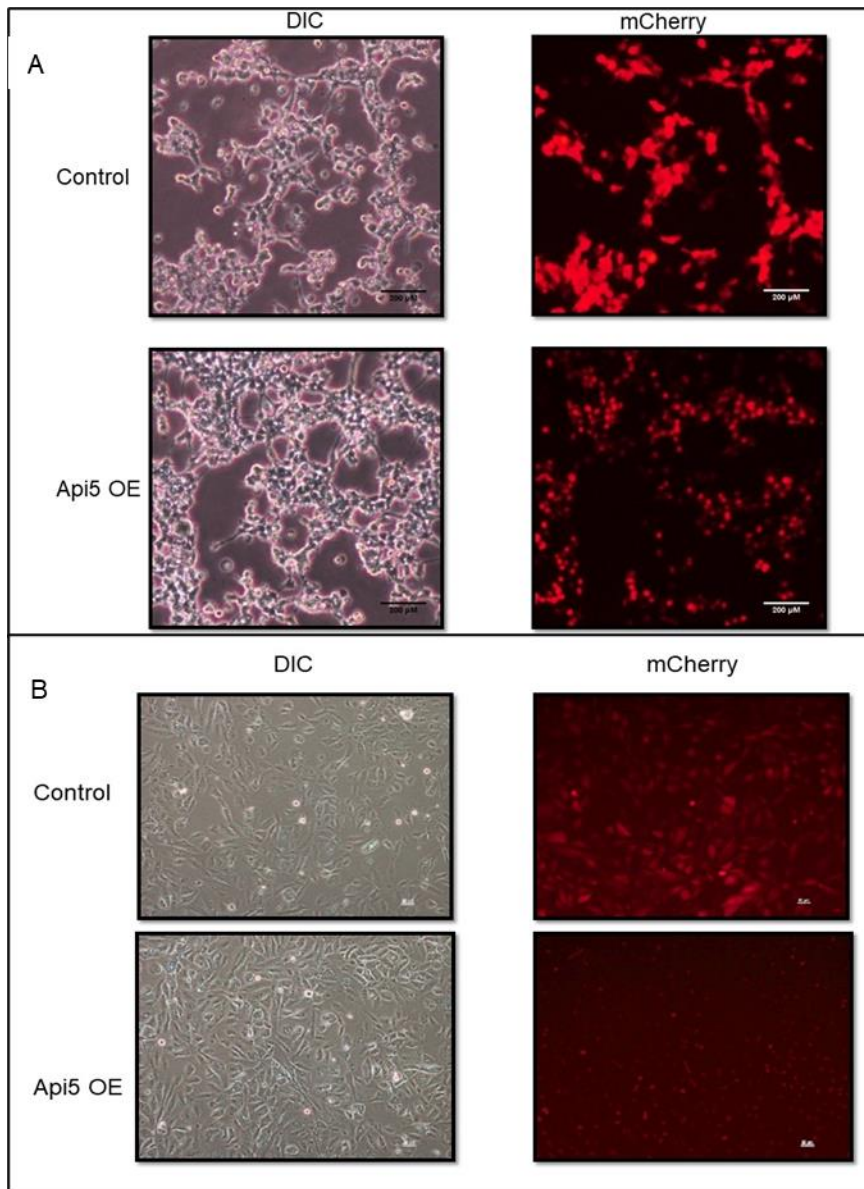


**Fig 3.1** Api5 OE stable cell line preparation.

Representative image showing mCherry fluorescence checked a) 21 hours post-transfection into HEK293T b) 28 hours after Transduction to MCF10A.

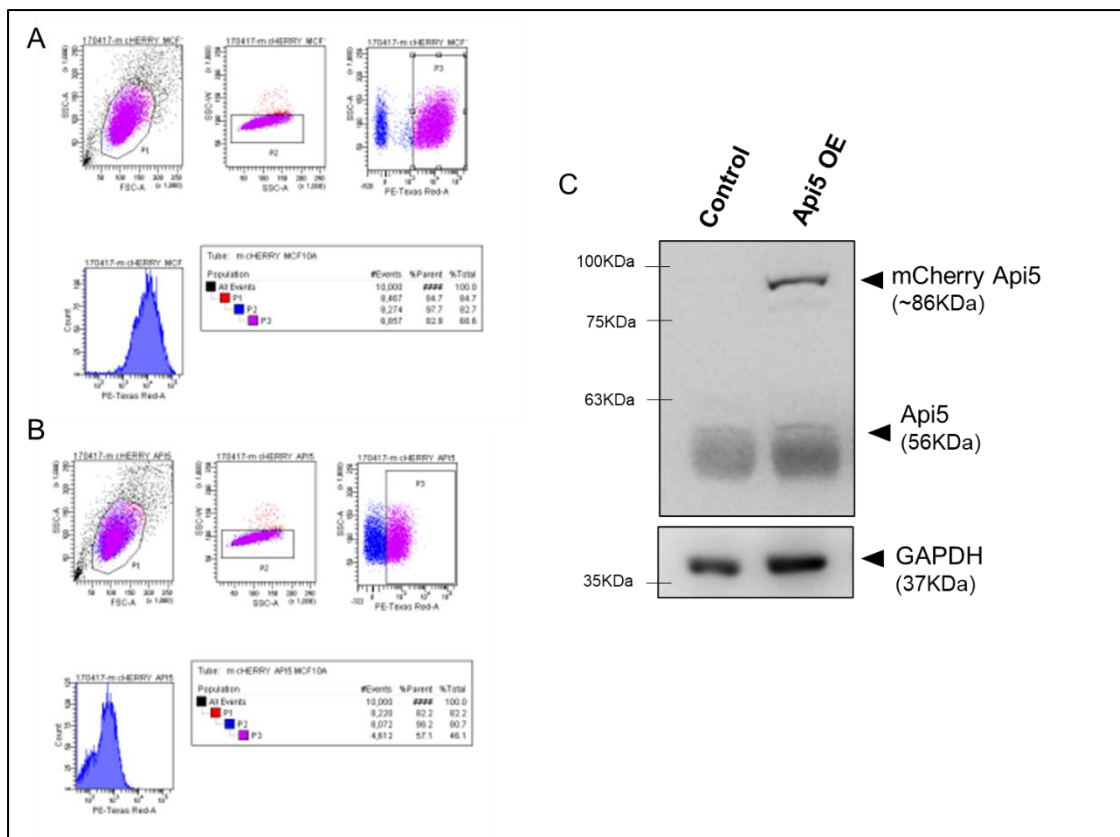


**Fig 3.2** FACS sorting of Api5 OE cells

a & b) Sorting of Api5 overexpressing MCF10A and the control cells using the mCherry fluorescence. c) Api5 overexpression was confirmed with immunoblot analysis. Api5 overexpressing MCF10A lysates collected after 16-day culture on Matrigel<sup>®</sup> probed against Api5.

Further for confirming the overexpression, lysates of Api5 overexpressing and control cells after 16-day culture on Matrigel<sup>®</sup> were collected. These lysates were used for immunoblotting analyses and probed against Api5. Overexpression of Api5 was observed as a separate band because of the increase in molecular weight. The approximate 28KDa shift is due to the presence of the mCherry tag along with Api5 (Fig 3.2).

Similarly, MCF10AT1 and MCF10CA1a cells with stable knockdown of Api5 were generated using lentiviral mediated transduction. pLKO1.eGFP plasmid carrying shApi5 was used for transfection in HEK293T, and the prepared viral particles were



used for transduction in the required cells. The vector backbone had eGFP, which was thus used as a selection marker during FACS sorting (Fig 3.3).

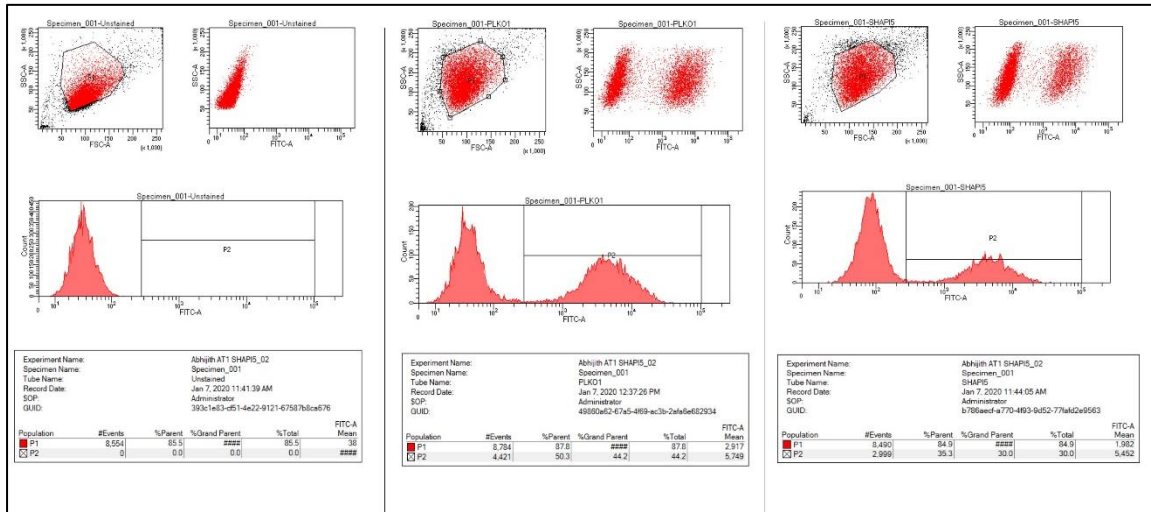


**Fig 3.3** Sorting parameters for selecting Api5 KD MCF10AAT1 and Api5 KD MCF10CA1a cells

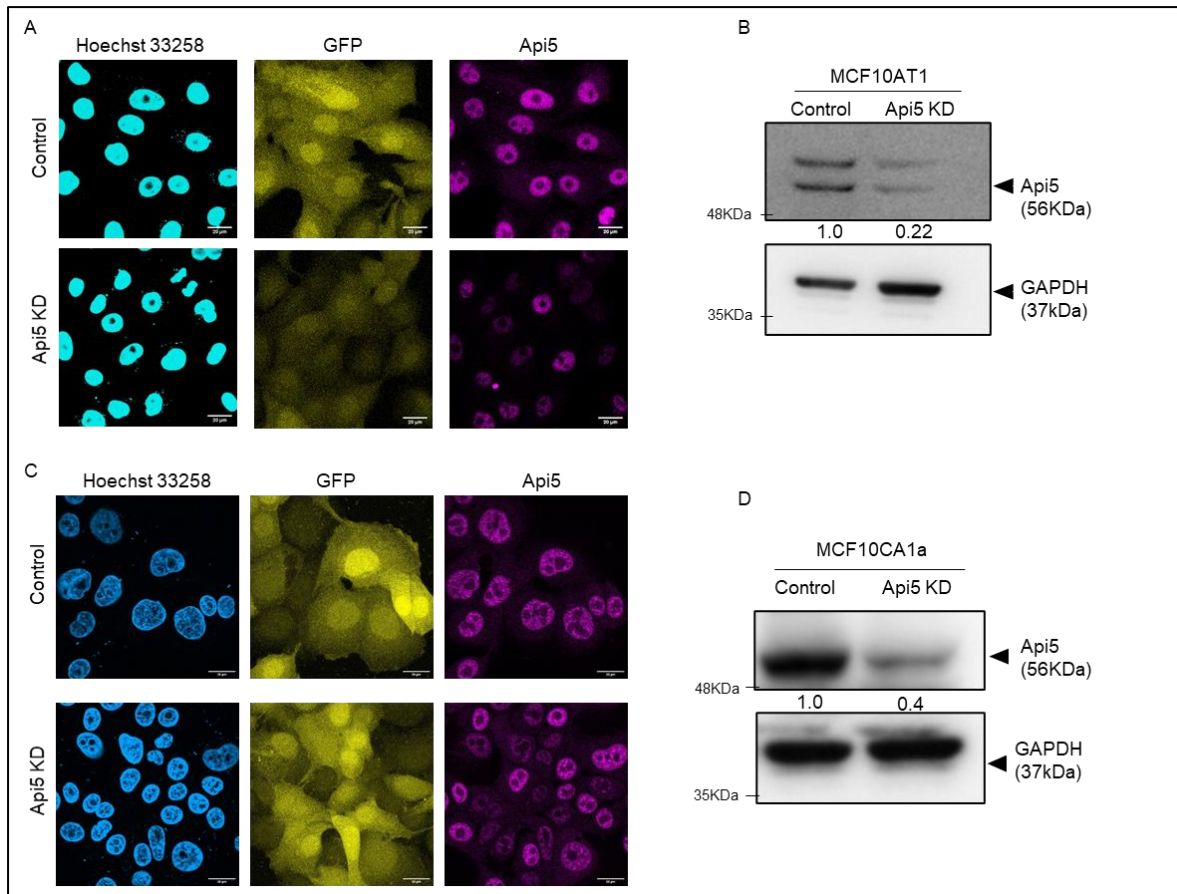


**Fig 3.4** MCF10AT1 and MCF10CA1a cells with Api5 knockdown were prepared and sorted using FACS.

Representative image of immunostaining and immunoblot against Api5 showing Api5 knockdown in MCF10AT1 (A and B) and MCF10CA1a (C & D).

The knockdown was further confirmed using both immunofluorescence and immunoblot assays (Fig 3.4). In the immunoblot, a minimum of 70% reduction in Api5 was observed in sorted MCF10AT1 cells while MCF10CA1a Api5 KD stable cells had around 60% reduction in Api5 expression.

### 3.2.2 Api5 overexpression resulted in altered morphology of MCF10A acinar cultures.

To understand the phenotypic changes, we cultured the MCF10A cells overexpressing mCherry Api5 in Matrigel® bed. This helps the 3D growth of MCF10A cells to form acinar structures which resemble the breast acini in human females. Cells were seeded as a single cell suspension in the Matrigel® bed and then grew into acinar structures for 16 days. By the 16<sup>th</sup> day, they form growth-arrested, hollow

lumen, breast acinar structures. The control mCherry MCF10A cells formed acinar structures that resemble the human mammary gland, while Api5 OE MCF10A had an altered morphology (Fig 3.5).

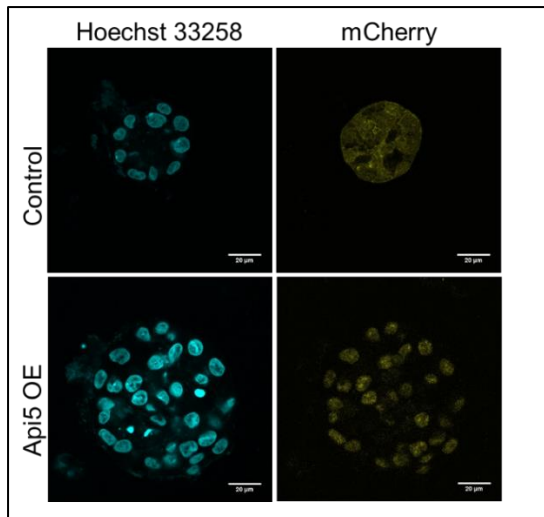


**Fig 3.5** Api5 OE results in altered MCF10A acinar morphology.

Representative image showing acinar structure formed by control and Api5 OE MCF10A cells after 16 days of culture on Matrigel. The nuclei are stained with Hoechst 33258.

For understanding the effect of Api5 overexpression, the morphological characteristics of the acini were analysed and compared to the acini formed by the control cells, MCF10A overexpressing only mCherry. Acinar size and volume are calculated and compared. Also, the nuclear size and volume were analysed to identify whether they are affected by Api5 overexpression. All the analyses were done using Huygens essentials and plotted using GraphPad Prism.

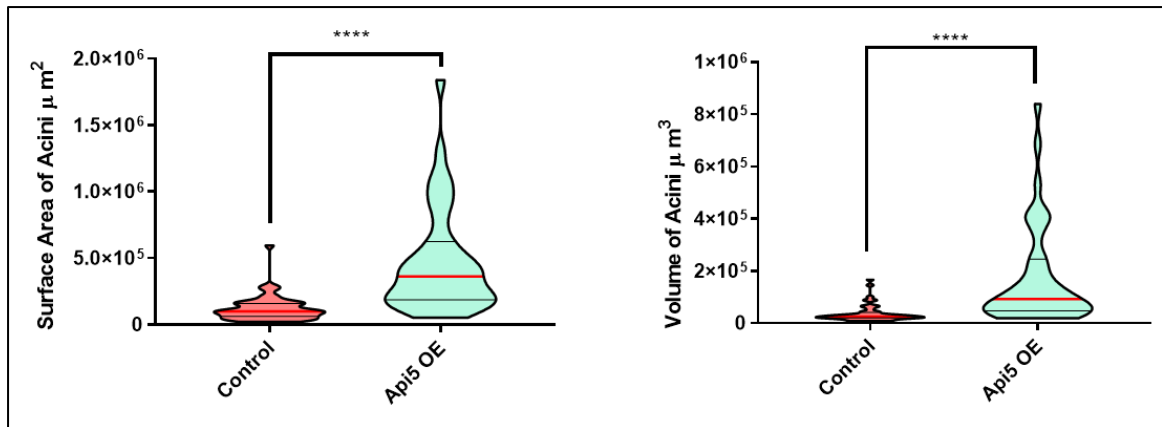


**Fig 3.6** Api5 OE results in altered size of MCF10A acini.

MCF10A overexpressing Api5 after grown in Matrigel® shows increased surface area and volume of acini. (N=4, n=50), Mann-Whitney test \*P<0.05, \*\*P<0.01, \*\*\*P<0.001 and \*\*\*\*P<0.0001

Api5 overexpression resulted in increased acinar volume and surface area, suggesting the possible transformation of the epithelial cell line (Fig 3.6). As a previous study in our lab observed a difference in nuclear size associated with the transformation of the cells, the nuclear volume and surface area between the Api5 overexpressing and control cells were compared.

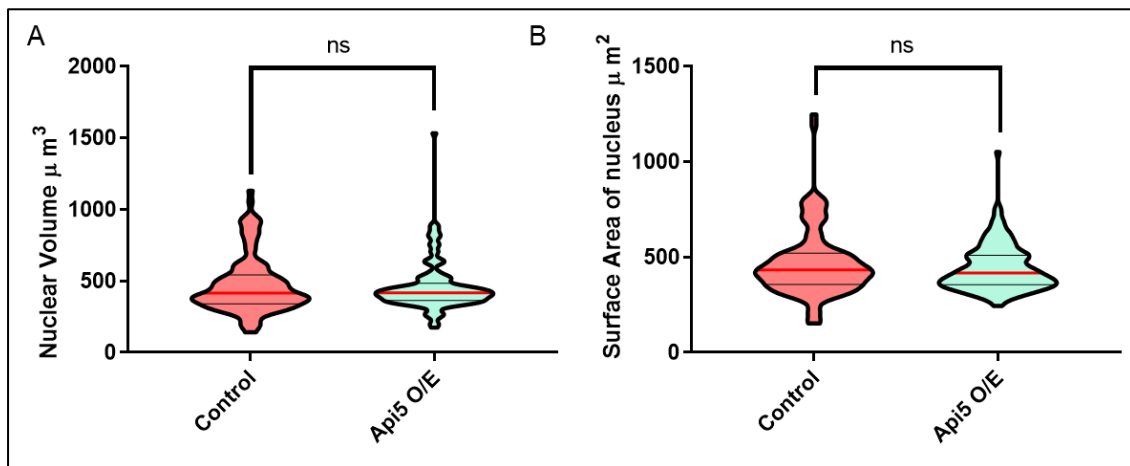


**Fig 3.7** Api5 OE did not alter nuclear size.

Api5 overexpression does not affect the a) volume and b) nuclear surface area of MCF10A cells grown in 3D culture (in Matrigel®) (N=2, n=110)

The data showed no significant difference in nuclear volume or surface area after Api5 overexpression compared to the control (Fig 3.7).

The increase in acinar size can be due to higher proliferation during acinar morphogenesis. To investigate this aspect, cell number per acini was calculated and compared to understand if Api5 overexpression altered cell number. Comparing the control with Api5 OE acini showed that overexpression significantly increased the number of cells per acini (Fig 3.8).

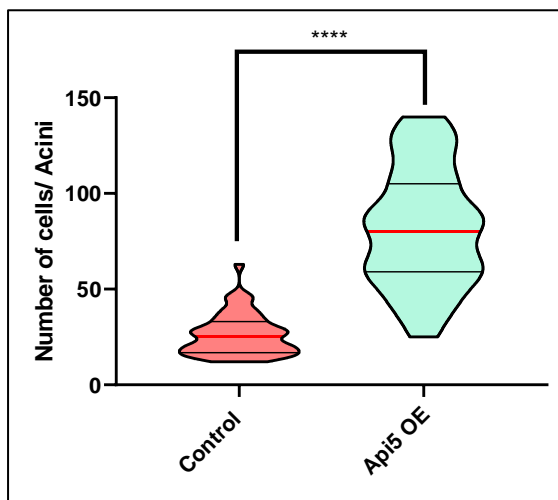


**Fig 3.8** Api5 overexpression leads to the increased number of cells per acini.

Violin plot showing number of cells per acini in Api5 OE MCF10A acinar cultures grown on Matrigel® (N=4, n=50) Mann-Whitney test \*P<0.05, \*\*P<0.01, \*\*\*P<0.001 and \*\*\*\*P<0.0001

Transformation of MCF10A cells is reported to lead to protrusion like structures from their 3D cultures (Debnath et al., 2003a). To investigate whether such a phenotype is initialised due to Api5 OE, phalloidin staining was carried out on the 16-day acinar cultures. The images were then analysed to identify if there are any protrusion like structures emanating from the acini.

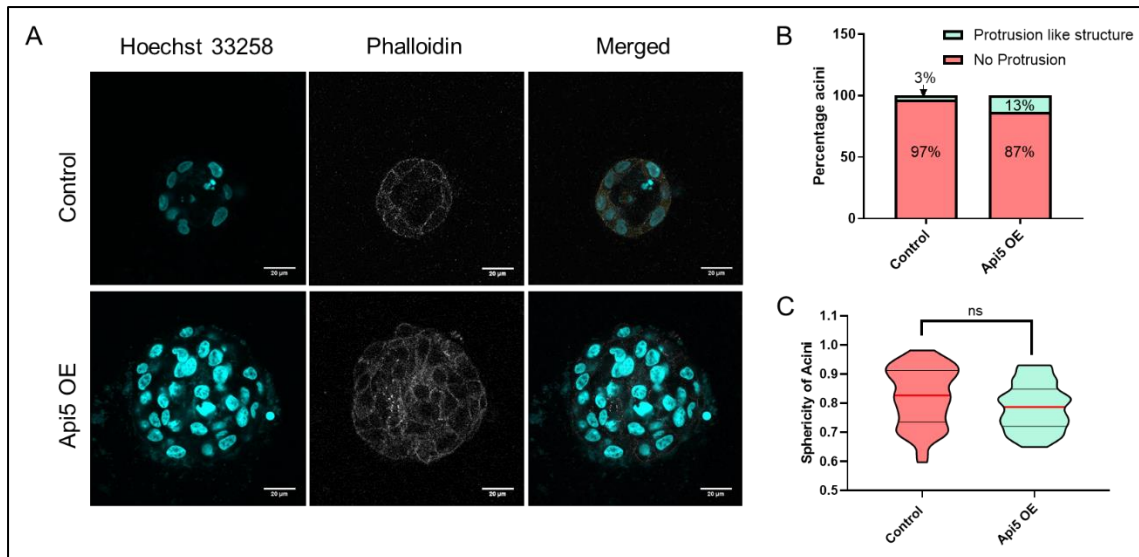


**Fig 3.9** MCF10A cells overexpressing Api5 does not form acini with protrusions  
a) Phalloidin staining showing the structure of acini formed by control and Api5 overexpressing cells. b) Quantification showing the percentage of acini having protrusion like structures. (c) Violin plot showing the sphericity of the acini formed by control and Api5 OE MCF10A cells. (N=3, n=33), Mann-Whitney test \*P<0.05, \*\*P<0.01, \*\*\*P<0.001 and \*\*\*\*P<0.0001

The results show that Api5 overexpression does not disrupt the spherical structure of the acini and does not lead to the formation of any protrusion like structures (Fig 3.9).

We also checked for cells in the lumen, which usually undergo apoptosis from the 8<sup>th</sup> day to the 16<sup>th</sup> day. The presence of cells in the lumen along with protrusion like structures suggests a transformed phenotype.

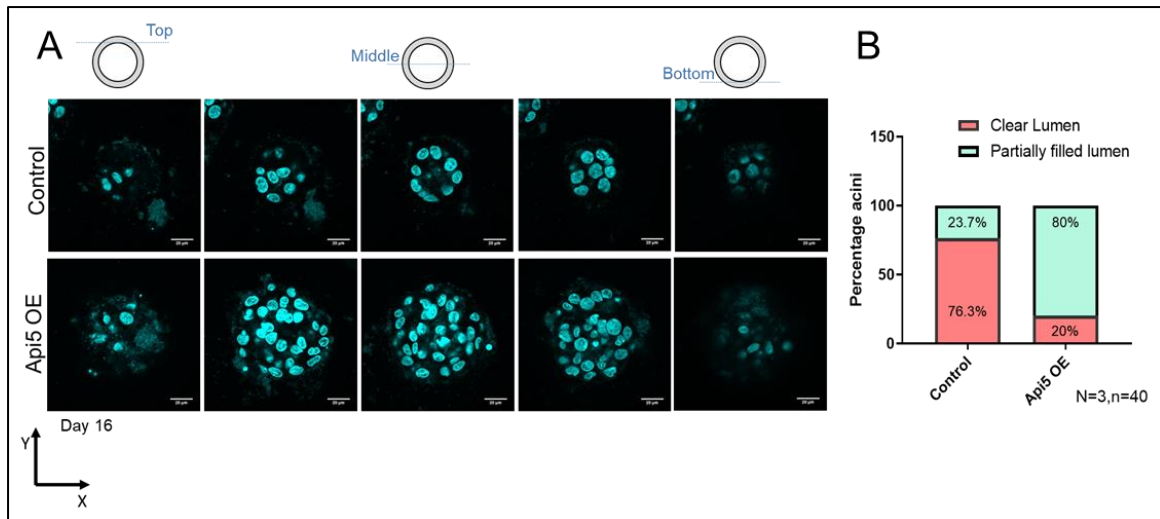


**Fig 3.10** Ap5 OE resulted in lumen filling of 16-day MCF10A acinar cultures  
a) Images of the acini from different stacks in order from top to bottom. b)  
Quantification of the percentage of acini showing filled lumen (N=3, n=40).

The results show that Ap5 overexpression has led to a wholly or partially filled lumen phenotype (Fig 3.10). The results from analysing the morphology of Ap5 OE MCF10A cells confirmed that the cells show transformed phenotypes. This indicates that Ap5 could be functioning as an oncogene and thus can be involved in promoting breast carcinogenesis.

### 3.2.3 Ap5 knockdown in MCF10AT1 and MCF10CA1a cells affects their growth in spheroid cultures

Ap5 overexpression studies showed that acinar morphology was altered and resulted in the transformation of the breast epithelial cell line. These studies concluded that Ap5 overexpression alone could trigger tumorigenic changes in the epithelial cell line. To further analyse whether Ap5 is essential for breast cancer cells, we decided to study the effect of Ap5 knockdown (KD) on spheroid cultures of MCF10AT1 and MCF10CA1a cells.

MCF10AT1 and MCF10CA1a with Ap5 KD were cultured on Matrigel. The spheroids formed by MCF10AT1 and MCF10CA1a with Ap5 KD show reduced volume and surface area than their respective controls. Also, there is a decrease in the number of cells per spheroid in Ap5 KD (Fig 3.11). This suggests Ap5 KD is either affecting the proliferation or activating apoptosis. Interestingly, in MCF10CA1a spheroids, we



observed apoptosis of cells visually not in contact with the extracellular matrix, as identified by nuclear fragmentation. However, this needs further analysis to confirm whether Api5 is necessary for the survival of cells in the lumen area without direct contact with the ECM.

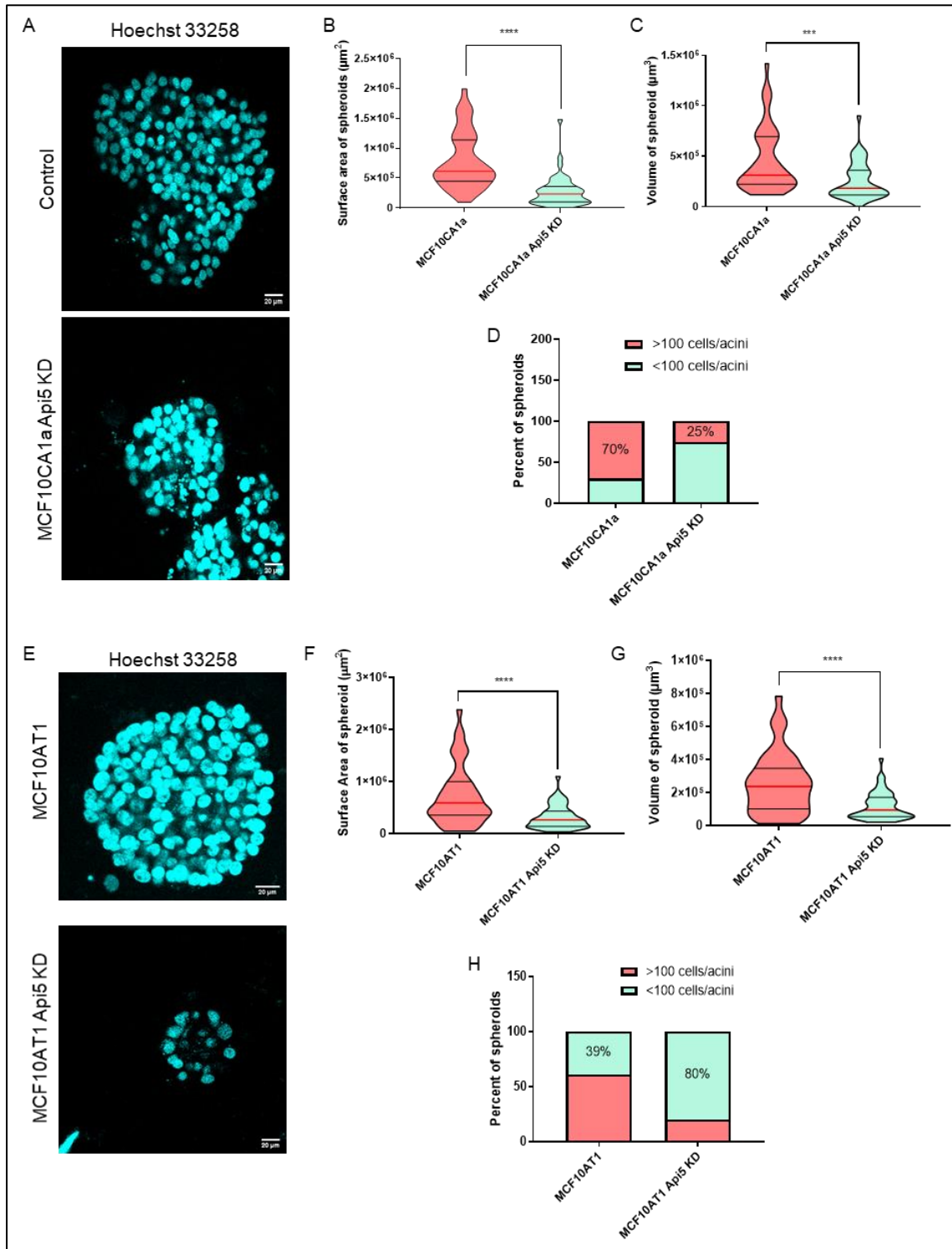




**Fig 3.11** Api5 KD in MCF10AT1 and MCF10CA1a affects spheroid formation in 3D cultures

a) MCF10CA1a spheroid culture showing reduced b) surface area and c) volume due to Api5 knockdown. c) Quantification representing the percentage of spheroids with >100 cells per spheroid. d) MCF10AT1 cells seeded on 3D culture showing reduced f) volume and g) surface area due to Api5 knockdown. h) Quantification represents the percentage of spheroids with >100 cells per spheroid. Mann-Whitney test, ns  $p > 0.05$ , \* $P < 0.05$ , \*\* $P < 0.01$ , \*\*\* $P < 0.001$  and \*\*\*\* $P < 0.0001$  (N=3, n=50)

### **3.2.4 Altered expression of Api5 affects proliferation and apoptosis in 3D cultures**

As the results suggest the possibility of altered expression of Api5 affecting proliferation and/or inhibition of apoptosis, we studied the expression of proliferative and apoptotic markers in acinar and spheroid cultures.

To compare the proliferation in MCF10A acinar cultures, the Ki67 positive nucleus per acini was counted, and the percentage of acini showing Ki67 staining in more than 33% cells per acini was plotted. The data shows that almost 81% of Api5 overexpressing MCF10A acini have Ki67 staining in more than 33% of cells (Fig 3.12). Also, western blotting against Ki67 using Day 16 3D lysates showed that Api5 overexpression increased Ki67 levels.

To confirm the effect of Api5 OE in the proliferation of MCF10A acinar cultures, we also studied the expression of PCNA, a cell cycle-related proliferation marker, in day 16 lysates. Similar to Ki67, a significant increase in the expression of PCNA was observed, confirming that Api5 overexpression resulted in higher proliferation.

Further to understand the effect of Api5 overexpression on apoptosis, lysates of the 3D acinar culture were collected at Day 4, 8, 12 and 16 post-seeding, and western blot analysis was carried out probing for different apoptosis markers.

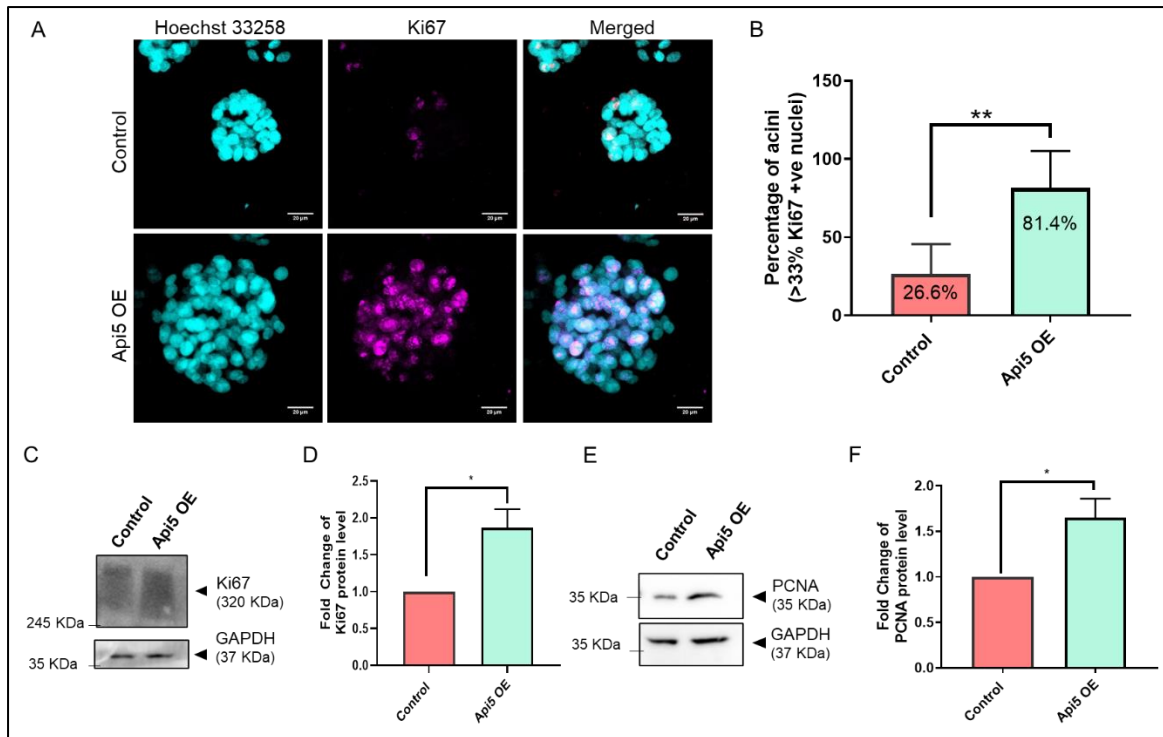


**Fig 3.12** Api5 overexpression leads to increased proliferation

a) Ki67 staining on 3D acinar structures shows high levels of Ki67 staining in Api5 overexpressing acini b) Percentage of acini having more than 33% cells with K67 positive are higher in Api5 OE compared to control. Mann Whitney t-test \*P<0.05, \*\*P<0.01, \*\*\*P<0.001 and \*\*\*\*P<0.0001. c) Representative image of western blot showing Ki67 expression in day 16 lysates of 3D acinar cultures. d) Quantification showing fold change of Ki67 protein levels. e) Representative blot showing expression of PCNA in day 16 3D acinar culture lysates and its f) quantification represented as fold change Paired t-test \*P<0.05, \*\*P<0.01, \*\*\*P<0.001 and \*\*\*\*P<0.0001

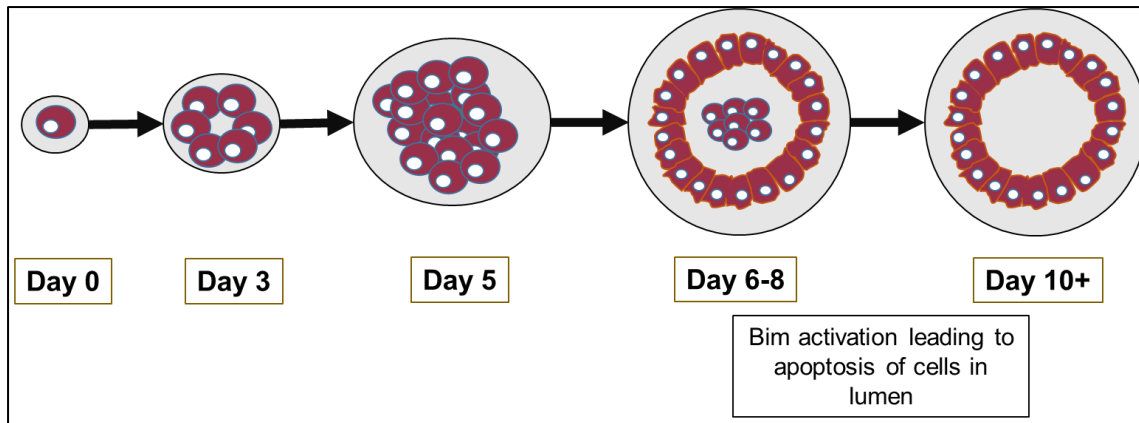


**Fig 3.13** Schematic showing apoptosis during acinar morphogenesis

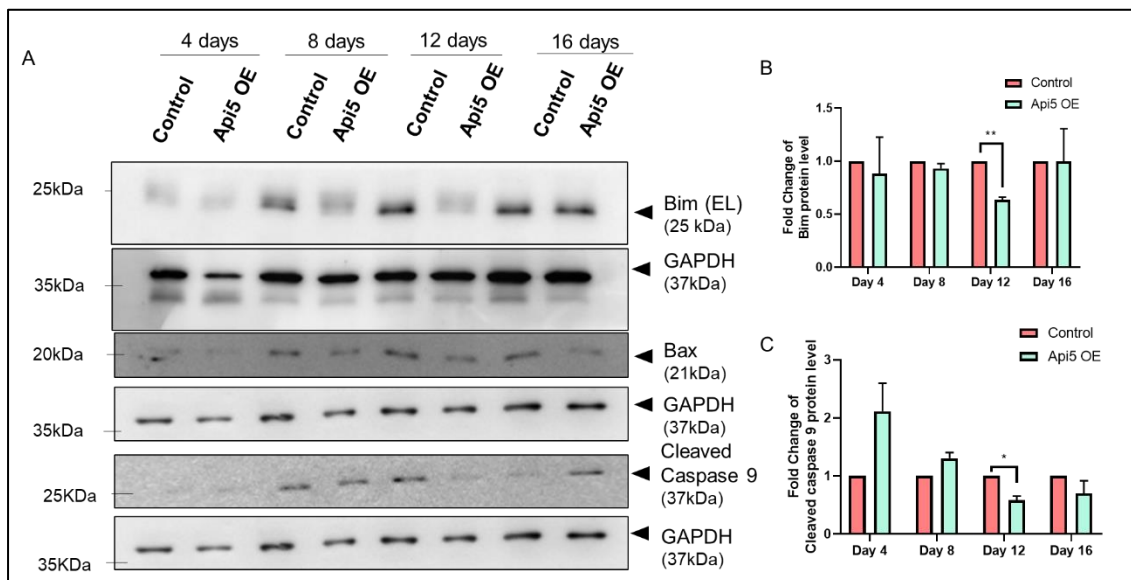


**Fig 3.14** Api5 overexpression results in reduced apoptosis during MCF10A breast acinar morphogenesis.

a) Western blot showing expression of apoptotic markers such as Bim, Bax and Cleaved Caspase 9 during the breast acinar morphogenesis. Bar graph showing fold change in expression of b) Bim and c) Cleaved Caspase 9 during the acinar morphogenesis normalised to GAPDH and compared to control each day. Paired t-test ns  $P < 0.05$ , \* $P < 0.05$ , \*\* $P < 0.01$ , \*\*\* $P < 0.001$  and \*\*\*\* $P < 0.0001$

Interestingly, Bim levels were reduced on day 12 in the Api5 OE set of lysates compared to the control set on the same day. Apoptosis of lumen cells during MCF10A acinar morphogenesis happens between day 8 and day 12. It is also known

that Bim is essential for apoptosis-mediated lumen clearance during breast acinar morphogenesis (Mailleux et al., 2007). This suggested that Api5 OE could be deregulating the apoptosis during breast acinar morphogenesis. Further, we also studied the expression pattern of other apoptosis markers such as Caspase 9 and Bax. A similar pattern was also observed with Bax and cleaved Caspase 9 (Fig 3.14).

To study whether Api5 KD affects proliferation, 7-day spheroid cultures of MCF10AT1 and MCF10CA1a were immunostained against Ki67. Percentage of a spheroid with more than 50% cells showing Ki67 positive cells were analysed. Quantification showed Api5 KD resulted in a significantly lower percentage of spheroids with more than 50% Ki67 positive nuclei in Api5 KD MCF10CA1a cells. However, no difference was observed between control and Api5 KD MCF10AT1 cells. To confirm the effect of Api5 KD on proliferation, immunoblot against proliferation markers Ki67 and PCNA were carried out in spheroid culture lysates of the respective cells.

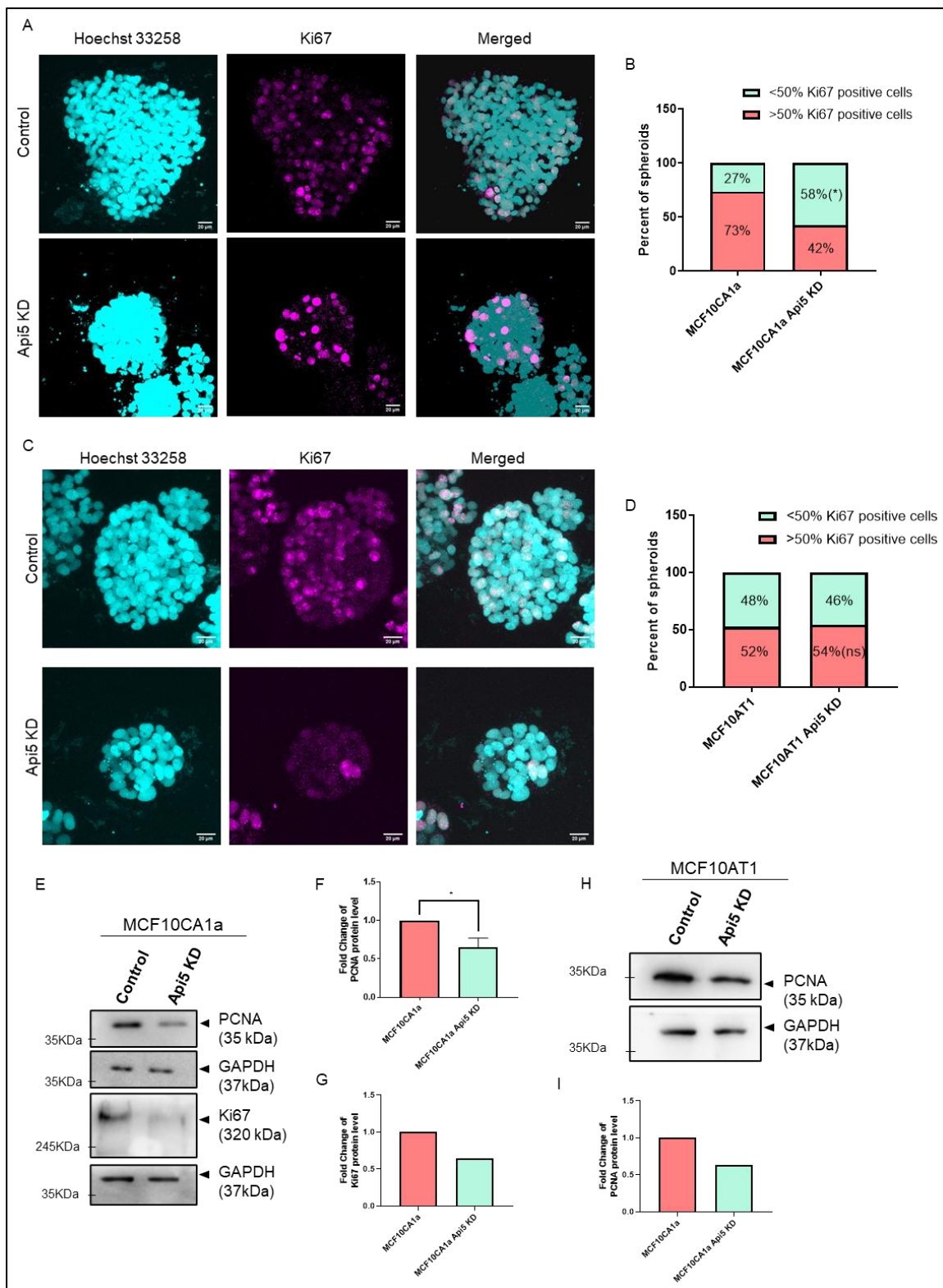


**Fig 3.15** Api5 knockdown results in reduced proliferation of malignant breast cells. Representative image of immunostaining and corresponding quantification showing Ki67 expression in spheroid cultures of (a & b) MCF10CA1a and (c & d) MCF10AT1. e) Representative image of blot showing expression of PCNA and Ki67 in

MCF10CA1a 3D spheroid culture lysates. Fold change of f) PCNA and g) Ki67 are plotted as box plots. h) Representative image of western blot showing expression of PCNA in the spheroid culture of MCF10AT1 and (i) quantified as fold change. Paired t-test ns P<0.05, \*P<0.05, \*\*P<0.01, \*\*\*P<0.001 and \*\*\*\*P<0.0001

Results indicated that Api5 KD in both the premalignant and malignant cells result in reduced proliferation of the cells. This was evident from reduced Ki67 positive nuclei staining as well as results from western blot assays. Thus, it confirms that Api5 can regulate the proliferation of breast epithelial cells and are necessary for the survival of malignant breast cells.

Since our results from overexpression studies indicate that Api5 can also regulate apoptosis during breast acinar morphogenesis, we decided to understand whether Api5 KD can lead to higher apoptosis. To analyse this, we studied the expression of active caspase 3 using immunofluorescence in 7 days spheroid cultures of Api5 KD MCF10CA1a and MCF10AT1 cells (Fig 3.15).

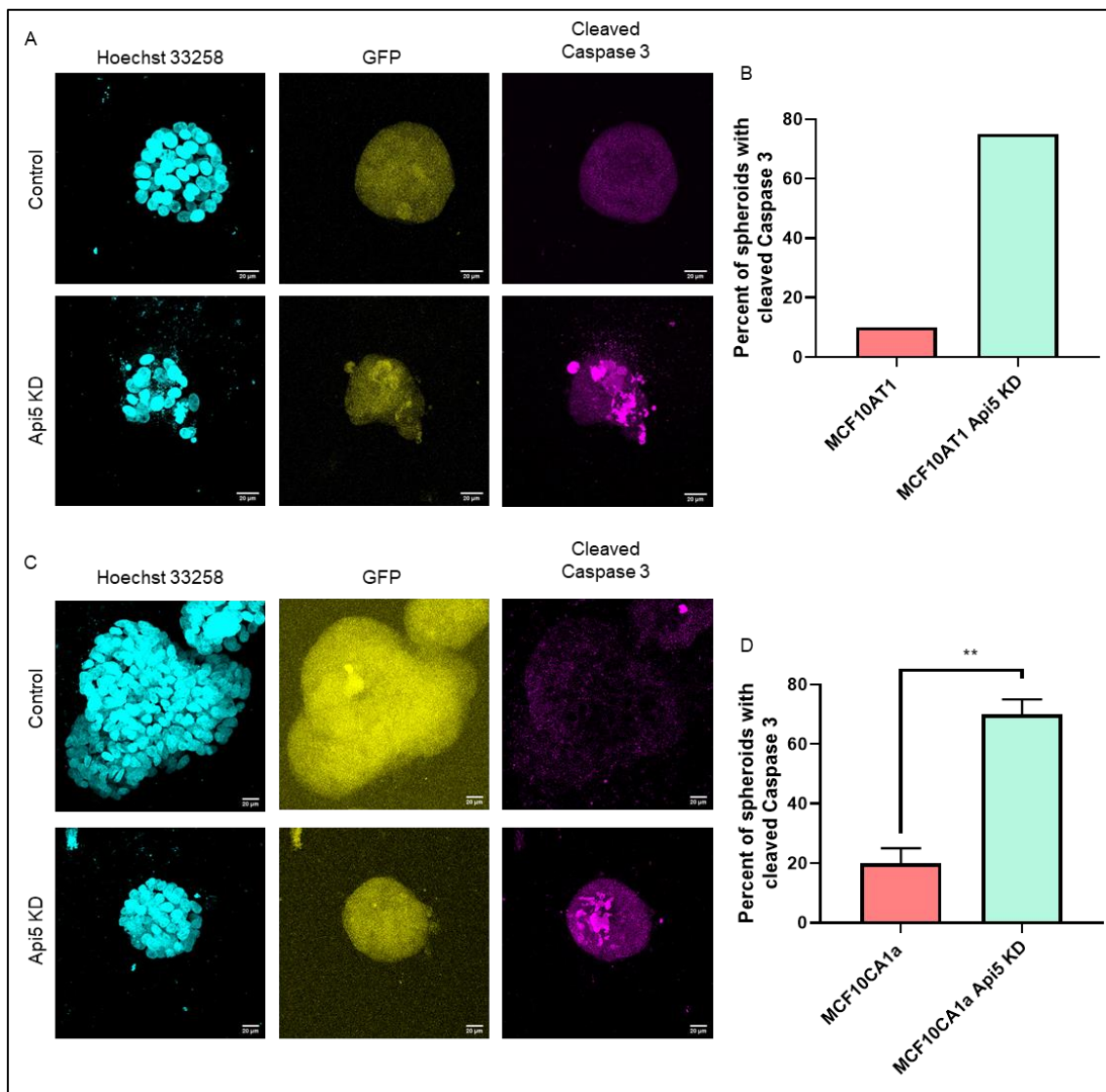


**Fig 3.16** Api5 KD leads to an increase in apoptosis.

Representative image of immunostaining against active Caspase-3 in (a & b) MCF10AT1 cells with Api5 KD and (c & d) MCF10CA1a Api5 KD cells.

Api5 KD resulted in higher levels of active caspase-3, suggesting activation of apoptosis in malignant cells. Both MCF10AT1 and MCF10CA1a cells with Api5 KD had almost 75% spheroids showing active caspase-3 staining (Fig 3.16).

To further validate the results, we also analysed the activation of caspase 9 and protein levels of Bim and Bax in the spheroid culture lysates.

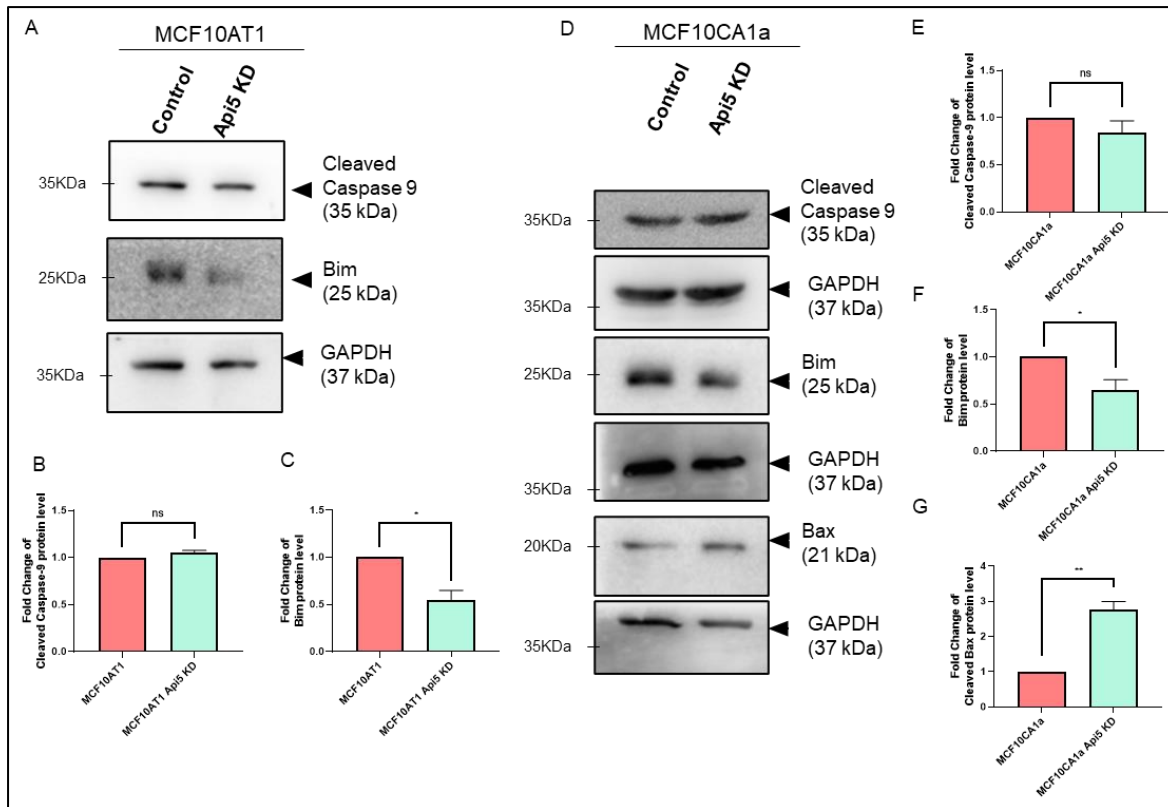


**Fig 3.17** Api5 KD in malignant cells activates apoptosis through Bax.

a) Representative blot showing cleaved caspase-9 and Bim expression in 7-day spheroid cultures of MCF10AT1 and corresponding quantification represented as fold change (b & c). d) Representative image of blot showing expression of cleaved caspase-9, Bim and Bax in 7-day spheroid cultures of Api5 KD MCF10CA1a and the corresponding quantification represented as fold change (e- g). Paired t-test ns  $P < 0.05$ , \* $P < 0.05$ , \*\* $P < 0.01$ , \*\*\* $P < 0.001$  and \*\*\*\* $P < 0.0001$

Western blot analyses suggested that Api5 KD in malignant breast cells result in apoptosis activation through Bax. However, Api5 KD did not affect caspase-9 activity and it resulted in reduced levels of Bim expression as well. The positive correlation between Api5 and Bim was also identified on the 16th day lysates of Api5 OE MCF10A acinar cultures (Fig 3.17).

In a nutshell, Api5 OE resulted in reduced apoptosis during acinar morphogenesis, as evident by reduced Bim protein level and caspase-9 activity. Upon Api5 KD in malignant breast cells, apoptosis was activated through Bax and Caspase-3.



### 3.2.5 Api5 overexpression results in disruption of polarity in 3D acinar structures

Apico-basal polarity in 3D cultures is an essential characteristic of epithelial cells (Rodriguez-Boulan and Macara, 2014). MCF10A 3D acinar culture maintains this characteristic feature similar to the human mammary gland acini (Debnath and Brugge, 2005) (Fig 3.18). Increased size, higher proliferation and reduced apoptosis suggested transformation of epithelial cells, which can also affect the polarity of the cells (Anandi et al., 2017). Also, there have been several reports that suggest loss of polarity is associated with transformation (Coradini et al., 2011; Royer and Lu, 2011).

Api5 overexpression in breast epithelial cells results in transformed acini like morphological features, to understand whether this led to changes in polarity,  $\alpha 6$  Integrin, the basal marker, and Laminin V, the basement membrane marker, were studied. Immunofluorescence analysis of these proteins in 3D breast acinar cultures was done for understanding their localisation.

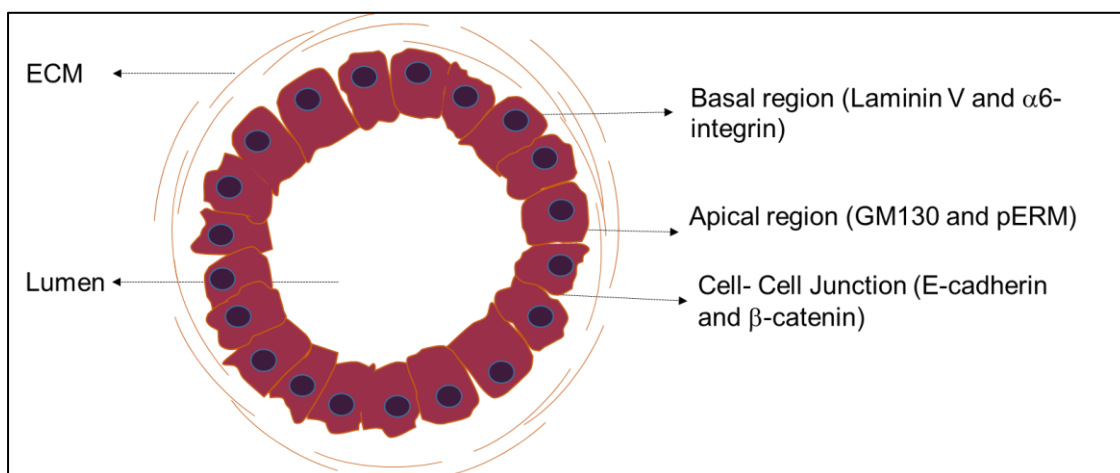


**Fig 3.18** Schematic showing polarity in MCF10A acinar structure

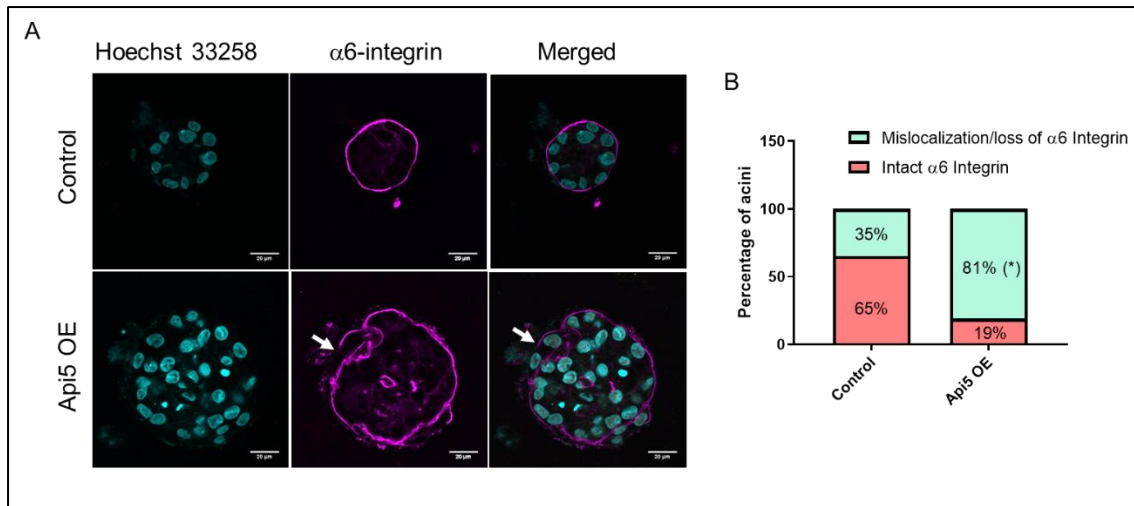


**Fig 3.19** Api5 overexpression in MCF10A cells disrupted  $\alpha 6$ -integrin localisation. a)  $\alpha 6$  Integrin staining showing the loss and mislocalisation of the basal marker. b) Quantification showing the percentage of acini which shows loss or mislocalisation of  $\alpha 6$  Integrin. (N=3, n=55) Paired t-test \*P<0.05, \*\*P<0.01, \*\*\*P<0.001 and \*\*\*\*P<0.0001

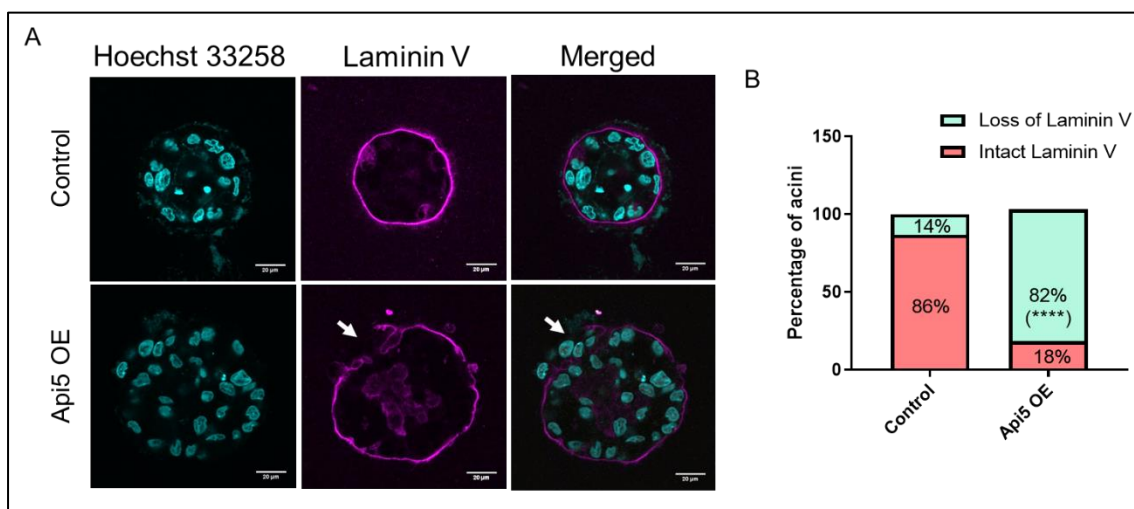


**Fig 3.20** Api5 OE in MCF10A led to loss of basal polarity marker, Laminin V. a) Immunofluorescence staining against Laminin V showing loss phenotype. b) Quantification showing the percentage of acini having loss phenotype for Laminin V. (N=4, n=60). Paired t-test \*P<0.05, \*\*P<0.01, \*\*\*P<0.001 and \*\*\*\*P<0.0001

The basal polarity markers were disrupted in Api5 overexpressing acini while intact in the control acini (Fig 3.19 & 3.20). A significant population of Api5 OE MCF10A acini showed loss or mislocalization of basal polarity markers. To further understand the effect of Api5 overexpression on polarity, we analysed the apical polarity marker, GM130. GM130 is a protein localised to cis-Golgi, which is apically localised in the MCF10A acini.

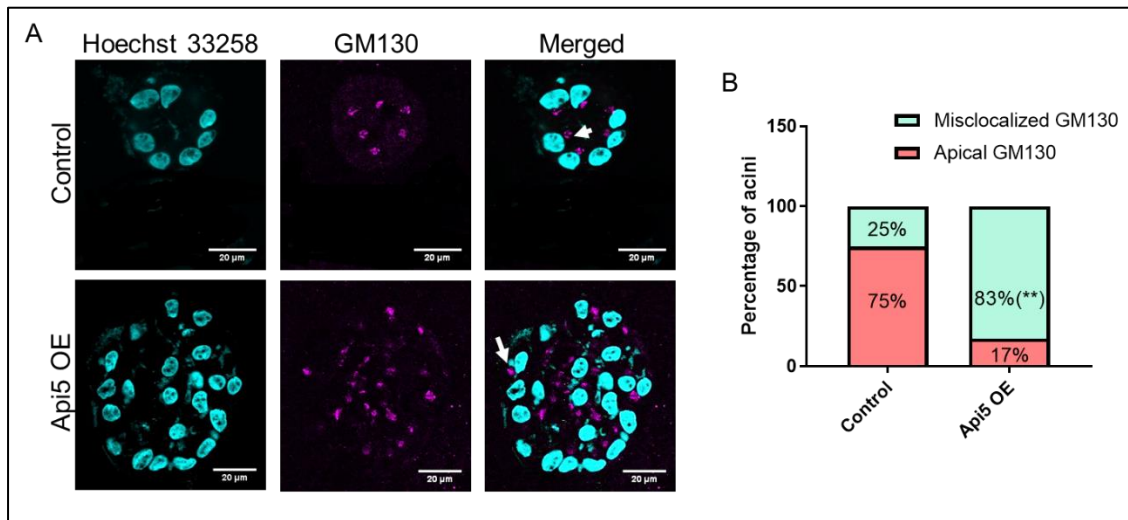


**Fig 3.21** Api5 OE disrupts apical polarity of MCF10A 3D acinar cultures.

a) GM130 staining showing Api5 overexpression leading to mislocalisation of the apical polarity marker. b) Quantification showing the percentage of acini having mislocalisation of GM130. (N=4, n=60). Paired t-test \*P<0.05, \*\*P<0.01, \*\*\*P<0.001 and \*\*\*\*P<0.0001

The apically localised GM130 was mislocalised in 85% of Api5 overexpressing MCF10A acini (Fig 3.21). This shows that Api5 overexpression alters the apical polarity as well.

Golgi bodies also play a significant role in cell polarity when cells cultured in 2D dishes as well. It also has a role in the directionality of cellular movement. Since we observed mislocalisation of GM130 in 3D acinar cultures, we further dissociated the 3D structures and assayed for the Golgi morphology using GM130 immunostaining.

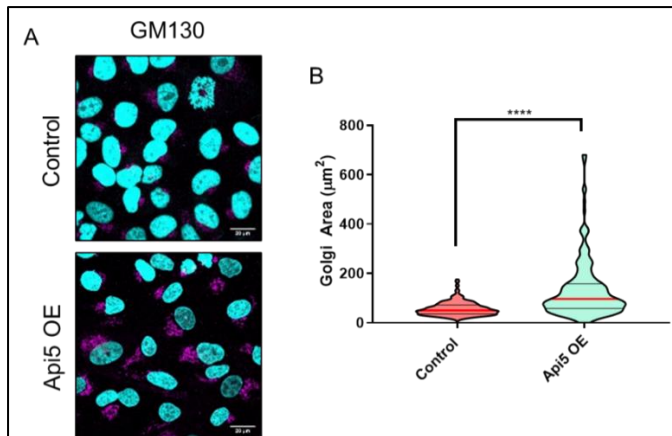


**Fig 3.22** Api5 overexpression results in dispersal of Golgi

a) Representative image showing GM130 immunostaining in 3D dissociated cells. b) Quantification showing Golgi area measured using ImageJ. Mann Whitney t-test \* $P < 0.05$ , \*\* $P < 0.01$ , \*\*\* $P < 0.001$  and \*\*\*\* $P < 0.0001$ .

Immunostaining in 3D dissociated cells revealed that Api5 overexpression resulted in the dispersal of Golgi bodies (Fig 3.22). Golgi dispersal is known to be associated with malignant cells (Anandi et al., 2017; Petrosyan, 2015). This also suggests that Api5 overexpression mediated polarity dispersal is not restricted to 3D cultures. Even if the cells are dissociated and plated as monolayer culture, it retains the altered morphology of cellular organelles.

ERM is a complex of ezrin, radixin and moesin localised to the plasma membrane. Tyrosine kinase-mediated activation of ERM protein leads to activated pERM complex. In MCF10A acinar cultures, these are known to have enrichment at the apical surface (Debnath and Brugge, 2005). To understand whether there is a global shift in the localisation of cellular components, we immunostained 16 days acinar cultures with pERM.

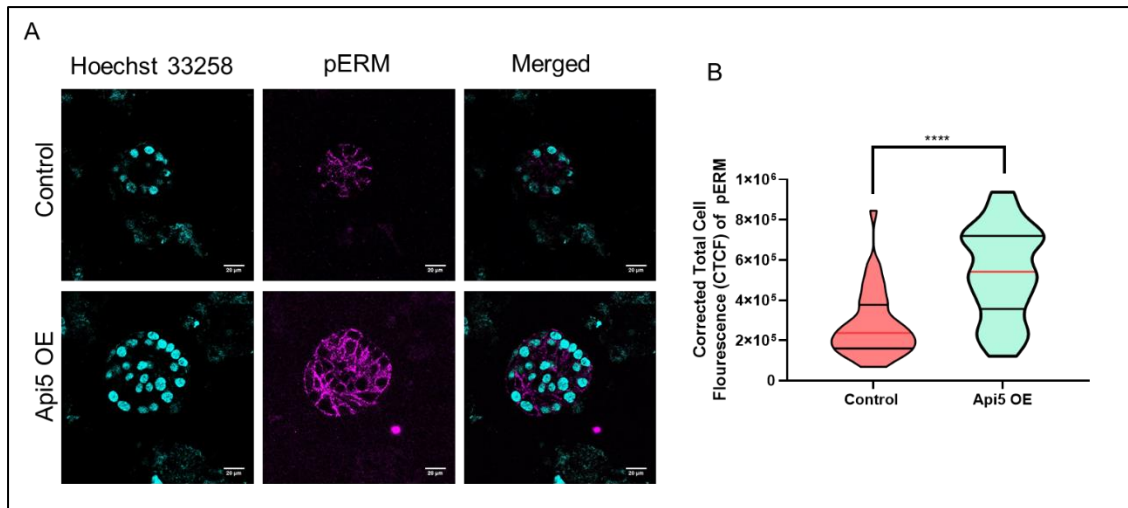


**Fig 3.23** Api5 overexpression resulted in higher pERM staining

a) Representative image showing pERM staining in day 16 acinar cultures b) Quantification showing corrected fluorescence intensity analysed using ImageJ. Mann Whitney t-test \* $P < 0.05$ , \*\* $P < 0.01$ , \*\*\* $P < 0.001$  and \*\*\*\* $P < 0.0001$ .

Api5 OE did not result in altered localisation of pERM, although there was an increase in staining intensity of pERM. This was confirmed by quantifying Corrected Total Cell Fluorescence (CTCF) (Fig 3.23). Though this needs further studies using western blot analysis and comparing the total levels of ERM protein, Api5 overexpression might be leading to higher activation of ERM proteins through elevated activation of membrane receptors. Multiple studies shows that pERM levels are upregulated in tumor tissues (Ponuwai, 2016; Zhang et al., 2013).

As we observed Api5 OE resulted in basal and apical polarity dispersal, we were interested in understanding its effect on cell-cell junctions. Breast epithelial cells form cadherin junctions between cells in acinar structures.

To understand whether Api5 overexpression can lead to altered cell-cell junctions, immunofluorescence and immunoblot assay against E cadherin,  $\beta$ -catenin were carried out. E-cadherin showed an apparent loss phenotype in IF while an increase in immunoblot, suggesting a lack of localisation even with a higher expression level. The increase in E-cadherin levels was also confirmed by quantifying the intensity of staining in 3D acini cultures (Fig 3.24).

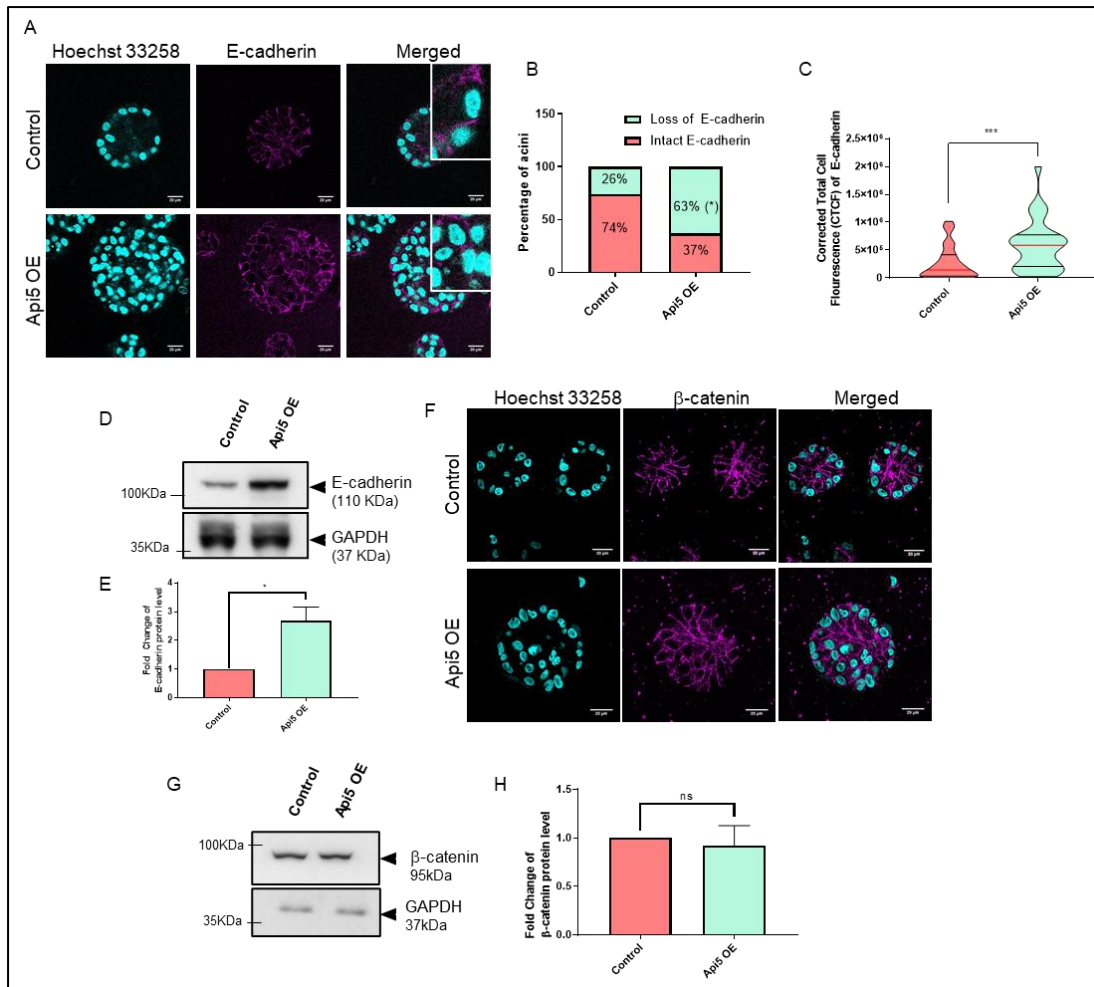


**Fig 3.24** Api5 overexpression results in variation in levels of cell-cell junction markers.

a) Immunofluorescence against E cadherin showing loss phenotype in Api5 overexpressing acini indicated by the arrow mark. b) Bar diagram shows the percentage of acini having loss phenotype (N=4, n=60). c) Violin plot showing the intensity of E-cadherin staining in 16-day 3D acinar cultures. d and e) Western blot showing protein levels of E-cadherin in 16-day breast acinar culture, which is quantified and plotted in bar diagram. f) Immunostaining against β catenin showing a similar staining pattern for both Api5 overexpressing and control acini. g-h) Western blot analysis show varying levels of β catenin and fold change of protein level compared to control and normalised with GAPDH. All lysates were collected after 16 days of culture on Matrigel®. Mann-Whitney test \*P<0.05, \*\*P<0.01, \*\*\*P<0.001 and \*\*\*\*P<0.0001



$\beta$ -catenin did not show any loss or mislocalisation when analysed in immunostaining of 16-day acini cultures. Similarly, western blot analysis confirmed no change in protein levels by day-16 (Fig 3.24).

Further to understand whether Api5 OE induced effect on cell junction is specific to 3D culture, we immunostained E-cadherin and  $\beta$ -catenin in dissociated monolayer cultures.

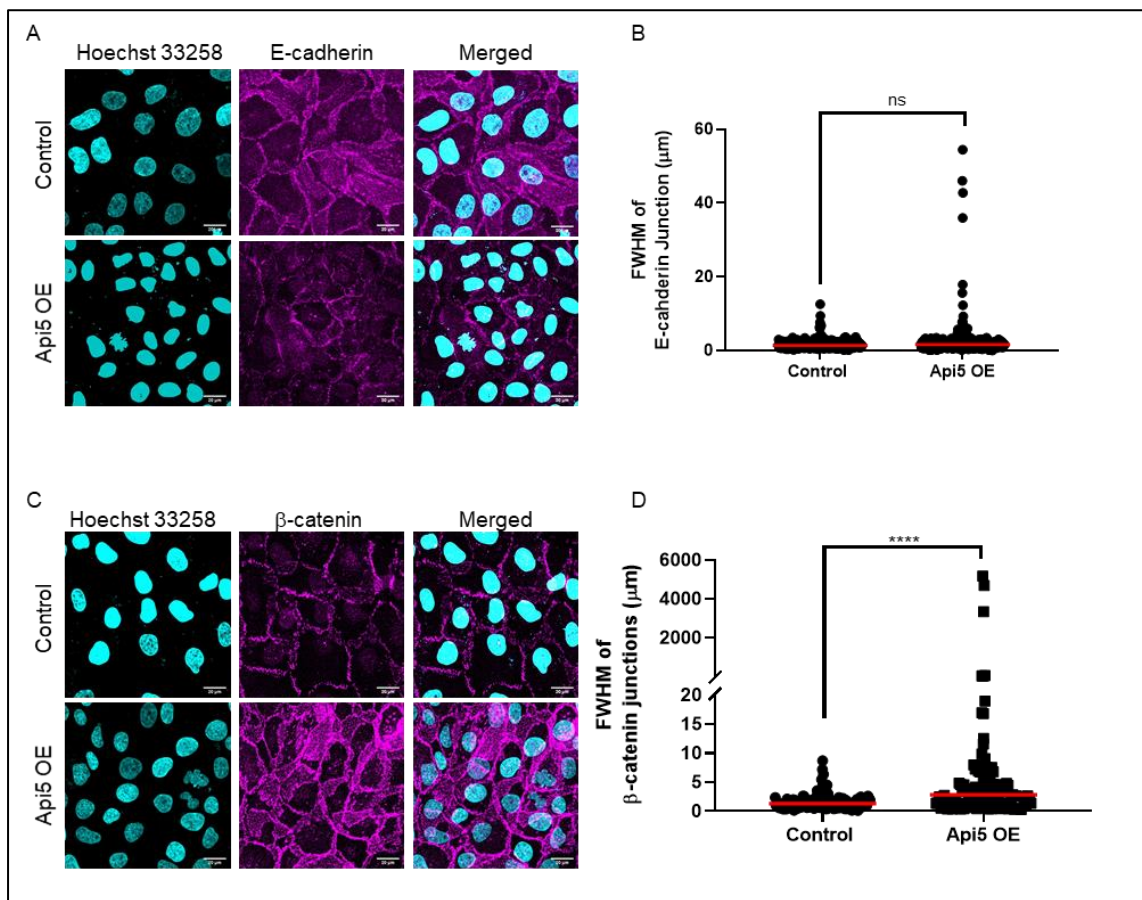


**Fig 3.25** Api5 overexpression affects cell-cell junctions

a) Representative image showing E-cadherin staining in 3D dissociated cells and b) quantification showing the Full-Width Half Max (FWHM) of the staining at the junctions. c) Representative image showing  $\beta$ -catenin staining in 3D dissociated cells and d) quantifications showing the FWHM at the junctions. Mann-Whitney test ns  $P > 0.05$ , \* $P < 0.05$ , \*\* $P < 0.01$ , \*\*\* $P < 0.001$  and \*\*\*\* $P < 0.0001$

We observed a loss of E-cadherin at cell-cell junctions in dissociated cells as well, although in the junction where E-cadherin were present, they had a similar thickness to that of the control cells (Fig 3.25). This suggests that Api5 overexpression results in loss of E-cadherin at cell-cell junctions, although it is possibly not through loosened junctions. Interestingly, We observed dispersed junctional staining of  $\beta$ -catenin as evident from higher FWHM values. Api5 OE could be leading to loss of E-cadherin at the junction but a loosely arranged b-catenin.

### **3.2.6 Api5 overexpression results in partial-EMT like phenotype.**

Our studies found that Api5 overexpression resulted in E-cadherin loss at cell-cell junctions, although the total expression levels were upregulated. E-cadherin is also used as an epithelial marker when studying Epithelial to Mesenchymal Transition (EMT). Oncogene induced transformation is often known to activate EMT. This transition helps change the phenotypic and molecular characteristics of the epithelial cell to adapt to the malignant transformation (Roche, 2018; Zeisberg and Neilson, 2009).

Further studies were carried out to identify whether Api5 overexpression can initiate EMT characteristics. The EMT can be studied using specific molecular markers specifically associated with the transition, including an increase in N cadherin, Slug, Vimentin, Fibronectin while reducing levels of E cadherin.

Immunoblot analyses of 3D acini lysates show an increase in Fibronectin, Twist, Vimentin and Slug (Fig 3.26). Data shows that the E cadherin levels get upregulated while N cadherin is not affected. This might be suggesting cells attaining a partial EMT characteristics when Api5 is overexpressed.



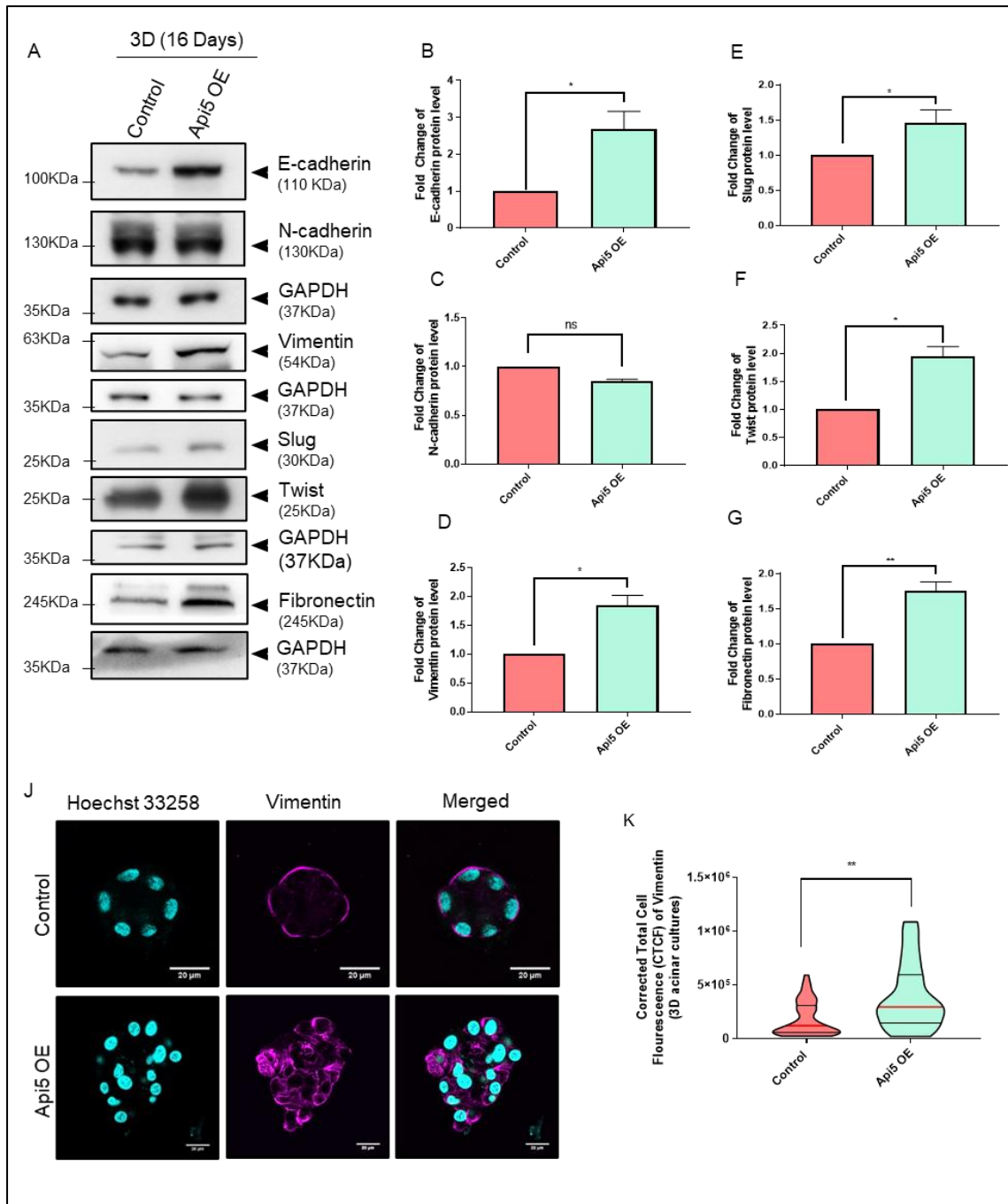


**Fig 3.26** Api5 overexpression might be resulting in partial EMT like characteristics.

a) Western blot analysis shows an increase in protein levels of mesenchymal markers like Vimentin, Twist and Slug in Api5 overexpressing MCF10A lysates collected after 16 days culture on Matrigel<sup>®</sup>. b) Relative expression of the Fibronectin, N-cadherin, Vimentin, Slug and Twist normalised with GAPDH. c) Representative images showing Immunostaining against Vimentin in 16-day acini cultures. d) Violin plot showing the intensity of Vimentin staining in 16-day acinar cultures. \*P<0.05, \*\*P<0.01, \*\*\*P<0.001 and \*\*\*\*P<0.0001

To investigate whether the partial-EMT characteristics attained led to a permanent characteristic change of MCF10A cells, 3D cultures were dissociated and seeded as 2D monolayer cultures. This was then used for immunostaining against Vimentin and western blot analysis against other EMT markers. Vimentin levels were upregulated in Api5 OE cells as confirmed with immunostaining and western blot analysis. Similarly, other markers such as E-cadherin, N-cadherin, Slug and Fibronectin showed a similar pattern as in 3D culture lysates. In addition, Cytokeratin-14 levels showed down regulation while cytokeratin-19 levels were increased in Api5 OE cells (Fig 3.27).

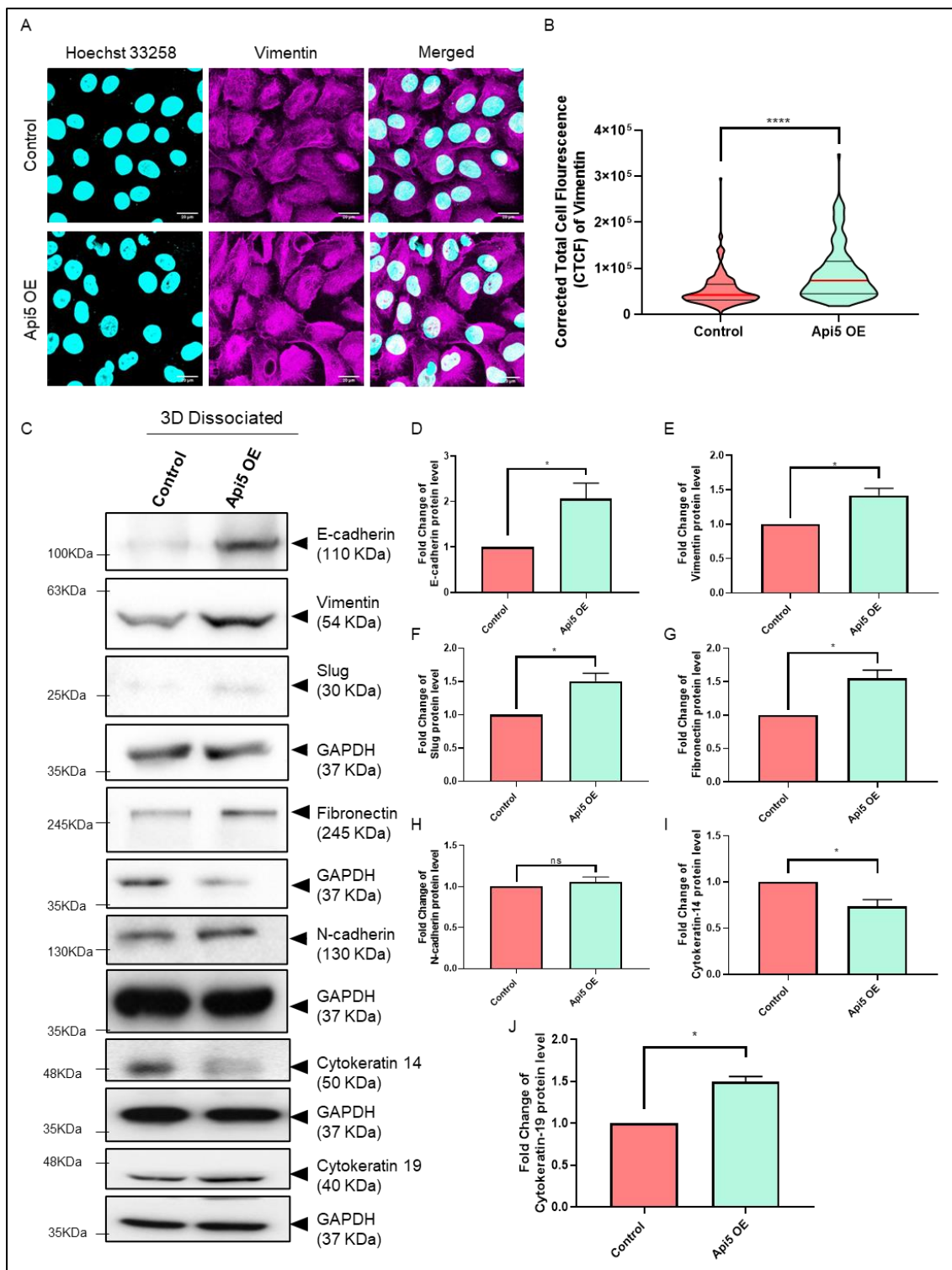


**Fig 3.27** Api5 OE results in partial-EMT characteristics, which are maintained even after dissociating from 3D culture.

a) Representative image of immunostaining against Vimentin in 3D dissociated cells and b) quantification showing the corrected fluorescence intensity of vimentin immunostaining. c) Western blot showing expression of different EMT markers in 3D

dissociated cells. Bar graphs showing fold change of d) E-cadherin, e) Vimentin, f) Slug, g) Fibronectin, h) N-cadherin, i) Cytokeratin-14 and j) cytokeratin-19 in 3D dissociated cells. Mann-Whitney test or paired t-test ns  $p > 0.05$ , \* $P < 0.05$ , \*\* $P < 0.01$ , \*\*\* $P < 0.001$  and \*\*\*\* $P < 0.0001$  ( $N \geq 3$ )

The results show that Api5 overexpression might be partially inducing some EMT characteristics like increased Vimentin and Slug expression. Higher levels of E-cadherin suggest maintenance of certain epithelial characteristics as well. The results strongly suggest that Api5 OE can result in partial-EMT. Evidences suggest partial-EMT as a transition phase that epithelial cells undergo during transformation (Jolly et al., 2015; Saitoh, 2018). Reports suggest that these characteristics can be associated with highly malignant cells as well.

At the same time, changes in cytokeratin levels were intriguing. To further understand the effect of Api5 OE on cytokeratin, the expression of different keratins was assayed using immunoblotting. 3D dissociated cell lysates were used for this study.

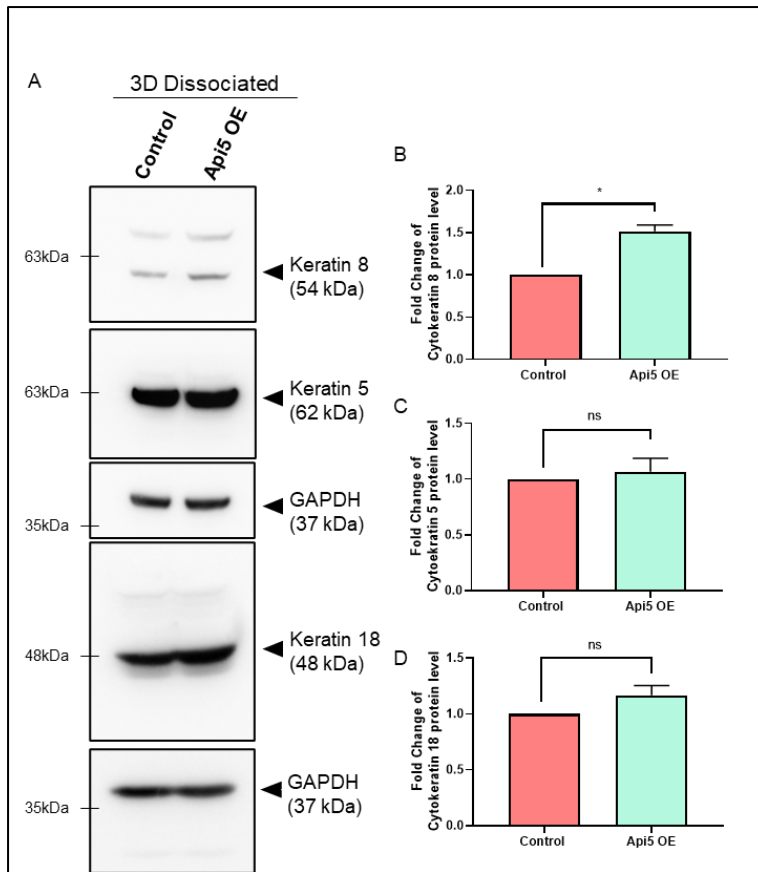


**Fig 3.28** Api5 overexpression results in higher cytoke­ratin-8 expressions.

a) Representative image of blots showing expression of different cytoke­ratin in 3D dissociated cells. Quantification showing fold change of b) Cytoke­ratin 8, c) Cytoke­ratin-5, and d) Cytoke­ratin-18 in Api5 OE 3D dissociated MCF10A cells. Paired t-test ns  $p > 0.05$ , \* $P < 0.05$ , \*\* $P < 0.01$ , \*\*\* $P < 0.001$  and \*\*\*\* $P < 0.0001$  ( $N \geq 3$ )

The results indicated that Api5 overexpression resulted in higher expression of Cytoke­ratin-8, although other keratins (Cytoke­ratin 5 and Cytoke­ratin 18) were not significantly altered (Fig 3.28).

Cytoke­ratin interacts with desmosome junction proteins and helps in maintenance of desmosome junctions. Since we observed loss of cadherin junctions due to Api5 OE, we were interested in studying whether desmosome junctions are also affected. Immunoblotting against some desmosome components was carried out using lysates from 3D dissociated cells.

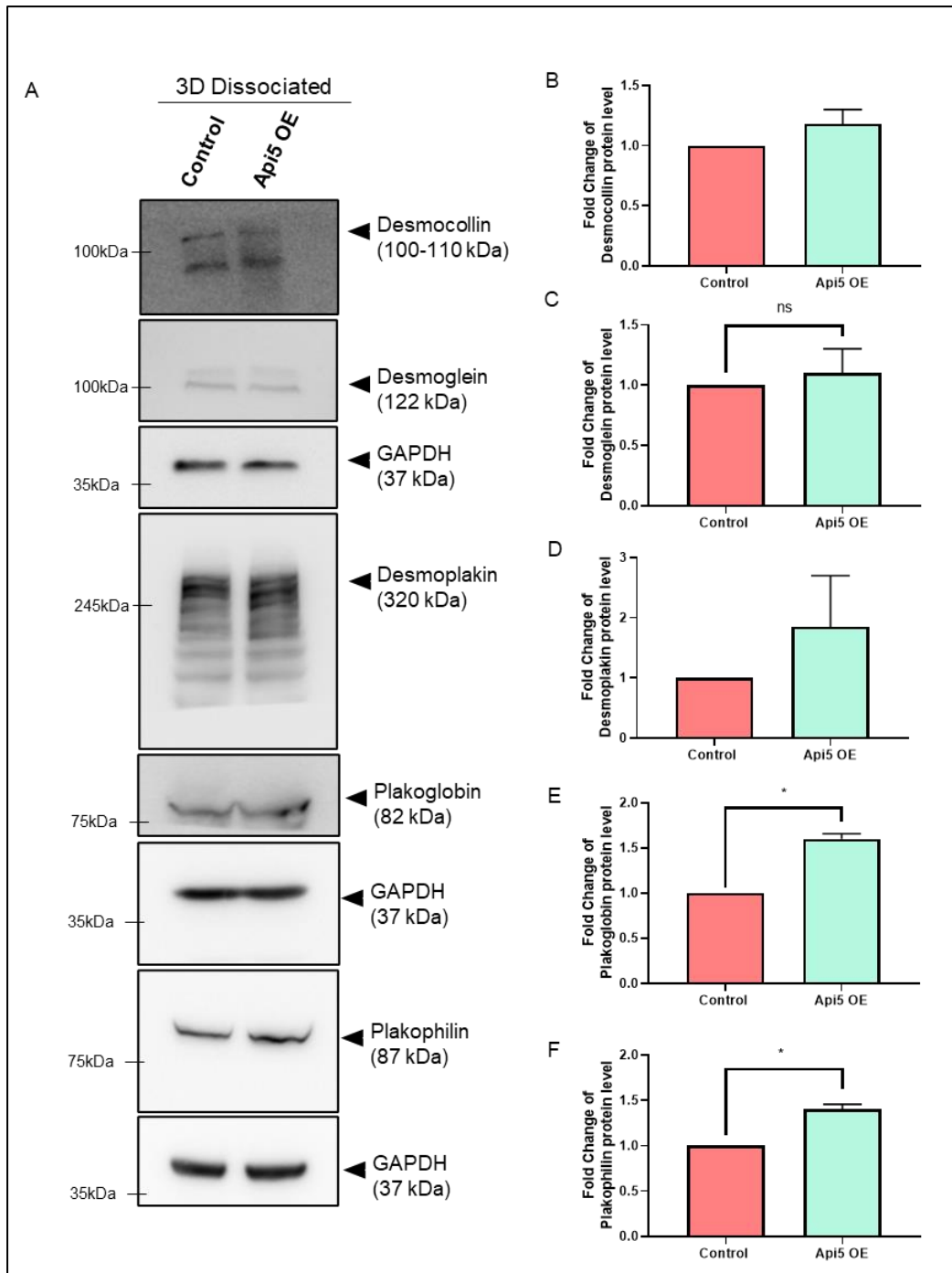


**Fig 3.29** Api5 overexpression results in altered expression of Desmosomal Armadillo proteins.

a) Representative image of immunoblot against desmosomal components in 3D dissociated cell lysates. Quantification showing fold change of b) Desmocollin, c) Desmoglein, d) Desmoplakin, e) Plakoglobin, and f) Plakophilin in Api5 OE 3D dissociated cell lysates. Paired t-test ns  $p > 0.05$ , \* $P < 0.05$ , \*\* $P < 0.01$ , \*\*\* $P < 0.001$  and \*\*\*\* $P < 0.0001$  ( $N \geq 3$ )

The results suggested that Api5 OE resulted in higher expression of Armadillo proteins in the desmosomal junctions (Fig 3.29). Interestingly, it is reported that these classes of proteins also play a role in EMT and are often associated with epithelial characteristics (Chidgey and Dawson, 2007; Knights et al., 2012).

Together this part of our study could confirm that Api5 overexpression resulted in a partial-EMT like phenotype and the cells represented characteristics of both epithelial and mesenchymal cells. Also Api5 OE have broadly affected the cell-cell junctions as evident from changes in cadherin and desmosome junction components.

### **3.2.7 Api5 knockdown affects EMT marker expression in malignant breast cells**

Api5 OE resulted in partial-EMT like molecular changes in breast epithelial cells. It was intriguing to understand the effect of Api5 KD in the EMT status of malignant breast cells.

Analysing the expression levels of E-cadherin,  $\beta$ -catenin and Vimentin in MCF10CA1a Api5 KD cells revealed that Api5 KD results in reduced expression of both epithelial and mesenchymal markers (Fig 3.30).

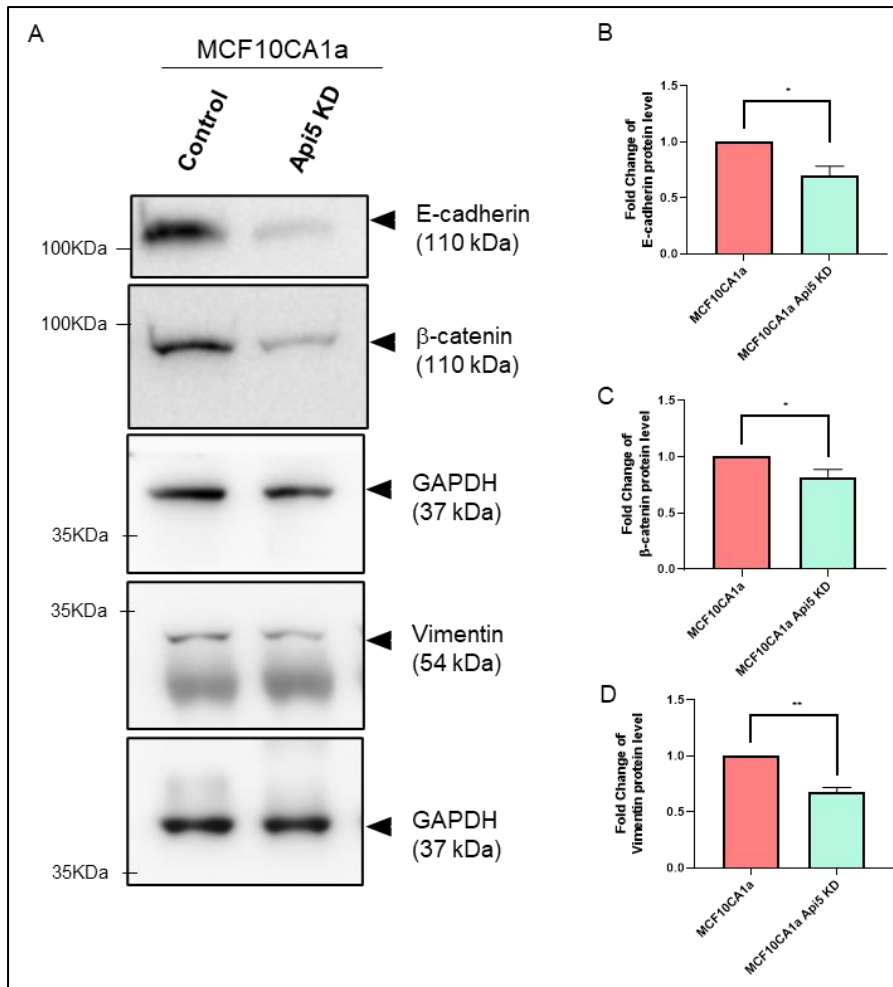


**Fig 3.30** Api5 KD results in altered EMT marker expression.

a) Representative image of blots showing expression of E-cadherin,  $\beta$ -catenin and Vimentin in Api5 KD MCF10CA1a spheroid cultures. Quantification of fold change in protein expression was plotted as bar graphs for the corresponding proteins (b-d). Paired t-test ns  $p > 0.05$ , \* $P < 0.05$ , \*\* $P < 0.01$ , \*\*\* $P < 0.001$  and \*\*\*\* $P < 0.0001$  ( $N \geq 3$ )

### 3.2.8 Api5 overexpression led to higher migratory potential

As Api5 overexpression led to transformation and partial EMT characteristics, it can also induce invasion and migration. To study whether Api5 OE could induce invasion, we analysed the activity of MMP2 and MMP9 using gelatin zymography. Results show that Api5 overexpression did not increase MMP2/9 activity. Further, conditioned media from different days during the acinar morphogenesis were used for gelatin zymography to confirm an altered invasion of the extracellular matrix due



to Api5 OE. Results suggest that Api5 OE elevated MMP2/9 activity during the early days of morphogenesis which then reduced and stabilised by Day 16 (Fig 3.31).

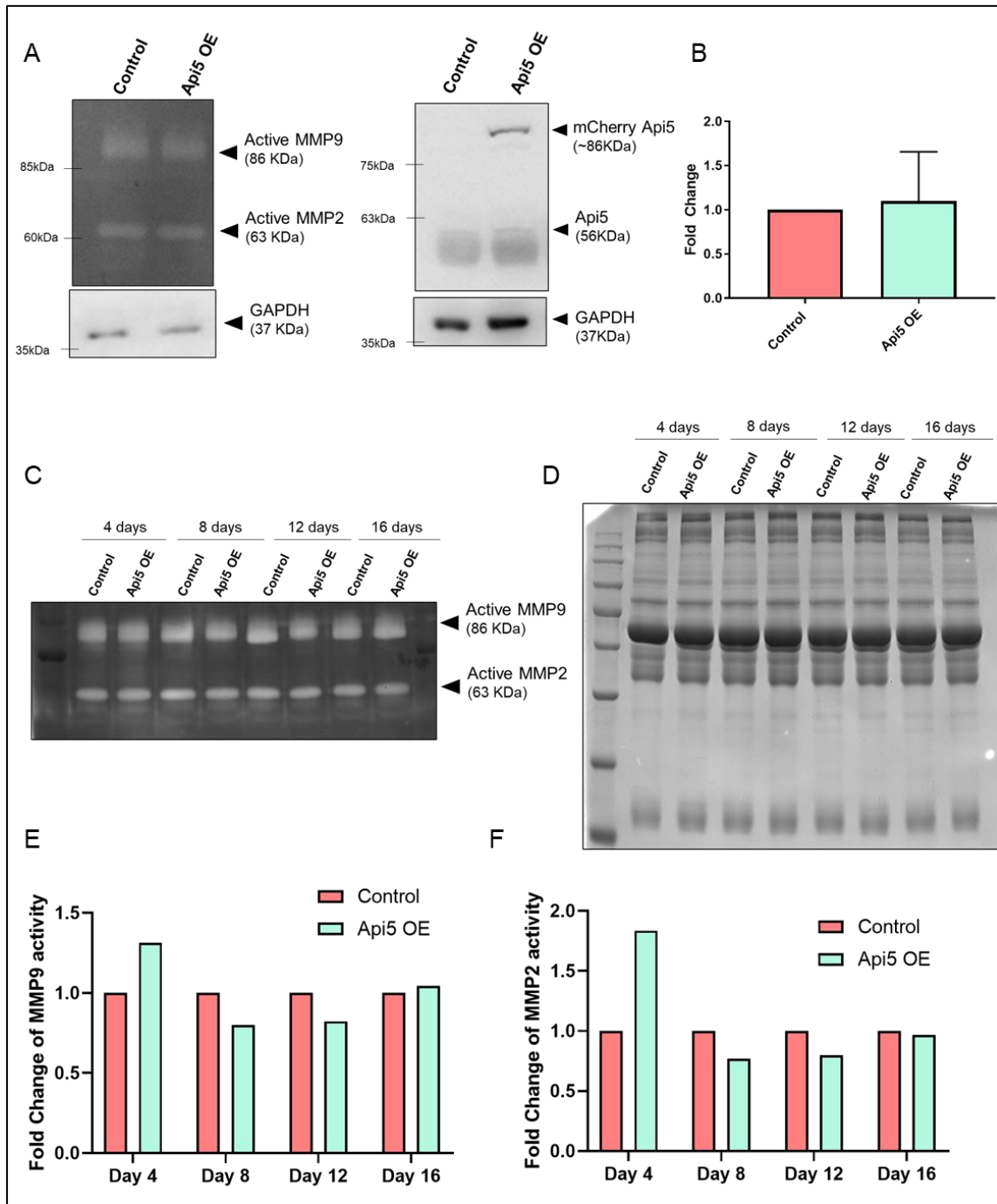


**Fig 3.31** Api5 OE affects MMP activity during early days of acinar morphogenesis. a,c) activity of MMP2 and MMP9 can be seen as clearing gelatin in the gel. b) Quantification showing MMP9 activity normalised to GAPDH levels. d) SDS gel stained with Coomassie blue to show the protein load in each conditioned media

sample in gelatin gel. Quantification of fold change in e) MMP9 and f) MMP2 activity compared to control of each day and normalised to protein load. (N≥2)

We also explored whether Api5 is required for the MMP2 and MMP9 activity in malignant breast cells. For this conditioned media was collected from Api5 KD MCF10CA1a spheroid cultures and assayed using Gelatin Zymography

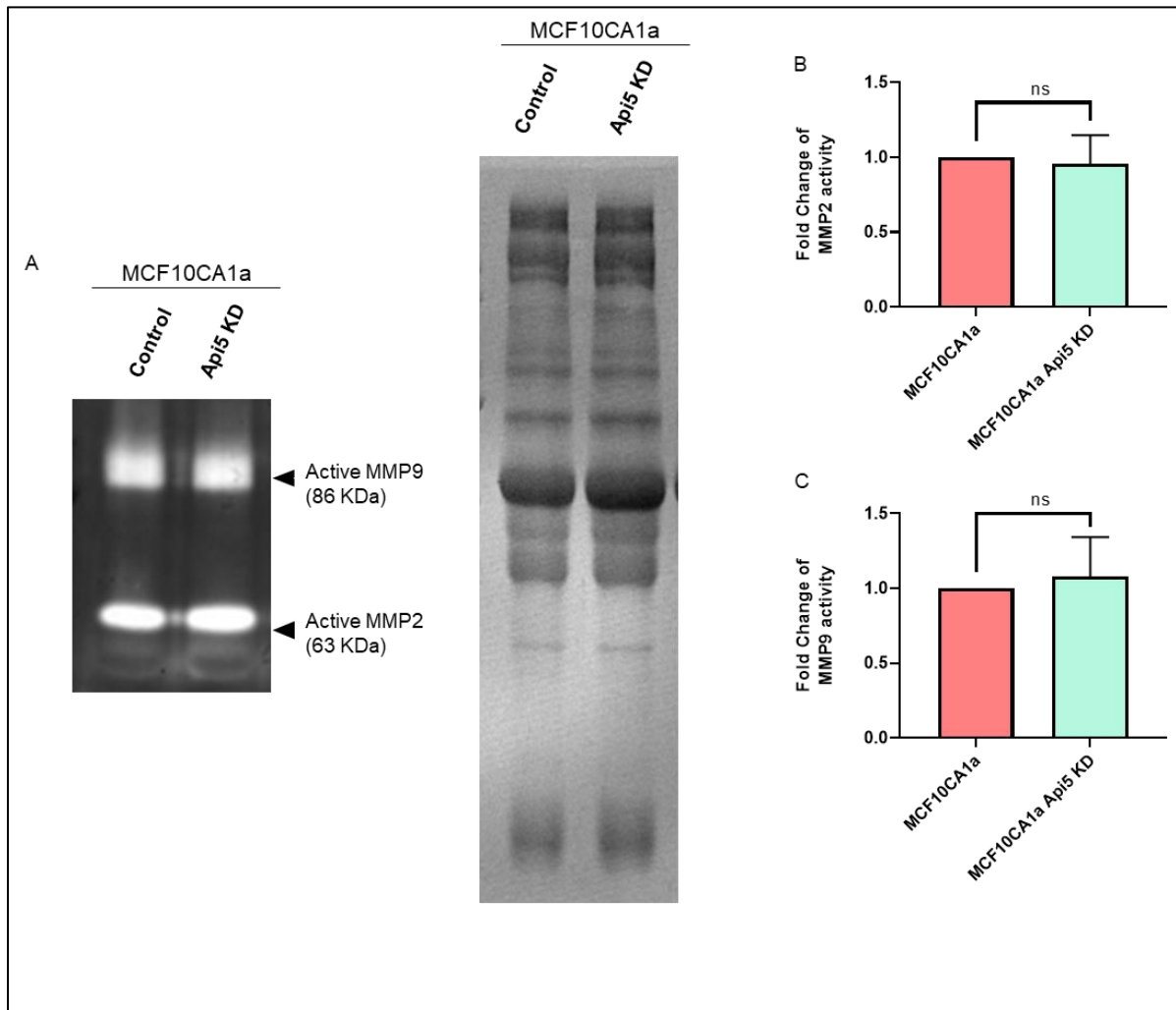


**Fig 3.32** Api5 KD does not affect MMP2 and MMP9 activity.

a) Representative image of gelatin zymography gel showing MMP2 and MMP9 activity. Quantification showing fold change in b) MMP2 and c) MMP9 activity. Paired t-test ns  $p > 0.05$ , \* $P < 0.05$ , \*\* $P < 0.01$ , \*\*\* $P < 0.001$  and \*\*\*\* $P < 0.0001$  (N≥3)

Gelatin zymography showed that Api5 KD did not alter the MMP-2 and MMP9 activity in MCF10CA1a cells as no significant difference was observed between control and Api5 KD cells (Fig 3.32).

To understand whether Api5 OE can affect MMP1 activity, a DQ collagen assay was carried out. 3D dissociated cells are seeded on DQ or Dye Quenched collagen-containing matrix and are observed using a fluorescent microscope 48 hours post-seeding. Those cells with MMP1 activity will cleave the collagen and dye to be active, showing fluorescence in the green channel. DQ collagen assay using Api5 OE 3D dissociated cells confirmed that Api5 OE does not lead to invasive potential in the epithelial cell line as there was no difference in the intensity of DQ collagen (Fig 3.33).

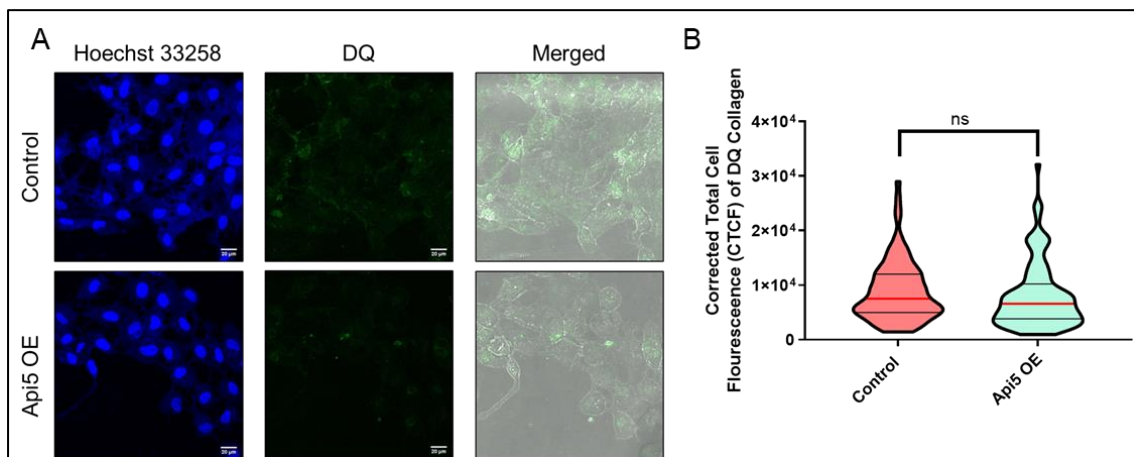


**Fig 3.33** Api5 OE does not induce invasive potential in the epithelial cell line.

a) Representative image showing DQ collagen fluorescence b) Violin plot showing the intensity of the dye fluorescence quantified using ImageJ. Mann-Whitney test, ns  $p > 0.05$ , \* $P < 0.05$ , \*\* $P < 0.01$ , \*\*\* $P < 0.001$  and \*\*\*\* $P < 0.0001$  ( $N \geq 3$ )

To understand the effect of Api5 overexpression on migration, a Single-cell migration analysis was carried out. The cells were tracked using the FastTracks tool. Each cell's velocity, displacement, distance, and persistence were calculated, and the tracks were plotted along with the trajectory plot. Api5 OE increased the distance travelled and velocity of the cells while displacement was not affected. This is supported by a decrease in persistence, suggesting a possible issue with directionality decision by the cells. Plotting the tracks on an XY plan confirmed that

Api5 OE cells were moving in a zig-zag fashion while the control cells were relatively on a straight line (Fig 3.34).

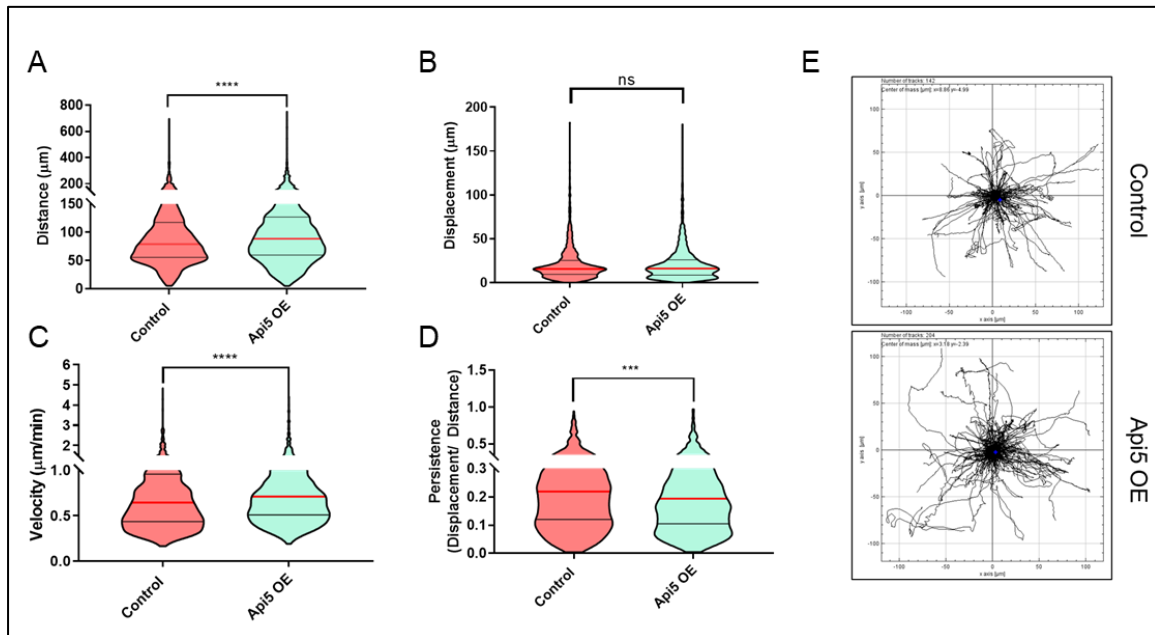


**Fig 3.34** Api5 overexpression increases single-cell migration.

Violin plot showing a) distance, b) displacement, c) velocity and d) persistence of cells tracked using fasttracks software. e) Trajectory plot showing the tracks of cells plotted onto an XY plane. Mann-Whitney test ns  $p > 0.05$ , \* $P < 0.05$ , \*\* $P < 0.01$ , \*\*\* $P < 0.001$  and \*\*\*\* $P < 0.0001$  ( $N \geq 3$ )

To understand whether Api5 is essential for the cellular migration of malignant cells, we carried out a single-cell migration analysis of Api5 KD MCF10CA1a cells. As stated previously, cells were tracked for 3 hours with imaging every 2 minutes. The tracks were analysed using FastTracks software.

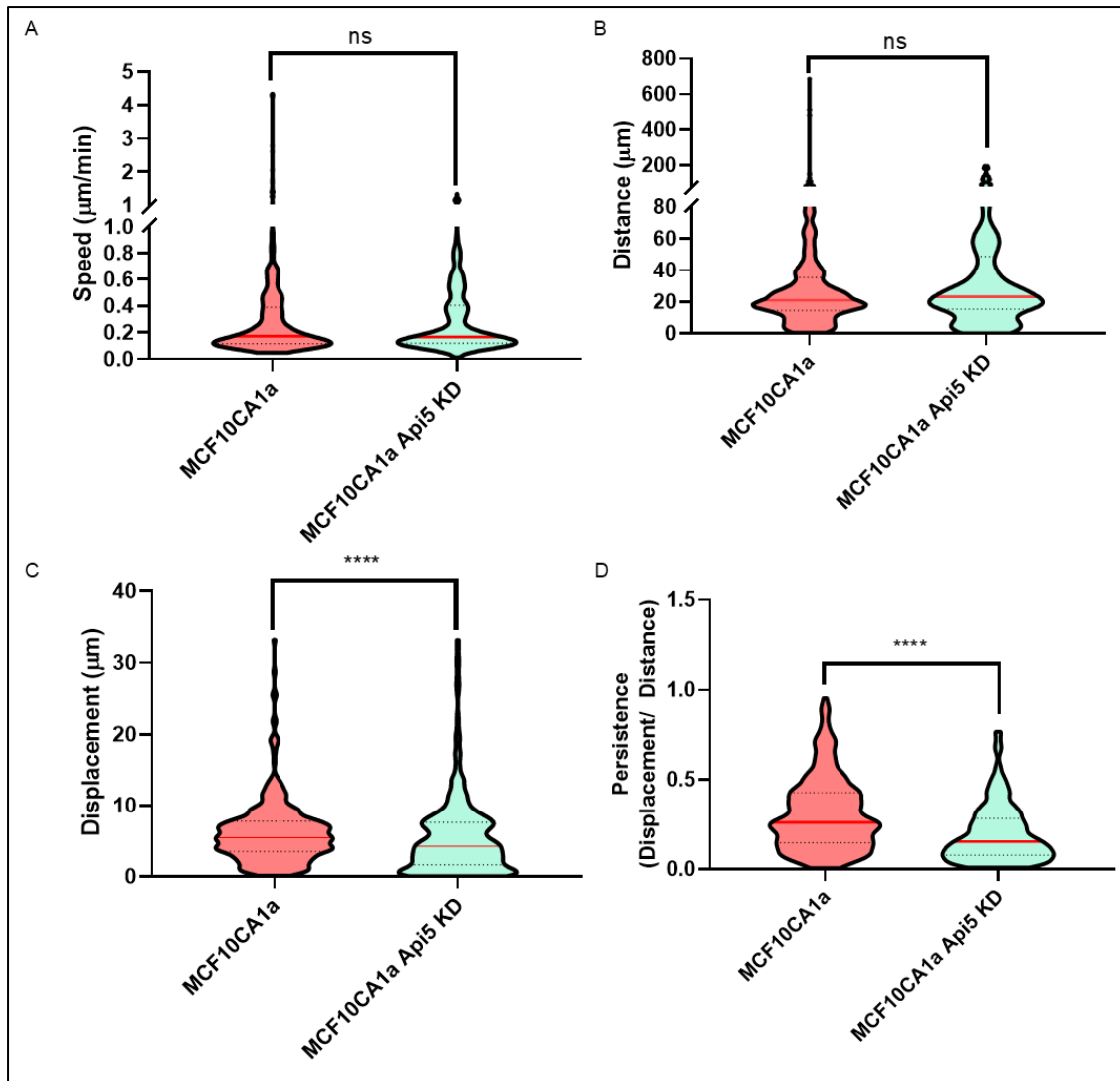


**Fig 3.35** Api5 KD results in reduced cell migratory potential.

Violin plot representing a) Speed b) Distance c) Displacement and d) Persistence of Api5 KD MCF10CA1a cells as compared against control cells. Mann-Whitney test ns  $p > 0.05$ , \* $P < 0.05$ , \*\* $P < 0.01$ , \*\*\* $P < 0.001$  and \*\*\*\* $P < 0.0001$  ( $N \geq 3$ )

Api5 KD in malignant breast cells resulted in the reduced displacement of cells as well as reduced persistence. Although the speed of cells and distance travelled were unaffected (Fig 3.35). This suggests that Api5 is necessary for the migration of cells, although the altered expression can affect various cell migration parameters.

Similarly, we also analysed the cell migration of Api5 KD MCF10AT1 cells, although there was no significant difference in distance travelled, displacement and

persistence between the control and Api5 KD cells. However, there was a significant increase in the speed of the cells upon Api5 KD (Fig 3.36).

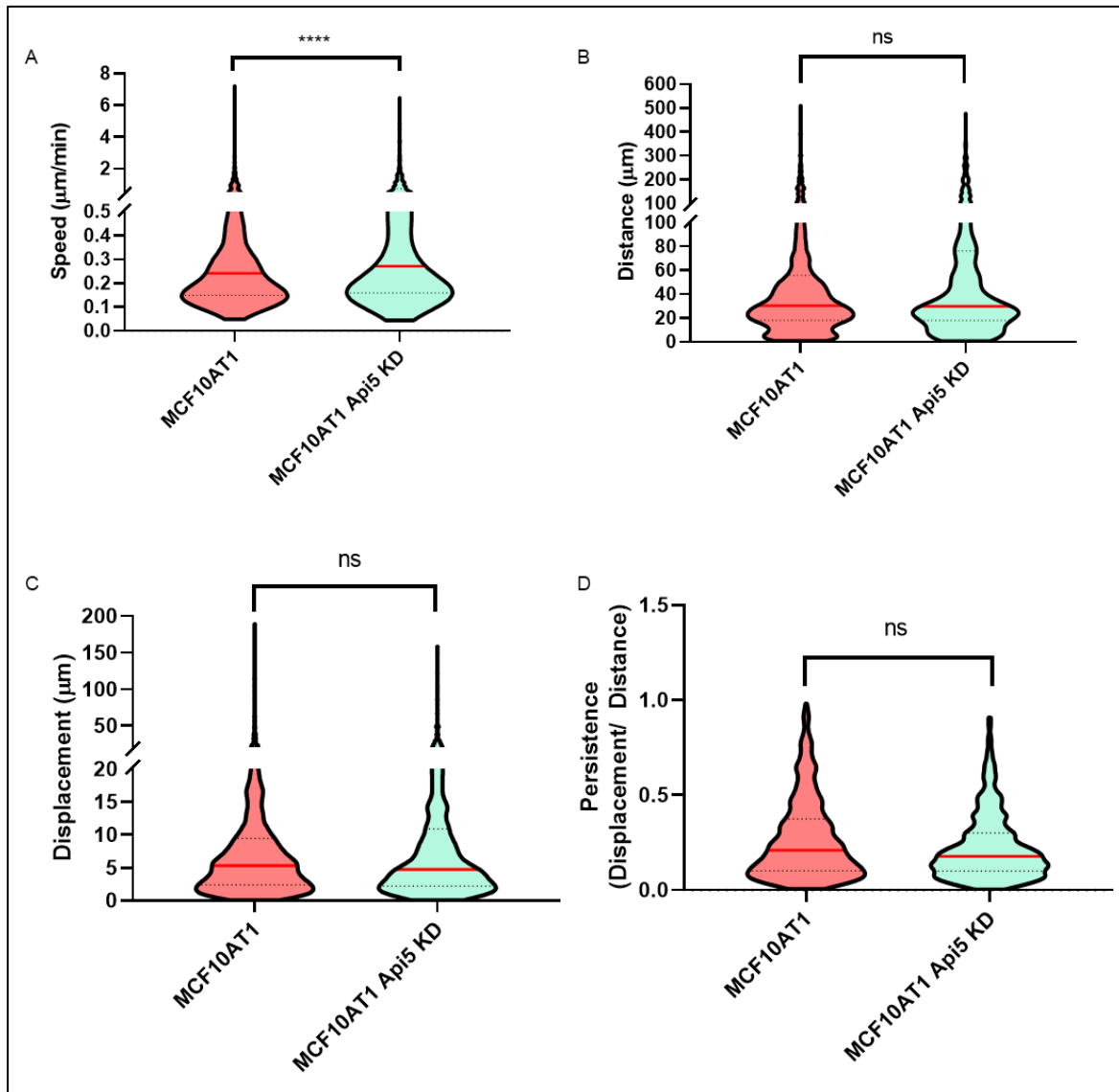


**Fig 3.36** Api5 KD results in reduced cell migratory potential.

Violin plot representing a) Speed b) Distance c) Displacement, and d) Persistence of Api5 KD MCF10AT1 cells as compared against control cells. Mann-Whitney test ns  $p > 0.05$ , \* $P < 0.05$ , \*\* $P < 0.01$ , \*\*\* $P < 0.001$  and \*\*\*\* $P < 0.0001$  ( $N \geq 3$ )

### 3.2.9 Api5 knockdown reduced colony formation ability of malignant cells

Transformed cells show the potential to form colonies from a single cell when they are sparsely seeded. Both MCF10CA1a and MCF10AT1 cells can form such colonies in 7 -14 days. To analyse if Api5 is essential for colony formation, we

sparsely seeded 100 cells in a 35 mm dish and cultured them for seven days. The survival was studied using crystal violet staining.

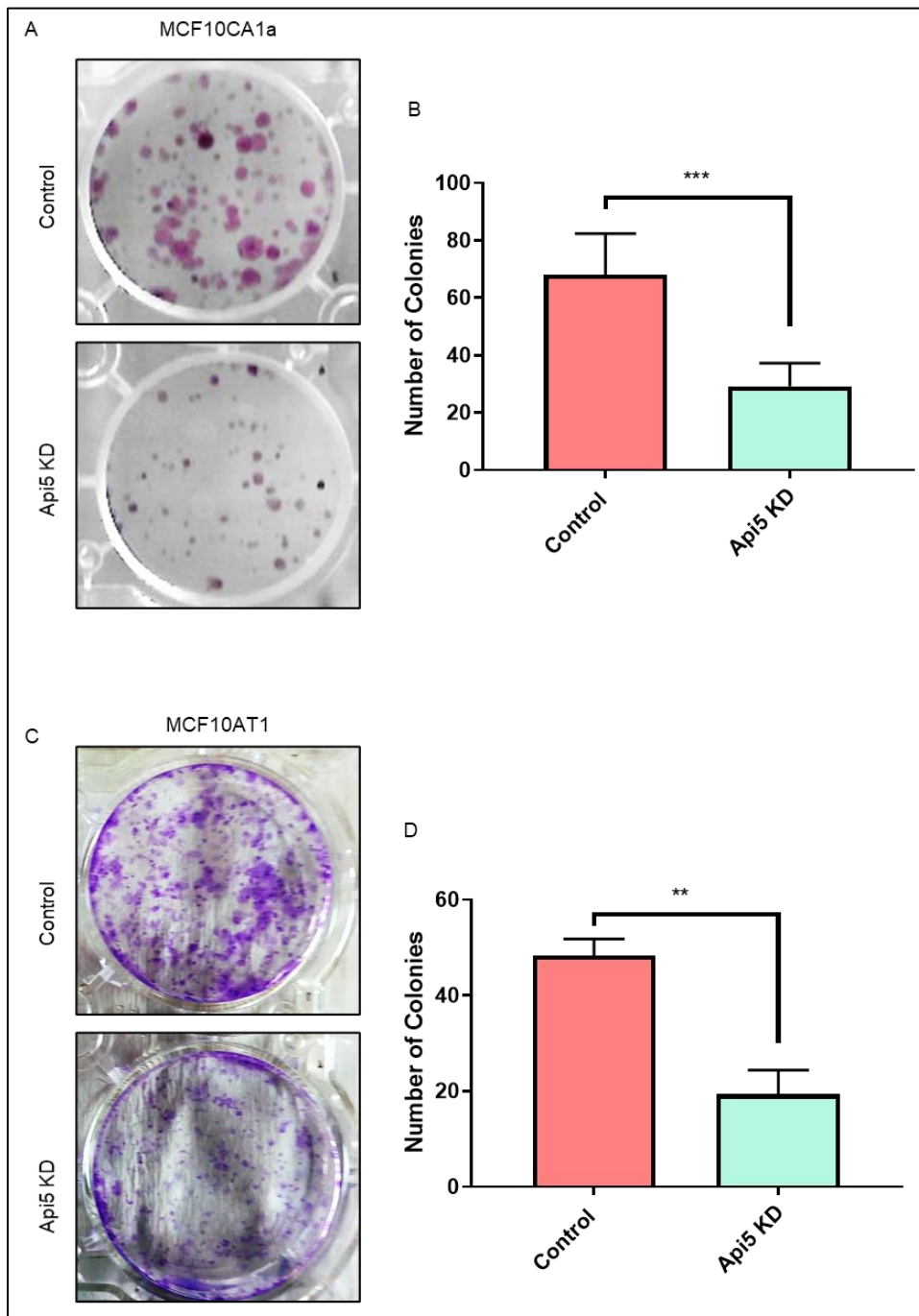


**Fig 3.37** Api5 knockdown results in reduced proliferation.

Representative image and corresponding quantification showing the number of colonies formed by (a & b) Api5 KD MCF10CA1a and (c & d) Api5 KD MCF10AT1

cells. The colonies were manually counted after crystal violet staining. Paired t-test ns  $p > 0.05$ , \* $P < 0.05$ , \*\* $P < 0.01$ , \*\*\* $P < 0.001$  and \*\*\*\* $P < 0.0001$  ( $N \geq 3$ )

Api5 KD MCF10AT1 and MCF10CA1a showed reduced colony formation ability as confirmed with fewer colonies (Fig 3.37). This suggests that Api5 is essential for the survival of malignant cells and the formation of their colonies.

### 3.2.10 Api5 overexpression results in anchorage-independent growth of breast epithelial cells.

Api5 OE cells are found to cause transformation of breast epithelial cells, induce partial-EMT, and increase cellular migration. These characteristics can often be associated with the ability to grow in an anchorage-independent manner. For studying this, 3D dissociated cells were grown on soft agar. Then, 21 days post-seeding, the cells were stained with MTT to find the number of live colonies. Colonies are counted manually using images from 10 random positions on each well of a six-well dish.

Api5 OE resulted in anchorage-independent growth, as evident from the increased number of colonies formed by the cells on soft agar (Fig 3.38).

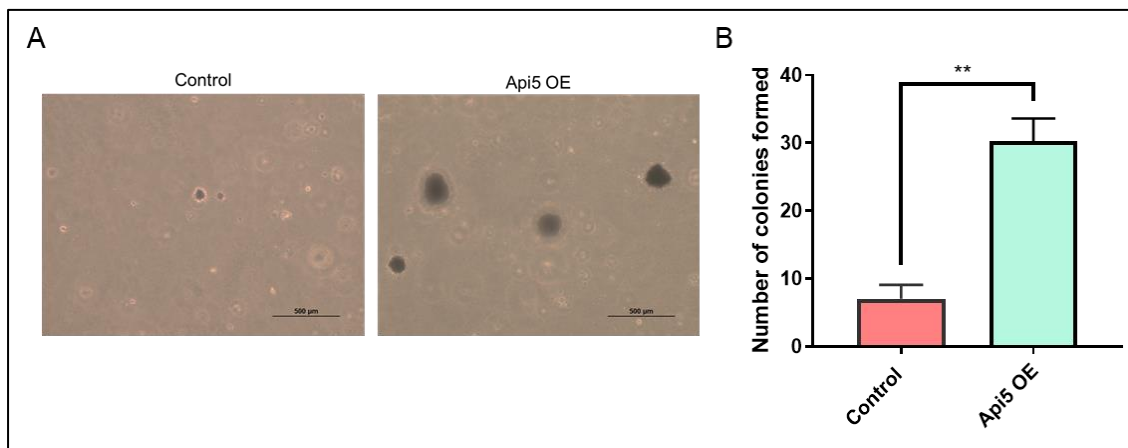


**Fig 3.38** Api5 overexpression induces the ability to grow in an anchorage-independent manner.

a) Representative image showing colonies of cells formed in soft agar post 21 days of seeding b) Quantification showing the number of colonies counted manually. Mann-Whitney test, ns  $p > 0.05$ , \* $P < 0.05$ , \*\* $P < 0.01$ , \*\*\* $P < 0.001$  and \*\*\*\* $P < 0.0001$  ( $N \geq 3$ )



Anchorage-independent growth is a common phenotypic characteristic shown by malignant cells. To understand whether Api5 is necessary for malignant cells to grow in an anchorage-independent manner, we carried out a soft agar colony formation assay using Api5 KD MCF10CA1a and MCF10AT1 cells.

The culture was supplemented with growth media, and it was changed every four days. MCF10CA1a cells were stained with MTT after seven days, while MCF10AT1 were stained after 21 days. MCF10CA1a forms large colonies by day 7, while Api5 knockdown reduced the number of colonies. Similar results were observed in MCF10AT1 cells as well (Fig 3.39). This suggests that Api5 is required for the anchorage-independent growth of breast cancer cells.

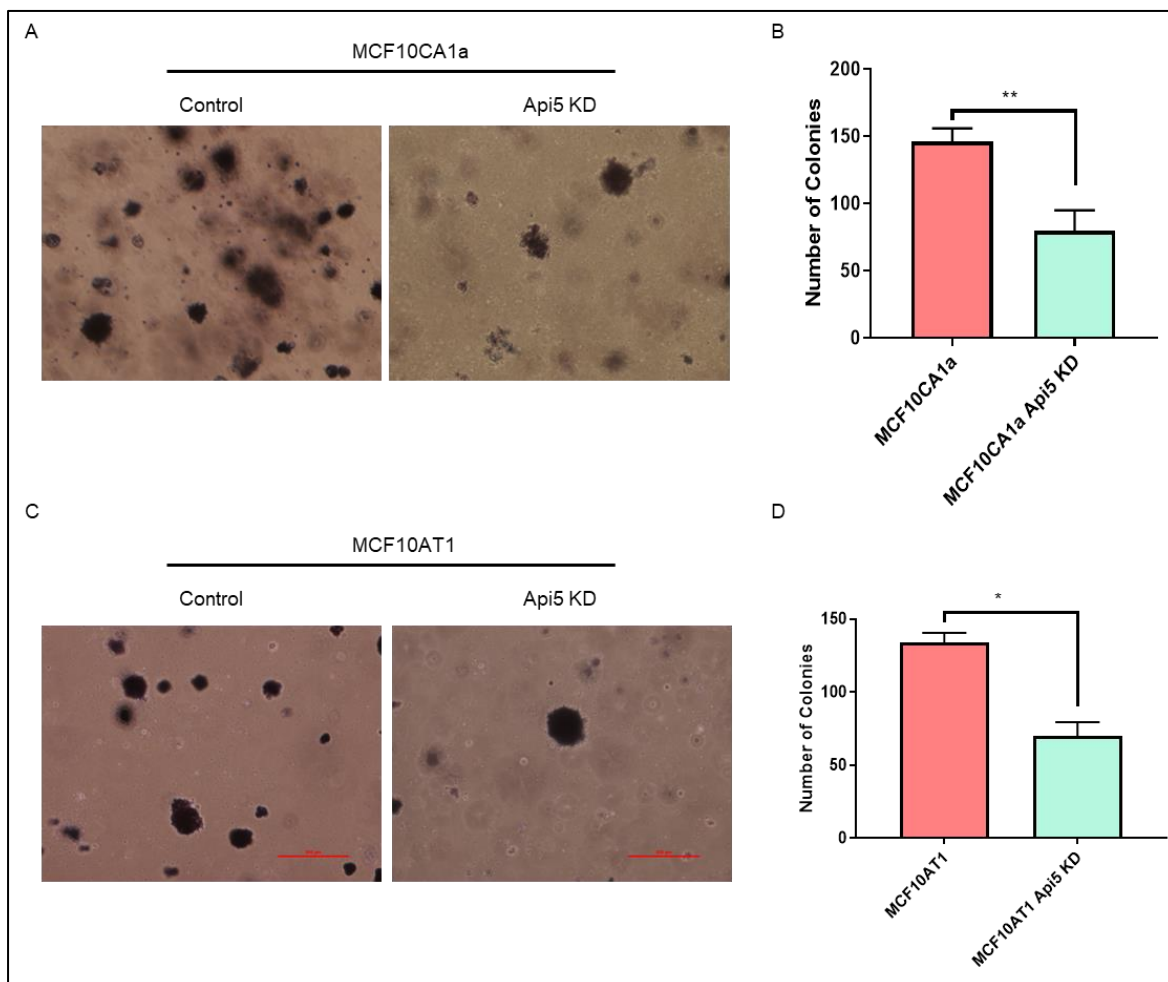


**Fig 3.39** Api5 knockdown results in reduced ability to grow in an anchorage-independent manner.

Representative image and quantification showing colonies formed by (a & b ) MCF10CA1a and (c & d) MCF10AT1 with Api5 KD compared to control cells.

Colonies are stained with MTT, and images were taken at 10X magnification using a

light microscope attached digital camera.  $N \geq 3$ , Mann Whitney test,  $ns\ p > 0.05$ ,  $*P < 0.05$ ,  $**P < 0.01$ ,  $***P < 0.001$  and  $****P < 0.0001$

### 3.2.11 To investigate whether Api5 overexpression can induce *in vivo* tumorigenic potential.

Anchorage independent growth is a characteristic shown by malignant cells. Our results showed that Api5 OE resulted in anchorage independent growth of epithelial cell line. This suggested that the cells might have also acquired malignant potential. To confirm this *in vivo* tumorigenicity assays were carried out.

Api5 overexpressing MCF10A and control cells were seeded on Matrigel and cultured for 16 days before dissociating the 3D acinar structures. The dissociated cells were injected into Athymic nude mice on their flanks. The animals were grown in environment-controlled chambers for 12 weeks. 2 weeks post-injection, a small growth was observed on the flank where Api5 overexpressing cells were injected but later, by the fifth week, the growth regressed. Repeating the studies using a single mouse injected with control cells on one flank and Api5 overexpressing cells on the other confirmed that Api5 overexpression did not lead to *in vivo* tumorigenesis in MCF10A cells (Fig 3.40).

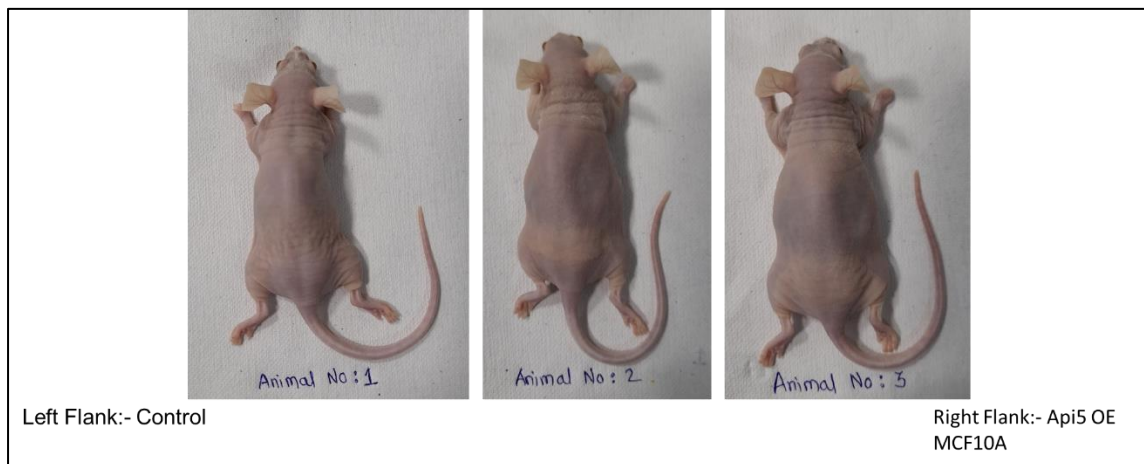


**Fig 3.40** Api5 OE does not induce *in vivo* tumorigenic potential in MCF10A cells. Athymic nude mice injected with control and Api5 overexpressing 3D dissociated cells. Images show mice after 12 weeks of injection of cells. ( $N=3, n=8$ )

MCF10CA1a cells in culture are confirmed to form a tumour in athymic mice when injected subcutaneously to the flank at a cell count of 4 million cells. The size of the tumour reached around 10% of the weight of the mice within 6 to 8 weeks post-injection. When MCF10CA1a cells with Api5 KD were injected similarly, it resulted in a more nominal growth as compared to the control (Fig 3.41-3.42).

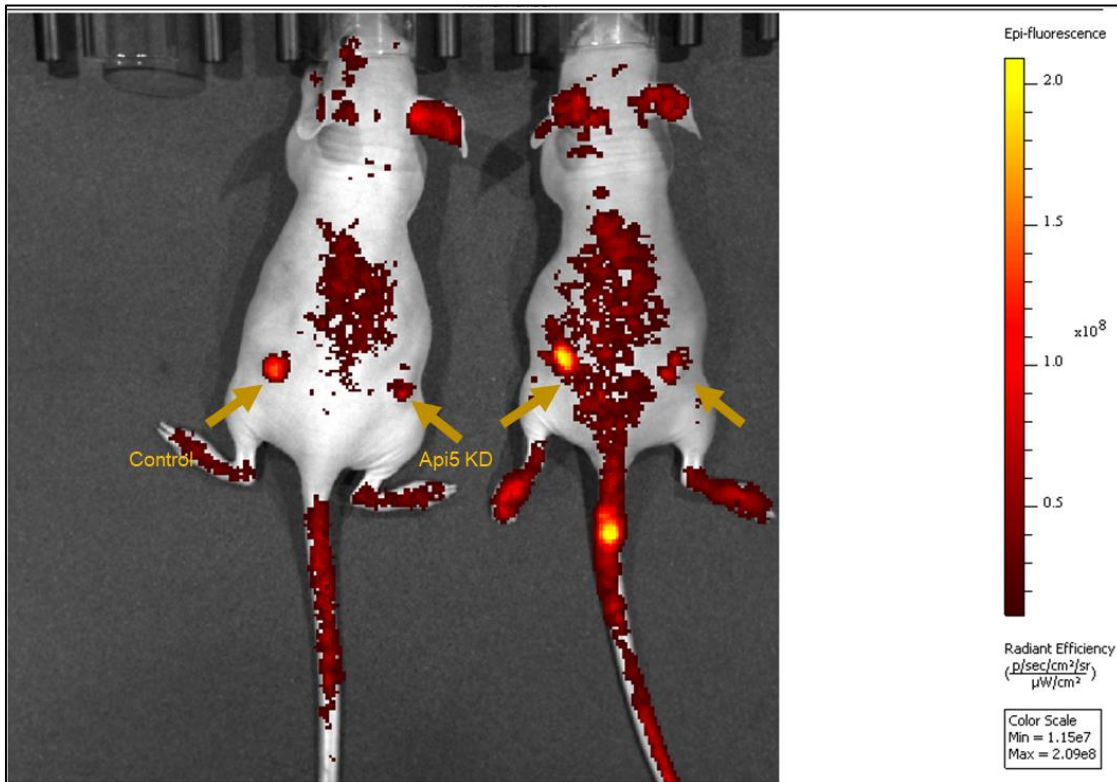


**Fig 3.41** Api5 KD in MCF10CA1a affects tumor growth *in vivo*.

Athymic nude mice injected with 4 million control MCF10CA1a cells (Left flank) and 4 million MCF10CA1a Api5 KD cells (Right flank). The fluorescence intensity images are taken on Week 2 post-injection.

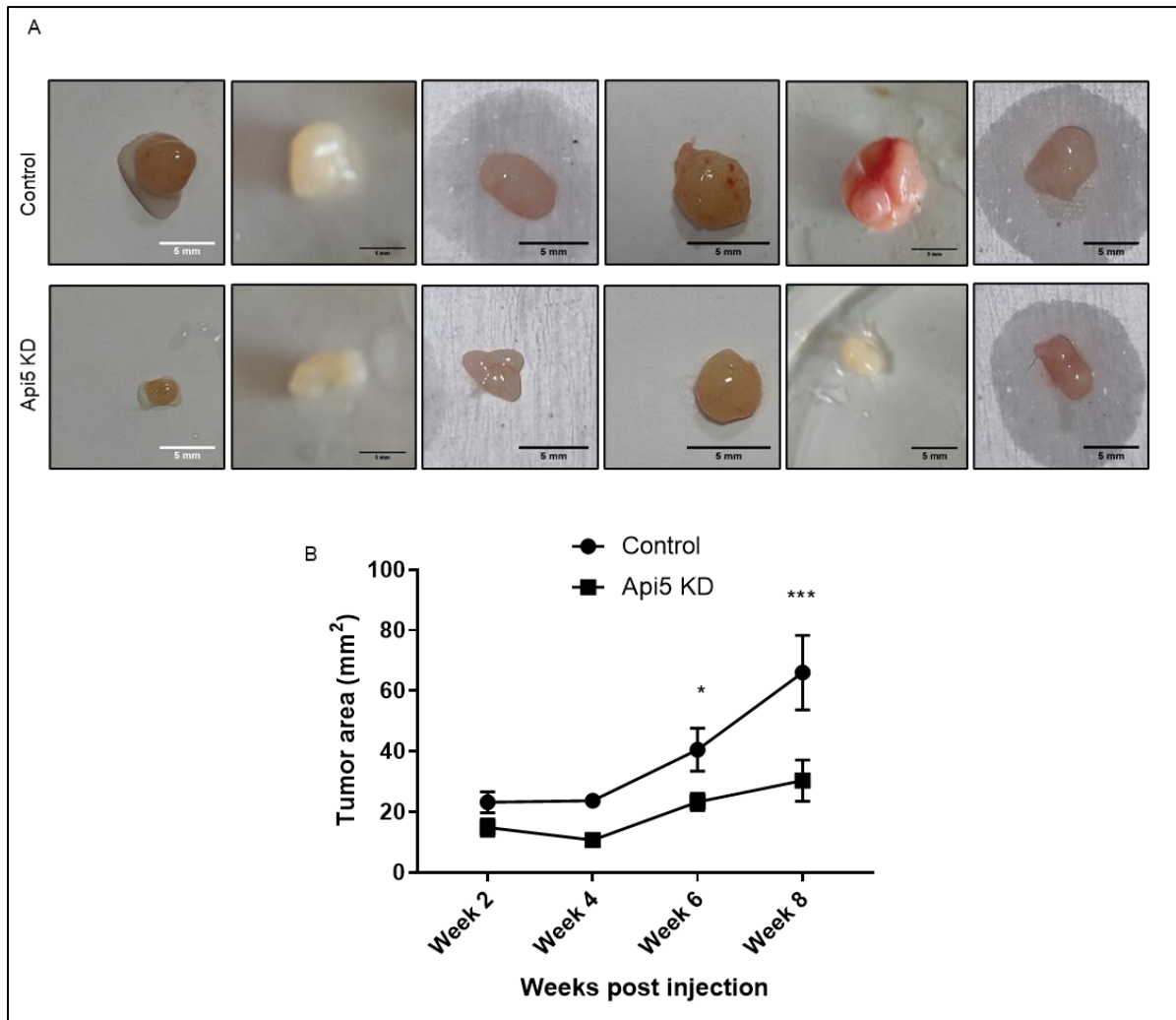


**Fig 3.42** Api5 knockdown reduces in vivo tumorigenicity potential.

a) Images of tumour dissected from Athymic mice injected with MCF10CA1a and MCF10CA1a Api5 KD cells after 8 weeks. b) Comparison of tumour area during the tumour growth measured using a vernier calliper. 2-way ANOVA followed by Sidak's multiple comparison test, \* $P < 0.05$ , \*\* $P < 0.01$ , \*\*\* $P < 0.001$  and \*\*\*\* $P < 0.0001$ ,  $N = 3$ ,  $n = 12$

Studies with both overexpression and knockdown confirmed that Api5 is involved in initiating and maintaining breast cancer. In addition, results confirm that Api5 can regulate various carcinogenic phenotypes such as proliferation, apoptosis, migration, and anchorage-independent growth.

### 3.3 Discussion

The breast is a glandular epithelium that undergoes constant remodelling during a female's lifetime (Javed and Lteif, 2013; Macias and Hinck, 2012). The changes in morphology and characteristics of the gland happen in response to hormonal changes. At the same time, Breast cancer is the primary cause of cancer-associated death in women worldwide (GLOBOCAN, 2020). Identifying molecular players associated with breast carcinogenesis would help in better management of the disease. Biomarkers that aid in early detection could help in extending the survival chances of the patient. Also, identifying oncogenes that drive breast carcinogenesis can create possible novel drug regimens that also helps in better patient survival (Ben-Hamo et al., 2020).

Studies have pointed out that understanding breast morphogenesis could provide insights into breast cancer management (Turashvili et al., 2005). Deregulation of the signalling cascades involved in breast morphogenesis can trigger carcinogenesis (Howard and Ashworth, 2006). Such changes also lead to altered morphology in breast acini. Apoptosis is a major mechanism involved in the proper development and maintenance of organs. In the breast, apoptosis plays an essential role during the cyclic events that happen in response to hormones, and it also mediates the involution process post lactation (Mailleux et al., 2008). Oncogene activation can hinder this apoptosis activation and thus favour carcinogenesis in the breast (Debnath et al., 2002). Apoptosis cascade signals mainly through extrinsic or intrinsic pathways. The intrinsic pathway activates the Bcl2 family of proteins, including Bim (Dewson et al., 2010; Elmore, 2007). Bim is an essential factor in apoptosis during breast acinar morphogenesis that regulates the lumen clearance (Reginato et al., 2005). Regulators of apoptosis, Bcl2 family proteins and IAPs, are often deregulated in various cancers (Pluta et al., 2015). Apart from these proteins, Api5 is an apoptosis inhibitor identified as a possible oncogene (Song et al., 2017). Api5 regulates apoptosis by regulating multiple molecular pathways such as ERK signalling, Caspase activation and E2F1 mediated gene expression regulation (Morris et al., 2006; Noh et al., 2014). Our study identifies the involvement of Api5 in breast carcinogenesis. A few recent reports have suggested the possibility of Api5 supporting breast carcinogenesis. However, a detailed explanation of the importance and the involvement of Api5 in breast carcinogenesis was not attempted. Using 3D

cultures, we identified the necessity of Api5 in breast malignancy and we also found that it can regulate various characteristics that once altered can promote cancer.

Oncogene overexpression can lead to the transformation of breast epithelial cells (Debnath et al., 2003b). Such transformation alters the morphological and biochemical characteristics of the epithelial cells. These changes in cellular characteristics are also observed in malignant breast cells *in vivo* (Halaoui et al., 2017; Makki, 2015). Acini is the basic functional unit of the breast gland. *In vivo* acini consist of a single layer of basal cells surrounded by myoepithelial cells. The hollow lumen connects to ducts that carry milk to the nipple (Vidi et al., 2013). Malignancy in the breast leads to the filling of lumen and ducts with transformed cells. MCF10A 3D acinar cultures present a reliable model for studying the impact of altered gene expression in breast epithelial cells. This can be utilised to understand the function of genes during breast morphogenesis as well as in cancers.

Using breast acinar cultures of MCF10A cells, we found Api5 OE results in a partially/wholly filled lumen. This suggests that Api5 OE in breast epithelial cells can trigger transformation potential. Furthermore, an increase in cell number and thus the size of the acinar structures confirmed that Api5 OE could transform breast epithelial cells. Furthermore, Api5 KD in breast malignant cell lines confirmed that the protein plays a significant role in breast carcinogenesis.

Epithelial cells form polarised acinar structures in the breast gland (Debnath and Brugge, 2005; Vidi et al., 2013). The polarised structures help in maintaining the structure and integrity of the glandular epithelium. Along with this, cadherin junction and desmosomal junctions play a significant role in maintaining glandular epithelium. These characteristic features prevent uncontrolled growth and migration of the cells (Andrews et al., 2012). Malignancy in the breast can result in altered or disrupted polarity in breast epithelial cells (Debnath et al., 2003a). Disruption of polarity helps in elevated cellular proliferation and migratory potential. Api5 OE resulted in the loss of apico-basal polarity. The characteristics are well known to be associated with the transformation of breast epithelial cells. We also observed that Api5 OE resulted in a loss of cadherin junction, thus suggesting a possibility of altered epithelial characteristics of the cells.

Malignant epithelial cells often tend to undergo EMT, which shifts the phenotypic and molecular characteristics of the cells (Roche, 2018). Loss of cell polarity is also often associated with EMT induction (Moreno-Bueno et al., 2008). Higher levels of mesenchymal molecular markers such as Vimentin, Slug and Twist suggest EMT in epithelial cells. Recent studies have also uncovered a partial-EMT state in malignant cells, exhibiting both epithelial and mesenchymal characteristics (Jolly et al., 2015). This hybrid-EMT or partial EMT state is found to promote malignant cell survival, migration and metastasis (Saitoh, 2018).

Interestingly, Api5 OE resulted in higher expression of Vimentin, Slug, and Twist. At the same time, the cells also showed higher E-cadherin levels. This suggested partial-EMT like characteristics. Furthermore, we observed that Api5 OE MCF10A cells dissociated from 3D cultures migrated faster than the control cells. Our result indicates that Api5 OE altered the epithelial cells' characteristics, attaining a higher migratory potential.

Further studies also revealed that Api5 OE results in anchorage-independent growth of breast epithelial cells, a well-known characteristic of malignant cells. Cancer cells can multiply and form colonies even without attachment to a matrix (Mori et al., 2009). This helps in the growth of these cells in adverse conditions as well. Our studies using Api5 KD MCF10CA1a cells confirmed that Api5 is necessary for the anchorage-independent growth of the cancer cells. *in vivo* tumorigenicity studies confirmed that Api5 plays a significant role in breast carcinogenesis. Although Api5 OE did not result in tumour growth *in vivo*, Api5 KD in malignant cells negatively affected tumour formation.

Taken together, our data indicate that Api5 is a significant player in breast carcinogenesis. We have also proved that Api5 expression is necessary to maintain multiple malignant phenotypes (Fig 3.43). The fact that overexpression of a single gene resulted in various characteristic changes in the epithelial cell suggests that Api5 could regulate various signalling events in breast carcinogenesis.

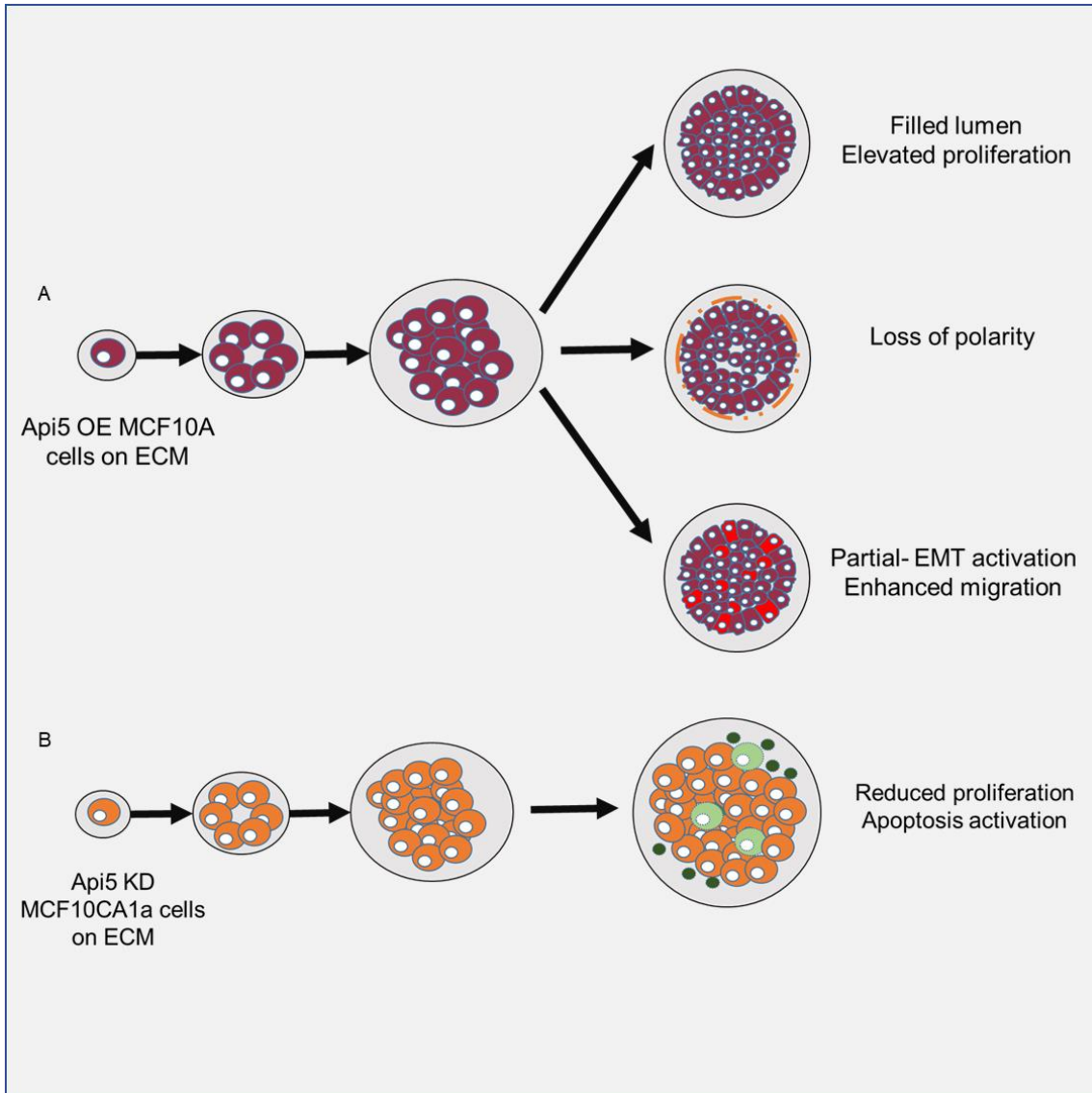


**Fig 3.43** Summary graphics showing the effect of Api5 OE in epithelial cell line and Api5 KD in the malignant breast cell line.



## **Chapter 4: Api5 regulates Akt and ERK signalling through FGF2**

### 3.1 Background

Api5 is reported to interact with FGF2 directly, a growth factor that is well known to be associated with development and malignancy (Maehara et al., 2017; Noh et al., 2014). Api5 is well established as significant regulator of FGF2 signalling (Jang et al., 2017; Noh et al., 2014). Api5 is also known to regulate apoptosis and cell proliferation (Garcia-Jove Navarro et al., 2013; Morris et al., 2006). The effects may be combined through the FGF2 signalling.

During breast acinar growth, the gland undergoes a series of proliferation, apoptosis, and polarisation. FGF2 is known to be a major player involved in the proliferation and growth of the breast gland (Zhang et al., 2014). The FGF-FGFR family members are significant regulators of breast ductal growth and differentiation. Reduced levels of the FGFR are known to slow down the process as well (Sumbal and Koledova, 2019).

FGF family members are upregulated in malignant cancers. The FGF upregulation can activate diverse signalling cascades, including PI3K/Akt and MAPK signalling (Okada et al., 2019). Api5 is known to regulate Bim expression through FGF2-ERK signalling (Noh et al., 2014). Bim is a proapoptotic molecule that is also known to regulate the apoptosis of cells in the lumen during MCF10A acinar morphogenesis (Mailleux et al., 2007). Overexpression of Api5 led to lumen filling, thus suggesting possible deregulation of Bim through FGF2- ERK signalling.

The morphometric changes strongly suggested that Api5 OE alters several of the characteristic features of the MCF10A acini. This suggested that Api5 might be regulating various cellular events during the growth of the MCF10A acini.

MCF10A acinar morphogenesis recapitulates the significant events that happen *in vivo* (Debnath et al., 2003a). This includes proliferation, polarisation and apoptosis of cells. Studies have shown the importance of various signalling events during acinar morphogenesis, such as ERK and Akt (Debnath et al., 2003b; Worster et al., 2012). The altered expression of Akt is also known to affect the morphometry of the acini. The results from this study showed filling up of lumen and loss of polarity due to Akt overexpression (Debnath et al., 2003b). Another group have reported the effect of cMYC overexpression. Interestingly, they observed that the morphogenesis of MCF10A acini could prevent the cMYC overexpression induced changes of the

acini(Simpson et al., 2011). ERK signalling has also been reported to be involved in the regulation of acini morphogenesis. Altered expression of several plausible oncogenes led to activation of ERK signalling as well.

Oure results indicate that Api5 OE resulted in altered signalling during the acinar morphogenesis. It upregulates FGF2-PDK1-Akt/cMYC signalling during early days of morphogenesis while the axis shifted to FGF2-Ras-ERK-Bim signalling during the later days.

## **4.2 Result**

### **4.2.1 To investigate the molecular mechanism behind Api5 mediated breast epithelial cell transformation**

Api5 overexpressing MCF10A grown in 3D cultures lysed every four days during the 16 days culture, and the lysates were used for immunoblotting assay probing for the possible pathway players. As the ERK-mediated Bim degradation pathway is known to be associated with Api5 mediated tumour formation in an immunodeficient murine cell line, we initially focused on the same pathway. Also, while analysing the apoptosis during MCF10A acinar morphogenesis, Bim showed a reduction on Day 12 compared to control cells. Therefore, molecular players involved in this signalling were studied to understand further if Api5 OE activated FGF2-ERK signalling.

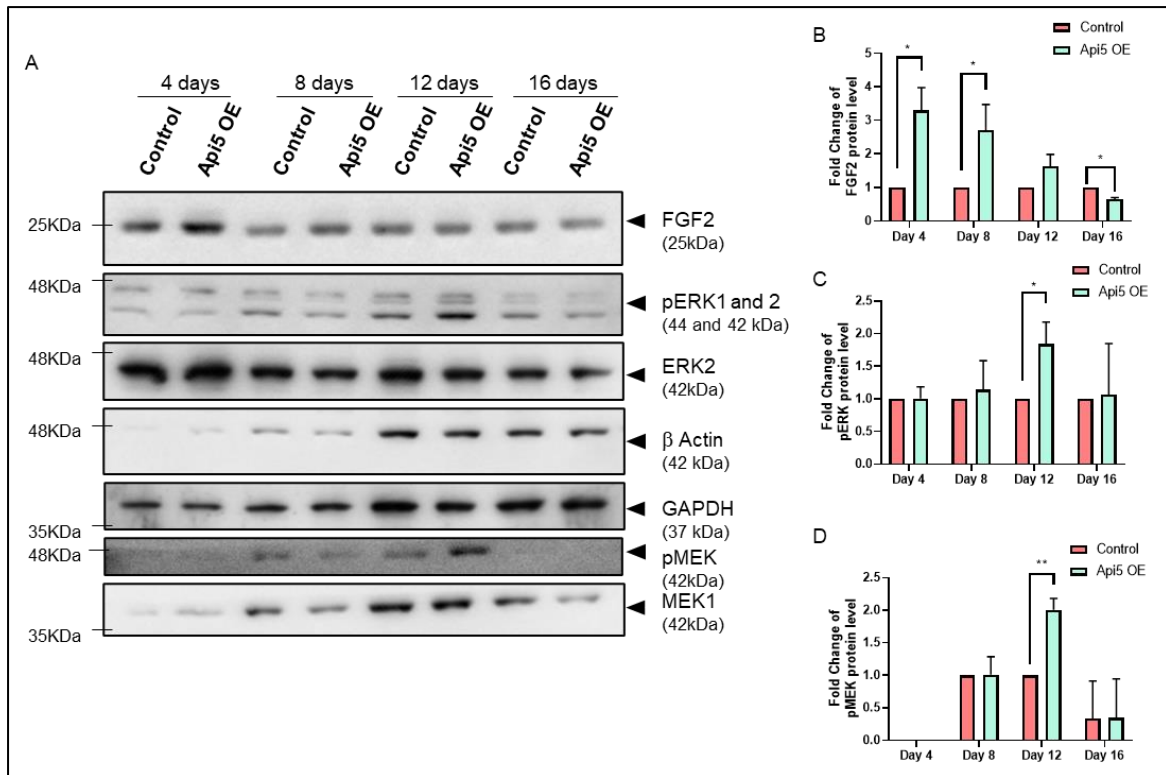


**Fig 4.1** Api5 overexpression results in ERK signalling activation during late days of MCF10A acinar morphogenesis.

a) Western blot showing expression of FGF, pERK 1&2, and pMEK. b) Graph showing fold change in FGF2 levels normalised to GAPDH and compared with Day 4. c) Graph showing fold change in pERK levels compared against control on each day and normalised to total ERK. d) Graph showing fold change in pMEK levels compared against control on each day and normalised to total MEK1. (N>3), Paired t-test, ns  $p>0.05$ , \* $P<0.05$ , \*\* $P<0.01$ , \*\*\* $P<0.001$  and \*\*\*\* $P<0.0001$  (N≥3)

Api5 OE resulted in activation of ERK and MEK during late days of acinar morphogenesis (Fig 4.1). This activation coincided with the Bim degradation observed, thus confirming ERK signalling leading to Bim degradation and reducing apoptosis. Also, ERK signalling is known to induce EMT and sustained proliferation (Huang et al., 2021; Shin et al., 2019).

Interestingly, FGF2 was upregulated from Day 4 through Day 12. This suggested that Api5 OE induced FGF2 activation might be activating some other signalling initially. Since FGF2 is known to activate PI3K/Akt signalling, Api5 OE MCF10A lysates were studied for Akt signalling.

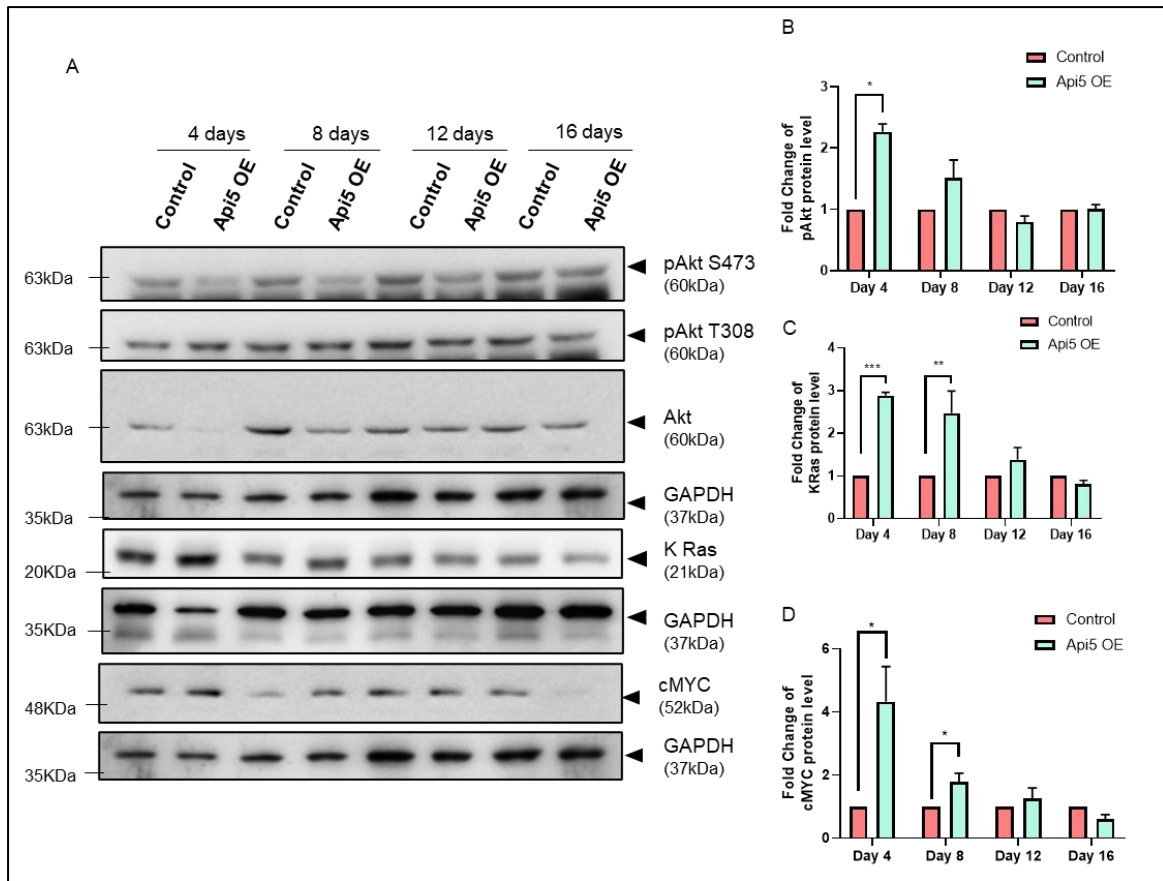


**Fig 4.2** Api5 OE results in FGF2 mediated PDK1-Akt signalling.

a) Immunoblot showing expression of pAkt, cMYC and KRas in Api5 OE MCF10A lysates, b) Fold change of pAkt T308, c) KRas, and d) cMYC during the morphogenesis of MCF10A acini culture. (N>3), Paired t-test, ns p>0.05, \*P<0.05, \*\*P<0.01, \*\*\*P<0.001 and \*\*\*\*P<0.0001 (N≥3)

Results indicated that Api5 OE resulted in phosphorylation of T308 residue of Akt during the early days of acinar morphogenesis. This phosphorylation is known to be carried out by the PDK1 enzyme (Dangelmaier et al., 2014). Activation of PDK1 leads to activation of cMYC. Immunoblot confirmed cMYC upregulation from Day 4 through Day 8 of acinar morphogenesis (Fig 4.2).

Immunoblotting also showed that KRas levels are upregulated similarly to cMYC during the early days of morphogenesis. This suggests that Api5 OE through FGF2 might signal PI3K/KRas-PDK1-Akt/ cMYC during the early days of morphogenesis while FGF2-KRas-MEK-ERK signalling functions during later days of

morphogenesis. To confirm that Api5 can regulate these signalling pathways, Api5 KD MCF10CA1a 3D culture lysates were assayed.

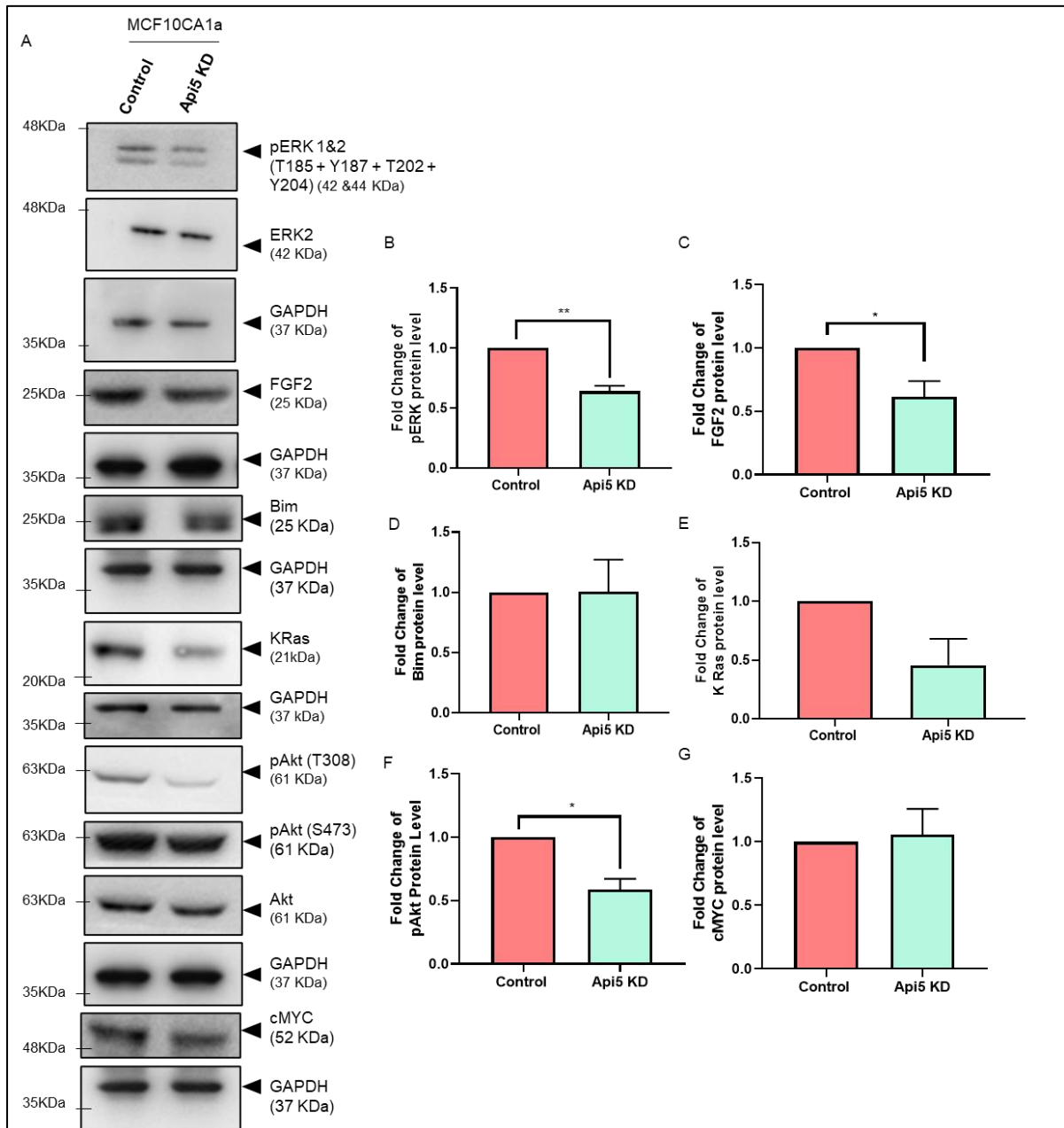


**Fig 4.3** Api5 KD results down-regulate FGF2-Akt/ ERK signalling

a) Western blot showing expression of pERK, pAkt, KRas, cMYC and FGF2 in Api5 KD MCF10CA1a 3D lysates. Fold change of b) pERK, c) FGF2, d) Bim, e) KRas, f) pAkt and g) cMYC in Api5 KD MCF10CA1a lysates compared to control and normalised to GAPDH or total proteins for phospho markers. (N>3), Paired t-test, ns  $p > 0.05$ , \* $P < 0.05$ , \*\* $P < 0.01$ , \*\*\* $P < 0.001$  and \*\*\*\* $P < 0.0001$  ( $N \geq 3$ )

Api5 KD in MCF10CA1a resulted in reduced ERK and Akt activation in 3D culture lysates. Also, FGF2 levels were reduced in Api5 KD lysates. Although Bim and cMYC did not show any change, possibly due to alternative signalling mechanisms present in the malignant cells (Fig 4.3).

### 4.3 Discussion

MCF10A acinar morphogenesis can provide insights into breast gland development. At the same time, the same complex signalling are altered during malignancy of the breast. Many events that regulate the morphogenesis of MCF10A acini are deregulated in breast cancer. This includes ERK signalling and Akt signalling (Bartholomeusz et al., 2012; Guo et al., 2020; Paplomata and O'Regan, 2014).

Debnath *et al.* have shown that activation of Akt can disrupt acinar morphogenesis(Debnath et al., 2003b). They found that activation of Akt elevates proliferation during the early stages of breast morphogenesis. In our study, we observed a similar event where Api5 OE resulted in Akt activation during the early days of morphogenesis. This could suggest proliferative signalling were activated by Akt due to Api5 OE. We also observed that FGF2 expressions were upregulated from early days to alter days of morphogenesis.

Increased levels of FGF in organoid cultures are known to induce invasion of the cells to the extracellular matrix(Zhao et al., 2015). We observe larger acinar structures formed by Api5 OE, possibly through the activated FGF signalling cascade. Interestingly, we also observed higher proliferative capacity and reduced apoptosis. FGF2 mediated Akt signalling could be supporting elevated proliferation during the early days of MCF10A acinar morphogenesis. Api5 through FGF2/ERK signalling is known to degrade Bim and thereby regulate apoptosis. Our studies also found that Bim levels are reduced during later days of MCF10A acinar morphogenesis. This coincided with the activation of MEK and ERK, as confirmed by phosphorylation of these signalling kinases. Bim is a significant regulator involved in lumen clearance during MCF10A acinar morphogenesis. Oncogene mediated filling of the lumen is known to be achieved through ERK-mediated Bim degradation (Reginato et al., 2005). Thus Api5 OE could be activating higher proliferation during the early days through FGF2 Akt signalling while later it suppresses apoptosis by Bim degradation. Moreover we also observed reduced levels of active caspase-9.

Early activation of Akt was only observed at the T308 site of Akt, which suggested the possibility of involvement of other signalling events due to Api5 OE. T308 site of Akt is phosphorylated by PDK1 kinase. Activation of PDK1 is also known to activate the PDK1-cMYC axis. This axis is known to cause the transformation of cells as well



as induce stem cell-like properties. Interestingly, we also observed that Api5 OE resulted in higher cMYC expression during the early days of morphogenesis. Along with cMYC, we also observed higher levels of KRas. Thus Api5 OE might be resulting in activation of FGF/ KRas/ PDK1/ Akt and PDK1/ cMYC axis. This early activation could promote polarity disruption and higher proliferation. This signalling gets switched to ERK pathway during the later days of acinar morphogenesis, reducing apoptosis and supporting sustained proliferation.

Our study unveils Api5 being a central regulator of multiple key signalling cascades (Fig 4.4). Overexpression of Api5 thus can result in disruption of several cellular which thereby promoted transformation events as observed in our studies.

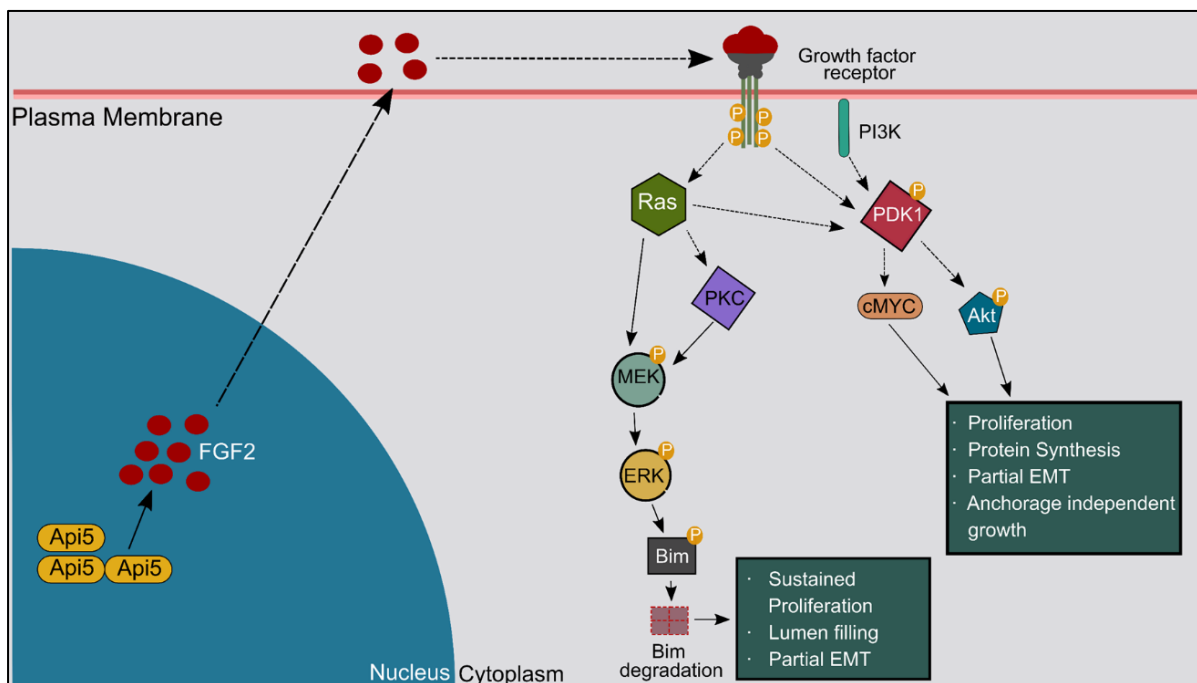


**Fig 4.4** Schematic showing the signalling mechanisms in which Api5 affect breast carcinogenesis.

**Chapter 5: Breast cancer patients have upregulated  
API5 levels which predicts poor patient survival**

## 5.1 Background

Apoptosis is a major pathway involved in cellular homeostasis. The central signalling cascades of apoptosis, extrinsic and intrinsic pathways, senses both external and internal stimuli for initiating programmed cell death(Elmore, 2007). Several proteins tightly regulate these signalling events. Deregulation of these proteins is very often associated with malignancies(Lowe and Lin, 2000; Wong, 2011). Increased levels of apoptosis inhibitors and reduced expression of proapoptotic molecules are reported in cancer patients. These changes can be at the protein level as well as transcript levels. Understanding this expression patterns can help in identifying cancer specific biomarkers and drug targets.

Studies have proven that using publicly available databases to understand genes' expression levels in cancers and correlate them to their role in disease progression could benefit in identifying biomarkers and new drug targets (Huang et al., 2015; Kalecky et al., 2020). One of the major databases that provide genomic expression data from patients is The Cancer Genome Atlas (TCGA). TCGA provides transcript level expression data of genes in 33 different types of cancer. The database provides access to clinico-pathological data of patients(Cancer Genome Atlas, 2012). These data have been widely used for understanding the role of candidate genes in cancers. Comparison studies of gene expression across different subtypes and adjacent normal tissues would provide a more significant base for building hypotheses.

GENT2 is another database that provides gene expression data of normal and tumour tissue, utilising multiple GEO datasets(Park et al., 2019). The same data can also be used to compare gene expression patterns across cancer subtypes and normal tissue. Putting data from TCGA and GENT2 together can provide a strong understanding of tumour tissue gene expression patterns.

A recent report shows that Api5 expression is upregulated in chemoresistant TNBC tissues(Bousquet et al., 2019). Another study has identified that API5 gene expression in breast cancer tissue is higher than normal using oncomine database(Basset et al., 2017). Otherwise, Api5 gene expression in breast cancer tissues remains largely unexplored. Identifying the gene expression pattern of Api5 in breast cancer could help in understanding the role of Api5 in breast cancer.

In this study, using TCGA and GENT2, we explored the expression pattern of API5 in breast cancer. Further, we also studied the correlation between API5 expression and patient survival using kmplotter. In addition to this, we identified the possible pathways that can alter due to higher expression of Api5 in breast cancer using coexpression analysis.

## **5.2 Results**

### **5.2.1 API5 expression is upregulated in tumour tissues as compared to adjacent normal tissue**

We have initially carried out the analyses to check the expression difference between tumour tissue and the adjacent normal tissue in breast cancer patients. Api5 transcript expressions were higher in tumour tissue than normal in the GENT2 database, although there were no differences in the TCGA database. This, along with the previous reports, confirms that Api5 transcript-level expression of Api5 is upregulated in breast cancer tissues compared to adjacent normal samples.

Thus, we analysed the possible difference in expression of Api5 in different subtypes (based on molecular subtype classification and receptor status).

The hormone receptors (estrogen receptor and progesterone receptor) and the Her2 receptor are molecular markers to help classify breast cancer. TNBC or Triple-negative breast cancer is a highly malignant type of breast cancer based on receptor status.

The data shows no significant difference except a significantly higher median for TNBC than hormone receptor positive, Her2 negative subset (According to Dunn's post hoc test).

To further understand the API5 expression in breast cancer patients, the TCGA dataset is divided based on molecular subtypes, either based on the Pam50 gene expression study or histopathological analyses. All these data are compared to adjacent normal data from the patients.

The data suggested significantly higher expression of API5 in basal subtype (which is the highly malignant subtype of breast cancer) compared to adjacent normal as well as Luminal A (which is the low malignancy subtype). Basal being a very

aggressive subtype of breast cancer, higher API5 expression suggests a correlation between aggressiveness and Api5 expression.

A similar analysis using the GENT2 database shows that API5 levels are significantly upregulated in all subtypes compared to normal tissues (Fig 5.1).

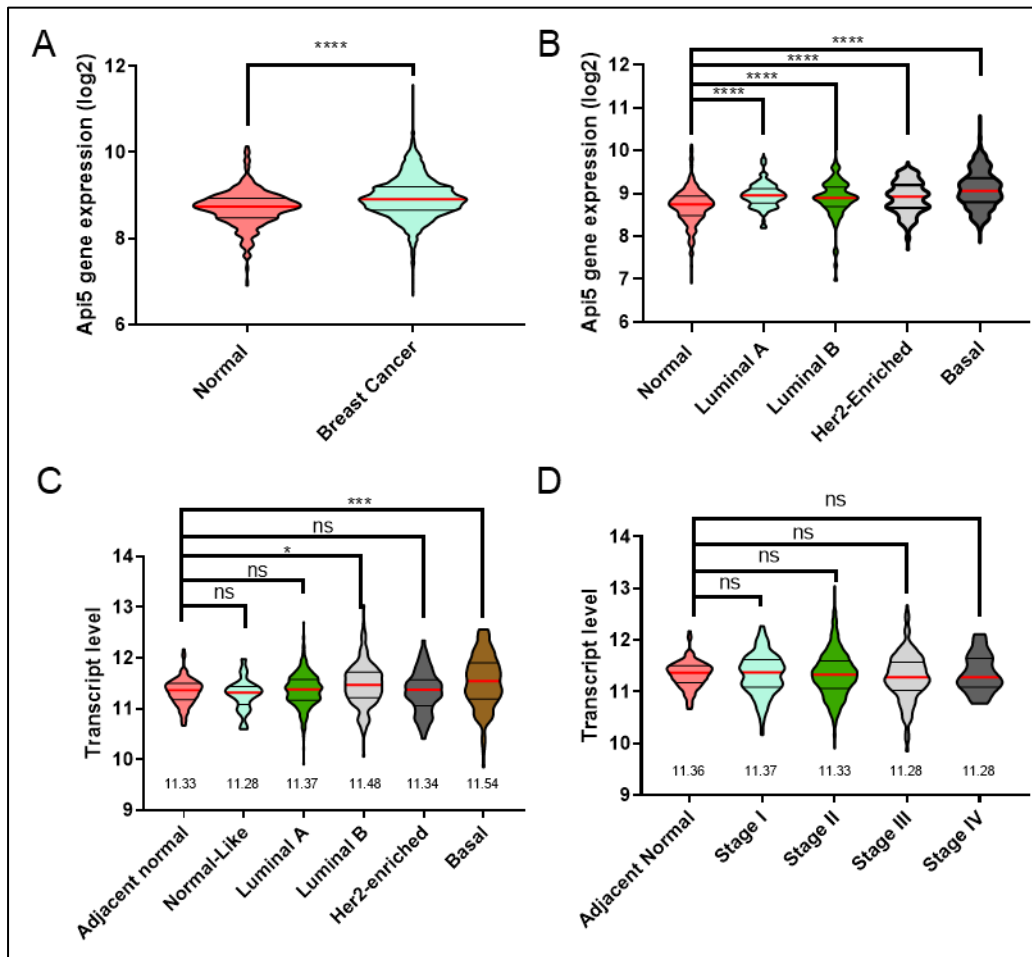


**Fig 5.1** Api5 transcript levels are upregulated in breast cancer.

a) Violin plot showing API5 expression in breast cancer tissue samples compared with normal tissue using GENT2 database. b) API5 expression compared across different molecular subtypes using GENT2 database, and c) TCGA database. d) API5 expression was compared across different stages compared using the TCGA dataset. Kruskal Wallis test and Dunn's post hoc test ns  $p > 0.05$ , \* $P < 0.05$ , \*\* $P < 0.01$ , \*\*\* $P < 0.001$  and \*\*\*\* $P < 0.0001$

We further tried to understand the expression of Api5 in different stages of breast cancer.

Data showed no significant difference in expression of Api5 between different stages. So, we further checked the expression based on menopause status, but that also did not show any significant difference in expression.

To understand if Api5 mRNA expression can predict patient outcome, kmplot analysis was carried out using the kmplotter tool and GENT2 database. Both the analysis revealed that high levels of API5 could predict poor survival of patients (Fig 5.2).

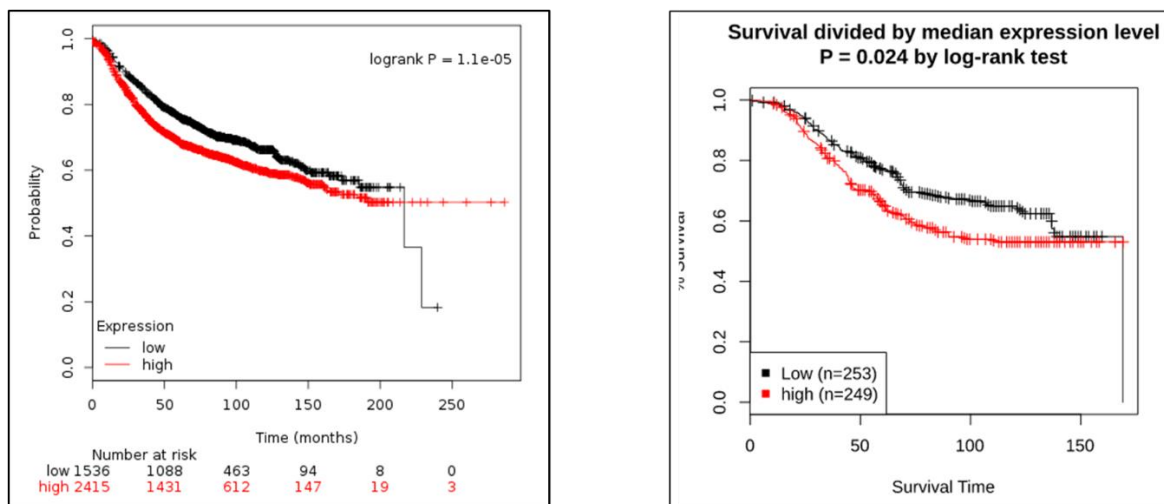


**Fig 5.2** Higher Api5 expression suggest poor patient survival.

Kaplan Meier plot shows the probability of patient survival based on API5 expression for 150-250 months plotted from kmplotter and GENT2. P-value mentioned as provided by the online tool.

The analysis was carried out with the help of kmplotter, an online tool that uses several microarray data for checking the disease-free survival based on the expression levels of any specific gene. We used the complete data set 201687\_s\_at, auto select best cut off, and only Jetset probe. We did not make any restrictions and asked the software to split the values based on the median. The data showed that higher expression of Api5 significantly correlates with poor survival of breast cancer patients. This suggests the possibility of a difference in expression at the protein level between highly malignant and less malignant breast tumours.

Similarly, in GENT2, the kmplot was plotted using the entire data available with the database without any filters.

### 5.2.2 Higher Api5 transcript expression correlates with elevated proliferation and affects cell-cell junction components

To delineate the molecular pathway associated with the Api5 mediated transformation of breast epithelial cells, we used 3D culture lysates and carried out immunoblot analyses. In addition, to further understand whether the same pathway are affected in breast cancer patients expressing higher levels of Api5, we used the TCGA data, and the expression of the possible molecular players was compared with API5 expression.

To narrow down the possible correlated genes, the entire TCGA database was divided based on API5 expression. Genes that are upregulated and downregulated in API5 high expression samples were selected. The survival plot for these genes was analysed to identify the genes that can predict patient survival in high API5 background. The final list of genes was used for DAVID platform-based pathway prediction. The results indicated that higher levels of API5 correlated with altered extracellular matrix composition, higher cell division and changes in plasma membrane composition (Fig 5.3-5.5). These results align with the *in vitro* data where we observed higher proliferation, polarity disruption and increase in migration. This suggests that Api5 could be regulating cell proliferation, polarity and migration *in vivo* as well.



**Fig 5.3** Steps involved in screening of genes used for DAVID based pathway prediction analysis.

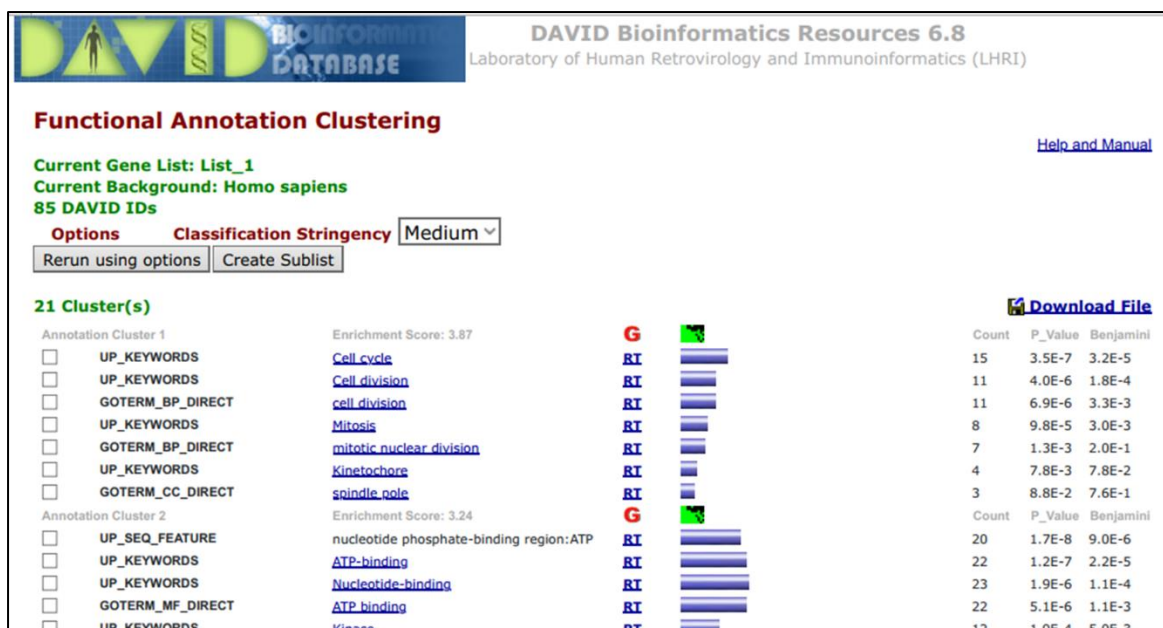


Fig 5.4 Results from DAVID analysis with Upregulated gene set as query genes.

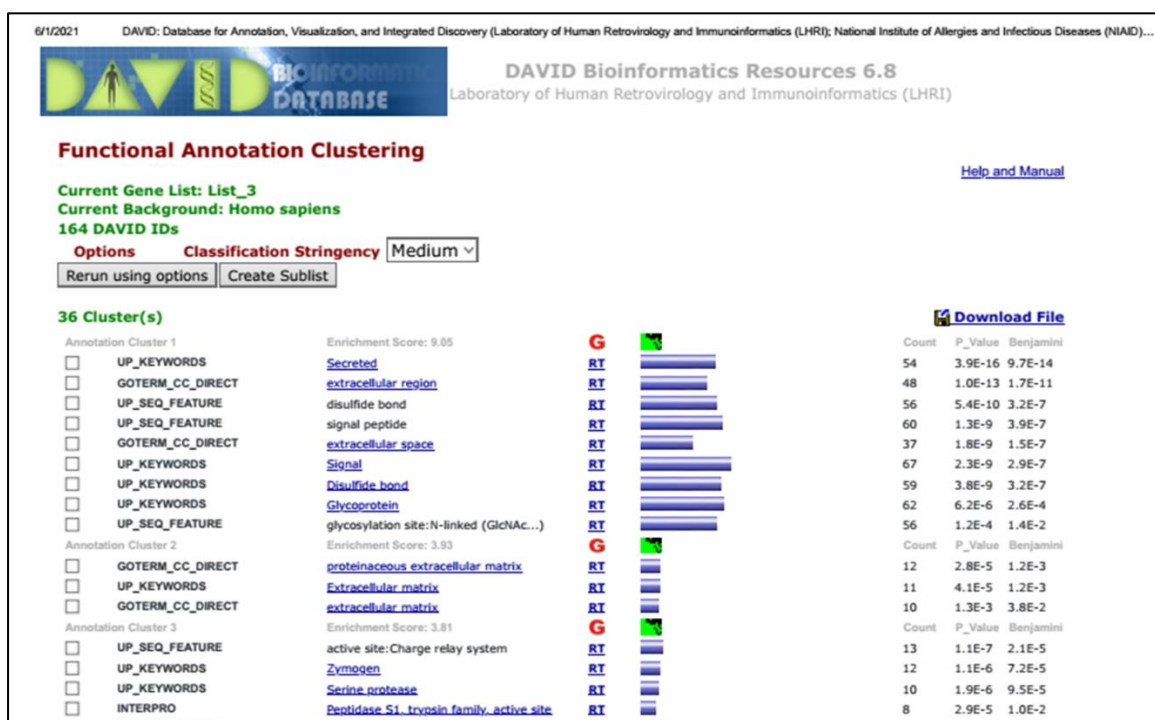


Fig 5.5 Results from DAVID analysis with down-regulated gene set as query genes.

KEGG pathways, cAMP signalling pathway and Cell cycle were found to be associated with higher Api5 expression (Fig 5.6 and 5.7). This suggests a possibility of elevated proliferative signalling through the cAMP pathway, which can also activate Akt signalling among other proliferative signalling in breast cancer patients with higher API5.



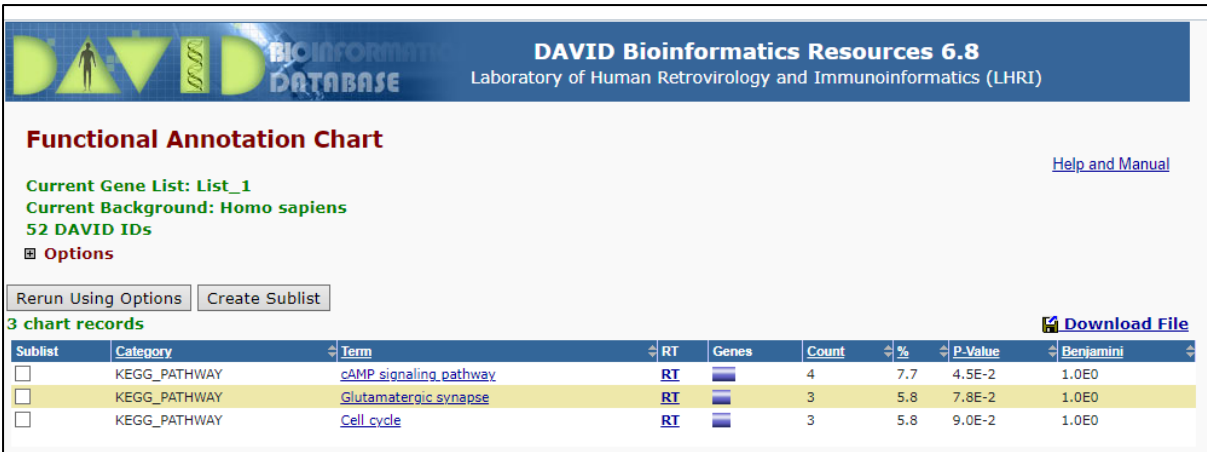


Fig 5.6 Results from DAVID platform when KEGG pathway terms were selected.

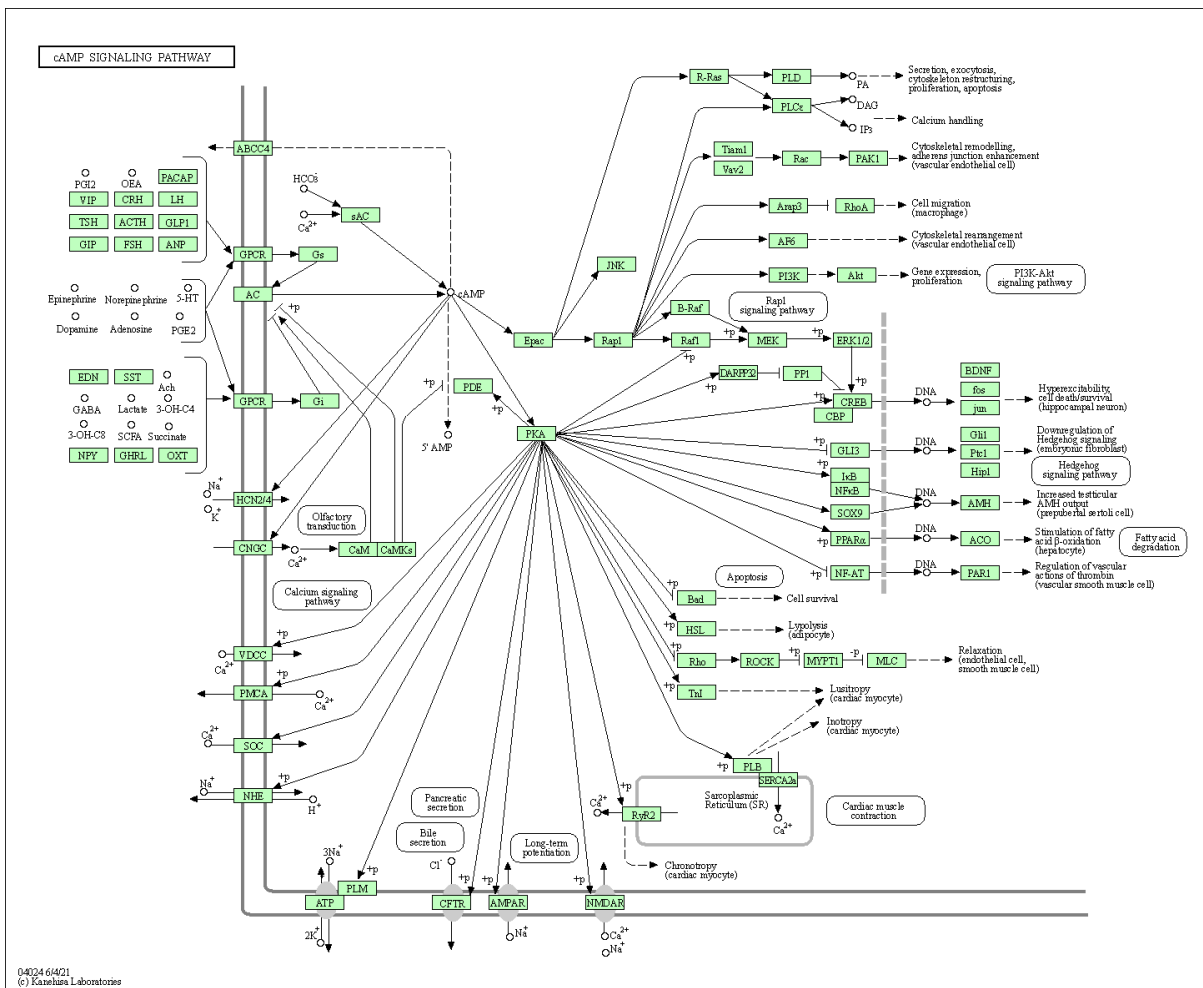
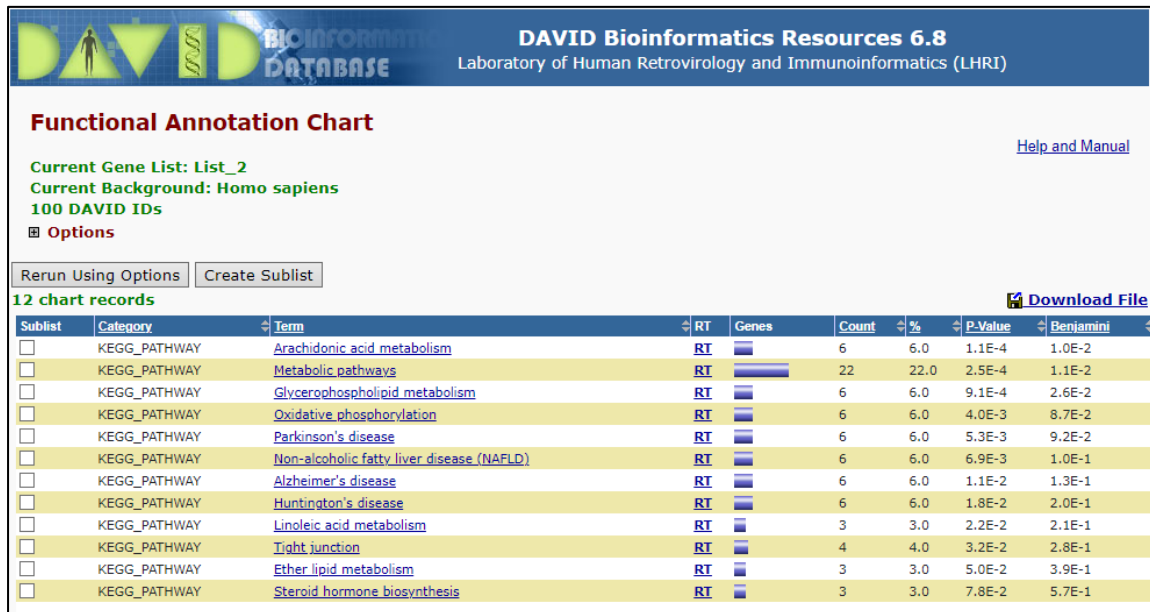


Fig 5.7 cAMP signalling pathway as shown by KEGG pathway

A similar analysis on downregulated genes showed a strong negative correlation with Metabolic pathways (Fig 5.8). This possibly can suggest regulation of metabolic

pathways by Api5 in breast cancer patients. Although how this would be supporting Api5's role in breast carcinogenesis would require further studies.



**Fig 5.8** Results from DAVID platform when KEGG pathway terms were selected after submitting negatively correlated gene list.

Interestingly Tight junction is also found in the list, suggesting a possible alteration of tight junctions in breast cancer patient samples with higher Api5.

Further using the TCGA dataset, correlation analysis was carried out to compare API5 and other genes identified by the *in vitro* studies. This revealed that API5 expression positively correlated with FGF2, ERK2, PDK1, KRAS and CMYC.

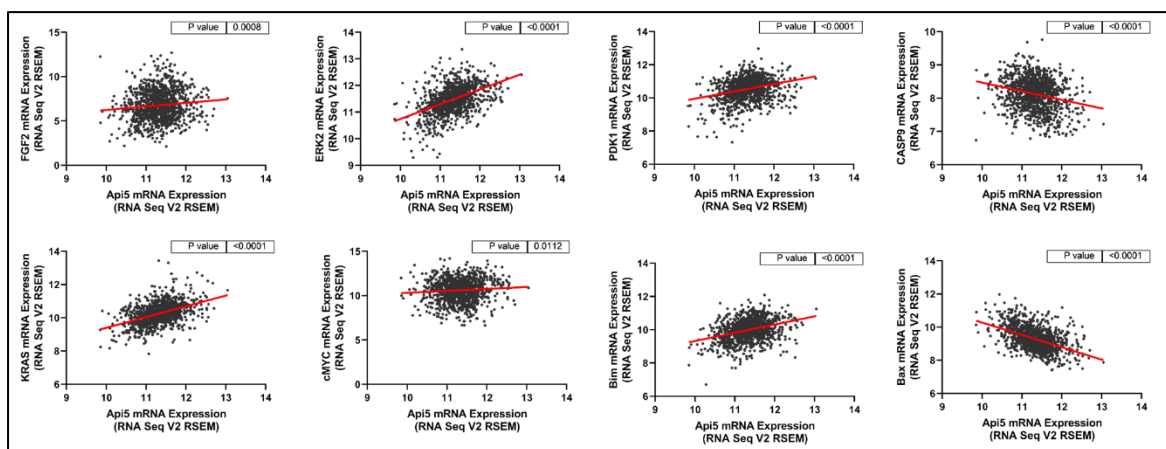


**Fig 5.9** Correlation between API5 expression and pathway players.

Plots show a correlation between API5 and mentioned genes in the TCGA database.

Results indicate that Api5 is possibly regulating both ERK and Akt signalling in breast cancer tissues as well. As observed in *in vitro* studies, this regulation would most probably be supported through FGF2-KRas signalling (Fig 5.9).

### 5.2.3 Immunohistochemical analysis of breast cancer samples

To understand the expression pattern of Api5 in Indian breast cancer patients, Immunohistochemical analysis was done using FFPE blocks. Prashanti Cancer Care Mission had provided breast cancer tissue blocks with the adjacent normal and reduction tissue of the other breast. Api5 expression levels were compared using IHC. We had standardised the dilution of the antibody by checking the staining in different breast tissues.

The staining was quantified as H scores. H scores are based on visual quantification of IHC staining based on positive percentage cells and staining intensity. The data is the median value of 3 independent observations.

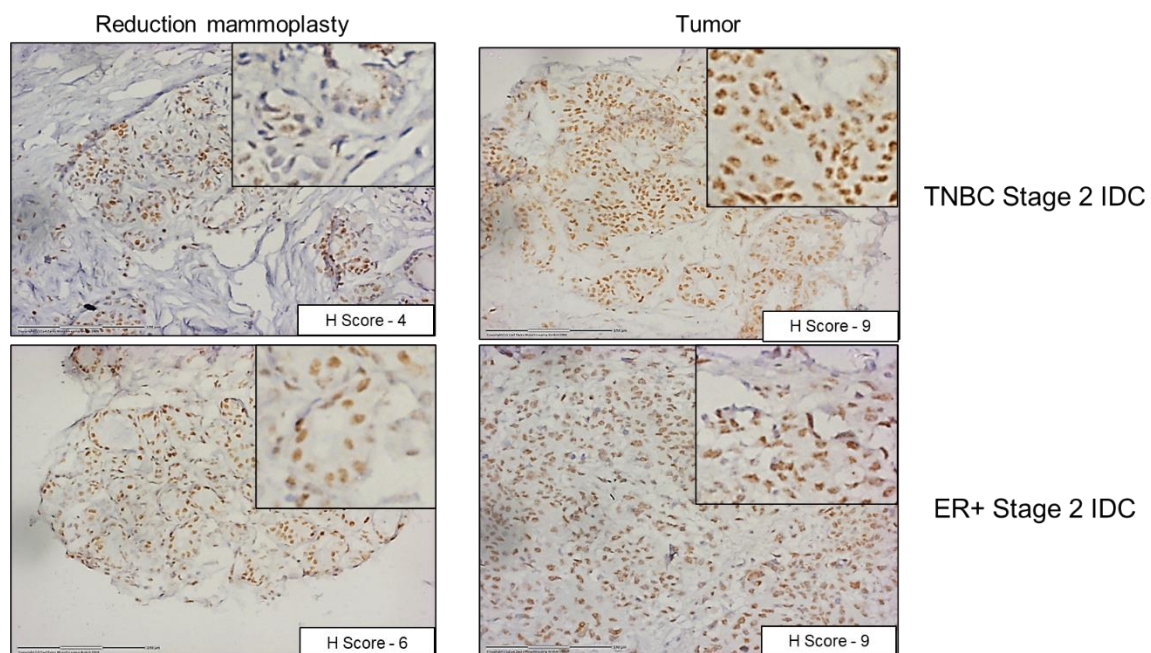


**Fig 5.10** Api5 protein expression in Indian breast cancer patients.

Immunohistochemical analysis of FFPE blocks of human breast cancer patients shows that Api5 levels are higher in tumour tissues than the corresponding reduction tissue. Scale bar- 150  $\mu$ m.

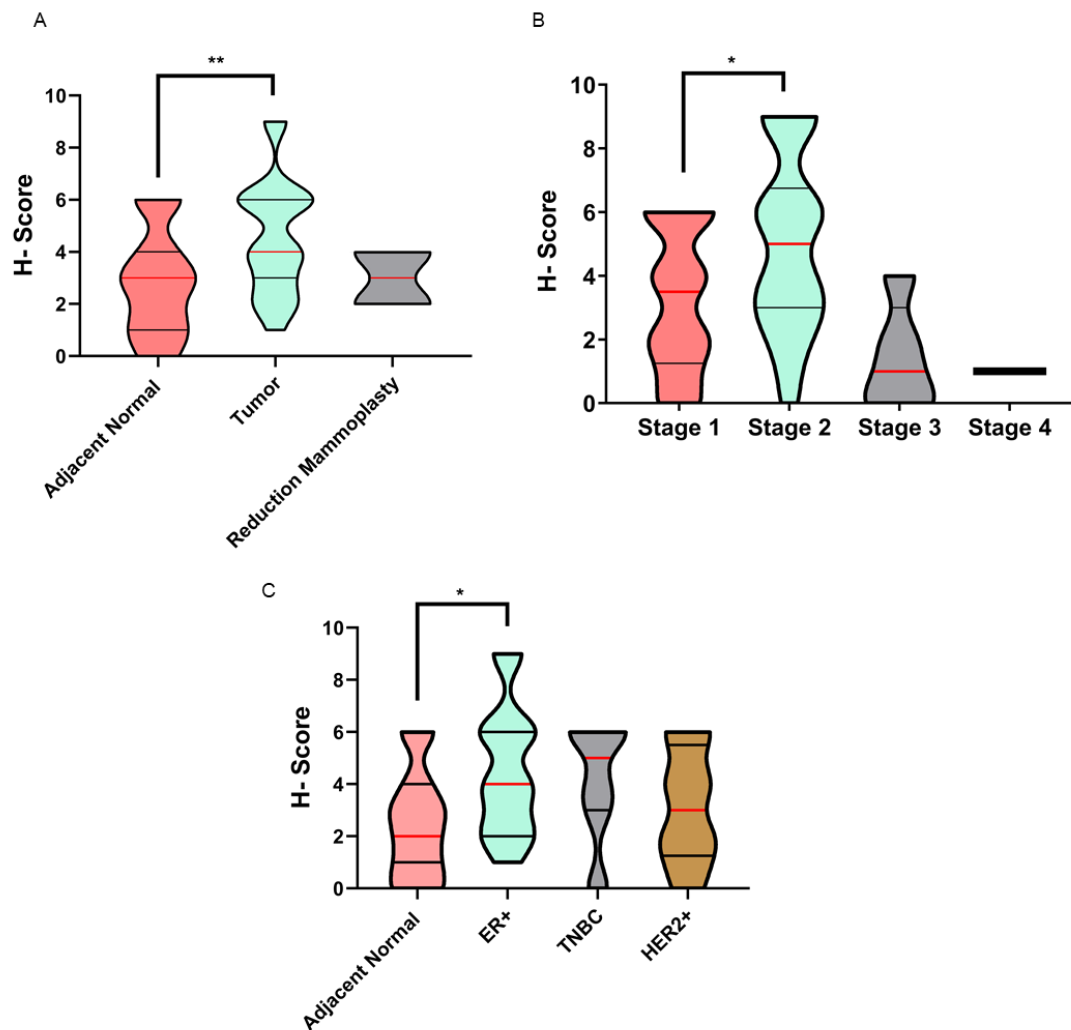


**Fig 5.11** Api5 proteins levels are upregulated in tumour tissues of Indian breast cancer patients.

Api5 expression compared between a) adjacent normal and tumour tissues, b) between different stages of breast cancer tissue samples, and c) adjacent normal and hormone receptor-based subtypes. (N $\geq$ 20 for Adjacent normal, Tumor tissue, Stage 1, Stage 2, and ER+ samples) Statistical analysis was performed using the Mann-Whitney test. \*P<0.05, \*\*P<0.01, \*\*\*P<0.001 and \*\*\*\*P<0.0001.

Results confirmed that Api5 expression is upregulated in Indian breast cancer patients as compared against their adjacent normal tissue. Interestingly, Api5 expression was higher in Stage 2 cancer samples when compared against stage 1 samples (Fig 5.10 and 5.11).

### 5.3 Discussion

*In vitro* studies often provide results that are different in *in vivo* conditions. This makes it necessary to conduct studies on patient samples after initial *in vitro* studies. Oncogenes that can cause transformation can be upregulated in cancers. Our result indicates that Api5 transcript, as well as protein levels, are upregulated in malignant samples. Api5 can be functioning as an oncogene in the breast and could be playing a vital role in carcinogenesis.

Recent advances in cancer genomics have helped in accessing big data, including gene expression patterns and clinical parameters. These data provide insights to gene expression patterns in several types of cancers. Using two such datasets, GENT2 and TCGA, we identified the transcript expression pattern of Api5 in breast cancer which indicates higher expression of API5 in cancer tissues.

The gene expression data are widely used to identify coexpression patterns and delineate the plausible molecular signalling associated with the gene of interest (Sanchez-Vega et al., 2018; Zhu et al., 2018). Studies have utilised TCGA data set expression profiles and identified highly altered signalling cascades in breast cancer, such as MAPK and PI3K signalling (Sinkala et al., 2021).

We utilised the transcript expression data and carried out analyses after categorising based on API5 expression. This list was further filtered based on those genes that affected patient survival in a high Api5 background. Our study confirmed that Api5 gene expression is positively correlated with high cell proliferation *in vivo* as well. These results indicate that Api5 could be playing a significant role during breast carcinogenesis. Also, the *in silico* results indicated that changes in Api5 expression might affect cell membrane composition, which are in line with the results from 3D acinar cultures.

Further, we also confirmed that Api5 proteins levels are upregulated in Indian breast cancer patient samples. Taking together, our results indicate a strong involvement of Api5 in breast cancer. Moreover, the signalling events that Api5 can regulate would be affecting cell proliferation and cell attachment majorly. Further *in vivo* studies using PDX based models and drug targeting could provide insights for developing Api5 as a biomarker and drug target.

## **Chapter 6: Conclusion and Future Prospective**

Api5 is an anti-apoptotic protein that is predicted to function as an oncogene and support carcinogenesis. It is known to regulate signalling events that can play a significant role in apoptosis and cell division. However, it is not entirely explored how Api5 could function in carcinogenesis. In this study, we investigated the role and necessity of Api5 in breast carcinogenesis.

The results identified that Api5 is a major regulator of breast carcinogenesis and altered expression of Api5 in breast cancer cells can suppress the tumour promoting abilities. Using 3D breast acinar cultures of Api5 OE MCF10A cells, we found that the OE enhanced proliferation and reduced apoptosis. The Api5 OE led to larger acinar structures with partially or entirely filled lumen. These characteristics changes suggested the transformation of the breast epithelial cell line. Our results also confirmed that it affected the morphometry and the cellular characteristics, including polarity. Api5 OE led to altered polarity in 3D acinar cultures. These results point at a possibility that Api5 OE can deregulate breast acinar morphogenesis as well. We also observed that Api5 could regulate Bim expression, which is known as a major factor involved in breast acinar lumen formation (Reginato et al., 2005). The fact that overexpression of single gene altered several cell characteristics, when grown in 3D cultures, confirms that maintaining its levels is extremely important.

The events that occur during breast morphogenesis also hold clues for breast carcinogenesis. The major events such as proliferation, polarisation, and apoptosis that regulate breast acinar morphogenesis are also altered in breast cancers (Howard and Ashworth, 2006). Thus our results identified that Api5 OE, through deregulating events that lead to breast acinar morphogenesis, can lead to the transformation of the cells.

Api5 OE activated Akt and cMYC signalling during the early days of acinar morphogenesis. These signalling cascades are known to regulate breast acinar morphogenesis, and when its expression is deregulated, it can promote carcinogenesis. Previous studies have reported that overexpression of Akt or cMYC can have morphometric changes similar to what we observed in Api5 OE MCF10A cells (Debnath et al., 2003b; Partanen et al., 2007). Interestingly, the Akt and cMYC expression in control acinar cultures are altered when compared between different

days of morphogenesis. This also suggests the possibility that Api5 could be functioning as a regulator for their signalling during the specific days.

During the later days of acinar morphogenesis, Api5 OE resulted in upregulated ERK signalling activation, which also regulated the Bim expression(Noh et al., 2014). The ability of Api5 to regulate multiple signalling cascades again confirms that it can function as a major regulator during the development cascade.

We also observed other characteristic changes upon Api5 OE: anchorage independent growth, enhanced migration, partial EMT, and Golgi dispersal. Our *in silico* studies found that higher Api5 expression can affect cell membrane and ECM dynamics, which supports our findings on changes in several membrane-bound proteins. This includes polarity markers and growth factors. It is possible that this altered membrane protein composition could be contributing to the polarity dispersal, partial EMT and anchorage-independent growth. *In silico* studies also found a positive correlation between API5 and cell cycle, which also supports the *in vitro* data showing elevated proliferation due to Api5 OE. This higher proliferative capacity can also be complemented by activating mitogenic signals by Akt and ERK signalling cascades.

Partial EMT characteristics attained by Api5 OE MCF10A cells can be attributed to the FGF2 signalling inducing Akt and ERK signalling. The result that we observe in terms of characteristic changes is predicted to be an outcome of the signalling and the 3D growth of the acinar structures. The altered signalling events could be leading to disruption of the regulatory networks during acinar morphogenesis, thus completely disrupting the epithelial behaviour of the cells.

Several earlier reports have identified the relation between Api5 and FGF2(Jang et al., 2017; Krejci et al., 2007; Song et al., 2017). Our results also point at the possibility that Api5 OE transforms MCF10A by deregulating FGF2 signalling. *in silico* results also confirmed that a positive correlation exists between FGF2 signalling components and Api5. The overexpression and knockdown studies confirmed that Api5 is involved in the direct regulation of FGF2 levels and the downstream signalling. FGF2 is a well-known oncogene that can signal multiple molecular pathways that contribute to malignancy. The possibility that Api5 is an upstream regulator of FGF2 signalling is compelling.



Our results provide more significant insights into the functional importance of Api5 in breast cancer. To our belief, we also report for the first time that deregulation of Api5 expression can alter various signalling events during breast acinar morphogenesis, which are plausibly signalled through FGF2.

### **Api5 as a regulator of breast acinar morphogenesis**

Considering the leads from our studies, we hypothesise that Api5 could regulate breast acinar morphogenesis. Initial understanding from *in silico* and *in vitro* studies suggests that Api5 can regulate cell proliferation and membrane dynamics. Thus, it is also possible that the expression of Api5 itself can be fluctuating during the acinar morphogenesis. It is possible that Api5 could be regulating the polarisation that happens from Day 5 and lumen clearance that initiates from Day 8. These events may be functioning through FGF2 as our result indicated FGF2 as a prime regulator downstream to Api5. Although further studies are required to confirm the possibility that Api5 is a major regulator involved in breast morphogenesis. The luminal cell death can also be initiated by a reduced expression of Api5 in cells present in the lumen of acini. This could be a response to the loss of attachment to the matrix. Reduced Api5 levels can trigger higher Bim mediated apoptosis signalling. Further investigations are required to delineate whether Api5 is major player in breast acinar morphogenesis and the functional role of the protein in the breast development.

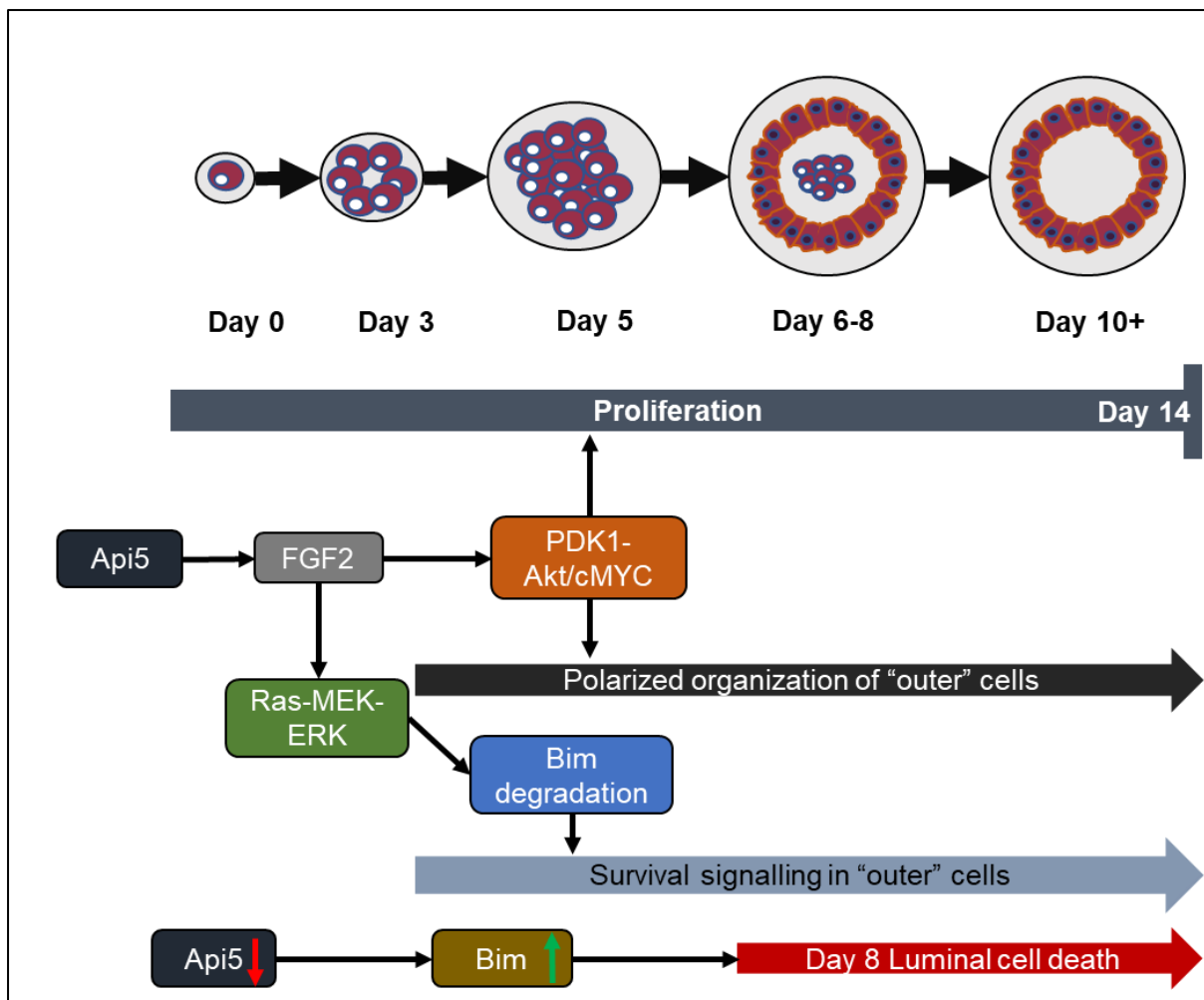


**Fig 6.1** Regulation of breast morphogenesis by Api5.

Plausible pathway illustration showing Api5 mediated regulation of molecular signalling and events during breast acinar morphogenesis

### **Api5-FGF2 signalling in breast carcinogenesis**

Our results could identify that the characteristic changes we observed in acinar morphogenesis can be due to enhanced proliferation, reduced apoptosis and changes in epithelial characteristics of the cells. These changes are found to be closely associated with early activation of PDK1-Akt/cMYC signalling and later through ERK signalling. Both the signalling cascades are found to be activated by FGF2. However, further studies are required to confirm if the complete changes are brought out through FGF2 or involve other proteins such as E2F1. We are interested in understanding whether Api5 is a master regulator of FGF2 signalling in breast carcinogenesis and also to identify whether Api5 mediated transformation is wholly mediated by FGF2 or not.

There are also a few interesting findings that may provide more insights into the function of Api5 in breast carcinogenesis. This includes the large number of changes observed in several cell membrane components. It is possible that the FGF2 signalling could lead to this or vice versa. Also, even though Api5 OE resulted in numerous changes that led to the transformation of MCF10A cells, they could not gain malignant potential. Comparing the results to previous studies on cMYC suggests an existing regulatory signalling that could be functioning during acinar morphogenesis. Identifying these mechanisms can bring in a detailed understanding of how Api5 could regulate breast carcinogenesis.

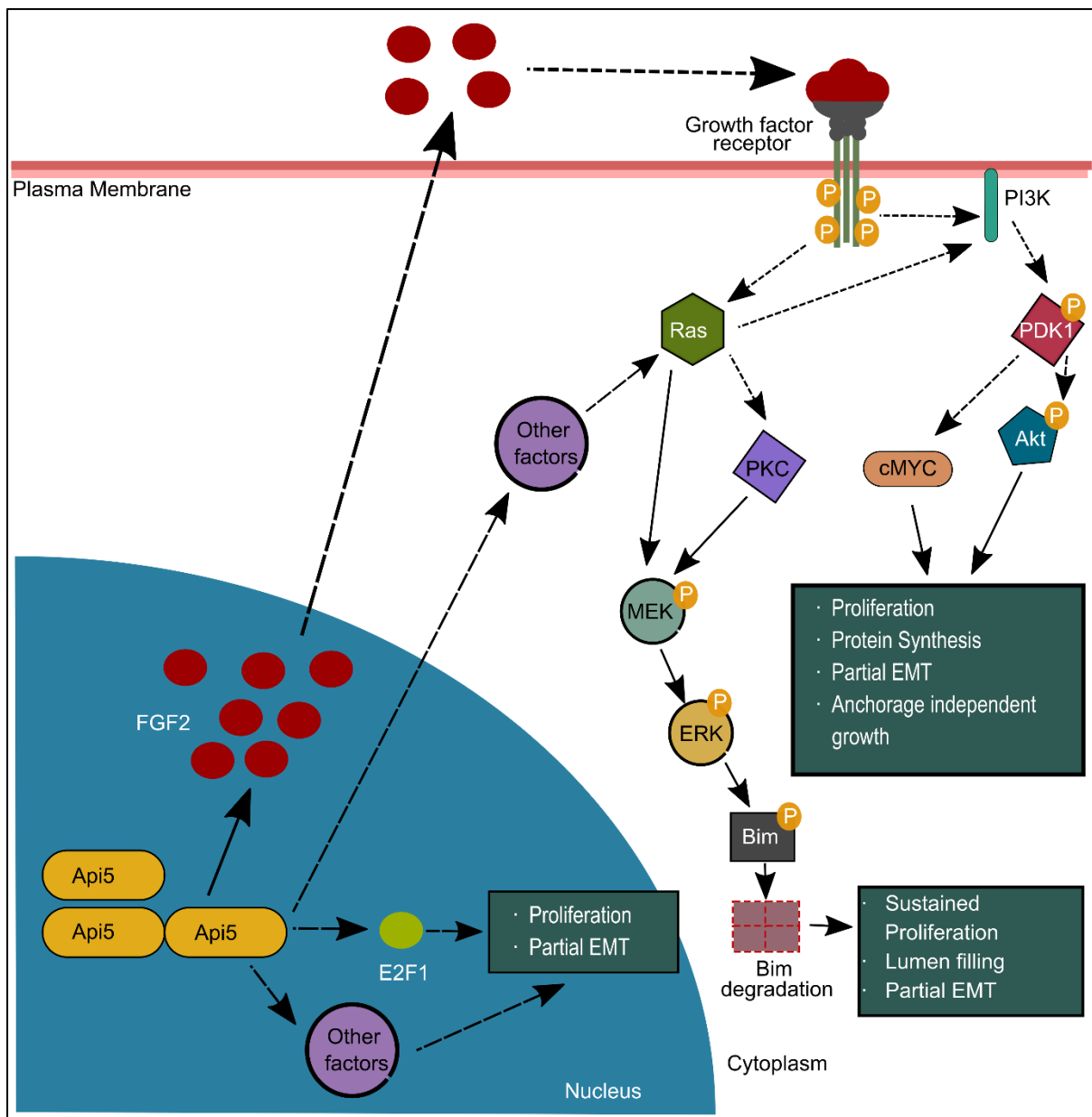


**Fig 6.2** Alternative signalling pathway in Api5 mediated transformation of breast epithelial cells.

Api5 could be functioning through E2F1 leading to transcription of other genes involved in EMT and proliferation. There can also be other factors involved in Api5 mediated regulation of Akt and ERK signalling.

## Bibliography

**Anandi, L., Chakravarty, V., Ashiq, K. A., Bodakuntla, S. and Lahiri, M.** (2017). DNA-dependent protein kinase plays a central role in transformation of breast epithelial cells following alkylation damage. *J Cell Sci* **130**, 3749-3763.

**Anandi, V. L., Ashiq, K. A., Nitheesh, K. and Lahiri, M.** (2016). Platelet-activating factor promotes motility in breast cancer cells and disrupts non-transformed breast acinar structures. *Oncol Rep* **35**, 179-88.

**Andrews, J. L., Kim, A. C. and Hens, J. R.** (2012). The role and function of cadherins in the mammary gland. *Breast Cancer Res* **14**, 203.

**Bartholomeusz, C., Gonzalez-Angulo, A. M., Liu, P., Hayashi, N., Lluch, A., Ferrer-Lozano, J. and Hortobagyi, G. N.** (2012). High ERK protein expression levels correlate with shorter survival in triple-negative breast cancer patients. *Oncologist* **17**, 766-74.

**Basset, C., Bonnet-Magnaval, F., Navarro, M. G., Touriol, C., Courtade, M., Prats, H., Garmy-Susini, B. and Lacazette, E.** (2017). Api5 a new cofactor of estrogen receptor alpha involved in breast cancer outcome. *Oncotarget* **8**, 52511-52526.

**Ben-Hamo, R., Jacob Berger, A., Gavert, N., Miller, M., Pines, G., Oren, R., Pikarsky, E., Benes, C. H., Neuman, T., Zwang, Y. et al.** (2020). Predicting and affecting response to cancer therapy based on pathway-level biomarkers. *Nat Commun* **11**, 3296.

**Bessette, D. C., Tilch, E., Seidens, T., Quinn, M. C., Wiegmanns, A. P., Shi, W., Cocciardi, S., McCart-Reed, A., Saunus, J. M., Simpson, P. T. et al.** (2015). Using the MCF10A/MCF10CA1a Breast Cancer Progression Cell Line Model to Investigate the Effect of Active, Mutant Forms of EGFR in Breast Cancer Development and Treatment Using Gefitinib. *PLoS One* **10**, e0125232.

**Bissell, M. J. and Radisky, D.** (2001). Putting tumours in context. *Nat Rev Cancer* **1**, 46-54.

**Bousquet, G., Feugeas, J. P., Gu, Y., Leboeuf, C., Bouchtaoui, M. E., Lu, H., Espie, M., Janin, A. and Benedetto, M. D.** (2019). High expression of apoptosis protein (Api-5) in chemoresistant triple-negative breast cancers: an innovative target. *Oncotarget* **10**, 6577-6588.

**Cancer Genome Atlas, N.** (2012). Comprehensive molecular portraits of human breast tumours. *Nature* **490**, 61-70.

**Chidgey, M. and Dawson, C.** (2007). Desmosomes: a role in cancer? *Br J Cancer* **96**, 1783-7.

**Cho, H., Chung, J. Y., Song, K. H., Noh, K. H., Kim, B. W., Chung, E. J., Ylaya, K., Kim, J. H., Kim, T. W., Hewitt, S. M. et al.** (2014). Apoptosis inhibitor-5 overexpression is associated with tumor progression and poor prognosis in patients with cervical cancer. *BMC Cancer* **14**, 545.

**Cooper, J. P. and Youle, R. J.** (2012). Balancing cell growth and death. *Curr Opin Cell Biol* **24**, 802-3.

**Coradini, D., Casarsa, C. and Oriana, S.** (2011). Epithelial cell polarity and tumorigenesis: new perspectives for cancer detection and treatment. *Acta Pharmacol Sin* **32**, 552-64.

**Dangelmaier, C., Manne, B. K., Liverani, E., Jin, J., Bray, P. and Kunapuli, S. P.** (2014). PDK1 selectively phosphorylates Thr(308) on Akt and contributes to human platelet functional responses. *Thromb Haemost* **111**, 508-17.

**Danial, N. N. and Korsmeyer, S. J.** (2004). Cell death: critical control points. *Cell* **116**, 205-19.

**Debnath, J. and Brugge, J. S.** (2005). Modelling glandular epithelial cancers in three-dimensional cultures. *Nat Rev Cancer* **5**, 675-88.

**Debnath, J., Mills, K. R., Collins, N. L., Reginato, M. J., Muthuswamy, S. K. and Brugge, J. S.** (2002). The role of apoptosis in creating and maintaining luminal space within normal and oncogene-expressing mammary acini. *Cell* **111**, 29-40.

**Debnath, J., Muthuswamy, S. K. and Brugge, J. S.** (2003a). Morphogenesis and oncogenesis of MCF-10A mammary epithelial acini grown in three-dimensional basement membrane cultures. *Methods* **30**, 256-68.

**Debnath, J., Walker, S. J. and Brugge, J. S.** (2003b). Akt activation disrupts mammary acinar architecture and enhances proliferation in an mTOR-dependent manner. *J Cell Biol* **163**, 315-26.

**Dewson, G., Kluck, R. M. J. C. H. and Cytoskeleton.** (2010). Bcl-2 family-regulated apoptosis in health and disease. **2**, 9-22.

**DuChez, B. J.** (2017). Automated Tracking of Cell Migration with Rapid Data Analysis. *Curr Protoc Cell Biol* **76**, 12 12 1-12 12 16.

**Edmondson, R., Broglie, J. J., Adcock, A. F. and Yang, L.** (2014). Three-dimensional cell culture systems and their applications in drug discovery and cell-based biosensors. *Assay Drug Dev Technol* **12**, 207-18.

**Elmore, S.** (2007). Apoptosis: a review of programmed cell death. *Toxicol Pathol* **35**, 495-516.

**Galluzzi, L., Maiuri, M. C., Vitale, I., Zischka, H., Castedo, M., Zitvogel, L. and Kroemer, G.** (2007). Cell death modalities: classification and pathophysiological implications. *Cell Death Differ* **14**, 1237-43.

**Garcia-Jove Navarro, M., Basset, C., Arcondeguy, T., Touriol, C., Perez, G., Prats, H. and Lacazette, E.** (2013). Api5 contributes to E2F1 control of the G1/S cell cycle phase transition. *PLoS One* **8**, e71443.

**Ghobrial, I. M., Witzig, T. E. and Adjei, A. A.** (2005). Targeting apoptosis pathways in cancer therapy. *CA Cancer J Clin* **55**, 178-94.

**Gudipaty, S. A., Conner, C. M., Rosenblatt, J. and Montell, D. J.** (2018). Unconventional Ways to Live and Die: Cell Death and Survival in Development, Homeostasis, and Disease. *Annu Rev Cell Dev Biol* **34**, 311-332.

**Guo, Y. J., Pan, W. W., Liu, S. B., Shen, Z. F., Xu, Y. and Hu, L. L.** (2020). ERK/MAPK signalling pathway and tumorigenesis. *Exp Ther Med* **19**, 1997-2007.

**Halaoui, R., Rejon, C., Chatterjee, S. J., Szymborski, J., Meterissian, S., Muller, W. J., Omeroglu, A. and McCaffrey, L.** (2017). Progressive polarity loss and luminal collapse disrupt tissue organization in carcinoma. *Genes Dev* **31**, 1573-1587.

**Han, B. G., Kim, K. H., Lee, S. J., Jeong, K. C., Cho, J. W., Noh, K. H., Kim, T. W., Kim, S. J., Yoon, H. J., Suh, S. W. et al.** (2012). Helical repeat structure of apoptosis inhibitor 5 reveals protein-protein interaction modules. *J Biol Chem* **287**, 10727-37.

**Hanahan, D. and Weinberg, R. A.** (2011). Hallmarks of cancer: the next generation. *Cell* **144**, 646-74.

**Hengartner, M. O.** (2001). Apoptosis: corralling the corpses. *Cell* **104**, 325-8.

**Horvitz, H. R.** (1999). Genetic control of programmed cell death in the nematode *Caenorhabditis elegans*. *Cancer Res* **59**, 1701s-1706s.

**Howard, B. and Ashworth, A.** (2006). Signalling pathways implicated in early mammary gland morphogenesis and breast cancer. *PLoS Genet* **2**, e112.

**Huang, L., Chen, S., Fan, H., Ji, D., Chen, C. and Sheng, W.** (2021). GINS2 promotes EMT in pancreatic cancer via specifically stimulating ERK/MAPK signaling. *Cancer Gene Ther* **28**, 839-849.

**Huang, Z., Duan, H. and Li, H.** (2015). Identification of Gene Expression Pattern Related to Breast Cancer Survival Using Integrated TCGA Datasets and Genomic Tools. *Biomed Res Int* **2015**, 878546.

**Imre, G., Berthelet, J., Heering, J., Kehrlöesser, S., Melzer, I. M., Lee, B. I., Thiede, B., Dotsch, V. and Rajalingam, K.** (2017). Apoptosis inhibitor 5 is an endogenous inhibitor of caspase-2. *EMBO Rep* **18**, 733-744.

**Jang, H. S., Woo, S. R., Song, K. H., Cho, H., Chay, D. B., Hong, S. O., Lee, H. J., Oh, S. J., Chung, J. Y., Kim, J. H. et al.** (2017). API5 induces cisplatin resistance through FGFR signaling in human cancer cells. *Exp Mol Med* **49**, e374.

**Jansen, M. P., Foekens, J. A., van Staveren, I. L., Dirkwager-Kiel, M. M., Ritstier, K., Look, M. P., Meijer-van Gelder, M. E., Sieuwerts, A. M., Portengen, H., Dorssers, L. C. et al.** (2005). Molecular classification of tamoxifen-resistant breast carcinomas by gene expression profiling. *J Clin Oncol* **23**, 732-40.

**Javed, A. and Lteif, A.** (2013). Development of the human breast. *Semin Plast Surg* **27**, 5-12.

**Jolly, M. K., Boareto, M., Huang, B., Jia, D., Lu, M., Ben-Jacob, E., Onuchic, J. N. and Levine, H.** (2015). Implications of the Hybrid Epithelial/Mesenchymal Phenotype in Metastasis. *Front Oncol* **5**, 155.

**Kalecky, K., Modisette, R., Pena, S., Cho, Y. R. and Taube, J.** (2020). Integrative analysis of breast cancer profiles in TCGA by TNBC subgrouping reveals novel microRNA-specific clusters, including miR-17-92a, distinguishing basal-like 1 and basal-like 2 TNBC subtypes. *BMC Cancer* **20**, 141.

**Kerr, J. F., Wyllie, A. H. and Currie, A. R.** (1972). Apoptosis: a basic biological phenomenon with wide-ranging implications in tissue kinetics. *Br J Cancer* **26**, 239-57.

**Kesari, A. L., Chandrasekhar, S. D., Rajan, B., Mathew, B. S. and Pillai, M. R.** (2003). Clinicopathological significance of tissue homeostasis in Indian breast cancer. *Breast Cancer* **10**, 241-8.

**Kim, J. W., Cho, H. S., Kim, J. H., Hur, S. Y., Kim, T. E., Lee, J. M., Kim, I. K. and Namkoong, S. E.** (2000). AAC-11 overexpression induces invasion and protects cervical cancer cells from apoptosis. *Lab Invest* **80**, 587-94.



**Kleinman, H. K. and Martin, G. R.** (2005). Matrigel: basement membrane matrix with biological activity. *Semin Cancer Biol* **15**, 378-86.

**Knights, A. J., Funnell, A. P., Crossley, M. and Pearson, R. C.** (2012). Holding Tight: Cell Junctions and Cancer Spread. *Trends Cancer Res* **8**, 61-69.

**Krejci, P., Pejchalova, K., Rosenbloom, B. E., Rosenfelt, F. P., Tran, E. L., Laurell, H. and Wilcox, W. R.** (2007). The antiapoptotic protein Api5 and its partner, high molecular weight FGF2, are up-regulated in B cell chronic lymphoid leukemia. *J Leukoc Biol* **82**, 1363-4.

**Kroemer, G., Galluzzi, L., Vandenabeele, P., Abrams, J., Alnemri, E. S., Baehrecke, E. H., Blagosklonny, M. V., El-Deiry, W. S., Golstein, P., Green, D. R. et al.** (2009). Classification of cell death: recommendations of the Nomenclature Committee on Cell Death 2009. *Cell Death Differ* **16**, 3-11.

**LaCasse, E. C., Mahoney, D. J., Cheung, H. H., Plenchette, S., Baird, S. and Korneluk, R. G.** (2008). IAP-targeted therapies for cancer. *Oncogene* **27**, 6252-75.

**Larsen, B. D. and Sorensen, C. S.** (2017). The caspase-activated DNase: apoptosis and beyond. *FEBS J* **284**, 1160-1170.

**Lowe, S. W. and Lin, A. W.** (2000). Apoptosis in cancer. *Carcinogenesis* **21**, 485-95.

**Macias, H. and Hinck, L.** (2012). Mammary gland development. *Wiley Interdiscip Rev Dev Biol* **1**, 533-57.

**Maehara, O., Suda, G., Natsuzaka, M., Ohnishi, S., Komatsu, Y., Sato, F., Nakai, M., Sho, T., Morikawa, K., Ogawa, K. et al.** (2017). Fibroblast growth factor-2-mediated FGFR/Erk signaling supports maintenance of cancer stem-like cells in esophageal squamous cell carcinoma. *Carcinogenesis* **38**, 1073-1083.

**Mailleux, A. A., Overholtzer, M. and Brugge, J. S.** (2008). Lumen formation during mammary epithelial morphogenesis: insights from in vitro and in vivo models. *Cell Cycle* **7**, 57-62.

**Mailleux, A. A., Overholtzer, M., Schmelzle, T., Bouillet, P., Strasser, A. and Brugge, J. S.** (2007). BIM regulates apoptosis during mammary ductal morphogenesis, and its absence reveals alternative cell death mechanisms. *Dev Cell* **12**, 221-34.

**Makki, J.** (2015). Diversity of Breast Carcinoma: Histological Subtypes and Clinical Relevance. *Clin Med Insights Pathol* **8**, 23-31.

**Moreno-Bueno, G., Portillo, F. and Cano, A.** (2008). Transcriptional regulation of cell polarity in EMT and cancer. *Oncogene* **27**, 6958-69.

**Mori, S., Chang, J. T., Andrechek, E. R., Matsumura, N., Baba, T., Yao, G., Kim, J. W., Gatza, M., Murphy, S. and Nevins, J. R.** (2009). Anchorage-independent cell growth signature identifies tumors with metastatic potential. *Oncogene* **28**, 2796-805.

**Morris, E. J., Michaud, W. A., Ji, J. Y., Moon, N. S., Rocco, J. W. and Dyson, N. J.** (2006). Functional identification of Api5 as a suppressor of E2F-dependent apoptosis in vivo. *PLoS Genet* **2**, e196.

**Noh, K. H., Kim, S. H., Kim, J. H., Song, K. H., Lee, Y. H., Kang, T. H., Han, H. D., Sood, A. K., Ng, J., Kim, K. et al.** (2014). API5 confers tumoral immune escape through FGF2-dependent cell survival pathway. *Cancer Res* **74**, 3556-66.

**O'Brien, M. A., Kirby, R. J. J. o. v. e. and care, c.** (2008). Apoptosis: A review of pro-apoptotic and anti-apoptotic pathways and dysregulation in disease. **18**, 572-585.

**Okada, T., Enkhjargal, B., Travis, Z. D., Ocak, U., Tang, J., Suzuki, H. and Zhang, J. H.** (2019). FGF-2 Attenuates Neuronal Apoptosis via FGFR3/PI3k/Akt Signaling Pathway After Subarachnoid Hemorrhage. *Mol Neurobiol* **56**, 8203-8219.

**Paplomata, E. and O'Regan, R.** (2014). The PI3K/AKT/mTOR pathway in breast cancer: targets, trials and biomarkers. *Ther Adv Med Oncol* **6**, 154-66.

**Park, S. J., Yoon, B. H., Kim, S. K. and Kim, S. Y.** (2019). GENT2: an updated gene expression database for normal and tumor tissues. *BMC Med Genomics* **12**, 101.

**Partanen, J. I., Nieminen, A. I., Makela, T. P. and Klefstrom, J.** (2007). Suppression of oncogenic properties of c-Myc by LKB1-controlled epithelial organization. *Proc Natl Acad Sci U S A* **104**, 14694-9.

**Petrosyan, A.** (2015). Onco-Golgi: Is Fragmentation a Gate to Cancer Progression? *Biochem Mol Biol J* **1**.

**Pluta, P., Jeziorski, A., Cebula-Obrzut, A. P., Wierzbowska, A., Piekarski, J. and Smolewski, P.** (2015). Expression of IAP family proteins and its clinical importance in breast cancer patients. *Neoplasma* **62**, 666-73.

**Ponuwai, G. A.** (2016). A glimpse of the ERM proteins. *J Biomed Sci* **23**, 35.

**Poon, I. K., Lucas, C. D., Rossi, A. G. and Ravichandran, K. S.** (2014). Apoptotic cell clearance: basic biology and therapeutic potential. *Nat Rev Immunol* **14**, 166-80.

**Qu, Y., Han, B., Yu, Y., Yao, W., Bose, S., Karlan, B. Y., Giuliano, A. E. and Cui, X.** (2015). Evaluation of MCF10A as a Reliable Model for Normal Human Mammary Epithelial Cells. *PLoS One* **10**, e0131285.

**Ramdas, P., Rajihuzzaman, M., Veerasenan, S. D., Selvaduray, K. R., Nesaretnam, K. and Radhakrishnan, A. K.** (2011). Tocotrienol-treated MCF-7 human breast cancer cells show down-regulation of API5 and up-regulation of MIG6 genes. *Cancer Genomics Proteomics* **8**, 19-31.

**Reed, J. C.** (1997). Bcl-2 family proteins: regulators of apoptosis and chemoresistance in hematologic malignancies. *Semin Hematol* **34**, 9-19.

**Reginato, M. J., Mills, K. R., Becker, E. B., Lynch, D. K., Bonni, A., Muthuswamy, S. K. and Brugge, J. S.** (2005). Bim regulation of lumen formation in cultured mammary epithelial acini is targeted by oncogenes. *Mol Cell Biol* **25**, 4591-601.

**Rigou, P., Piddubnyak, V., Faye, A., Rain, J. C., Michel, L., Calvo, F. and Poyet, J. L.** (2009). The antiapoptotic protein AAC-11 interacts with and regulates Acinus-mediated DNA fragmentation. *EMBO J* **28**, 1576-88.

**Roche, J.** (2018). The Epithelial-to-Mesenchymal Transition in Cancer. *Cancers (Basel)* **10**.

**Rodriguez-Boulan, E. and Macara, I. G.** (2014). Organization and execution of the epithelial polarity programme. *Nat Rev Mol Cell Biol* **15**, 225-42.

**Royer, C. and Lu, X.** (2011). Epithelial cell polarity: a major gatekeeper against cancer? *Cell Death Differ* **18**, 1470-7.

**Russo, J. and Russo, I. H.** (2004). Development of the human breast. *Maturitas* **49**, 2-15.

**Saitoh, M.** (2018). Involvement of partial EMT in cancer progression. *J Biochem* **164**, 257-264.

**Sanchez-Vega, F., Mina, M., Armenia, J., Chatila, W. K., Luna, A., La, K. C., Dimitriadoy, S., Liu, D. L., Kantheti, H. S., Saghafinia, S. et al.** (2018). Oncogenic Signaling Pathways in The Cancer Genome Atlas. *Cell* **173**, 321-337 e10.

**Sasaki, H., Moriyama, S., Yukiue, H., Kobayashi, Y., Nakashima, Y., Kaji, M., Fukai, I., Kiriya, M., Yamakawa, Y. and Fujii, Y.** (2001). Expression of the antiapoptosis gene, AAC-11, as a prognosis marker in non-small cell lung cancer. *Lung Cancer* **34**, 53-7.

**Schmeichel, K. L. and Bissell, M. J.** (2003). Modeling tissue-specific signaling and organ function in three dimensions. *J Cell Sci* **116**, 2377-88.

**Schneider, P. and Tschopp, J.** (2000). Apoptosis induced by death receptors. *Pharm Acta Helv* **74**, 281-6.

**Sharma, V. K. and Lahiri, M.** (2021). Interplay between p300 and HDAC1 regulate acetylation and stability of Api5 to regulate cell proliferation. *Sci Rep* **11**, 16427.

**Shin, S., Buel, G. R., Nagiec, M. J., Han, M. J., Roux, P. P., Blenis, J. and Yoon, S. O.** (2019). ERK2 regulates epithelial-to-mesenchymal plasticity through DOCK10-dependent Rac1/FoxO1 activation. *Proc Natl Acad Sci U S A* **116**, 2967-2976.

**Siegel, R. L., Miller, K. D. and Jemal, A.** (2018). Cancer statistics, 2018. *CA Cancer J Clin* **68**, 7-30.

**Simpson, D. R., Yu, M., Zheng, S., Zhao, Z., Muthuswamy, S. K. and Tansey, W. P.** (2011). Epithelial cell organization suppresses Myc function by attenuating Myc expression. *Cancer Res* **71**, 3822-30.

**Sinkala, M., Nkhoma, P., Mulder, N. and Martin, D. P.** (2021). Integrated molecular characterisation of the MAPK pathways in human cancers reveals pharmacologically vulnerable mutations and gene dependencies. *Commun Biol* **4**, 9.

**Song, K. H., Cho, H., Kim, S., Lee, H. J., Oh, S. J., Woo, S. R., Hong, S. O., Jang, H. S., Noh, K. H., Choi, C. H. et al.** (2017). API5 confers cancer stem cell-like properties through the FGF2-NANOG axis. *Oncogenesis* **6**, e285.

**Sumbal, J. and Koledova, Z.** (2019). FGF signaling in mammary gland fibroblasts regulates multiple fibroblast functions and mammary epithelial morphogenesis. *Development* **146**.

**Tewari, M., Yu, M., Ross, B., Dean, C., Giordano, A. and Rubin, R.** (1997). AAC-11, a novel cDNA that inhibits apoptosis after growth factor withdrawal. *Cancer Res* **57**, 4063-9.

**Tsujimoto, Y., Finger, L. R., Yunis, J., Nowell, P. C. and Croce, C. M.** (1984). Cloning of the chromosome breakpoint of neoplastic B cells with the t(14;18) chromosome translocation. *Science* **226**, 1097-9.

**Turashvili, G., Bouchal, J., Burkadze, G. and Kolar, Z.** (2005). Mammary gland development and cancer. *Cesk Patol* **41**, 94-101.

**Vidi, P. A., Bissell, M. J. and Lelievre, S. A.** (2013). Three-dimensional culture of human breast epithelial cells: the how and the why. *Methods Mol Biol* **945**, 193-219.

**Wei, Y., Fan, T. and Yu, M.** (2008). Inhibitor of apoptosis proteins and apoptosis. *Acta Biochim Biophys Sin (Shanghai)* **40**, 278-88.

**Wong, R. S.** (2011). Apoptosis in cancer: from pathogenesis to treatment. *J Exp Clin Cancer Res* **30**, 87.

**Worster, D. T., Schmelzle, T., Solimini, N. L., Lightcap, E. S., Millard, B., Mills, G. B., Brugge, J. S. and Albeck, J. G.** (2012). Akt and ERK control the proliferative response of mammary epithelial cells to the growth factors IGF-1 and EGF through the cell cycle inhibitor p57Kip2. *Sci Signal* **5**, ra19.

**Zeisberg, M. and Neilson, E. G.** (2009). Biomarkers for epithelial-mesenchymal transitions. *J Clin Invest* **119**, 1429-37.

**Zhang, L., Xiao, R., Xiong, J., Leng, J., Ehtisham, A., Hu, Y., Ding, Q., Xu, H., Liu, S., Wang, J. et al.** (2013). Activated ERM protein plays a critical role in drug resistance of MOLT4 cells induced by CCL25. *PLoS One* **8**, e52384.

**Zhang, X., Martinez, D., Koledova, Z., Qiao, G., Streuli, C. H. and Lu, P.** (2014). FGF ligands of the postnatal mammary stroma regulate distinct aspects of epithelial morphogenesis. *Development* **141**, 3352-62.

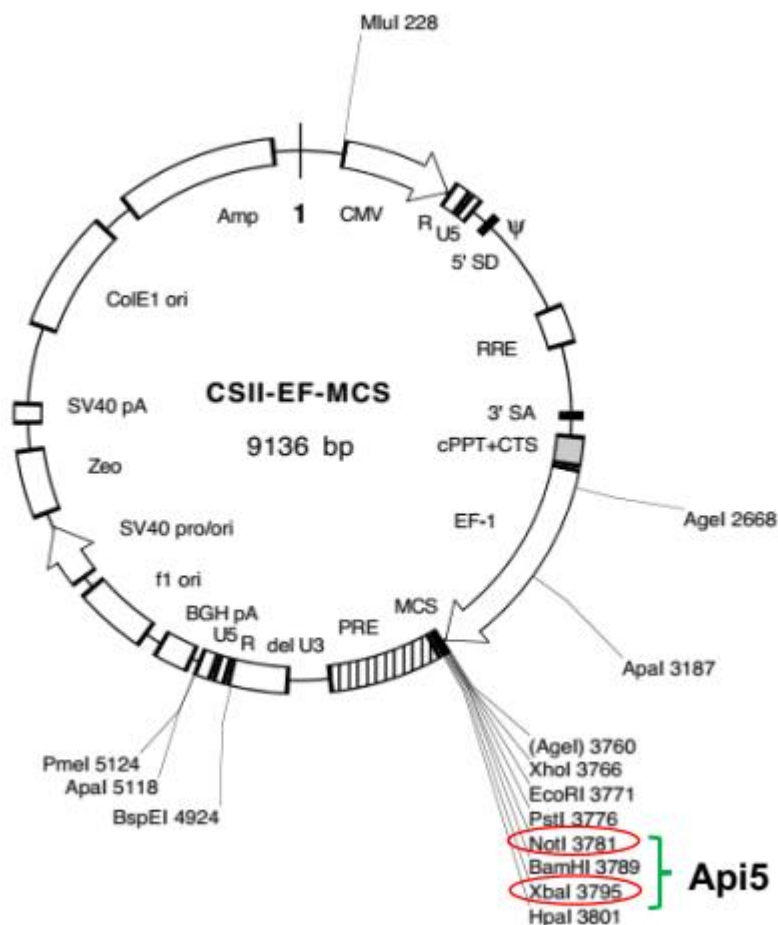
**Zhao, D., Lu, Y., Yang, C., Zhou, X. and Xu, Z.** (2015). Activation of FGF receptor signaling promotes invasion of non-small-cell lung cancer. *Tumour Biol* **36**, 3637-42.

**Zhu, Q., Sun, Y., Zhou, Q., He, Q. and Qian, H.** (2018). Identification of key genes and pathways by bioinformatics analysis with TCGA RNA sequencing data in hepatocellular carcinoma. *Mol Clin Oncol* **9**, 597-606.

# Appendix

## Appendix I- Vector maps

### I.1 Vector map of a mCherry-CSII-EF-MCS vector with Api5 insertion sites.



**Plasmid name:** CSII-EF-MCS

**Source:** RIKEN BRC DNA bank

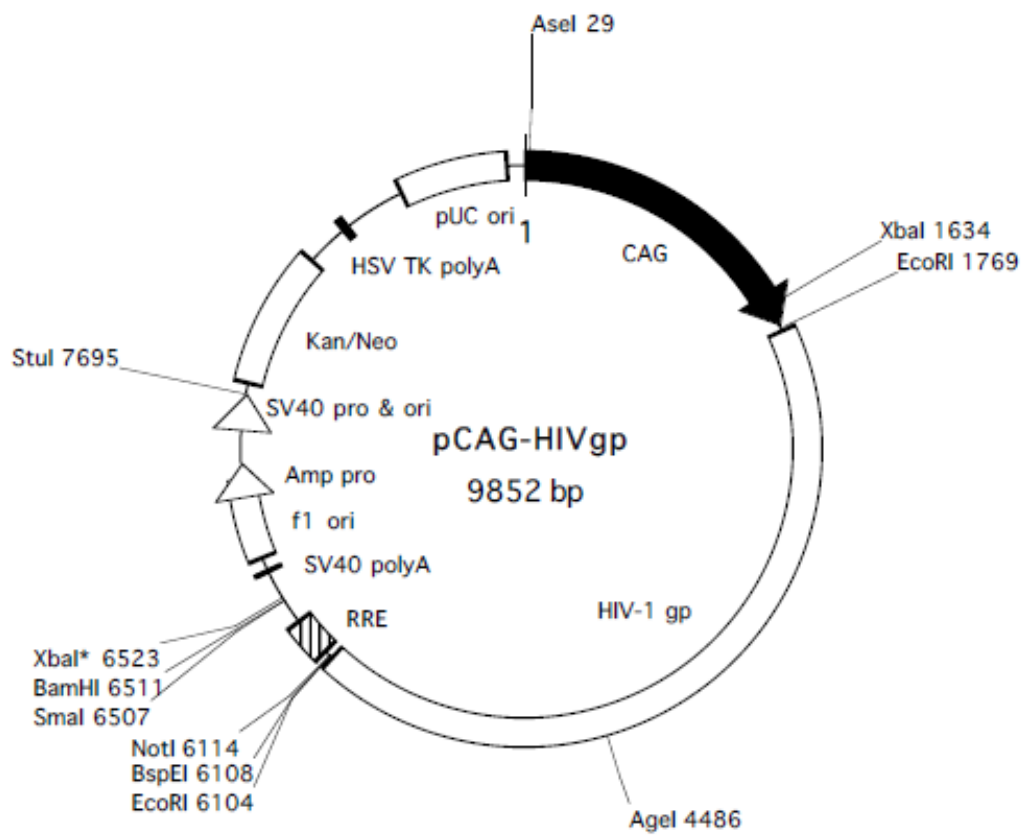
**Restriction sites:** Not1 and Xba1

**Primer sequences used for amplification of Api5:**

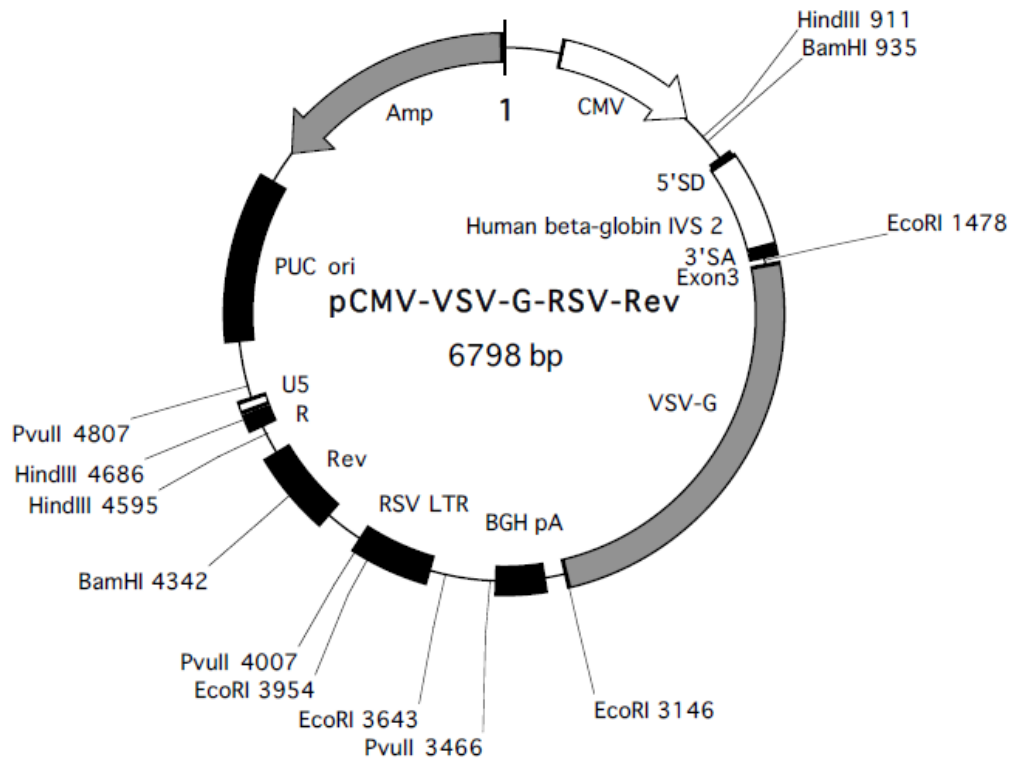
Forward: AAGGAAAAAGCGGCCGCATATGCCGACAGTAGAGGAGCT

Reverse: GCTCTAGATCAGTAGAGTCTTCCCCGAC

I.2 Vector map of packaging plasmid for generation of Api5 overexpression lentiviral particles.

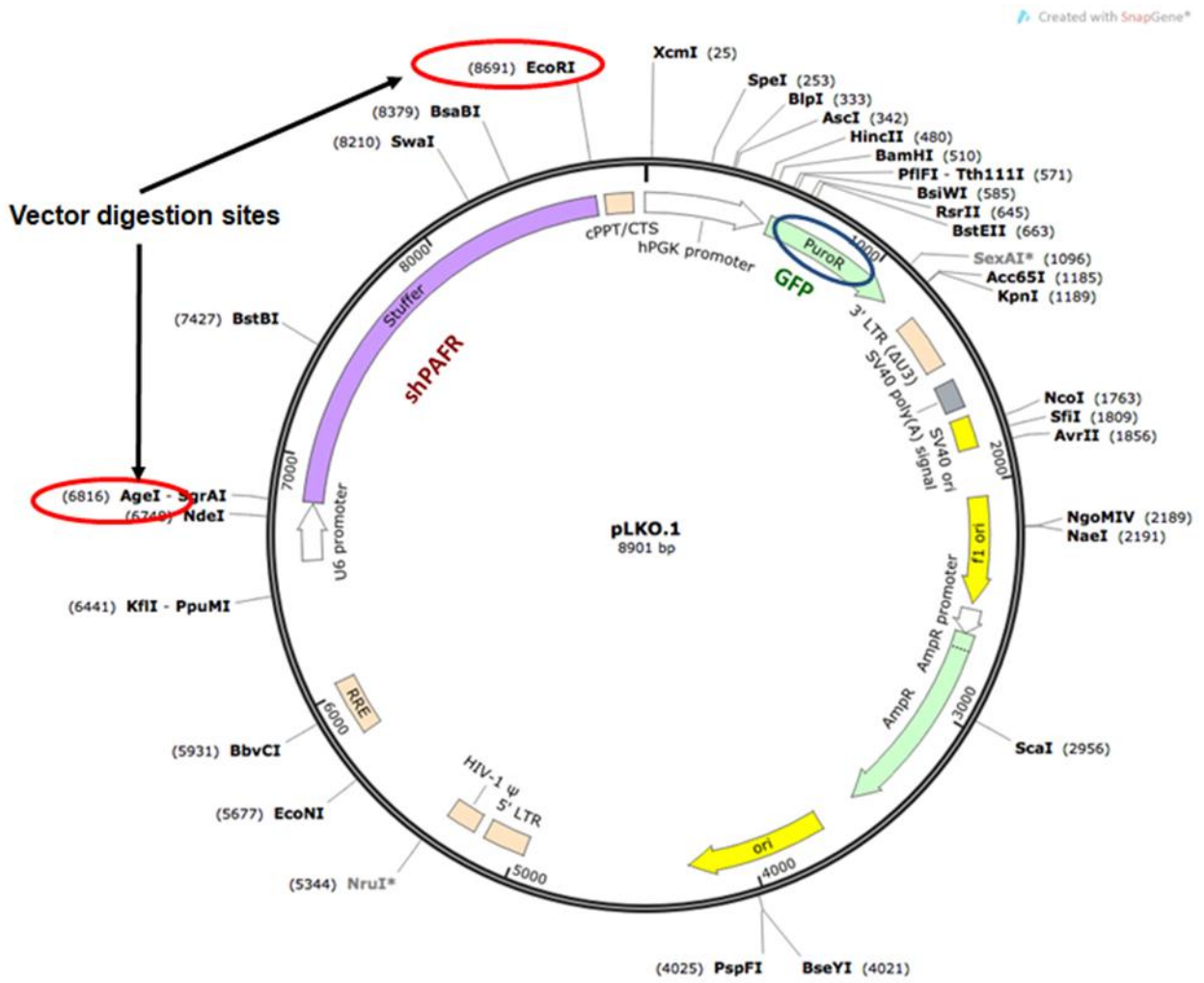


I.3 Vector map of the envelop plasmid for generation of Api5 overexpression lentiviral particles.

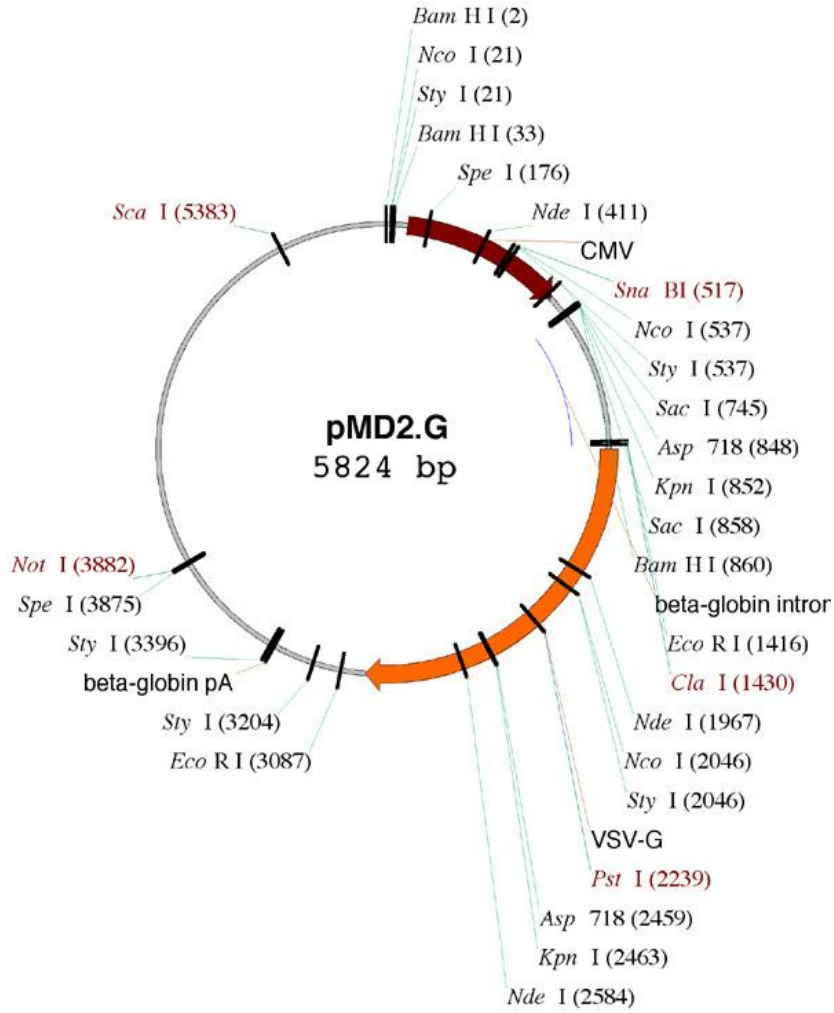




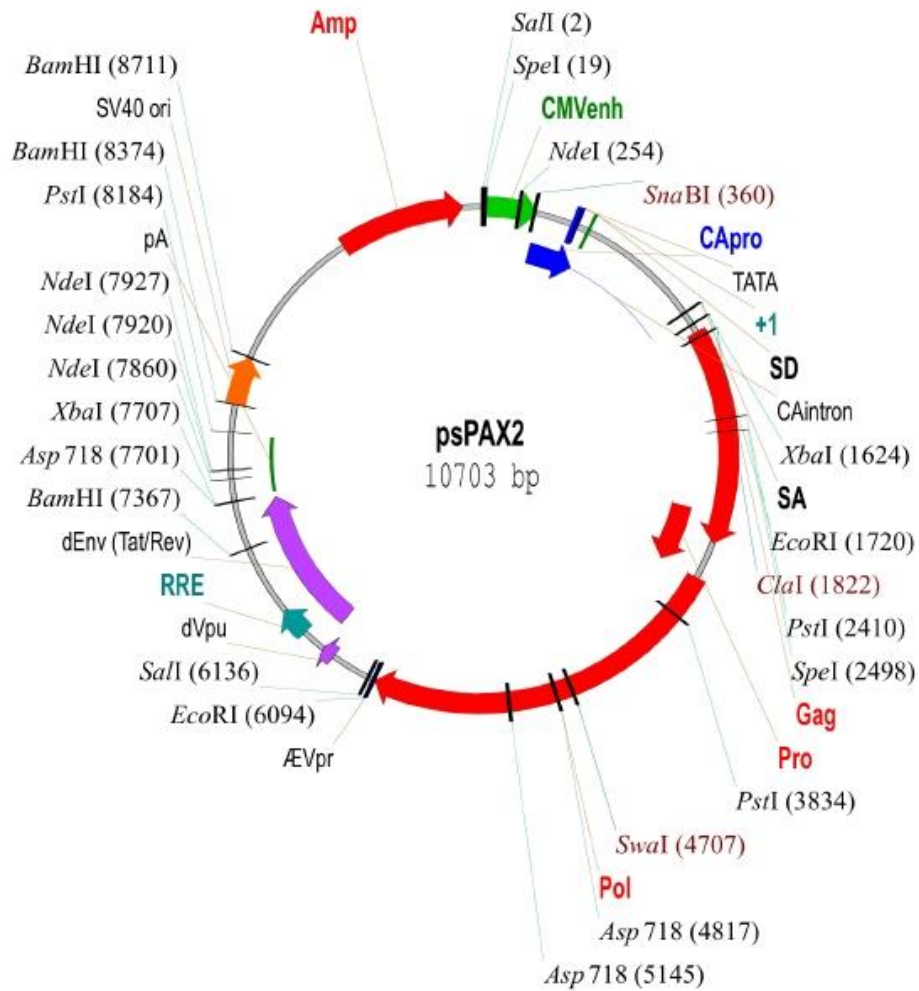
I.4 Vector map of pLKO1.GFP vector with shApi5 insertion sites.



I.5 Vector map of the envelop plasmid for generation of Api5 knockdown lentiviral particles.



I.6 Vector map of packaging plasmid for generation of Api5 knockdown lentiviral particles.



## Appendix II- Media Composition

### II.1 MCF10A media composition

Components	Stock concentration	Growth Medium	Resuspension Medium	Assay Medium
Horse Serum (Invitrogen)		5%	20%	5%
Insulin (Sigma-Aldrich)	10 mg/ml	10 µg/ml	-	10 µg/ml
Hydrocortisone (Sigma-Aldrich)	1 mg/ml	0.5 µg/ml	-	0.5 µg/ml
Choleratoxin (Sigma Aldrich)	1 mg/ml	100ng/ml	-	100ng/ml
Epidermal growth factor (EGF-Sigma Aldrich)	100 µg/ml	20 ng/ml	-	5 ng/ml
Matrigel® (BD Biosciences)	NA	-	-	2% (5% for MCF10AT1 and MCF10CA1a)
Pencillin-Streptomycin (Invitrogen)	100X	2X	2X	2X

## Appendix III: Buffers for Immunofluorescence:

### III.1 Phosphate buffered Saline (PBS)

Component	Concentration
Na <sub>2</sub> HPO <sub>4</sub>	10 mM
KH <sub>2</sub> PO <sub>4</sub>	1.8 mM
NaCl	137 mM
KCl	2.7 mM

### III.2 Phosphate buffer Saline-EDTA (PBS-EDTA)

Component	Concentration
EDTA	5 mM
Sodium orthovanadate	1 mM
Sodium Fluoride	1.5 mM
Protease Inhibitor Cocktail	1X
PBS	1X

### III.3 Immunofluorescence Buffer (IF Buffer)

Component	Concentration
PBS	1 X
Sodium Azide	0.05% [w/v]
BSA	0.1% [w/v]
Triton-X-100	0.2% [v/v]
Tween 20	0.05%
PBS	1 X

## Appendix IV- Buffers for Immunoblotting

### IV.1 6X sample buffer (10 ml)

1M Tris pH6.8	3.5 ml
DTT	0.93 g
Glycerol	3.6 ml
SDS	1.1 g
1% bromo-phenol blue	0.6 ml

### IV.2 10X SDS Running Buffer (2L)

Tris base	60.6 g
Glycine	288 g
SDS	20 g

### IV.3 10X Transfer Buffer (2L)

Tris base	58g
Glycine	293g

### IV.4 20X TBS (2L)

Tris base	120 g
NaCl	320 g
KCl	8 g
pH 7.6 with HCl	

## Appendix V: Buffers and staining solution for Gelatin Zymography

### V.1 Non-reducing sample buffer

Component	Concentration
Tris-HCl (pH 7.5)	25mM
NaCl	100mM
NP-40	1%

### V.2 Renaturing buffer

Component	Concentration
Triton X-100	2.5%
Water	100ml

### V.3 Developing buffer

Component	Concentration
Tris-HCL (pH-7.8)	0.5 M
NaCl	2M
CaCl <sub>2</sub>	0.05M
Brij35	0.2%

#### V.4 Staining solution

<b>Component</b>	<b>Concentration</b>
Coomassie blue	0.1% w/v
Methanol	50% v/v
Acetic acid	10% v/v

#### V.5 Destaining solution

<b>Component</b>	<b>Concentration</b>
Methanol	40% v/v
Acetic acid	10% v/v

## **Publications**



## List of Publications

### Research Articles

1. **Abhijith K**, Debiprasad Panda, Radhika Malaviya, Gautami Gaidhani, and Mayurika Lahiri, Altered expression of Api5 affects breast carcinogenesis by modulating FGF2 signalling. **BioRxiv**, 2021.

### Collaborative research articles

1. Chakravarty V, Anandi L, Ashiq KA, **Abhijith K**, Umesh R, Lahiri M. Prolonged Exposure to Platelet Activating Factor Transforms Breast Epithelial Cells. **Front Genet.** 2021 Mar 25; 12:634938.

## **Research Articles**

# Altered expression of Api5 affects breast carcinogenesis by modulating FGF2 signalling

Abhijith K<sup>1</sup>, Debiprasad Panda<sup>1</sup>, Radhika Malaviya<sup>1</sup>, Gautami Gaidhani<sup>1,2</sup>, Mayurika Lahiri<sup>1\*</sup>

<sup>1</sup>Department of Biology, Indian Institute of Science Education and Research, Dr. Homi Bhabha Road, Pune, Maharashtra 411008, India

<sup>2</sup>The School of Chemistry and Molecular Biology, St. Lucia Campus, The University of Queensland, Brisbane, QLD 4072, Australia.

\*Author for correspondence ([mayurika.lahiri@iiserpune.ac.in](mailto:mayurika.lahiri@iiserpune.ac.in))

**Orcid ID:** M.L.: 0000-0001-9456-4920

A.K: 0000-0003-3643-0291

**Key words:** Breast cancer, Apoptosis, Api5, FGF2, Transformation, Proliferation, Morphogenesis

**Short title:** Role of Api5 in breast carcinogenesis

## Abstract

Apoptosis or programmed cell death plays a vital role in maintaining homeostasis and, therefore, is a tightly regulated process. Deregulation of apoptosis signalling can favour carcinogenesis. Apoptosis inhibitor 5 (Api5), an inhibitor of apoptosis, is upregulated in cancers. Interestingly, Api5 is shown to regulate both apoptosis and cell proliferation. To address the precise functional significance of Api5 in carcinogenesis here we investigate the role of Api5 in breast carcinogenesis.

Consistently, *in-silico* analysis revealed elevated levels of Api5 transcript in breast cancer patients which correlated with poor prognosis. Overexpression of Api5 in non-tumorigenic breast acinar cultures resulted in increased proliferation and cells exhibited a partial EMT-like phenotype with higher migratory potential and disruption in cell polarity. Furthermore, during acini development, the influence of Api5 is mediated via the combined action of FGF2 activated PDK1-Akt/cMYC signalling and Ras-ERK pathways. Conversely, Api5 knock-down downregulated FGF2 signalling leading to reduced proliferation and diminished *in vivo* tumorigenic potential of the breast cancer cells. Thus, taken together, our study identifies Api5 as a central player involved in regulating multiple events during breast carcinogenesis.

## Introduction

Apoptosis Inhibitor 5 (Api5), also known as Aac11 (Anti-apoptotic clone 11)/ MIG 8 (Migration Inducing Gene 8) and FIF (FGF2 interacting factor), is a 55 kDa protein localised in the nucleus (Tewari et al. 1997). The protein has a Leucine Zipper Domain (LZD), an LxxLL motif and a nuclear localisation signal (NLS) (Han et al. 2012). Tiwari *et al.* discovered Api5 as a cDNA clone that helped in the survival of cells upon serum deprivation (Tewari et al. 1997). Following this study there have been several studies to understand the function and regulation of the protein. In 2006, Morris *et al.* identified the role of Aac-11 in the transcriptional regulation of E2F1, where they demonstrated Aac-11 to inhibit E2F1-mediated apoptosis (Morris et al. 2006). Interestingly, Navarro *et al.* in 2013 reported Api5, a mammalian homolog of Aac-11, to regulate the expression of several genes required for G1/S transition that are under the control of E2F1 (Garcia-Jove Navarro et al. 2013). Together the data confirmed that Api5 could regulate both apoptosis and proliferation through E2F1. Further studies mainly focused on the regulation of apoptosis by Api5 such as its interaction and inhibition of Caspase-2 (Imre et al. 2017) and activation of ERK-mediated Bim degradation through FGF2 (Noh et al. 2014). A recent study from our lab has identified the regulators of Api5 acetylation and its' requirement during the cell cycle (Sharma and Lahiri 2021).

Early reports started pointing at the possible tumour promoting role of Api5. In 2000, Kim et al. demonstrated that Aac11 overexpression could protect human cervical cancer cells from apoptosis (Kim et al. 2000), followed by a report on non-small cell lung cancer (NSCLC) and breast cancer. In NSCLC, higher levels of API5 were associated with poor survival of patients (Sasaki et al. 2001), while Api5 expression levels were observed to be elevated in Tamoxifen (a hormonal therapy drug that binds to the oestrogen receptor)-resistant breast carcinomas (Jansen et al. 2005).

Cho *et al.* reported higher expression of Api5 in cervical cancer tissues as well (Cho et al. 2014). A recent report by Basset et al. shed more light on the role of Api5 on breast cancer, where they reported that Api5 interacted with oestrogen receptor alpha (ER $\alpha$ ) through the LxxLL motif. They also showed reduced *in vivo* tumorigenicity upon knock-down of Api5 in xenografted MCF7 cells in mice (Basset et al. 2017).

Interestingly, Di Benedetto and her group reported that Api5 inhibition reduced angiogenesis and elevated apoptosis in xenograft models, thereby highlighting the potential use of Api5 as a therapeutic target in metastatic breast cancers that are resistant to chemotherapy (Bousquet et al. 2019). These reports suggested that Api5 could be functioning as a tumour promoter by regulating various signalling mechanisms. However, further investigations are required for establishing the role and necessity of this protein during carcinogenesis. Investigating the role of Api5 in breast cancer could be interesting as earlier reports do suggest a strong involvement of this protein in breast carcinogenesis.

Moreover, breast cancer is also a leading cause of mortality in women worldwide. GLOBOCAN 2020 data reports that breast cancer-associated mortality to incidence ratio is higher in developing countries like India. Continuous research and development have paved the way for better diagnosis and targeted therapy for breast cancer; however, taming the increase in incidence and mortality is still a challenging problem that needs to be attended to. Studying the function of Api5 in breast carcinogenesis could provide a possible biomarker or drug target for better management of the disease.

In our study, we report the role of Api5 in breast carcinogenesis using multiple models by altering the level of Api5 protein expression. Altered expression of Api5

affected proliferation, apoptosis, cell polarity and cell migration in both non-tumorigenic and tumorigenic cell lines. Api5 overexpression in MCF10A breast epithelial cells activated FGF2 signalling, leading to PDK1-Akt/cMYC activation during the early days of acinar morphogenesis. Activation of this led to elevated proliferation, migration, partial EMT and loss of polarity as was observed in Api5 overexpressed MCF10A cells. 3D cultures of these cells showed altered morphological changes and reduced apoptosis, which is speculated to be functioning through the FGF2-mediated activation of ERK signalling that was observed in the later days of acinar growth. Interestingly, reduced levels of Api5 resulted in the lower tumorigenic potential of the malignant breast cancer cell line, MCF10CA1a and impeded FGF2 signalling. Our findings provide insights into the requirement of Api5 and how it regulates several cellular processes that, upon deregulation, can lead to breast carcinogenesis.

## **Results**

### **Api5 transcript levels are up-regulated in breast cancer and is associated with poor patient survival**

To investigate the expression pattern of *API5* in breast cancers, *in silico* analysis was performed to compare *API5* expression between normal and tumour tissues of the breast using the GENT2 database. GENT2 is an online tool containing gene expression data from different cancers and compares it to normal tissues (Park et al. 2019). The log<sub>2</sub> gene expression plot shows that Api5 transcript levels are up-regulated in breast cancer tissue samples when compared to normal breast tissues (Figure 1A). Molecular subtyping of breast cancer helps to classify breast cancer patients based on the Pam50 analysis or hormone receptor, proliferation marker and other factors. This subtyping also helps in creating treatment regimens and targeted

therapies. Based on the subtyping, breast cancer can be divided into luminal A, luminal B, Her2-enriched and basal subtypes (Giuu et al. 2012). The basal subtype comprises mostly triple-negative breast cancers (TNBC) and presents the most difficult to manage breast cancer population. On comparing the *API5* transcript expression between the normal breast tissue and the various molecular subtypes of breast cancer, expression of *API5* was observed in all the subtypes (Figure 1B). Further Kaplan-Meier survival analysis of the survival probability of a patient with high / low expression of *Api5* (divided by median cut-off) demonstrated poor survival of patients with high *Api5* expression (Figure 1C). Both these analyses were performed using data from the GENT2 database.

When *Api5* transcript levels were compared across the different molecular subtypes of breast cancer using data from the TCGA database, the basal subtype showed higher expression of *API5* when compared to the other molecular subtypes and adjacent normal tissues (Figure 1D). However, no significant changes were observed when *Api5* transcript levels were compared between adjacent normal and the hormone-receptor based subtypes as well as with the various stages of breast cancer (Figure 1E-G).

To validate *Api5* mRNA expression-based patient survival prediction, a Kaplan-Meier plot was generated using KM-plotter (Nagy et al. 2021). KM-plotter uses data from multiple online databases including GEO (NCBI). Using Jetset best probe for *API5* expression and median cut-off for high versus low, the plot suggested that higher *API5* expression is associated with poor breast cancer patient survival (Figure 1H). Using TCGAportal (Xu et al. 2019) online tool, we found higher *Api5* expression is associated with mutations in *PIK3CA* (PI3-kinase catalytic subunit alpha), *TP53* and *CDH1* (E-cadherin), suggesting the possible deregulation of critical pathways associated with high *API5* levels (Figure 1I).



Furthermore, immunohistochemical analyses on breast cancer tissue samples were carried out to investigate Api5 expression pattern in Indian breast cancer patients. The expression levels were assayed by visual quantification followed by H-score calculation. When compared with adjacent normal or reduction mammoplasty tissues, tumour tissues showed significantly higher Api5 expression. Also, Api5 expression levels were high in Stage 2 breast cancer samples compared to Stage 1. However, there was no difference in Api5 expression between ER+ and TNBC subtypes (Supplementary Figure S1A-D).

Data from the patient samples confirm that Api5 plays a significant role in breast cancer. Elevated expression of Api5 in tumour tissues further supports the possibility that Api5 is a tumour promoter in breast malignancies. To investigate this further, we decided to overexpress Api5 in a non-tumorigenic breast epithelial cell line and study its effects on acinar phenotypes.

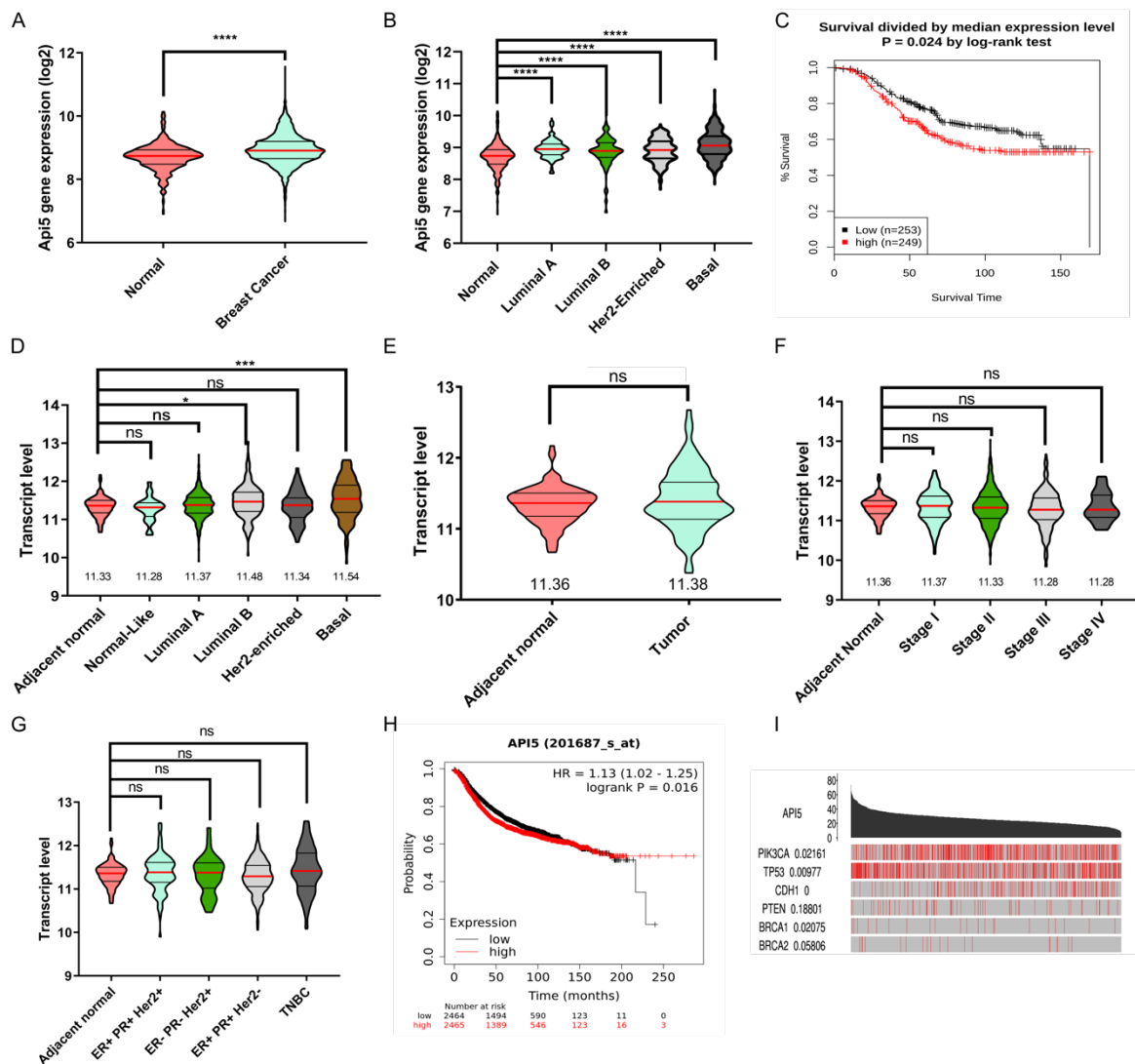


**Figure 1: Api5 transcript levels are up-regulated in breast cancer and is associated with poor patient survival.** (A) Transcript expression data (log<sub>2</sub>) of Api5 obtained from the GENT2 database is plotted. Significantly higher expression of Api5 is observed in cancer samples than in normal. Statistical analysis was performed using the Mann-Whitney test. \*P<0.05, \*\*P<0.01, \*\*\*P<0.001 and \*\*\*\*P<0.0001. (B) API5 expression data downloaded from GENT2 was used to compare the expression across different subtypes in comparison to the adjacent normal. Statistical analysis was performed using the Kruskal-Wallis test followed by Dunn's post hoc test. \*P<0.05, \*\*P<0.01, \*\*\*P<0.001 and \*\*\*\*P<0.0001. (C) Kaplan Meier plot showing survival probability of breast cancer patients divided into high or

low API5 expression (Median cutoff). Black line indicate survival probability of low API5 expressing patients, and red indicates high API5 expression. Significance test data is provided by the online tool. \* $P < 0.05$ . (D) API5 transcript level expression obtained from TCGA database and manually analysed using Graph Pad Prism and plotted. Expression of API5 across different molecular subtype was compared to the adjacent normal sample. Transcript expression of API5 from TCGA database compared across (E) adjacent normal and tumour tissues, (F) different stages of breast cancer, and (G) receptor status-based subtypes. Statistical analysis performed using the Kruskal-Wallis test followed by Dunn's post hoc test. \* $P < 0.05$ , \*\* $P < 0.01$ , \*\*\* $P < 0.001$  and \*\*\*\* $P < 0.0001$ . (The results published here are in whole or part based upon data generated by the TCGA Research Network: <https://www.cancer.gov/tcga>). (H) Kaplan Meier plot showing the probability of patient survival compared between API5 mRNA high or low samples. Data obtained from online tool kmpplot. Expression data is divided based on the median value of the expression. Black points show low API5 expression while red show high API5 expression. The significance test was carried out by the online tool and displayed as provided. (I) API5 expression and occurrence of mutations in genes were compared and plotted using the TCGA portal online tool. Significance test was performed using the online tool and displayed as provided.

### **Api5 overexpression in non-tumorigenic breast epithelial cells alter acinar morphogenesis due to increase in proliferation**

MCF10A is a non-tumorigenic breast epithelial cell line that form growth-arrested acinar cultures when cultured in laminin-rich extracellular matrix (Matrigel®). This is a well-established model to study the transformation of breast epithelial cells in response to tumorigenic signalling (Anandi et al. 2017). To study the effect of Api5 overexpression on cellular transformation of the breast acini, Api5 was

overexpressed in MCF10A cells (will be called Api5 OE henceforth) using lentiviral transduction followed by FACS sorting (Supplementary Figure S2A). Following 16 days of culturing, Api5 OE cells formed acini as shown in Figure 2A. On performing morphometric analysis, it was observed that Api5 OE acini have larger surface area (Figure 2B), volume (Figure 2C), increase in number of cells per acini (Figure 2D) and filled lumen phenotype (Figure 2E). There was no difference in the sphericity of Api5 OE acini when compared to the control acini (Supplementary Figure S2B) suggesting that the overall sphericity is maintained. Similarly, Api5 overexpression did not produce protrusion-like structures in the 3D cultures (Supplementary Figure S2C). Api5 OE acini were not growth arrested by day 16 and continued to proliferate as increased Ki67 protein expression was observed when compared to the control (Figure 2F-G). More than 80% of Api5 OE acini showed greater than six Ki67 positive nuclei per acini (6 cells per acini= approx. 33% of cell/acini) as shown in Figure 2H-I. On checking for the expression of PCNA, another proliferation marker, in the Api5 OE acini, an increase in PCNA levels was observed in Api5 OE when compared to the control (Figure 2J-K), thus further confirming that Api5 overexpression leads to increased proliferation. These results indicate the possibility that overexpression of Api5 in a non-tumorigenic epithelial cell line grown as acinar cultures may result in cellular transformation. To further prove this, anchorage independent growth of Api5 OE cells dissociated from the 16-day acini was investigated. Api5 OE cells formed colonies on soft agar (Figure 2L), indicating that overexpression of Api5 leads to a transformation of non-tumorigenic breast epithelial cells grown as acinar cultures.

The transformation of epithelial cells can also lead to increased migratory potential. To assess whether overexpression of Api5 in MCF10A cells increased its migratory potential, cells dissociated from 3D acinar culture were sparsely seeded and imaged

for 3 hours after they had attained their morphology. The cells were tracked using Fasttracks software (DuChez 2017) (FastTracks (<https://www.mathworks.com/matlabcentral/fileexchange/66034-fasttracks>), MATLAB Central File Exchange. Retrieved June 1, 2021) and parameters such as speed, displacement, distance, and persistence were calculated. Significant increase in the distance travelled (Figure 2M), velocity (Figure 2N) decrease in persistence (Figure 2O) while no change in displacement (Figure 2P) was observed in Api5 OE cells when compared to the controls. The track data was further used for plotting the cellular movement on an XY plot using ImageJ (Figure 2Q). The tracking parameters suggest that Api5 OE cells move faster and cover a longer distance than the control. Further Api5 OE cells showed lower persistence suggesting that the cells were moving in a zigzag fashion rather than taking a relatively straight direction as was observed in control cells. To understand the transformative potential of Api5, Api5 OE MCF10A cells dissociated from the acinar cultures were injected subcutaneously into the flanks of athymic mice and followed for eight weeks to check if the cells had become tumorigenic *in-vivo*. The Api5 OE cells did not form tumours (data not shown) suggesting that overexpression of Api5 is capable of partially transforming breast epithelial cells grown as acinar cultures with diminished tumorigenic potential. Interestingly our results showed that Api5 overexpression not only led to higher proliferation but also faster migration and anchorage-independent growth. This further hints at the regulation of several cellular characteristics, such as cell polarity and cell-cell junctions.

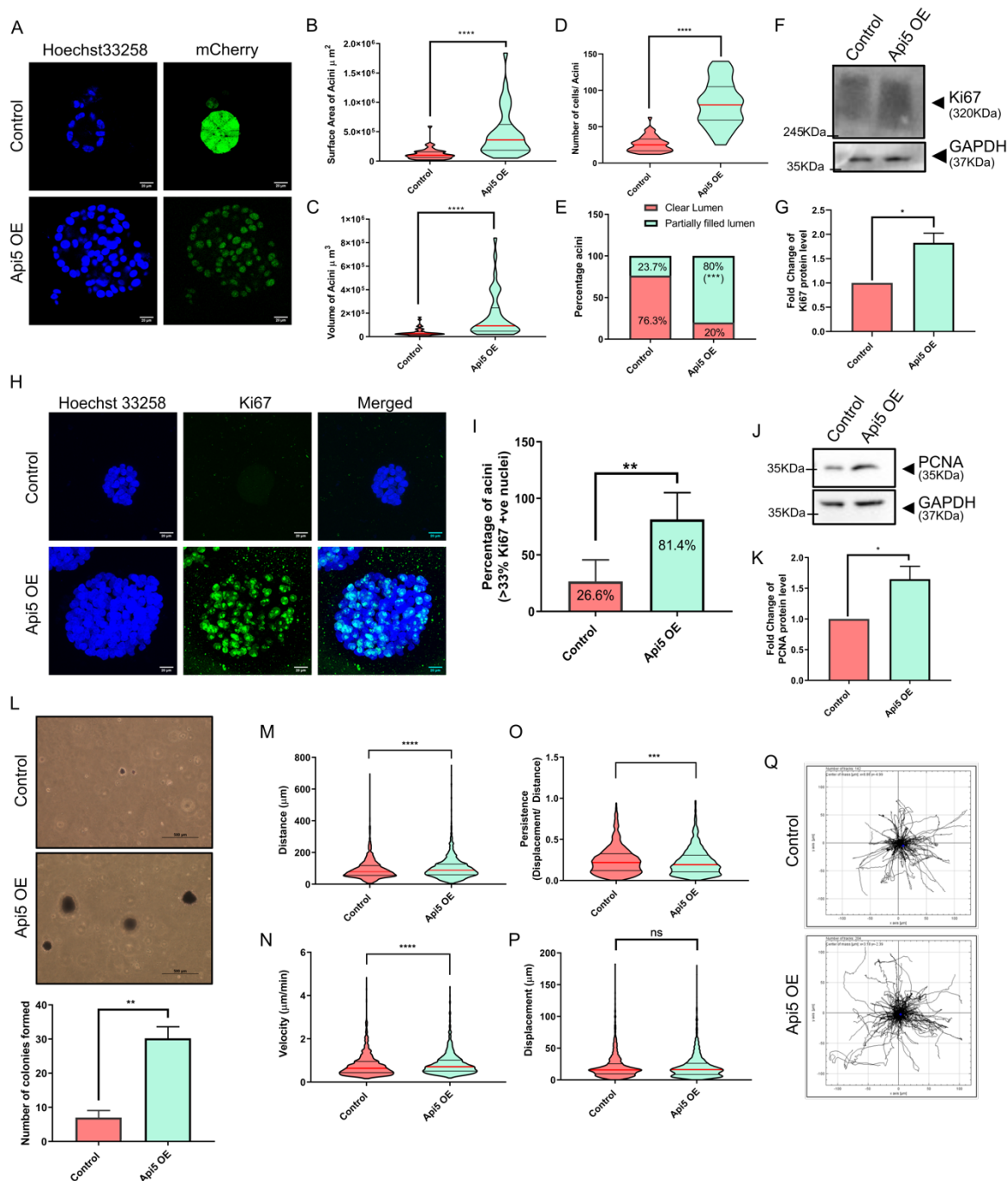


**Figure 2: Overexpression of Api5 in MCF10A cells alter acinar morphology with increased proliferation.** (A) Representative image of day 16 acini showing nuclei stained with Hoechst 33258 (blue) and mCherry (green). Violin plot showing (B) surface area and (C) volume of day 16 acini measured using Huygens software (SVI, Hilversum, Netherlands). (D) Violin plot showing number of cells in each acini, manually counted in day 16 Hoechst 33258-stained acini. Statistical analysis was performed using the Mann-Whitney test. \* $P < 0.05$ , \*\* $P < 0.01$ , \*\*\* $P < 0.001$  and

\*\*\*\*P<0.0001. (E) Bar diagram showing percentage of acini with partially or entirely filled lumen. Day 16 acini stained with Hoechst 33258 were analysed manually by Huygens software. (F) Lysates collected from Api5 OE day 16 acini were immunoblotted for Ki67, a proliferation marker (G) Quantification showing fold change in Ki67 protein level normalised to GAPDH. Statistical analysis was performed using the paired t-test. \*P<0.05, \*\*P<0.01, \*\*\*P<0.001 and \*\*\*\*P<0.0001. (H) Representative image of day 16 acini immunostained for Ki67 (green) and nuclei with Hoechst 33258 (blue) showing increased proliferation in Api5 OE acini when compared to control. (I) The percentage of acini with more than 33% Ki67 positive nuclei were manually analysed and plotted as a bar graph. Statistical analysis was performed using unpaired t-test. \*P<0.05, \*\*P<0.01, \*\*\*P<0.001 and \*\*\*\*P<0.0001. Data pooled from N≥3 independent experiments. (J) Protein expression of PCNA in day 16 acinar cultures obtained using western blot and quantified in (K) showing fold change of PCNA protein levels. Statistical analysis was performed using the paired t-test. \*P<0.05, \*\*P<0.01, \*\*\*P<0.001 and \*\*\*\*P<0.0001. (L) Representative image showing colony formed on soft agar assay stained with MTT after 21 days of seeding, manually counted and represented as a bar graph showing the total number of colonies formed on soft agar assay. Statistical analysis was performed using the Mann-Whitney test. \*P<0.05, \*\*P<0.01, \*\*\*P<0.001 and \*\*\*\*P<0.0001. Data was pooled from n≥5 independent experiments. Control and Api5 OE cells were sparsely seeded and tracked for 3 hours to analyse (M) distance travelled (N) velocity, (O) persistence and (P) displacement. All the parameters were calculated using Fasttracks tool utilising the time-course data of the cells tracked for 3 hours. (Q) Representative data showing movement of single cells in control and Api5 OE grown as monolayer cultures, sparsely seeded and tracked for 3 hours. Statistical

analysis was performed using the Mann-Whitney test. \* $P < 0.05$ , \*\* $P < 0.01$ , \*\*\* $P < 0.001$  and \*\*\*\* $P < 0.0001$ . Data was pooled from  $n \geq 5$  independent experiments.

### **Overexpression of Api5 in breast epithelial results in polarity disruption**

MCF10A cells cultured on Matrigel<sup>®</sup> form acinar structures with a single polarised layer of epithelial cells surrounding a hollow lumen that resemble the human mammary gland acini *in vivo*. Oncogene mediated transformation is often associated with loss or disruption of polarity (Javier 2008; Halaoui and McCaffrey 2015) and is one of the hallmarks of transformation. To understand whether overexpression of Api5 can lead to disruption of polarity in the acini, Api5 OE cells were cultured for 16 days and immunostained for the different polarity markers.  $\alpha 6$ -integrin that marks the basal region of the acini (Debnath et al. 2003a) was observed to be mislocalised in 81% of the Api5 OE acini compared to the control (Figure 3A and B). Similarly, laminin V, a basement membrane marker showed loss in 82% of acini with Api5 OE (Figure 3C and D), thus, confirming that overexpression of Api5 leads to basal polarity disruption. To further understand the effect of Api5 overexpression on the other polarity components in the acinar cultures, the apical polarity marker GM130 (cis-Golgi protein) and the cell-cell junction markers E-cadherin and  $\beta$ -catenin were studied. 83% of the Api5 OE acini had mislocalised GM130 (Figure 3E and F), where GM130 was not observed to be apically positioned to the cell nucleus (Debnath et al. 2003a). In addition, 63% of the Api5 OE acini showed loss of E-cadherin (Figure 3G and H). Interestingly,  $\beta$ -catenin, another cell-cell junction marker remained unaffected in the Api5 overexpressed acinar cultures (Supplementary Figure S2D and E). Taken together, our data suggests that overexpression of Api5 leads to polarity disruption in the breast acinar cultures, which can be associated with oncogene-mediated transformation. These results indicated that Api5



overexpression resulted in several characteristics changes in the epithelial cell line, possibly through epithelial to mesenchymal transition (EMT).

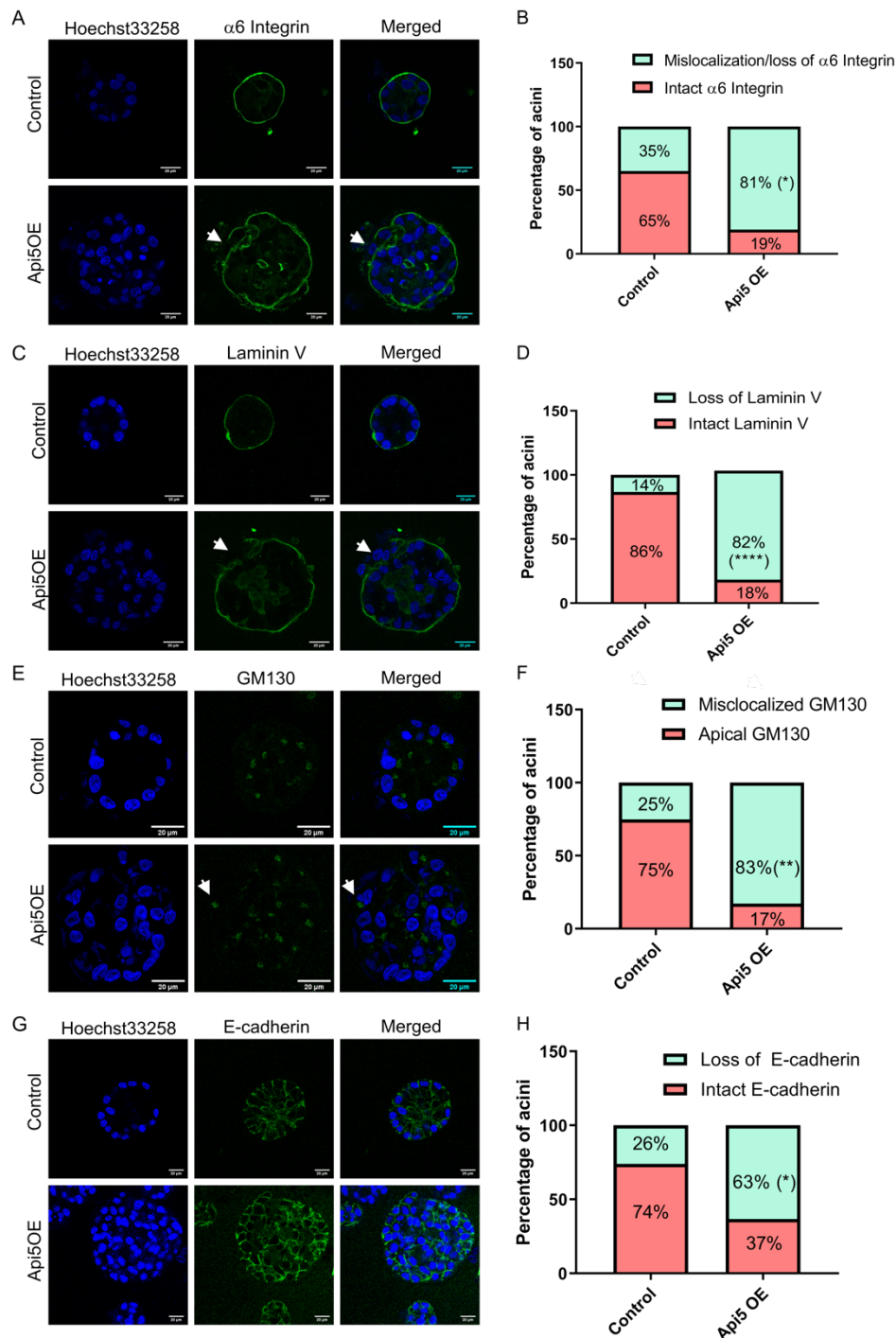


**Figure 3: Overexpression of Api5 disrupts breast acinar polarity. (A)**

Representative image showing basal polarity marker,  $\alpha 6$ -integrin (green)

immunostained in day 16 acini. (B) Bar diagram showing the percentage of acini with

mislocalisation / loss of  $\alpha 6$ -integrin staining. (C) Representative image showing basal polarity marker Laminin V immunostaining (green) in day 16 control and Api5 OE acini. (D) Bar diagram showing the percentage of acini with mislocalisation/ loss of Laminin V staining. (E) Representative image showing GM130 (green) immunostaining in day 16 control and Api5 OE acini. (F) Quantification showing percentage of acini with mislocalised GM130 staining. (G) Representative image showing cell-cell junction marker E-cadherin (green) immunostaining in control and Api5 OE day 16 acini. (H) Bar diagram showing percentage of acini with loss of E-cadherin staining. Statistical analysis for percentage of acini was performed using unpaired t-test. \* $P < 0.05$ , \*\* $P < 0.01$ , \*\*\* $P < 0.001$  and \*\*\*\* $P < 0.0001$ . Data pooled from  $N \geq 3$  independent experiments.

### **Overexpression of Api5 in non-tumorigenic breast epithelial cells induce partial EMT-like characteristics**

Transformation of breast epithelial cells are often associated with epithelial to mesenchymal transition (EMT). MCF10A cells exhibits epithelial characteristics, including expression of epithelial markers such as E-cadherin and cytokeratin. Cells acquire mesenchymal characteristics such as a change in shape and expression of mesenchymal markers such as vimentin, slug and twist upon oncogene-mediated transformation. To study whether overexpression of Api5 leads to EMT, Api5 OE cells were cultured for 16 days, lysates collected, and immunoblotting was performed. Vimentin, twist, slug and fibronectin showed 1.5-fold upregulation in Api5 OE acini when compared to the control (Figure 4A and Supplementary Figure S3A-D). However, there was no change in  $\beta$ -catenin and N-cadherin expression levels (Figure 4A and Supplementary Figure S3E and F). Interestingly the epithelial marker, E-cadherin showed a 2-fold increase in Api5 OE cells in comparison to the control

(Figure 4A, and Supplementary Figure S3G). This was confirmed by calculating the corrected fluorescence intensity of E-cadherin in day 16 acini (Figure 4C) where a significant increase in the fluorescence intensity was observed, thereby suggesting an increase in E-cadherin levels. To further investigate whether the EMT-like phenotype that was observed upon overexpression of Api5 was a transient phenomenon or not, cells dissociated from the 16-day breast acinar cultures were grown as monolayer cultures and analysed. Similar to the phenotype observed in the acinar cultures, an increase in vimentin, slug, fibronectin and E-cadherin was observed in the Api5 OE dissociated cells (Figure 4B and Supplementary Figure S3H-K). N-cadherin expression remained unaltered in the Api5 OE dissociated cells (Figure 4B and Supplementary Figure S3L). The epithelial cell markers cytokeratin 14 and 19 both showed differential regulation in the Api5 OE dissociated cells. Cytokeratin 14 was downregulated while cytokeratin 19 was up-regulated (Figure 4B and Supplementary Figure S3M and N). The upregulation of vimentin was further confirmed when the 16-day Api5 OE breast acini as well as dissociated cells were immunostained for vimentin and increased fluorescence intensity was demonstrated for the mesenchymal marker (Figure 4D-F and Supplementary Figure S3O). Thus, taken together our data suggests that overexpression of Api5 leads to a partial EMT-like phenotype in the breast epithelial cells.

The Golgi structure has been a topic of interest in several recent studies in cancer biology. Glandular epithelial structures like breast acini have intact Golgi localised towards the apical region while more transformed or cancerous cells have dispersed Golgi (Petrosyan 2015). Anandi and group in their studies have demonstrated methylation damage leading to an aberrant Golgi phenotype in transformed MCF10A breast acinar cultures (Anandi et al. 2017). In order to investigate whether overexpression of Api5 can also lead to an aberrant Golgi morphology, Api5 OE cells

were dissociated from 3D cultures and immunostained for the cis-Golgi marker GM130. Following quantification, it was observed that Api5 OE dissociated cells showed a significant increase in Golgi area compared to the control, thereby suggesting an aberrant phenotype (Figure 4G and H). Studies have reported Golgi bodies to play a major role in cell migration (Pouthas et al. 2008; Millarte and Farhan 2012; Saraste and Prydz 2019), and therefore the increase in the migratory potential along with reduced persistence that was observed in Api5 OE cells may be associated with the aberrant Golgi phenotype.

Api5 OE in MCF10A cells grown as acinar cultures resulted in significant characteristic changes in the epithelial cell line, where higher cell proliferation, loss of polarity, acquiring anchorage-independent growth and attaining a partial EMT-like phenotype were observed. Overexpression of Api5 thus resulted in the transformation of these cells.

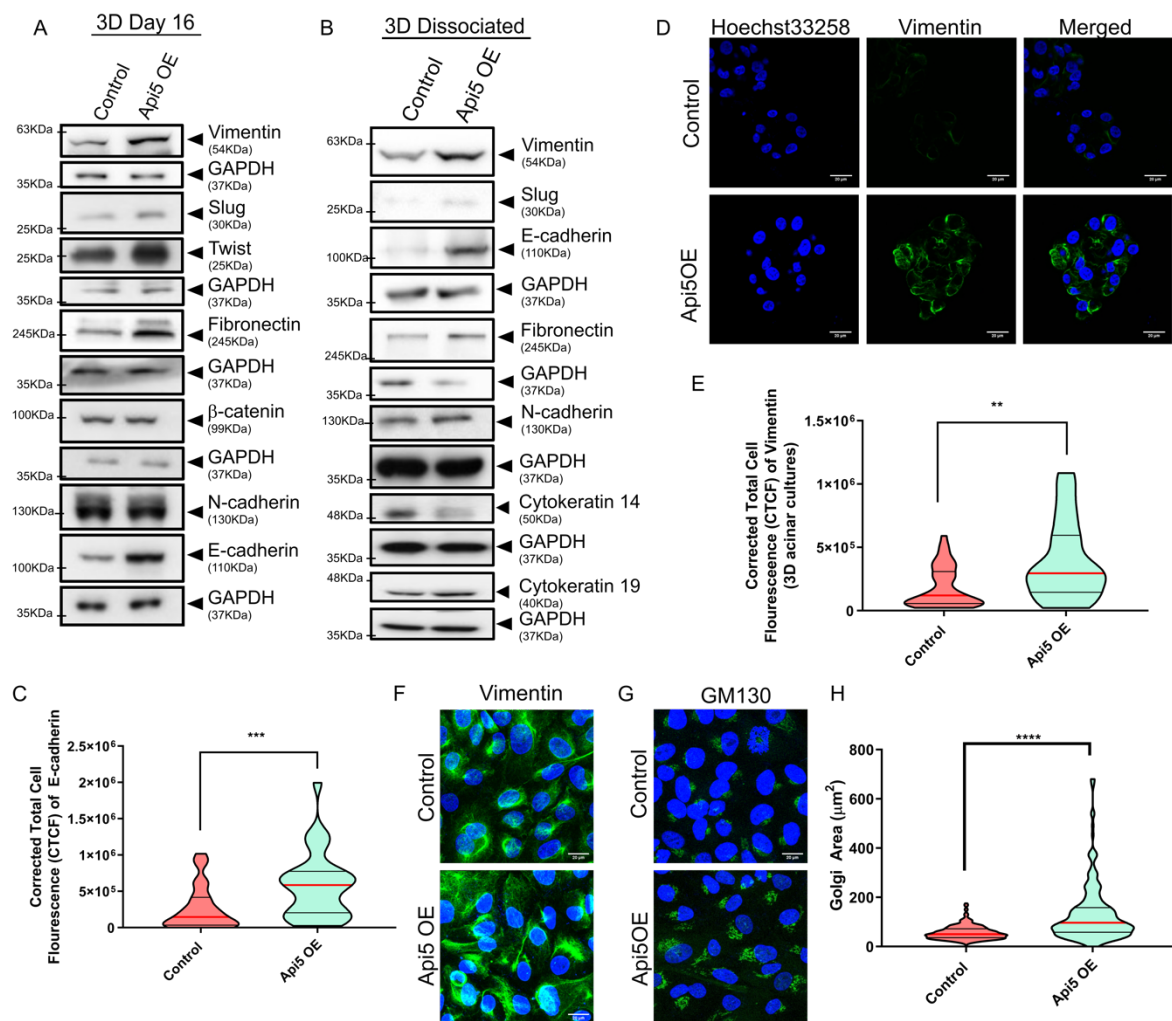


**Figure 4: Api5 overexpression in breast acini lead to the epithelial cells acquiring partial EMT-like characteristics.** Immunoblotting of lysates collected from (A) day 16 acini and (B) dissociated cells from day 16 acini and grown as monolayer cultures showing differential expression of epithelial and mesenchymal markers in Api5 OE compared to the control. (C) Violin plot showing corrected cell fluorescence of E-cadherin immunostaining of day 16 control and Api5 OE acini. (D) Representative image of Vimentin (green) immunostaining of control and Api5 OE day 16 acini. Nuclei were counterstained with Hoechst 33258 (blue). (E) Corrected cell fluorescence of vimentin quantified using ImageJ and represented as violin plot. (F) Representative image of immunostained control and Api5 dissociated cells for Vimentin (green). Nuclei was stained with Hoechst 33258 (blue). (G) Representative

image of GM130 immunostained control and Api5 OE dissociated cells (GM130: green, nuclei: blue). (H) Golgi area was measured using ImageJ. Statistical analysis performed using the Mann-Whitney test. \* $P < 0.05$ , \*\* $P < 0.01$ , \*\*\* $P < 0.001$  and \*\*\*\* $P < 0.0001$ . Data pooled from  $n > 5$  independent experiments.

### **Reduced expression of Api5 in premalignant and malignant breast cancer cells lead to partial reversal of cancerous phenotypes**

Since overexpression of Api5 was leading to a transformed phenotype, we wanted to explore whether down-regulation of Api5 could alter the cancerous phenotype in pre-malignant and malignant breast cancer cells. On investigating the protein expression of Api5 in the MCF10 cell line series (Soule et al. 1990; Dawson et al. 1996; Santner et al. 2001; Imbalzano et al. 2009), Api5 protein expression was observed to be up-regulated in MCF10CA1a cells in comparison to the non-tumorigenic MCF10A or pre-malignant MCF10AT1 cells (Figure 5A-B). shApi5 knock-down stable cells were prepared in both MCF10AT1 and MCF10CA1a and FACS-sorted (Supplementary Figure S4A and G). When Api5 KD MCF10CA1a cells were cultured for 8 days, they formed smaller spheroids as was observed by a significant reduction in surface area and volume when compared to MCF10CA1a control (Figure 5C-E). This reduction in size was further corroborated with a significant reduction in the number of cells forming the Api5 KD MCF10CA1a spheroids. 75% of the Api5 KD MCF10CA1a spheroids had structures composed of less than 100 cells (Figure 5C and F). Since overexpression of Api5 showed increased proliferation, it was intriguing to investigate whether knock-down of Api5 in the malignant cells could lead to reduced proliferation. 58% of Api5 KD MCF10CA1a spheroids showed a reduction in proliferation as was analysed by less than 50% cells per spheroid being Ki67 positive (Figure 5G and Supplementary Figure S4B). The levels of PCNA was also reduced upon knock down of Api5 (Figure 5H and Supplementary Figure S4C), thus further

corroborating the observation that knock down of Api5 in malignant breast cells results in a reduction in proliferation. Furthermore, Api5 KD MCF10CA1a cells formed fewer colonies on soft agar thereby indicating that a reduction in Api5 expression negatively affected anchorage independent growth (Figure 5I and Supplementary Figure S4D). When these Api5 KD MCF10CA1a cells were injected into the flanks of athymic mice they formed tumours, although the tumour volume was significantly reduced compared to the control MCF10CA1a cells. Tumours were measured using a vernier calliper every alternative week for 8 weeks. Upon quantification, it was observed that while the MCF10CA1a control tumours continued to grow, Api5 KD MCF10CA1a tumours stopped growing and maintained a size similar to that of week 2 tumours (Figure 5J and K, Supplementary Figure S4E and F).

Similarly, knock-down of Api5 in the pre-malignant cell line MCF10AT1 also led to a reduction in the surface area and volume of the spheroids (Figure 5L-N). 80% of spheroids formed by Api5 KD MCF10AT1 had less than 100 cells per spheroid, while in the MCF10AT1 control spheroids, more than 60% of the spheroids had more than 100 cells in the spheroid (Figure 5O). Interestingly, knock down of Api5 in MCF10AT1 spheroids did not affect proliferation as no difference was observed in the number of Ki67 positive cells between the MCF10AT1 control and Api5 KD MCF10AT1 spheroids (Supplementary Figure S4H-I). Similar to the results observed in Api5 KD MCF10CA1a cells, knock-down of Api5 in the MCF10AT1 cells also resulted in a reduced ability to grow on soft agar suggesting partial reversal of the malignant phenotype (Supplementary Figure S4J-K).

Thus, we could confirm that while Api5 overexpression alters epithelial characteristics and leads to transformation, knock down of Api5 partially reversed



malignant phenotypes in malignant cells. These results confirm that Api5 is a major player involved in breast carcinogenesis.

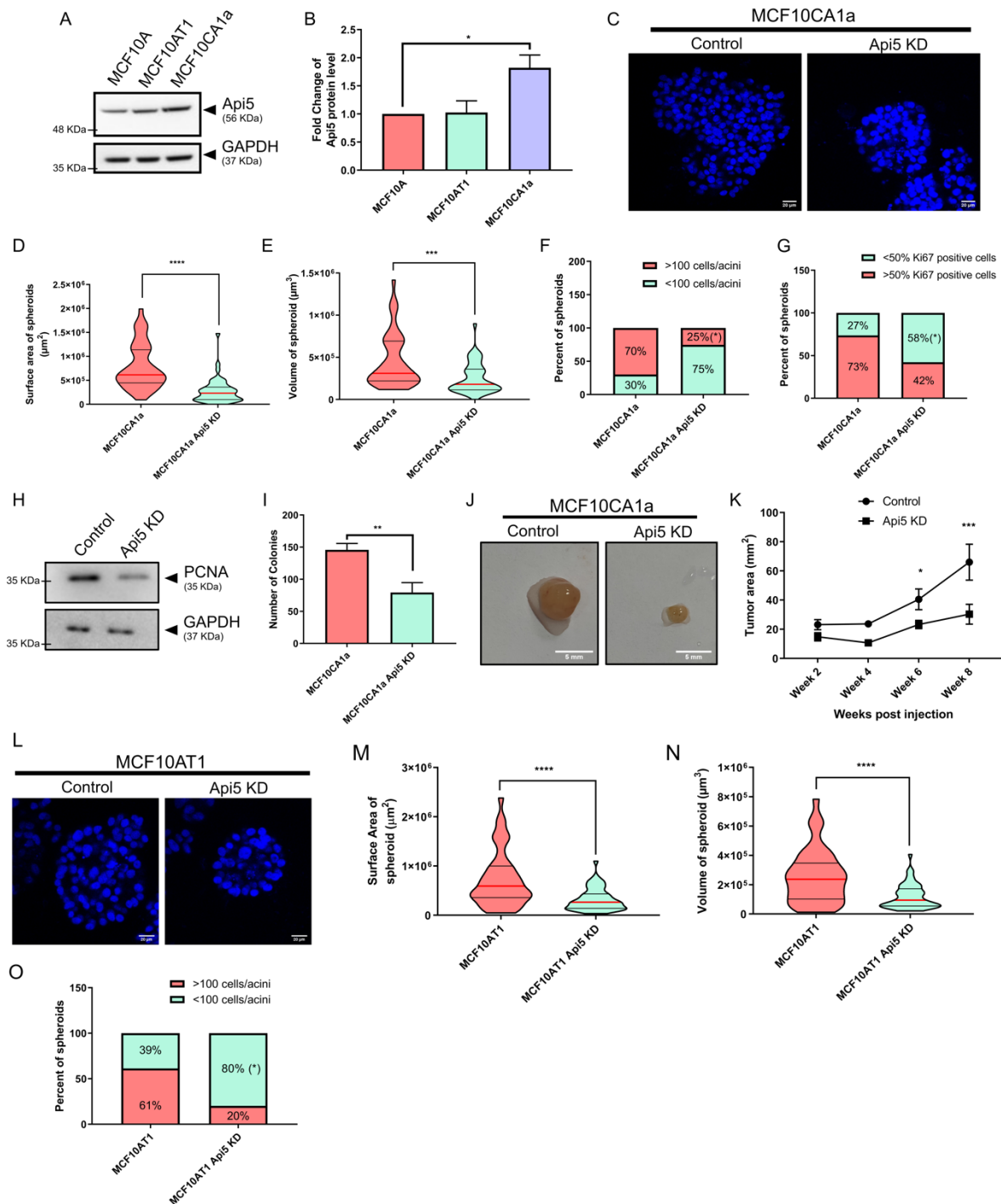


**Figure 5: Api5 knock-down in malignant breast cells resulted in a partial reversal of cancerous phenotypes.** (A) Api5 protein expression in MCF10A cell line series. (B) Quantification showing the expression levels of Api5 across the MCF10A cell line series normalised to loading control GAPDH. Statistical analysis



was performed using the paired t-test. \*P<0.05, \*\*P<0.01, \*\*\*P<0.001 and \*\*\*\*P<0.0001. Data pooled from N≥3 independent experiments. (C) Api5 KD and control MCF10CA1a cells cultured on Matrigel® for seven days stained with nuclear stain Hoechst 33258 (blue). MCF10CA1a control and MCF10CA1a Api5 KD cells were immunostained with phalloidin after 7 days of culture on Matrigel®, and morphometric analysis was performed to calculate (D) surface area and (E) volume of spheroids using Huygens software (SVI, Hilversum, Netherlands). Statistical analysis was performed using the Mann-Whitney test. \*P<0.05, \*\*P<0.01, \*\*\*P<0.001 and \*\*\*\*P<0.0001. Data pooled from N≥3 independent experiments. (F) The percentage of cells with >100 or <100 cells per spheroids were calculated and plotted. (G) Percentage of spheroids with more than 50% Ki67 positive cells per spheroid. Statistical analysis was performed using unpaired t-test. \*P<0.05, \*\*P<0.01, \*\*\*P<0.001 and \*\*\*\*P<0.0001. Data pooled from N≥3 independent experiments. (H) Immunoblotting of lysates collected from day 7 3D culture probed for PCNA. (I) Plot showing total number of MTT-stained colonies formed on soft agar assay that were manually counted. Statistical analysis was performed using the Mann-Whitney test. \*P<0.05, \*\*P<0.01, \*\*\*P<0.001 and \*\*\*\*P<0.0001. Data pooled from n>5 independent experiments. (J) Representative image of tumour dissected from flanks of athymic mice, 8 weeks post subcutaneous injection. The left panel shows MCF10CA1a control cells, while the right panel shows Api5 KD MCF10CA1a. (K) Graph showing tumour area as measured using vernier calliper at the mentioned time. For area calculation, the length of the longer axis and shorter axis were multiplied. Statistical analysis was performed using 2-way Anova followed by Sidak's multiple comparison test. \*P<0.05, \*\*P<0.01, \*\*\*P<0.001 and \*\*\*\*P<0.0001. Data are pooled from n>5 independent experiments. (L) Api5 KD and control MCF10AT1 cells cultured on Matrigel® for 7 days and stained with Hoechst 33258. Morphometric

analysis was performed on MCF10AT1 control and Api5 KD cells stained with phalloidin after 7 days of culture on Matrigel<sup>®</sup>, and (M) surface area and (N) volume of spheroid was measured using Huygens software. Statistical analysis was performed using the Mann-Whitney test. \*P<0.05, \*\*P<0.01, \*\*\*P<0.001 and \*\*\*\*P<0.0001. Data pooled from N≥3 independent experiments. (O) The number of cells per spheroids was counted based on nuclear staining and plotted for percentage of spheroids with >100 (red) and <100 cells (green). Statistical analysis was performed using unpaired t-test. \*P<0.05, \*\*P<0.01, \*\*\*P<0.001 and \*\*\*\*P<0.0001. Data pooled from N≥3 independent experiments.

### **Api5 regulates FGF2-mediated Akt and ERK signalling**

Our studies using non-tumorigenic breast epithelial and malignant cells confirmed that Api5 regulates several phenotypic characteristics that are altered due to transformation. To further understand the importance of Api5 in breast carcinogenesis, it is essential to delineate the molecular signalling involved. The coordinated functioning of Api5 and FGF2 has been intensely researched for a number of years. Studies have reported Api5 along with FGF2 to regulate ERK signalling thereby leading to Bim degradation (Krejci et al. 2007; Noh et al. 2014). Since Api5 OE MCF10A cells had filled lumen on day 16 and Bim, being an important player known to induce apoptosis during days 8 to 12 of acinar morphogenesis, a number of apoptotic markers, including Bim, were studied during the 3D growth of MCF10A and Api5 OE MCF10A acini. Whole cell lysates were collected on days 4, 8, 12 and 16 of acinar growth. Overexpression of Api5 led to reduction in Bim, and active caspase 9 on day 12 of morphogenesis (Figure 6A-C). Since ERK-mediated Bim degradation has been reported to be through Api5 signalling (Noh et al. 2014), we checked whether overexpression of Api5 could lead to an alteration in ERK and MEK activity. Phosphorylation of ERK and MEK kinases

were observed upon Api5 OE during day 12 of acinar growth (Figure 6A, D and E). Since ERK signalling was activated, we were interested in studying the effect on FGF2 expression levels upon overexpression of Api5 in the MCF10A acinar cultures. Increase in FGF2 protein expression was observed from days 4 to 12 in Api5 OE acini when compared to the control. This increase was a little over 3-fold on day 4 while it was 1.5-fold on day 12. By day 16, FGF2 was marginally lower in Api5 OE cells compared to the control (Figure 6A and F). Thus, overexpression of Api5 modulates a number of signalling pathways that play a role during acinar morphogenesis. Although an increase in FGF2 levels was observed on day 4, an increase in ERK signalling was observed only from day 12. Therefore, further investigation of other alternative pathways were performed. FGF2 is known to activate tyrosine kinase receptors that then activate the PI3K signalling cascade (Okada et al. 2019; Mossahebi-Mohammadi et al. 2020). In order to identify whether PI3K signalling is activated in Api5 OE MCF10A cells, phosphorylation of Akt at T308 and S473 residues were investigated. Complete activation of Akt requires initial phosphorylation at tyrosine 308 residue followed by activation at serine 473 residue. The enzyme PDK1 phosphorylates T308 residue on Akt. Overexpression of Api5 increased phosphorylation of Akt at T308 on days 4 and 8, while the Akt S473 phosphorylation was similar to that of the control cells (Figure 6A, G). Therefore it can be inferred that PDK1 is activated that may possibly lead to further activation of its downstream signalling molecule, cMYC. Upon probing for cMYC in these lysates, days 4 and 8 Api5 OE lysates showed significant increase in cMYC expression, which coincided with the phosphorylation of Akt at T308 residue (Figure 6A and H). Thus, the FGF2-mediated activation of PDK1-Akt/cMYC signalling during the initial days of growth supports the increased proliferation, protein synthesis and transformation of MCF10A cells while later activation of the ERK signalling cascade

leads to reduced apoptosis and lumen filling. FGF2- PDK1/ ERK signalling is very often linked through RAS and a recent study has shown that Api5 interacts with KRAS(Bong et al. 2020), thus KRAS expression pattern was also studied.

Interestingly, KRAS was up-regulated in Api5 OE 3D lysates from day 4 to day 12 and by day 16, KRAS levels were similar to that of the control (Figure 6A and I).

Taken together, we propose Api5 to activate FGF2-mediated Ras-ERK and Akt signalling cascades.

To confirm whether Api5 can regulate the FGF2 mediated Akt and ERK signalling, Api5 KD in MCF10CA1a cells cultured on Matrigel<sup>®</sup> were lysed and immunoblotted.

Api5 KD resulted in a decrease in ERK phosphorylation (Figure 6J and K),

suggesting Api5 may play a role in ERK signalling. Further, a reduction in FGF2

levels was also observed in Api5 KD cells compared to the control (Figure 6L and

M). Interestingly, Bim and cMYC levels remained unaltered (Figure 6L,

Supplementary Figure S5A and B). This may be due to the acquiring of an

alternative signalling pathway when the MCF10A cells became malignant. Similarly,

Akt activation was also hampered upon Api5 KD, as was demonstrated by

diminished Akt phosphorylation at both S473 and T308 sites (Figure 6N and O).

Western blot analysis from 3D culture lysates confirmed that Api5 played a role in

both Akt and ERK signalling mediated by FGF2. Increase in cMYC expression could

be responsible for the increase in the expression of mesenchymal markers. Also,

growth factor-mediated signalling cascade may be providing a sustained proliferative

signalling throughout morphogenesis of MCF10A, leading to partial or complete

transformation of the cells even though these cells failed to form tumours in athymic

mice, suggesting that there may still be other regulatory mechanism(s) playing a

role. However, it is interesting to note that alteration in the expression of an anti-

apoptotic protein was able to lead to an array of morphometric changes and signalling activation in the cells.

To further investigate the existence of this regulation in breast cancer patients, co-expression analysis was performed using the TCGA database. Interestingly, *BAX* and *CASPASE-9* showed a negative correlation with *API5* transcript levels, but *BIM* mRNA levels showed a positive correlation with *API5* (Supplementary Figure S5C-E). We had observed a similar trend in the protein expression levels in *Api5* OE MCF10A lysates collected on day 16. *ERK2*, *FGF2*, *PDK1*, *KRAS* and *cMYC* transcript levels also showed a positive correlation with *API5* transcript (Supplementary Figure S5F-J) supporting the data obtained from the 3D acinar cultures. These data indicate that *Api5* is regulating the *FGF2*-mediated *PDK1* and *ERK* signalling in breast cancer and can possibly be used as a target for therapy.

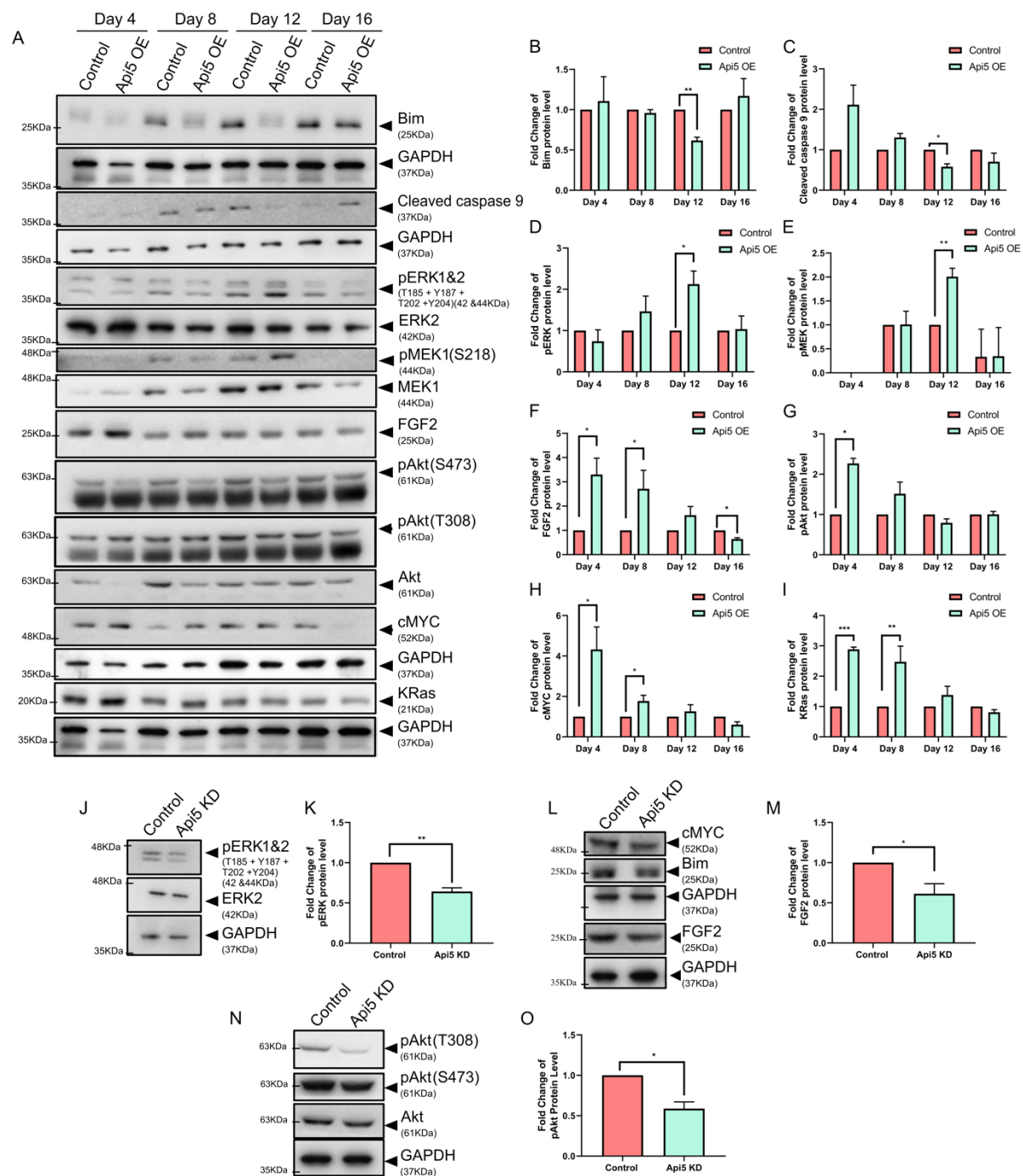


**Figure 6: Api5 regulates PDK1/Akt and ERK pathways through FGF2. (A)**

Lysates were collected from control and Api5 OE acinar cultures on days 4, 8, 12 and 16 and immunoblotted to study the expression of a number of proteins. Fold change in expression between control and Api5 OE were calculated for (B) Bim, (C) cleaved caspase 9, (D) pERK 1/2, (E) pMEK1, (F) FGF2, (G) pAkt (T308), (H) cMYC and (I) KRas. Normalisation of expression was done with GAPDH for Bim, cleaved

caspace 9, cMYC, and FGF2, while for pERK, pMEK and pAkt, it was with their respective total protein. (J) Immunoblotting of pERK 1&2 in day 7 MCF10CA1a control and Api5 KD spheroid cultures. (K) Quantification of the fold change in expression of pERK 1&2 normalised to total ERK2. (L) cMYC, Bim and FGF2 protein expression in Api5 KD MCF10CA1a compared to control MCF10CA1a spheroids cultured for seven days (M) Quantification of the fold-change in FGF2 expression normalised to GAPDH. (N) Lysates from day 7 MCF10CA1a control and Api5 KD spheroid cultures were immunoblotted for pAkt T308, S473 and total Akt expression levels. (O) Quantification of the fold change in expression of pAkt T308 normalised to total Akt. Data pooled from n>5 independent experiments. Statistical analysis was performed using the paired t-test. \*P<0.05, \*\*P<0.01, \*\*\*P<0.001 and \*\*\*\*P<0.0001. Data pooled from N≥3 independent experiments.

## Discussion

Apoptosis is an important cellular process required during constant remodelling of glandular epithelium in the human breast, which is often deregulated in cancers (Mailleux et al. 2007). The role of Api5, one of the regulators in the apoptotic signalling cascade, is not well established in breast carcinogenesis. In this study, we report that deregulation of Api5 expression in breast epithelial cells leads to activation of Akt and ERK signalling pathways that affect breast morphogenesis (Figure 7).

Analyses performed using multiple online tools and databases revealed that API5 transcript levels are higher in breast tumour tissues than in normal breast samples. A significant positive correlation was observed between *API5* expression and mutations in key signalling molecules such as p53 and PI3K. Mutations in these genes are known to be pathogenic and favour tumor progression (Duffy et al. 2018;

Shahbandi et al. 2020; Wang et al. 2020). The data demonstrates Api5 to play an important role that favours breast tumour progression. Interestingly, recent studies have also shown that Api5 expression pattern associated with chemo-resistant TNBC patients (Bousquet et al. 2019). Furthermore, an anti-Api5 peptide, which can bind and block Api5 activity, showed anti-cancer properties and was suggested to be used as a therapeutic option (Jagot-Lacoussiere et al. 2016).

Human breast contains lobules made of numerous acini which produces milk. In each acinus, epithelial cells surround an empty lumen in which milk is secreted and is then carried through the ducts (Javed and Lteif 2013). When cultured on specific extra cellular matrices, breast epithelial cells can form similar structures *in vitro* (Swamydas et al. 2010). Such 3D acinar cultures can resemble the human mammary gland acini structurally and functionally. These spheroid cultures could provide insights into molecular events that occurs during breast carcinogenesis. MCF10A, a non-tumorigenic breast epithelial cell line, forms growth arrested acinar structures when cultured on laminin-rich extra cellular matrix (Debnath et al. 2003a). Overexpression of oncogenes such as Erbb2, Akt and cMYC led to morphometric changes in the MCF10A acini (Debnath et al. 2003b; Partanen et al. 2007). Oncogenic transformation in 3D acinar cultures can result in filled lumen, larger acinar size and formation of protrusions from the spherical structures (Debnath and Brugge 2005). These characteristic changes that epithelial cells acquire have been enumerated in the hallmarks of cancer, coined by Hanahan and Weinberg (Hanahan and Weinberg 2011) such as resisting cell death, sustained proliferative signalling, invasion and metastasis. This makes MCF10A breast acinar cultures an effective model system for studying breast acinar morphogenesis and carcinogenesis (Bessette et al. 2015; Qu et al. 2015).



In our study, MCF10A cells stably overexpressing Api5 were cultured as spheroids. Distinct differences were observed between the control and Api5 OE cells. Morphometric changes including increase in size and cell number indicated the possibility of cellular transformation, thus suggesting a plausible role of Api5 in breast cancer. Api5 OE cells showed sustained proliferative capacity even at day 16 as was demonstrated by increased levels of Ki67 and PCNA. Furthermore, knock-down of Api5 in MCF10A isogenic cell lines, MCF10CA1a (malignant) (Santner et al. 2001) and MCF10AT1 (pre-malignant) (Dawson et al. 1996) led to reduction in both the size of spheroids as well as proliferation.

MCF10A acini have epithelial cell characteristics with basal and apical polarity (Debnath et al. 2003a). Several reports have demonstrated that loss of polarity and reduced lumen size are associated with breast cancer progression (Debnath and Brugge 2005; Imbalzano et al. 2009; Halaoui et al. 2017). In our study we observed a similar phenotype in MCF10A acini overexpressing Api5. Both Laminin V and  $\alpha 6$ -integrin were mislocalised or lost at several regions in the Api5 OE MCF10A acini. Golgi, in MCF10A acini, is localised to the apical region (Gaiko-Shcherbak et al. 2015). Api5 OE led to the mis-localisation of Golgi to the basal regions.

Epithelial cell characteristics are mostly altered during transformation (Roche 2018). Epithelial cells gain mesenchymal characteristics such as the expression of proteins like Slug, Twist, and Vimentin. We observed that Api5 OE led to a partial EMT-like phenotype. A partial/hybrid EMT state is observed when a cell expresses both epithelial and mesenchymal markers (Aiello and Kang 2019). Such a state can support collective cell migration and promote circulating tumour cell movement (Jolly et al. 2015). Recent reports have demonstrated that the hybrid EMT state helps cells to attain stemness characteristics and drug resistance (Saitoh 2018), both of which

are also associated with Api5-FGF2 signalling (Jang et al. 2017; Song et al. 2017).

Identifying whether Api5-induced partial EMT could drive drug resistance and induce stemness characteristics in cancer cells will aid in developing treatment strategies against chemo-resistant cancers.

Increase in migratory potential is a common phenotype observed in malignant cancer cells (Paul et al. 2017). In some scenarios they follow collective cell migration while single cell migration is also observed. The single cells detached from the tumour travel to another tissue, often leading to metastasis (Blockhuys et al. 2020). We report that overexpression of Api5 led to increased single cell migration. The cells attained higher speed and travelled longer distance, however, with reduced persistence. A similar result was earlier reported when fibroblast and glioblastoma cells were treated with EGF (Kim et al. 2008). A lower persistence indicates that the directionality of cellular movement is affected. Golgi plays a major role in cell migration and directionality of movement (Millarte and Farhan 2012). Since Api5 OE resulted in the dispersal of Golgi, this may be promoting the elevated migratory potential, however, with reduced persistence (Tang et al. 2019).

Further, we also demonstrated that Api5 regulates anchorage-independent growth, a well-established property suggesting malignant transformation. Api5 OE led to anchorage-independent growth of MCF10A cells, while knock down in MCF10CA1a and MCF10AT1 showed reduced colony formation on soft agar. When the Api5 KD cells (MCF10CA1a) were injected into the flanks of mice, they formed tumours, although the size was smaller when compared to MCF10CA1a control cells. However, Api5 OE cells did not form tumours in athymic mice. This suggests that overexpression of only Api5 may not be sufficient to cause complete transformation and carcinogenesis of breast epithelial cells. A series of deregulation and genomic changes are required for a cell to be completely transformed.

During MCF10A acinar morphogenesis, cells in the lumen undergo Bim-mediated apoptosis during days 10 to 16 (Reginato et al. 2005). Api5 OE led to reduced Bim levels, thereby inhibiting apoptosis. Studies have reported that oncogenes such as ErbB2 and v-Src show a similar inhibition of Bim, thus preventing luminal cell death (Reginato et al. 2005). This reduction in apoptosis explains the presence of a partially or entirely filled lumen that was observed in the Api5 OE acini. Bim protein levels are regulated by ERK signalling where ERK activation leads to phosphorylation of Bim and thereby its degradation (O'Reilly et al. 2009). We identified that Api5 OE activated FGF2-MEK-ERK signalling during day 12 of acinar morphogenesis, which coincided with the observed Bim degradation. Knock-down of Api5 in the malignant breast cell line confirmed that Api5 can regulate the FGF2-MEK-ERK signalling cascade (Figure 7).

Api5 OE induced higher FGF2 expression from day 4 of acinar morphogenesis which activated PDK1-Akt/cMYC signalling. Knock-down of Api5 resulted in reduced activation of this signalling cascade. c-MYC expression is known to be up-regulated in several breast cancers. Higher expression is also predicted to cause poor patient outcome (Green et al. 2016). Elevated c-MYC expression also mediates EMT in breast cancers (Cho et al. 2010; Yin et al. 2017), thus possibly explaining the partial-EMT observed in Api5 OE cells. Interestingly, Partanen and group in 2007 reported that overexpression of c-MYC in MCF10A led to filling of lumen and possible transformation-like phenotypes, although interestingly, the organised and polarised acinar architecture suppressed the transforming capability of c-MYC (Partanen et al. 2007). Later Simpson *et al.* reported that endogenous and exogenous c-MYC expression are suppressed during later stages of MCF10A acinar cultures (Simpson et al. 2011). Although Api5 overexpression led to a transformed phenotype in our study, the cells did not acquire malignant potential. Interestingly, our results also

indicate that Api5 overexpression induced altered signalling was restored by day 16 of acinar morphogenesis. Therefore, it is possible that acinar morphogenesis could have prevented a complete malignant transformation of overexpressed Api5 in MCF10A cells.

The ability of Api5 to regulate multiple signalling pathways may be an advantage for developing novel breast cancer treatment strategies. Chemoresistance is a complicated phenomenon that further reduces the survival chance of patients. Activation of Akt and ERK signalling are often found to be associated with chemoresistance in cancers. As mentioned earlier, several reports also implicate Api5 to play a role in chemoresistance (Jang et al. 2017; Bousquet et al. 2019). Thus, targeting Api5 might be an excellent strategy for managing such cancers.

Our investigations have uncovered a detailed understanding of the role of Api5 in breast carcinogenesis. We report that Api5 through FGF2, regulates ERK and Akt signalling, thereby leading to transformation of breast epithelial cells (Figure 7). Our data indicate Api5 to be a major regulator of several key events during breast carcinogenesis including elevated proliferation, decreased apoptosis, polarity disruption and anchorage-independent growth. This study opens up a plethora of new research opportunities as well as new possibilities for drug development.

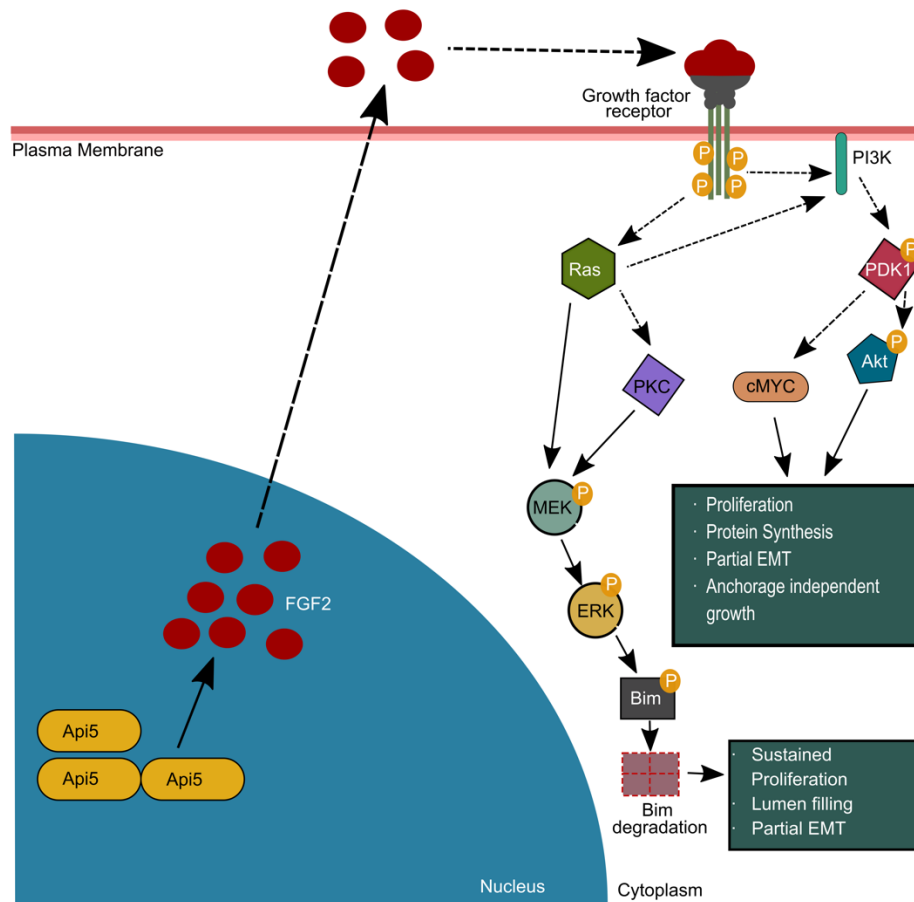


**Figure 7:** Schematic depicting the molecular mechanism of Api5-mediated regulation of PDK1/ Akt and ERK pathways, leading to the transformation of breast epithelial cells. Thick lines show signalling mechanisms revealed from experiments conducted in this study while dotted lines represents signalling mechanisms obtained from published literature. Api5 through FGF2 led to activation of growth factor receptor signalling. During the early days of morphogenesis, overexpression of Api5 led to elevated proliferation via the PDK1- Akt/cMYC pathway thus, aiding in the transformation of breast epithelial cells. Further, during the later days of morphogenesis, FGF2 signalling activated ERK-mediated Bim degradation, thereby inhibiting apoptosis and supporting sustained proliferation.

## **Materials and Methods**

### **Chemicals and antibodies**

Cholera Toxin (C8052), Epidermal Growth Factor (E9644), Hydrocortisone (H0888), Insulin (I1882), Polybrene (H9268), Triton X-100 (T8787), Tris Base (B9754), EDTA (E6758), Na<sub>3</sub>VO<sub>4</sub> (S6508), Protease inhibitor cocktail (P8340) and Poly-L-Lysine (P8920) were purchased from Sigma-Aldrich. Lipofectamine-2000 (11668-500) was purchased from Invitrogen, Thermo Fisher Scientific. Dispase (354235) was purchased from Corning, Sigma-Aldrich. NaF (RM1081) Na<sub>2</sub>HPO<sub>4</sub> (GRM1417), and KH<sub>2</sub>PO<sub>4</sub> (MB050) were purchased from HiMedia. NaCl (15918), Xylene (Q35417), Isopropanol (Q26897), and 30% H<sub>2</sub>O<sub>2</sub> (Q15465) were purchased from Qualigens. 16% paraformaldehyde (AA433689M) was purchased from Alfa Aesar.

Immunofluorescence staining was carried out using Ki67 (Abcam, monoclonal, ab16667),  $\alpha$ 6-integrin (Merck, monoclonal, MAB1378), Laminin V (Merck, monoclonal, MAB19562), GM130 (Abcam, polyclonal, ab30637), E-cadherin (Abcam, monoclonal, ab1416), Vimentin (Abcam, monoclonal, ab92547), and  $\beta$ -catenin (Abcam, monoclonal, ab32572). IHC against Api5 was performed using Api5 (Sigma polyclonal, HPA026598). Api5 (Sigma, polyclonal HPA026598 or Abnova, polyclonal, PAB7951), PCNA (Cell signalling, monoclonal, 2586), E-cadherin (BD, monoclonal, 610182), N-cadherin (Abcam, polyclonal, ab18203), GAPDH (Sigma, polyclonal, G9545), Vimentin (Abcam, monoclonal, ab92547), Slug (Cell Signalling, monoclonal, 9585), Twist (Abcam, Polyclonal, ab50581), Fibronectin (BD, monoclonal, 610077),  $\beta$ -catenin (BD, monoclonal, 610153), Cytokeratin 14 (Abcam, monoclonal, ab7800), Cytokeratin 19 (Abcam, monoclonal, ab52625), Bim (Abcam, monoclonal, ab32158), Cleaved Caspase-9 (Abcam, polyclonal, ab2324), pERK 1&2 (Abcam, monoclonal, ab50011), ERK2 (Abcam, monoclonal, ab32081), pMEK1

(Abcam, monoclonal, ab32088), MEK1 (Abcam, monoclonal, ab32091), FGF2 (Millipore, monoclonal, 05-118), pAkt T308 (Cell Signalling, monoclonal, 4056), pAkt S473 (Invitrogen/ Biosource, monoclonal, 44-621G), Akt (Cell Signalling, monoclonal, 9272S), and cMYC (Santacruz, monoclonal, SC-40) were used for the immunoblotting experiments. Peroxidase-conjugated AffiniPure goat anti-mouse (115-035-003) and anti-rabbit(111-035-003), as well as AffiniPure F(ab')<sub>2</sub> fragment goat anti-mouse IgG, F(ab')<sub>2</sub> fragment specific (115-006-006), were obtained from Jackson Immuno Research. Hoechst 33342 (H3570), Hoechst 33258 (H3569), Alexa Fluor® 488 conjugated anti-mouse secondary antibody(A-11029), Alexa Fluor® 488 conjugated anti-rabbit secondary antibody (A-11034), Alexa Fluor® 568 conjugated anti-mouse secondary antibody(A-11004), Alexa Fluor® 568 conjugated anti-rabbit secondary antibody(A-11036), Alexa Fluor® 568 conjugated anti-rat secondary antibody(A-11077), Alexa Fluor® 633 conjugated anti-mouse secondary antibody (A-21052), Alexa Fluor® 633 conjugated anti-rabbit secondary antibody (A-21071), and Alexa Fluor® 568 phalloidin (A-12380) were bought from Invitrogen, Thermo Fisher Scientific.

### Plasmids

CSII-EF-MCS plasmid was a gift from Dr Sourav Banerjee, NBRC, Manesar, India. pCAG-HIVgp and pCMV-VSV-G-RSV-Rev plasmids were purchased from RIKEN BioResource Centre. mVenusC1 was gifted by Jennifer Lippincott-Schwartz, NIH, USA in which Api5 was cloned.

Primers used for Api5 CDS insertion to CSII-EF-MCS vector were: Forward primer: 5'- AAGGAAAAAAGCGGCCGCATATGCCGACAGTAGAGGAGCT- 3' and reverse primer: 5'-GCTCTAGATCAGTAGAGTCTTCCCCGAC - 3'.

pMD2.G and pPax2 were generous gift from Dr Manas Kumar Santra, NCCS, Pune, India. pLKO1.EGFP was a generous gift from Dr Sorab Dalal, ACTREC, Mumbai, India.

Primers used for shApi5 insertion to pLKO1 vector were: Forward primer: 5'-

CCGGAAGACCTAGAACAGACCTTCACTCGAGTGAAGGTCTGTTCTAGGTCTTTT

TTTG - 3' and reverse primer: 5'-

AATTCAAAAAAGACCTAGAACAGACCTTCACTCGAGTGAAGGTCTGTTCTAGG

TCTT - 3'.

### *In-silico analyses*

Using the GENT2 website, the subtype-based expression profile was plotted by selecting the subtype profile tab and providing “Api5” as gene symbol. Survival plot is presented as provided by the tool with overall survival of the patients. TCGA data (Legacy dataset) downloaded from Xena Browser (UCSC Xena) by selecting IlluminaHiSeq dataset along with clinical data. The data, merged with expression data based on sample ID using R package, is then sorted to separate adjacent normal and tumour data (Sample ID ending with “11” represents adjacent normal data while “01” represents tumour data.) Graph Pad prism (Graph Pad Software, La Jolla, CA, USA) is used for plotting the extracted data. Further Kaplan Meier analysis was carried out using the kmplot online tool. Under breast cancer, “API5” was given as a gene symbol and “201687\_s at” dataset was selected and using median cut-off, the survival plot was generated. Mutation data were analysed using the TCGAportal online tool. TCGA BRCA was selected as a dataset, and Api5 was given as a gene symbol.

### *Cell lines and culture conditions*



The MCF10A cell line was a generous gift from Prof. Raymond C. Stevens (The Scripps Research Institute, La Jolla, CA), while MCF10AT1 and MCF10CA1a were purchased from ATCC. These cells were grown in DMEM with high glucose and without sodium pyruvate (Invitrogen) containing 5% horse serum (Invitrogen), 20 ng/ml EGF (Sigma-Aldrich), 0.5 µg/ml hydrocortisone (Sigma-Aldrich), 100 ng/ml cholera toxin (Sigma-Aldrich), 10 µg/ml insulin (Sigma-Aldrich) and 100 units/ml penicillin-streptomycin (Invitrogen). Cells were resuspended in high glucose DMEM without sodium pyruvate, containing 20% horse serum and 100 units/ml penicillin-streptomycin (Invitrogen) during passaging. The overlay medium in which the cell suspension was made for seeding (assay medium) contained DMEM without sodium pyruvate, horse serum, hydrocortisone, cholera toxin, insulin, EGF and penicillin-streptomycin. HEK 293T cell line was a generous gift from Dr Jomon Joseph (National Centre for Cell Science, Pune, India). The cells were grown in DMEM with high glucose and sodium pyruvate (Invitrogen) containing 10% foetal bovine serum (Invitrogen), and 100 units/ml penicillin-streptomycin (Invitrogen). Cells were resuspended in the same media for passaging. All cell lines were maintained in 100 mm petri dishes (Corning, Sigma-Aldrich / Nunc, Thermo Fisher Scientific / Eppendorf) at 37°C in a humidified 5% CO<sub>2</sub> incubator (Eppendorf). Stable cell lines overexpressing Api5 was prepared using lentiviral-mediated transduction. Briefly, HEK293T cells were transfected with 1µg CSII-EF MCS mCherry Api5 vector having a mCherry-Api5 sequence, along with 0.5µg pCMV-VSV-G-RSV-Rev and 1µg pCAG-HIVgp for viral particle preparation using Lipofectamine 2000 (Invitrogen)-mediated transfection. Opti-MEM® used for transfection was obtained from Invitrogen. DMEM containing 15% horse serum was added to the cells 24 hours post transfection. 48 hours post transfection, viral supernatant was collected and filtered through a 0.45 µm filter to remove cell debris. The viruses were then used to

transduce MCF10A. 4 µg polybrene was added to the cells to increase the transduction efficiency. As control, a stable cell line expressing only mCherry was also prepared. The transduced cells were sorted using BD FACS Aria (BD Biosciences) to get a pure population with maximum number of transduced cells. Api5 KD stable cells were generated in MCF10AT1 and MCF10CA1a in a similar manner. The shRNA was cloned in pLKO.1-EGFP vector, and packaging plasmids pMD2.G and pPax2 were used for lentiviral preparation. Cells were then sorted in BD FACS Aria.

### 3D 'on-top' culture

3D breast acinar cultures were set up in an 8-well chamber cover glass plates (Nunc Lab-Tek, Thermo Fisher Scientific) or 12-well plates (Eppendorf) using standard protocols(Debnath et al. 2003a; Anandi et al. 2016; Anandi et al. 2017). Cultures were grown in a humidified incubator with 5% CO<sub>2</sub> and maintained at 37°C (Eppendorf). The medium was changed every four days. For lysate collection on different days, higher cell density was seeded for Day 4 and Day 8.

For dissociation of acinar culture, Dispase™ (Corning, Sigma-Aldrich) was used. After the addition of Dispase™, the culture was incubated for 20 minutes. The dislodged acini were spun down at 900 rpm for 10 minutes, followed by 2 rounds of 1X PBS wash before plating in 12-well petri plates.

### Immunofluorescence staining

3D spheroid cultures were immune-stained with specific antibodies by established protocols(Anandi et al. 2017). For MCF10CA1a and MCF10AT1 spheroid staining, the 1X PBS and 1X IF buffer washes were added with 0.5% Triton X to aid for better penetration of antibodies. Images were captured using Leica SP8 or Zeiss LSM 710 laser scanning confocal microscope.

## Immunoblotting

Lysates from 2D or 3D cultures were collected in lysis buffer containing 50 mM Tris-HCl, pH 7.4, 0.1% Triton X-100, 5 mM EDTA, 250 mM NaCl, 50 mM NaF, 0.1 mM  $\text{Na}_3\text{VO}_4$  and protease inhibitors. Immunoblotting against specific proteins was performed as per established protocols (Bodakuntla et al. 2014). The blot images represented shows all the bands that were captured using the imaging system. None of the images have been cropped. The entire blots were cut as per experimental requirement and probed for different antibodies.

## Immunohistochemistry

Formalin-fixed and paraffin-embedded breast cancer patient samples were collected from Prashanti Cancer Care Mission, Pune. The samples from each patient may contain tumour area, adjacent normal tissue, lymph nodes, and the reduction mammoplasty tissue. Tissue sectioned using Leica Microtome at 3  $\mu\text{m}$  thickness were taken to poly-L-Lysine (Sigma) coated slides. Tissues are deparaffinised by overnight incubation at 62°C followed by xylene (Fisher scientific) washes. After rehydration of tissues with decreasing concentration of iso-propanol followed by water, endogenous peroxidases are blocked by incubating with 3%  $\text{H}_2\text{O}_2$  (made from 30%  $\text{H}_2\text{O}_2$ , Fisher scientific, by diluting with methanol). Antigen retrieval was carried out using 0.001M EDTA buffer (pH 7.4). Following blocking using 3% BSA, Api5 Antibody (1:2000 dilution, Sigma HPA026598) was added on top of the tissues and incubated at room temperature for 2 hours. Further, tissue is probed with HRP conjugated secondary antibody (Dako) for 30 minutes and then developed with DAB (Dako). The nuclei are counterstained with 10% haematoxylin and mounted with DPX mountant (Fisher Scientific). The analysis was carried out by observing slides at 20X magnification of compound microscope.

H-score for IHC is calculated as follows:

H-Score = Intensity score X Percentage positivity score

The intensity score and percentage positivity score ranges from 0 to 3, and the maximum H score is 9. Three individuals calculated the scores independently by observing ten different positions on the slide corresponding to the tissue ID. The median value from this observation was plotted on the graph.

### Single Cell Migration

Cells were sparsely seeded in 8-well Lab-Tek chamber cover glass slides and incubated for 16 hours in a 37°C incubator supplied with 5% CO<sub>2</sub>. After staining the nuclei with Hoechst 33342 (Invitrogen), cells were imaged at 20X magnification using Leica SP8 confocal microscope for 3 hours. 10 positions were selected for each well, and images were taken every 2 minutes. The data was processed using Fasttracks software (DuChez 2017) and plotted using Graph Pad Prism (Graph Pad Software, La Jolla, CA, USA).

### Soft Agar Assay

Soft agar colony formation assay was performed as detailed earlier (Anandi et al. 2017). Images were acquired using the 10X objective of a Nikon phase-contrast microscope. Ten randomly selected fields were imaged, and the colonies were manually counted. Clonogenicity assay was performed by sparsely seeding cells in 6-well plates (Corning) with three replicates for each set. After 7 days of incubation, cells were stained with crystal violet (HiMedia) and images were captured using HP Scanner after drying the plates.

### *In-vivo* tumorigenicity assay

$6 \times 10^6$  cells were injected subcutaneously in the flanks of athymic mice (Foxnl<sup>nu</sup> / Foxnl<sup>nu</sup>, 6-8 weeks old) mixed with 1:1 diluted Matrigel<sup>®</sup> PBS mixture. Tumour size was measured with a vernier calliper. Furthermore, after 8-12 weeks, mice were sacrificed, and the tumour was dissected out. The tumour was then fixed with 10% formaldehyde and embedded in paraffin wax. Tumour area was calculated by multiplying the major and minor axis of the tumour as measured with a vernier calliper.

### Statistical analysis

Different morphometric parameters were tested for significance using the Mann-Whitney test. Significance test for the *in-silico* data was performed using either Mann-Whitney or Kruskal- Wallis test. The Mann–Whitney U-test was used to analyse the statistical significance of relative Golgi area changes and relative fluorescence intensity in the 3D culture immunostaining. The different parameters for analysing cell migration was tested for significance using the Mann-Whitney test. Statistical analysis for mice tumour area was performed using the 2-way ANOVA followed by Sidak's multiple comparison test.  $P < 0.05$  was considered statistically significant. Graph Pad Prism software (Graph Pad Software, La Jolla, CA, USA) was used to analyse data.

### Ethics approvals

Ethics approval from Institutional Human Ethics Committee (IHEC) was obtained for using patient paraffin embedded tissue blocks in this study (IHEC/Admin/2021/012). Written informed consent was obtained by Prashanti Cancer Care Mission, Pune from all patients, and the study was conducted in accordance with the Declaration of Helsinki, institutional guidelines, and all local, state and national regulations. For preparing Api5 OE MCF10A cells, Api5 KD MCF10AT1 and Api5 KD MCF10CA1a

cells Institutional Biosafety Committee (IBSC) clearance was approved by the institute. The *in vivo* tumorigenicity studies were approved by the Institutional Animal Ethics Committee (IAEC) (IAEC/2018\_02/010 and IISER\_Pune/IAEC/2021\_01/06).

### **Competing interests**

The authors declare no competing or financial interests.

### **Acknowledgements**

We thank Dr Richa Rikhy, (IISER Pune, India) and Dr Sorab Dalal (ACTREC, Mumbai, India) for their useful suggestions. The authors sincerely acknowledge Dr Girish Deshpande (Princeton University, USA) and Prof L S Shashidhara (Ashoka University, India) for their valuable comments and edits in the manuscript. We also thank Dr Manas Kumar Santra (NCCS, Pune, India) and IISER Pune-BD FACS facility for help with sorting of cells. The authors acknowledge Dr T.S. Sridhar and his lab members (SJRI, Bangalore, India) for help with IHC protocols and Dr C.B. Koppikar and team (Prashanti Cancer Care Mission, Pune, India) for providing the paraffin-embedded tissue blocks. We thank Prof. Anjan Banerjee for allowing us to use the microtome for tissue sectioning. We also would like to acknowledge the IISER Pune Microscopy Facility for access to equipment and infrastructure and National Facility for Gene Function in Health and Disease (IISER, Pune, India) for access to the animal facility and support for experiments. We also thank Lahiri lab members for helpful comments and discussions.

### **Author contributions**

Conceptualisation: A.K, M.L.; Methodology: A.K, D.P., R.M., G.G., M.L.; Validation: A.K; Formal analysis: A.K, D.P., R.M., G.G., M.L.; Investigation: A.K, D.P., R.M.,

G.G.; Writing - original draft: A.K.; Writing - review & editing: M.L.; Visualisation: A.K,  
M.L.; Supervision: M.L.; Project administration: M.L.; Funding acquisition: M.L.

## References

- Aiello NM, Kang Y. 2019. Context-dependent EMT programs in cancer metastasis. *J Exp Med* **216**: 1016-1026.
- Almasan A, Ashkenazi A. 2003. Apo2L/TRAIL: apoptosis signaling, biology, and potential for cancer therapy. *Cytokine Growth Factor Rev* **14**: 337-348.
- Anandi L, Chakravarty V, Ashiq KA, Bodakuntla S, Lahiri M. 2017. DNA-dependent protein kinase plays a central role in transformation of breast epithelial cells following alkylation damage. *J Cell Sci* **130**: 3749-3763.
- Anandi VL, Ashiq KA, Nitheesh K, Lahiri M. 2016. Platelet-activating factor promotes motility in breast cancer cells and disrupts non-transformed breast acinar structures. *Oncol Rep* **35**: 179-188.
- Basset C, Bonnet-Magnaval F, Navarro MG, Touriol C, Courtade M, Prats H, Garmy-Susini B, Lacazette E. 2017. Api5 a new cofactor of estrogen receptor alpha involved in breast cancer outcome. *Oncotarget* **8**: 52511-52526.
- Bessette DC, Tilch E, Seidens T, Quinn MC, Wiegman AP, Shi W, Cocciardi S, McCart-Reed A, Saunus JM, Simpson PT et al. 2015. Using the MCF10A/MCF10CA1a Breast Cancer Progression Cell Line Model to Investigate the Effect of Active, Mutant Forms of EGFR in Breast Cancer Development and Treatment Using Gefitinib. *PLoS One* **10**: e0125232.
- Blockhuys S, Zhang X, Wittung-Stafshede P. 2020. Single-cell tracking demonstrates copper chaperone Atox1 to be required for breast cancer cell migration. *Proc Natl Acad Sci U S A* **117**: 2014-2019.
- Bodakuntla S, Libi AV, Sural S, Trivedi P, Lahiri M. 2014. N-nitroso-N-ethylurea activates DNA damage surveillance pathways and induces transformation in mammalian cells. *BMC Cancer* **14**: 287.
- Bong SM, Bae SH, Song B, Gwak H, Yang SW, Kim S, Nam S, Rajalingam K, Oh SJ, Kim TW et al. 2020. Regulation of mRNA export through API5 and nuclear FGF2 interaction. *Nucleic Acids Res* **48**: 6340-6352.
- Bousquet G, Feugeas JP, Gu Y, Leboeuf C, Bouchtaoui ME, Lu H, Espie M, Janin A, Benedetto MD. 2019. High expression of apoptosis protein (Api-5) in chemoresistant triple-negative breast cancers: an innovative target. *Oncotarget* **10**: 6577-6588.
- Cho H, Chung JY, Song KH, Noh KH, Kim BW, Chung EJ, Ylaya K, Kim JH, Kim TW, Hewitt SM et al. 2014. Apoptosis inhibitor-5 overexpression is associated with tumor progression and poor prognosis in patients with cervical cancer. *BMC Cancer* **14**: 545.
- Cho KB, Cho MK, Lee WY, Kang KW. 2010. Overexpression of c-myc induces epithelial mesenchymal transition in mammary epithelial cells. *Cancer Lett* **293**: 230-239.
- Dawson PJ, Wolman SR, Tait L, Heppner GH, Miller FR. 1996. MCF10AT: a model for the evolution of cancer from proliferative breast disease. *Am J Pathol* **148**: 313-319.
- Debnath J, Brugge JS. 2005. Modelling glandular epithelial cancers in three-dimensional cultures. *Nat Rev Cancer* **5**: 675-688.
- Debnath J, Muthuswamy SK, Brugge JS. 2003a. Morphogenesis and oncogenesis of MCF-10A mammary epithelial acini grown in three-dimensional basement membrane cultures. *Methods* **30**: 256-268.
- Debnath J, Walker SJ, Brugge JS. 2003b. Akt activation disrupts mammary acinar architecture and enhances proliferation in an mTOR-dependent manner. *J Cell Biol* **163**: 315-326.
- DuChes BJ. 2017. Automated Tracking of Cell Migration with Rapid Data Analysis. *Curr Protoc Cell Biol* **76**: 12.12.11-12.12.16.
- Duffy MJ, Synnott NC, Crown J. 2018. Mutant p53 in breast cancer: potential as a therapeutic target and biomarker. *Breast Cancer Res Treat* **170**: 213-219.
- Gaiko-Shcherbak A, Fabris G, Dreissen G, Merkel R, Hoffmann B, Noetzel E. 2015. The Acinar Cage: Basement Membranes Determine Molecule Exchange and Mechanical Stability of Human Breast Cell Acini. *PLoS One* **10**: e0145174.

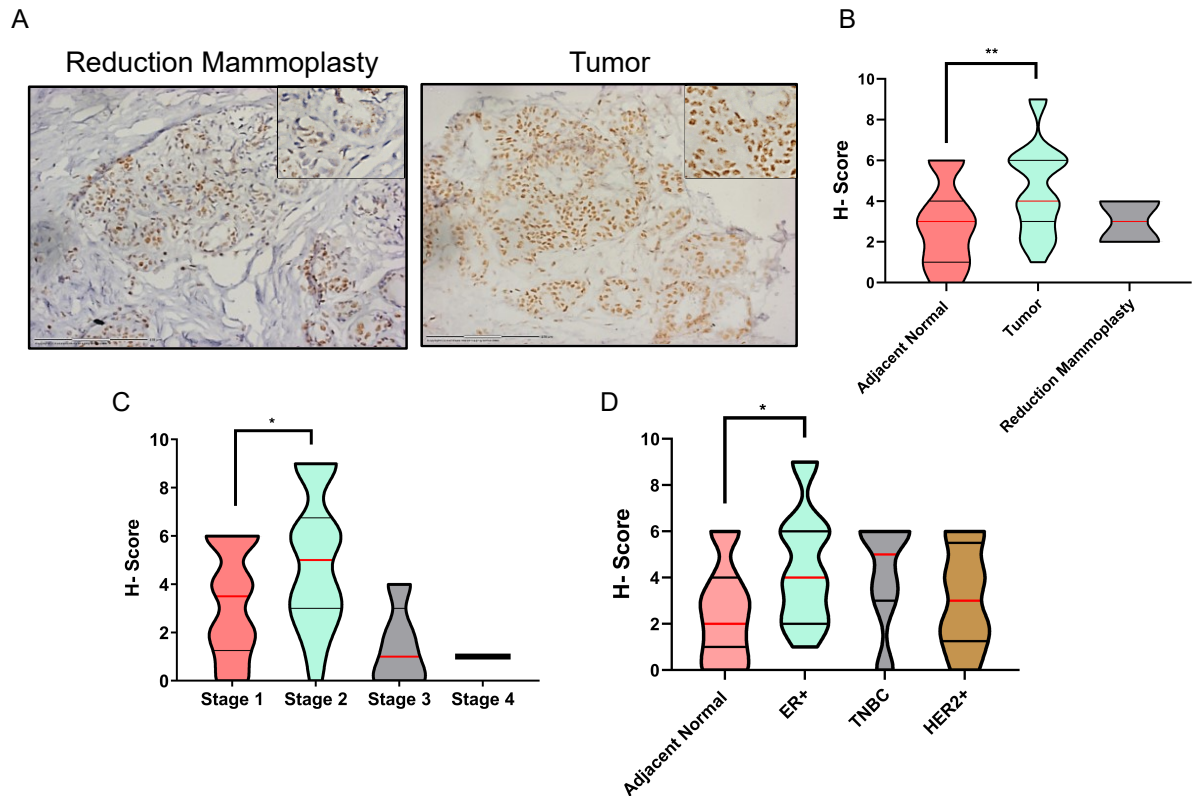


- Garcia-Jove Navarro M, Basset C, Arcondeguy T, Touriol C, Perez G, Prats H, Lacazette E. 2013. Api5 contributes to E2F1 control of the G1/S cell cycle phase transition. *PLoS One* **8**: e71443.
- Green AR, Aleskandarany MA, Agarwal D, Elsheikh S, Nolan CC, Diez-Rodriguez M, Macmillan RD, Ball GR, Caldas C, Madhusudan S et al. 2016. MYC functions are specific in biological subtypes of breast cancer and confers resistance to endocrine therapy in luminal tumours. *Br J Cancer* **114**: 917-928.
- Guiu S, Michiels S, Andre F, Cortes J, Denkert C, Di Leo A, Hennessy BT, Sorlie T, Sotiriou C, Turner N et al. 2012. Molecular subclasses of breast cancer: how do we define them? The IMPAKT 2012 Working Group Statement. *Ann Oncol* **23**: 2997-3006.
- Halaoui R, McCaffrey L. 2015. Rewiring cell polarity signaling in cancer. *Oncogene* **34**: 939-950.
- Halaoui R, Rejon C, Chatterjee SJ, Szymborski J, Meterissian S, Muller WJ, Omeroglu A, McCaffrey L. 2017. Progressive polarity loss and luminal collapse disrupt tissue organisation in carcinoma. *Genes Dev* **31**: 1573-1587.
- Han BG, Kim KH, Lee SJ, Jeong KC, Cho JW, Noh KH, Kim TW, Kim SJ, Yoon HJ, Suh SW et al. 2012. Helical repeat structure of apoptosis inhibitor 5 reveals protein-protein interaction modules. *J Biol Chem* **287**: 10727-10737.
- Hanahan D, Weinberg RA. 2011. Hallmarks of cancer: the next generation. *Cell* **144**: 646-674.
- Imbalzano KM, Tatarkova I, Imbalzano AN, Nickerson JA. 2009. Increasingly transformed MCF-10A cells have a progressively tumor-like phenotype in three-dimensional basement membrane culture. *Cancer Cell Int* **9**: 7.
- Imre G, Berthelet J, Heering J, Kehrlöesser S, Melzer IM, Lee BI, Thiede B, Dotsch V, Rajalingam K. 2017. Apoptosis inhibitor 5 is an endogenous inhibitor of caspase-2. *EMBO Rep* **18**: 733-744.
- Jagot-Lacoussiere L, Kotula E, Villoutreix BO, Bruzzoni-Giovanelli H, Poyet JL. 2016. A Cell-Penetrating Peptide Targeting AAC-11 Specifically Induces Cancer Cells Death. *Cancer Res* **76**: 5479-5490.
- Jang HS, Woo SR, Song KH, Cho H, Chay DB, Hong SO, Lee HJ, Oh SJ, Chung JY, Kim JH et al. 2017. API5 induces cisplatin resistance through FGFR signaling in human cancer cells. *Exp Mol Med* **49**: e374.
- Jansen MP, Foekens JA, van Staveren IL, Dirkzwager-Kiel MM, Ritstier K, Look MP, Meijer-van Gelder ME, Sieuwerts AM, Portengen H, Dorssers LC et al. 2005. Molecular classification of tamoxifen-resistant breast carcinomas by gene expression profiling. *J Clin Oncol* **23**: 732-740.
- Javed A, Lteif A. 2013. Development of the human breast. *Semin Plast Surg* **27**: 5-12.
- Javier RT. 2008. Cell polarity proteins: common targets for tumorigenic human viruses. *Oncogene* **27**: 7031-7046.
- Jolly MK, Boareto M, Huang B, Jia D, Lu M, Ben-Jacob E, Onuchic JN, Levine H. 2015. Implications of the Hybrid Epithelial/Mesenchymal Phenotype in Metastasis. *Front Oncol* **5**: 155.
- Kim HD, Guo TW, Wu AP, Wells A, Gertler FB, Lauffenburger DA. 2008. Epidermal growth factor-induced enhancement of glioblastoma cell migration in 3D arises from an intrinsic increase in speed but an extrinsic matrix- and proteolysis-dependent increase in persistence. *Mol Biol Cell* **19**: 4249-4259.
- Kim JW, Cho HS, Kim JH, Hur SY, Kim TE, Lee JM, Kim IK, Namkoong SE. 2000. AAC-11 overexpression induces invasion and protects cervical cancer cells from apoptosis. *Lab Invest* **80**: 587-594.
- Krejci P, Pejchalova K, Rosenbloom BE, Rosenfelt FP, Tran EL, Laurell H, Wilcox WR. 2007. The antiapoptotic protein Api5 and its partner, high molecular weight FGF2, are up-regulated in B cell chronic lymphoid leukemia. *J Leukoc Biol* **82**: 1363-1364.
- Mailleux AA, Overholtzer M, Schmelzle T, Bouillet P, Strasser A, Brugge JS. 2007. BIM regulates apoptosis during mammary ductal morphogenesis, and its absence reveals alternative cell death mechanisms. *Dev Cell* **12**: 221-234.

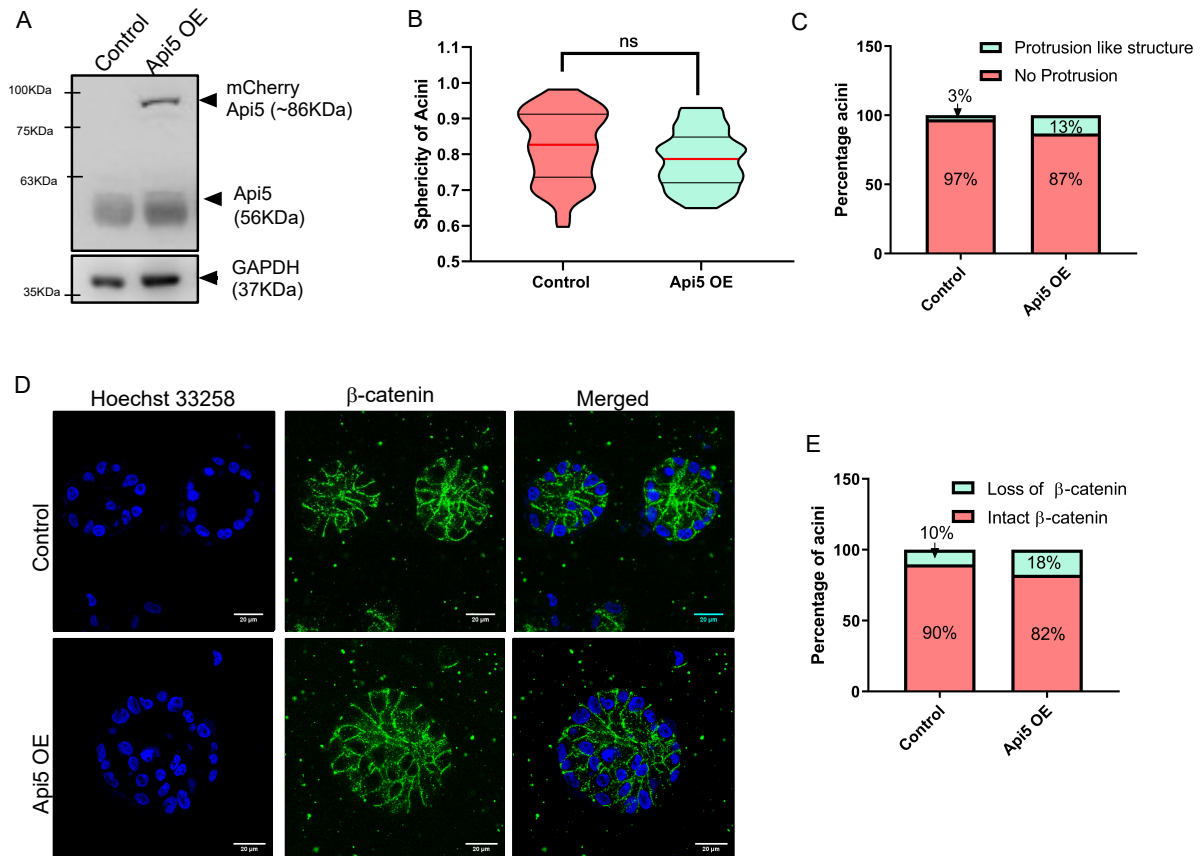
- Millarte V, Farhan H. 2012. The Golgi in cell migration: regulation by signal transduction and its implications for cancer cell metastasis. *ScientificWorldJournal* **2012**: 498278.
- Morris EJ, Michaud WA, Ji JY, Moon NS, Rocco JW, Dyson NJ. 2006. Functional identification of Api5 as a suppressor of E2F-dependent apoptosis in vivo. *PLoS Genet* **2**: e196.
- Mossahebi-Mohammadi M, Quan M, Zhang JS, Li X. 2020. FGF Signaling Pathway: A Key Regulator of Stem Cell Pluripotency. *Front Cell Dev Biol* **8**: 79.
- Nagy A, Munkacsy G, Gyorffy B. 2021. Pancancer survival analysis of cancer hallmark genes. *Sci Rep* **11**: 6047.
- Noh KH, Kim SH, Kim JH, Song KH, Lee YH, Kang TH, Han HD, Sood AK, Ng J, Kim K et al. 2014. API5 confers tumoral immune escape through FGF2-dependent cell survival pathway. *Cancer Res* **74**: 3556-3566.
- O'Reilly LA, Kruse EA, Puthalakath H, Kelly PN, Kaufmann T, Huang DC, Strasser A. 2009. MEK/ERK-mediated phosphorylation of Bim is required to ensure survival of T and B lymphocytes during mitogenic stimulation. *J Immunol* **183**: 261-269.
- Okada T, Enkhjargal B, Travis ZD, Ocak U, Tang J, Suzuki H, Zhang JH. 2019. FGF-2 Attenuates Neuronal Apoptosis via FGFR3/PI3k/Akt Signaling Pathway After Subarachnoid Hemorrhage. *Mol Neurobiol* **56**: 8203-8219.
- Park SJ, Yoon BH, Kim SK, Kim SY. 2019. GENT2: an updated gene expression database for normal and tumor tissues. *BMC Med Genomics* **12**: 101.
- Partanen JI, Nieminen AI, Makela TP, Klefstrom J. 2007. Suppression of oncogenic properties of c-Myc by LKB1-controlled epithelial organisation. *Proc Natl Acad Sci U S A* **104**: 14694-14699.
- Paul CD, Mistriotis P, Konstantopoulos K. 2017. Cancer cell motility: lessons from migration in confined spaces. *Nat Rev Cancer* **17**: 131-140.
- Petrosyan A. 2015. Onco-Golgi: Is Fragmentation a Gate to Cancer Progression? *Biochem Mol Biol J* **1**.
- Plati J, Bucur O, Khosravi-Far R. 2008. Dysregulation of apoptotic signaling in cancer: molecular mechanisms and therapeutic opportunities. *J Cell Biochem* **104**: 1124-1149.
- . 2011. Apoptotic cell signaling in cancer progression and therapy. *Integr Biol (Camb)* **3**: 279-296.
- Pouthas F, Girard P, Lecaudey V, Ly TB, Gilmour D, Boulin C, Pepperkok R, Reynaud EG. 2008. In migrating cells, the Golgi complex and the position of the centrosome depend on geometrical constraints of the substratum. *J Cell Sci* **121**: 2406-2414.
- Qu Y, Han B, Yu Y, Yao W, Bose S, Karlan BY, Giuliano AE, Cui X. 2015. Evaluation of MCF10A as a Reliable Model for Normal Human Mammary Epithelial Cells. *PLoS One* **10**: e0131285.
- Ramdas P, Rajihuzzaman M, Veerasenan SD, Selvaduray KR, Nesaretnam K, Radhakrishnan AK. 2011. Tocotrienol-treated MCF-7 human breast cancer cells show down-regulation of API5 and up-regulation of MIG6 genes. *Cancer Genomics Proteomics* **8**: 19-31.
- Reginato MJ, Mills KR, Becker EB, Lynch DK, Bonni A, Muthuswamy SK, Brugge JS. 2005. Bim regulation of lumen formation in cultured mammary epithelial acini is targeted by oncogenes. *Mol Cell Biol* **25**: 4591-4601.
- Roche J. 2018. The Epithelial-to-Mesenchymal Transition in Cancer. *Cancers (Basel)* **10**.
- Saitoh M. 2018. Involvement of partial EMT in cancer progression. *J Biochem* **164**: 257-264.
- Santner SJ, Dawson PJ, Tait L, Soule HD, Eliason J, Mohamed AN, Wolman SR, Heppner GH, Miller FR. 2001. Malignant MCF10CA1 cell lines derived from premalignant human breast epithelial MCF10AT cells. *Breast Cancer Res Treat* **65**: 101-110.
- Saraste J, Prydz K. 2019. A New Look at the Functional Organization of the Golgi Ribbon. *Front Cell Dev Biol* **7**: 171.
- Sasaki H, Moriyama S, Yukiue H, Kobayashi Y, Nakashima Y, Kaji M, Fukai I, Kiriya M, Yamakawa Y, Fujii Y. 2001. Expression of the antiapoptosis gene, AAC-11, as a prognosis marker in non-small cell lung cancer. *Lung Cancer* **34**: 53-57.

- Shahbandi A, Nguyen HD, Jackson JG. 2020. TP53 Mutations and Outcomes in Breast Cancer: Reading beyond the Headlines. *Trends Cancer* **6**: 98-110.
- Sharma VK, Lahiri M. 2021. Interplay between p300 and HDAC1 regulate acetylation and stability of Api5 to regulate cell proliferation. *Sci Rep* **11**: 16427.
- Simpson DR, Yu M, Zheng S, Zhao Z, Muthuswamy SK, Tansey WP. 2011. Epithelial cell organisation suppresses Myc function by attenuating Myc expression. *Cancer Res* **71**: 3822-3830.
- Song KH, Cho H, Kim S, Lee HJ, Oh SJ, Woo SR, Hong SO, Jang HS, Noh KH, Choi CH et al. 2017. API5 confers cancer stem cell-like properties through the FGF2-NANOG axis. *Oncogenesis* **6**: e285.
- Soule HD, Maloney TM, Wolman SR, Peterson WD, Jr., Brenz R, McGrath CM, Russo J, Pauley RJ, Jones RF, Brooks SC. 1990. Isolation and characterisation of a spontaneously immortalised human breast epithelial cell line, MCF-10. *Cancer Res* **50**: 6075-6086.
- Swamydas M, Eddy JM, Burg KJ, Dreau D. 2010. Matrix compositions and the development of breast acini and ducts in 3D cultures. *In Vitro Cell Dev Biol Anim* **46**: 673-684.
- Tang CX, Luan L, Zhang L, Wang Y, Liu XF, Wang J, Xiong Y, Wang D, Huang LY, Gao DS. 2019. Golgin-160 and GMAP210 play an important role in U251 cells migration and invasion initiated by GDNF. *PLoS One* **14**: e0211501.
- Tewari M, Yu M, Ross B, Dean C, Giordano A, Rubin R. 1997. AAC-11, a novel cDNA that inhibits apoptosis after growth factor withdrawal. *Cancer Res* **57**: 4063-4069.
- Wang M, Li J, Huang J, Luo M. 2020. The Predictive Role of PIK3CA Mutation Status on PI3K Inhibitors in HR+ Breast Cancer Therapy: A Systematic Review and Meta-Analysis. *Biomed Res Int* **2020**: 1598037.
- Wong RS. 2011. Apoptosis in cancer: from pathogenesis to treatment. *J Exp Clin Cancer Res* **30**: 87.
- Xu S, Feng Y, Zhao S. 2019. Proteins with Evolutionarily Hypervariable Domains are Associated with Immune Response and Better Survival of Basal-like Breast Cancer Patients. *Comput Struct Biotechnol J* **17**: 430-440.
- Yin S, Cheryan VT, Xu L, Rishi AK, Reddy KB. 2017. Myc mediates cancer stem-like cells and EMT changes in triple negative breast cancers cells. *PLoS One* **12**: e0183578.

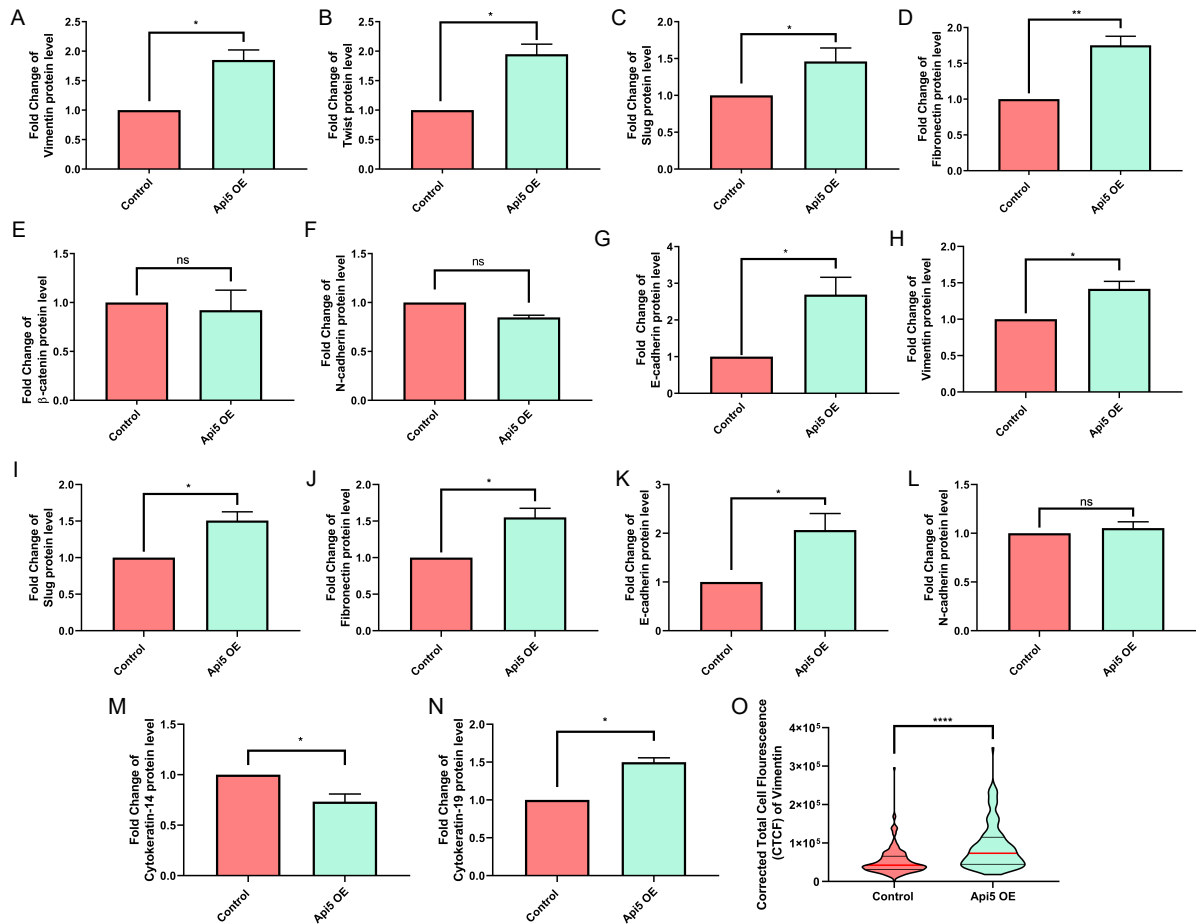
## Supplementary Information



**Supplementary Figure 1:** (A) Representative image of Api5 immunostained section of a paraffin-embedded breast cancer tissue block and the corresponding reduction mammoplasty section. Inset shows a zoomed-in image. H score of tissue sample compared between (B) adjacent normal and tumour tissues, (C) different stages of breast cancer and (D) subtypes of breast cancer plotted as violin plots. Statistical analysis was performed using the Mann-Whitney test. \* $P < 0.05$ , \*\* $P < 0.01$ , \*\*\* $P < 0.001$  and \*\*\*\* $P < 0.0001$ .  $N \geq 25$ .

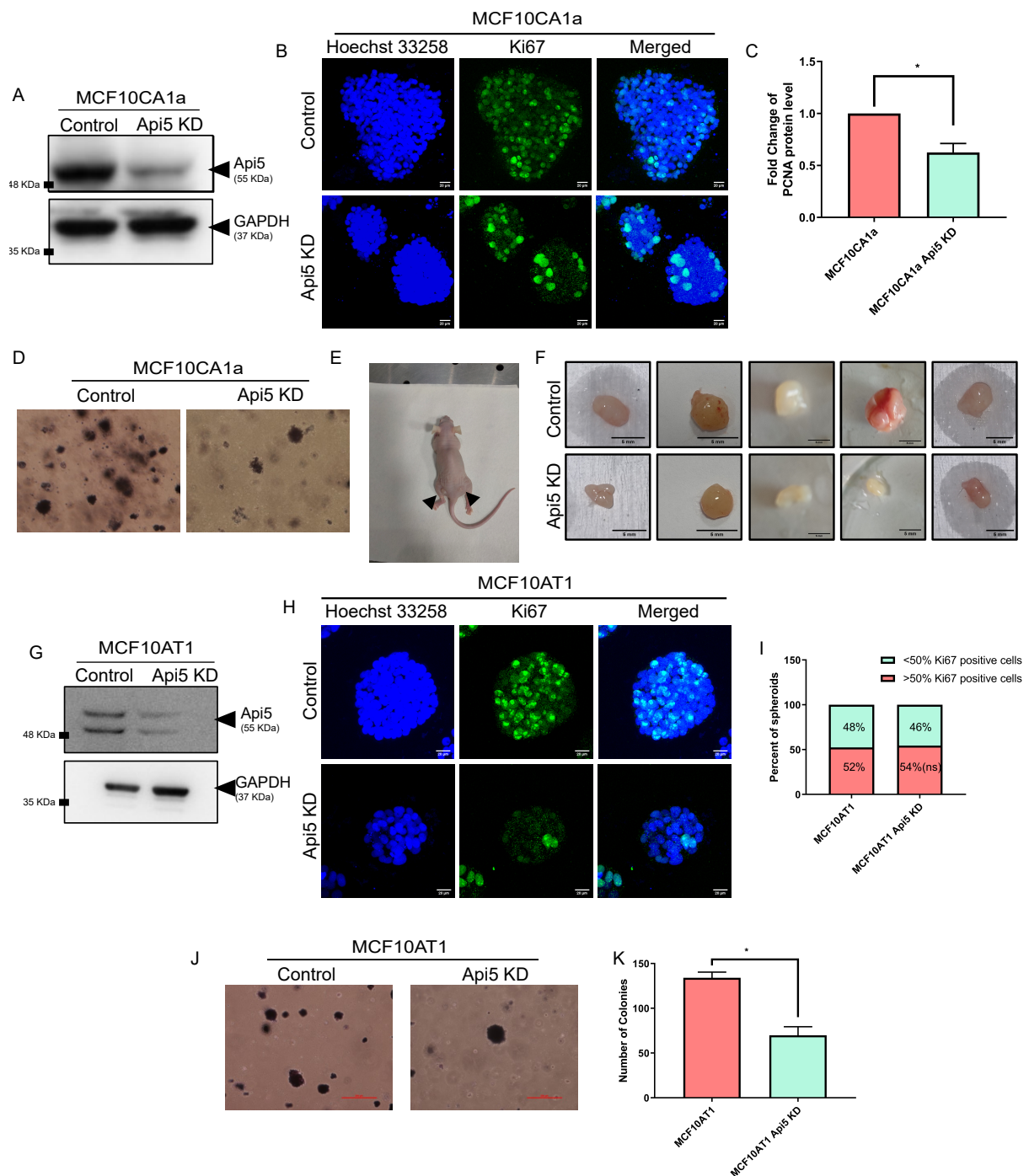


**Supplementary Figure 2:** (A) Western blot image showing overexpression of Api5 in MCF10A lysates collected from day 16 acini. (B) Graph showing sphericity of day 16 acini analysed based on phalloidin staining using Huygens software (C) Graph showing percentage of acini with protrusion-like structure manually analysed based on phalloidin staining in MCF10A cells. (D) Representative image of  $\beta$ -catenin staining (green) in day 16 acini. (E) Graph showing percentage of acini with intact and loss of  $\beta$ -catenin.



**Supplementary Figure 3: Breast epithelial cells overexpressing Api5 acquires partial EMT-like characteristics.** Graph showing fold change of (A) Vimentin, (B) Twist (C) Slug, (D) Fibronectin, (E)  $\beta$ -catenin, (F) N-cadherin and (G) E-cadherin protein expression lysates collected from day 16 lysates of 3D culture. Graph showing fold change of (H) Vimentin, (I) Slug, (J) Fibronectin, (K) E-cadherin, (L) N-cadherin, (M) Cytokeratin-14 and (N) Cytokeratin-19 in lysates collected from 3D dissociated cells of control and Api5 OE MCF10A. (O) Violin plot showing the corrected fluorescence intensity of vimentin in 3D dissociated cells. Fold change in protein levels were calculated in comparison to the control lane and normalised to GAPDH. Statistical analysis was performed using the paired t-test. \* $P < 0.05$ , \*\* $P < 0.01$ , \*\*\* $P < 0.001$  and \*\*\*\* $P < 0.0001$ . Data pooled from  $N \geq 3$  independent experiments.

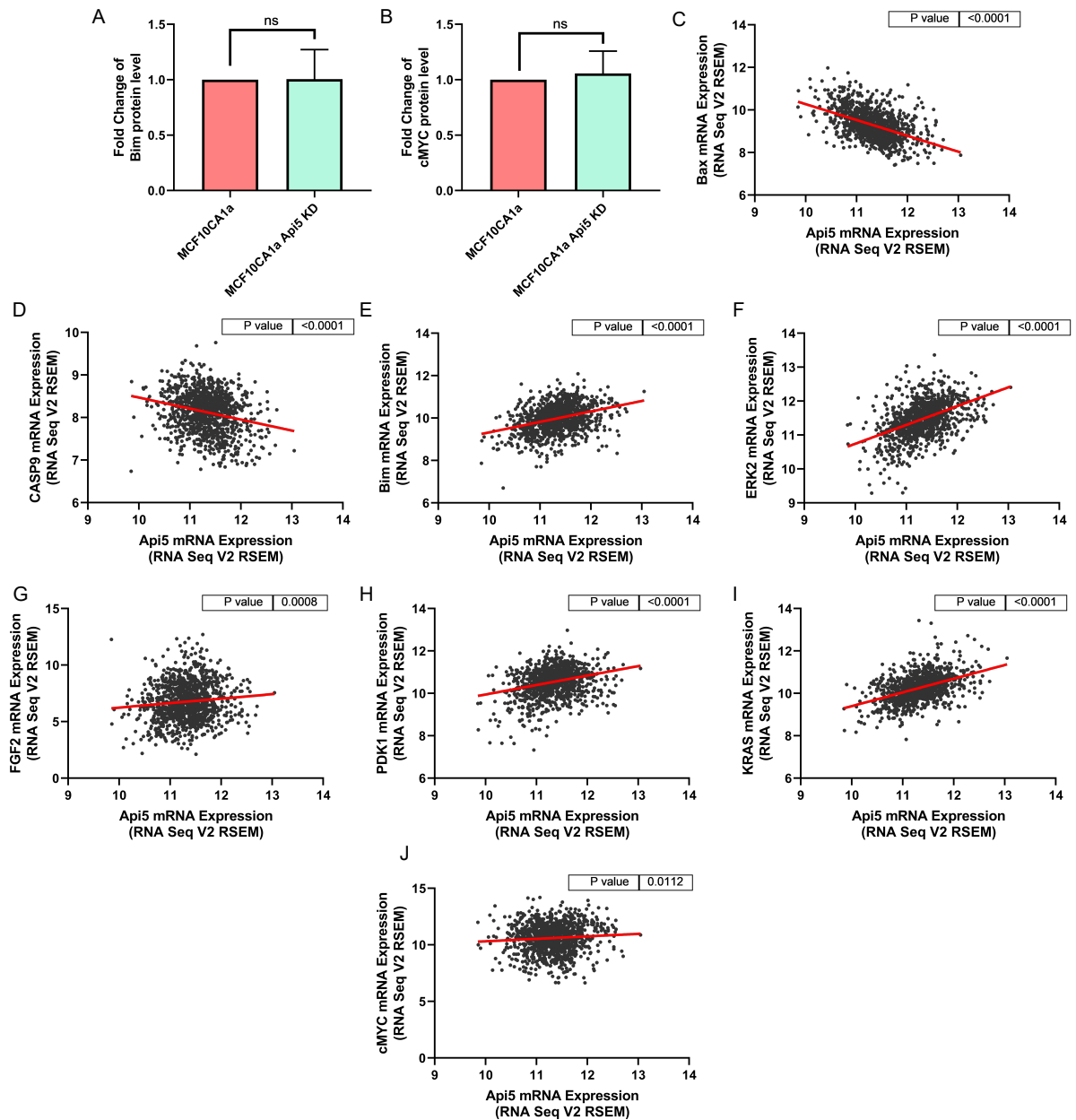




**Supplementary Figure 4** (A) Western blot showing Api5 levels in stable cells of MCF10CA1a transduced with shApi5 construct. (B) Representative image of Api5 KD MCF10CA1a cells immunostained for proliferation marker, Ki67 after 7 days of culturing in Matrigel® (Ki67: green, nuclei: blue) (C) Graph showing the fold change in PCNA protein levels in lysates collected from day 7 spheroid cultures. (D) Representative image showing colony formed in soft agar assay by MCF10CA1a

cells with Api5 KD stained with MTT after 21 days of seeding. (E) Representative image of mice sacrificed for tumour dissection post 8 weeks. Left flank was injected with control cells and the right flank with Api5 KD cells. (F) Representative images of tumour dissected from flanks of athymic mice after week 8 post subcutaneous injection. The upper panel shows MCF10CA1a control cells, while the lower panel shows Api5 KD MCF10CA1a. (G) Western blot showing Api5 levels in stable cells of MCF10AT1 transduced with shApi5 construct. (H) Representative image of Api5 KD MCF10AT1 cells immunostained for Ki67 after 7 days of culturing in Matrigel® (Ki67: green, nuclei: blue). (I) Graph showing the percentage of spheroids with 50% or more cells showing Ki67 staining. (J) Representative image showing colony formed in soft agar assay by MCF10AT1 cells with Api5 KD stained with MTT after 21 days of seeding. (K) Bar graph representing the number of colonies formed by MCF10AT1 cells compared between control and Api5 KD. Statistical analysis was performed using the Mann-Whitney test. \*P<0.05, \*\*P<0.01, \*\*\*P<0.001 and \*\*\*\*P<0.0001 or paired t-test. \*P<0.05, \*\*P<0.01, \*\*\*P<0.001 and \*\*\*\*P<0.0001. Data pooled from n>4 independent.





**Supplementary Figure 5:** Bar diagram representing the expression of (A) Bim and (B) cMYC in lysates collected from day 7 MCF10CA1a spheroids. (C-J) TCGA-based co-expression analysis performed between transcript expression of proteins involved in the pathway depicted in Figure 7 and Api5. Graphs are generated using TCGA data downloaded using UCSC Xena Browser(Goldman et al. 2020).



OPEN ACCESS

# Prolonged Exposure to Platelet Activating Factor Transforms Breast Epithelial Cells

**Edited by:**

Hari S. Misra,  
Bhabha Atomic Research Centre  
(BARC), India

**Reviewed by:**

Chandrima Das,  
Saha Institute of Nuclear Physics  
(SINP), India  
Constantinos Demopoulos,  
National and Kapodistrian University  
of Athens, Greece

**\*Correspondence:**

Mayurika Lahiri  
mayurika.lahiri@iiserpune.ac.in  
orcid.org/0000-0001-9456-4920

<sup>†</sup>These authors have contributed  
equally to this work

**\*Present address:**

Vaishali Chakravarty,  
Enveda Therapeutics India Pvt. Ltd.,  
VCR Park, Vishakhapatnam, India  
Libi Anandi,  
Department of Biology,  
Center for Genomics and Systems  
Biology, New York University,  
New York, NY, United States  
K. A. Ashiq,  
National Centre for Cell Science,  
Pune, India

**Specialty section:**

This article was submitted to  
Genetics of Common and Rare  
Diseases,  
a section of the journal  
Frontiers in Genetics

**Received:** 29 November 2020

**Accepted:** 03 March 2021

**Published:** 25 March 2021

**Citation:**

Chakravarty V, Anandi L, Ashiq KA,  
Abhijith K, Umesh R and  
Lahiri M (2021) Prolonged Exposure  
to Platelet Activating Factor  
Transforms Breast Epithelial Cells.  
*Front. Genet.* 12:634938.  
doi: 10.3389/fgene.2021.634938

**Vaishali Chakravarty<sup>††</sup>, Libi Anandi<sup>††</sup>, K. A. Ashiq<sup>††</sup>, K. Abhijith, Rintu Umesh and  
Mayurika Lahiri<sup>\*</sup>**

*Department of Biology, Indian Institute of Science Education and Research, Pune, India*

Lipid species are known to have various biological functions owing to their structural differences, and each of them possesses a specific role to play depending upon their location and distribution in the cell. Some of these lipids interact with proteins on the cell membrane and acts as second messengers. The level of lipid mediators is generally maintained in the cell by feedback mechanisms; however, their improper degradation or enhanced production leads to their accumulation in the tumor microenvironment and disturbs the homeostasis of the cell. Platelet activating factor (PAF) is a known phospholipid mediator secreted upon immunological challenges by platelets, neutrophils, basophils, and macrophages. PAF, as a potent inflammatory molecule, is well studied, and its role in various cancers and cardiovascular diseases has also been investigated. Interestingly, increased levels of PAF have been found in the blood plasma of smokers, and breast cancer cells have shown the accumulation of PAF in presence of cigarette smoke extract. This accumulation was found to increase tumor cell motility that in turn could promote metastasis. Beyond this, however, the effect of PAF on tumorigenesis has not yet been well explored. Here, we show that the continuous exposure of 3D breast acinar cultures to PAF resulted in the activation of various oncogenic signaling pathways leading to transformation. We also found that the presence of PAF in the micro-environment increased the expression of PAF receptor (PAF-R), which corroborated with the higher expression of PAF-R detected in some epithelial cancers, as per literature. Thus, this study impresses on the fact that the presence of PAF alters the cellular microenvironment and eventually triggers irreversible effects that can cumulatively lead to transformation.

**Keywords:** platelet activating factor, transformation, breast cancer, epithelial-mesenchymal transition, polarity

## INTRODUCTION

Immune system holds a key position in maintaining cellular homeostasis, and an imbalance can lead to various abnormalities including cancer. Hence, it is one of the primary targets while designing therapy for malignancies. Tumor infiltrating cells, such as leukocytes and macrophages, are common entities in cancers, and their interaction with the tumor micro-environment components is widely studied (Hanahan and Weinberg, 2011). Such entities are known to promote tumor progression and invasion, and thus hold a clinical relevance in

various cancers (Man et al., 2013). The interaction of the immune cells and the cancer cells could be through direct cell-cell contact or may also be mediated by secretory molecules. One such molecule is platelet activating factor (PAF). PAF is an autacoid phospholipid mediator, which is secreted in response to an agonist by various immune cells and elicits various immunoregulatory reactions such as platelet aggregation, allergy, anaphylaxis, and many more (Foa et al., 1985; Hanahan and Weinberg, 2011). Overall, it is known to induce various physiological and pathological processes that eventually affect the respiratory, vascular, and even reproductive system (Papakonstantinou et al., 2017). PAF production is tightly regulated by biosynthetic and degradative mechanisms since uncontrolled levels can cause various pathologies. PAF acetyl hydrolase (PAF-AH) controls the level of PAF in the system by degradative mechanisms (Chen et al., 2007).

In the early studies, after the role of PAF was established in various pleiotropic activities, its effects were observed in various diseases as well (Lordan et al., 2019). PAF-AH activity was seen to be inhibited when human plasma was treated with cigarette smoke extract (CSE). This was also strengthened by the results that showed increased plasma concentration of PAF in smokers, indicating the role of PAF in the development of cardiovascular diseases in smokers (Miyaura et al., 1992). Kispert et al. (2015) has shown that CSE inhibits PAF-AH activity, thus leading to the accumulation of PAF in the endothelial cells. In a recent study with a bladder cancer cell line, the same group has reported similar results, wherein grade III HT-1376 cells showed higher PAF accumulation followed by greater adherence in presence of CSE, exhibiting highly aggressive manifestations (Kispert et al., 2019). Investigations by Bussolati et al. showed the presence of high amounts of PAF in MCF-7, MDA-MB 231, and T47D cells. This synthesized PAF enhanced cell motility as well as increased proliferation in MDA-MB 231 cells (Bussolati et al., 2000). An early report from Bennett et al. demonstrates that PAF induces phenotypic transformation in rat embryonic cells. They have shown increased cell density, growth in low serum condition, and anchorage-independent growth, which are the indicators of transformation, in the presence of dose-dependent increase in PAF concentration (Bennett et al., 1993).

Although PAF is a lipid mediator, it is not known to freely diffuse through the cell membrane and studies clearly state that PAF activates a G-protein coupled receptor, PAF-R and mediates its activities through this axis. PAF-R is ubiquitously expressed across tissues, and its role in various cancers has been established (Ishii and Shimizu, 2000; Jancar and Chammas, 2014). The PAF-PAFR axis activation suggests a feedback control loop that maintains the PAFR levels in pathological conditions (Chen et al., 2015a; Lv et al., 2017). Two groups in 2015 have shown the role of PAFR in non small cell lung carcinoma (NSCLC) and esophageal squamous cell carcinoma (ESCC). In NSCLC, the activation of PAF-PAF-R axis induces epithelial-mesenchymal transition (EMT), leading to invasion and metastasis of NSCLC cells (Chen et al., 2015a). Role of PAF-R in ESCC malignancy has been stated *via* the activation of oncogenic signaling through FAK/PI3K/AKT/NF- $\kappa$ B axis (Chen et al., 2015b).

Previous report from the lab has shown that breast cancer cells in the presence of PAF shows higher motility and when MCF10A, a non-tumorigenic breast epithelial cell line, was grown on an ECM, in presence of PAF, disrupts the luminal phenotype (Anandi et al., 2016). Results from the lab as well as mounting evidence from literature imposed heavily on the necessity to investigate the role of PAF in the transformation of three-dimensional (3D) cultures of MCF10A cells. In the current study, we have focused on elucidating the transformation phenotypes acquired by MCF10A breast acinar cultures in the presence of PAF and the activation of PI3-K/AKT signaling pathway to strengthen the oncogenic potential of PAF.

## MATERIALS AND METHODS

### Cell Lines and Culture Conditions

MCF10A cell line was a generous gift from Prof. Raymond C. Stevens (The Scripps Research Institute, California, United States) and 2D monolayer cultures and 3D cultures were grown according to the standard protocols (Debnath et al., 2003). 3D cultures were maintained for 20 days by supplementing fresh media every 4 days. Methylcarbaryl PAF C-16, procured as a 10 mg/ml solution in ethanol (Cayman chemicals, 60908), was diluted in sterile PBS to make a working stock of 100  $\mu$ M. Required volume of the working stock was directly added to the desired volume of media, to achieve a final concentration of 200 nM. PAF treatment was given 3 h post seeding and along with every media change.

### Immunofluorescence

Acini from the 3D cultures were extracted using PBS-EDTA treatment for apical proteins and other proteins using normal method of extraction. Immunostaining was done using a previously described protocol (Anandi et al., 2017). Samples were imaged using 40X oil immersion objective of SP8 confocal microscope (Leica, Germany).

Details of chemical, antibodies, and statistical analysis used and methods for 3D “on top” cultures, immunoblot analysis, RNA Extraction, cDNA preparation, semi-quantitative PCR, soft agar assay, DQ collagen invasion assay, and gelatin zymography can be found in **Supplementary Material**.

## RESULTS

### PAF Treatment on 3D Cultures of MCF10A Leads to Increased Proliferation

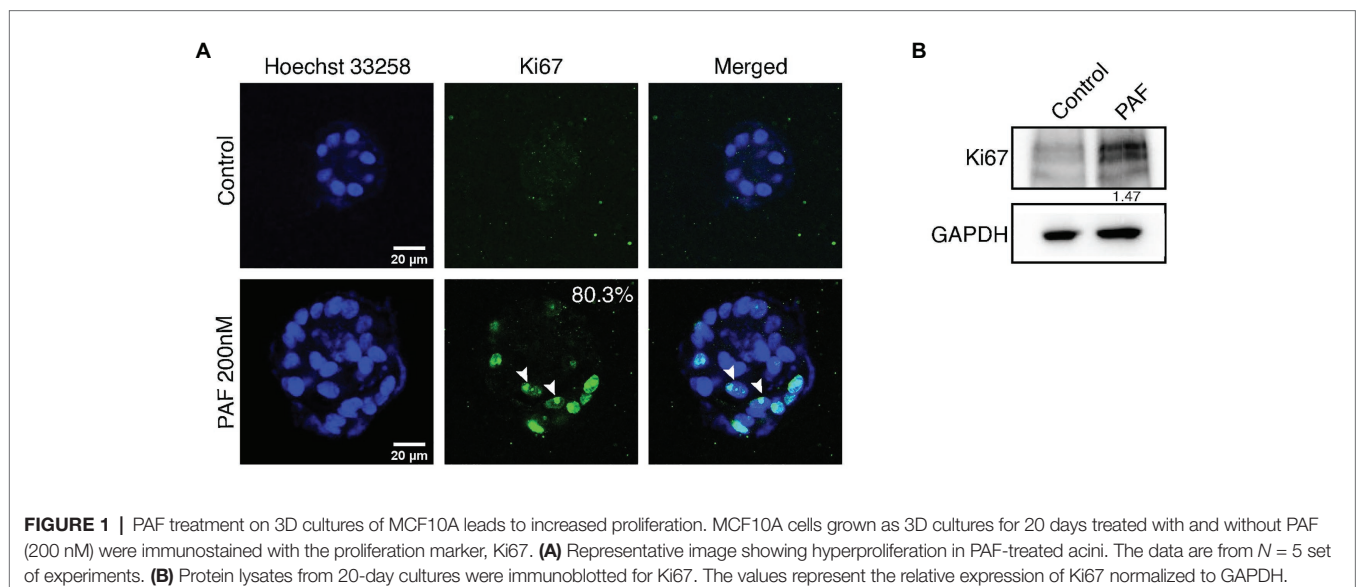
3D breast acinar cultures, grown on laminin rich matrix, attain a growth arrested state with a monolayer of cells around a hollow lumen, after 12 days of culturing. Cells in such stable structures are usually arrested in the G1 Phase (Fournier et al., 2006). Based on our previous data (Anandi et al., 2016), to ascertain if PAF treatment resulted in the presence of hyperproliferating and actively dividing cells, that resulted in large acini, we immunostained the PAF-treated 20-day cultures with Ki67, a proliferation marker. Acini with more than five

cells positive for Ki67 are considered to be hyperproliferating (Wu and Gallo, 2013). Eighty percent of the PAF treated acini were found to be hyperproliferating (**Figure 1A**). Further, immunoblotting revealed a 1.4-fold upregulation in Ki67 protein levels (**Figure 1B**). This shows that PAF leads to the formation of large multiple layered acini that have evaded the growth-arrested state and are hyperproliferating thus qualifying as a transformation phenotype.

## Apico-Basal Polarity and Cell-Cell Junctions Gets Disrupted in the Presence of PAF Treatment

One of the important features of epithelial architecture is polarization. Epithelial cells attain apico-basal polarity when placed in a 3D environment unlike cells on a 2D plane, which only have front and rear polarities. Alongside, cell-cell junction is an important component in maintaining the epithelial tissue homeostasis. In this study, it is evident that PAF affects the orientation of epithelial polarity and leads to compromised cell-cell junctions. There are various proteins that are known to act as markers of polarity such as integrins, laminins, and also Golgi (Debnath et al., 2003; Debnath and Brugge, 2005). E-cadherin is an adherens junction protein, which is well-established in MCF10A unlike the tight junctions, which are poorly developed (Ivers et al., 2014). E-cadherin is a central component of the zona adherens junction complex, and the loss of E-cadherin is a key indicator of tumor aggressiveness (Kourtidis et al., 2017). The 3D cultures of MCF10A treated with PAF were extracted after 20 days and immunostained with apical and basal markers such as GM130,  $\alpha 6$ -integrin, and Laminin-V.  $\alpha 6$ -integrin, receptors for the ECM, marks the basal region of the acini and stains across the basolateral regions. In the presence of PAF, the staining pattern was altered dramatically by change in expression level as well as membrane distribution of the protein (**Figure 2A**).

Seventy-three percent of acini treated with PAF exhibited marked loss of  $\alpha 6$ -integrin from the basal region and also enhanced cytoplasmic staining was observed, which we quantified as loss and mis-localized phenotype. Epithelial cells have a remarkable property of attachment to the ECM *via* the basement membrane (BM). This BM is disrupted in the cases of primary metastasis in breast carcinomas (Shaw et al., 2004). Laminins are a group of BM proteins and LamininV is one of the components of BM (Shaw et al., 2004). Acini grown in the presence of PAF showed gross disruption in LamininV staining, thus indicating loss of BM protein due to PAF treatment. Seventy-two percent of acini show disrupted as well as the loss of membrane localization of LamininV (**Figure 2B**). GM130, which is a cis-Golgi marker, was mislocalized to the basal and lateral regions in PAF-treated acini, whereas in the control acini Golgi localization remained apical. Upon quantifying, it was observed that 100% of Golgi was mislocalized in PAF-treated acini (**Figure 2C**). These results indicate a clear loss of apical as well as basal polarity in MCF10A 3D cultures grown in the presence of PAF. Immunostaining for  $\beta$ -catenin revealed a diffused localization of  $\beta$ -catenin at cell-cell junction as well as in intercellular granular pockets, which is also indicative of aberrant protein trafficking (**Figure 2D**). To further confirm the disruption of the cell-cell junctions, cells from day 20 spheroids were dissociated (referred to as dissociated cells hereafter) and immunostained for E-cadherin and  $\beta$ -catenin. Loss of E-cadherin by immunostaining was observed in the presence of PAF (**Figure 2E**) and analyzed using intensity plot profiling (**Figure 2G**).  $\beta$ -catenin also showed similar diffused patterns in the dissociated cells as was observed in the acinar cultures (**Figure 2F**). The diffused pattern was analyzed using a plot profiling of lines drawn across cell-cell junctions and then calculating Full Width Half Max (FWHM) as depicted in the schematic in **Figure 2H**. The FWHM values were significantly higher in PAF exposed cells as compared to





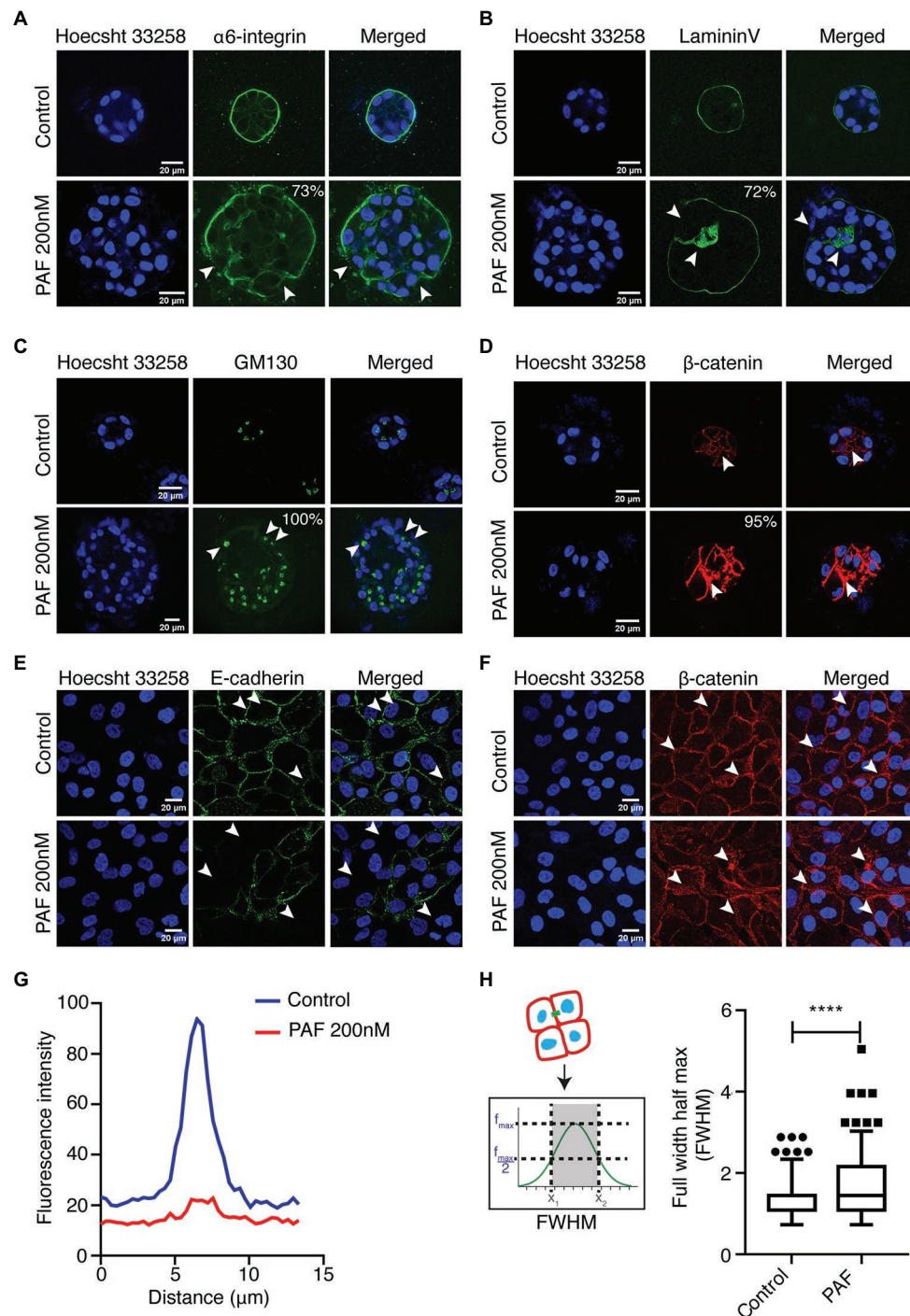


**FIGURE 2** | PAF treatment alters acinar polarity and leads to the disruption of cell-cell junctions. PAF-treated 20 days 3D cultures of MCF10A were immunostained with polarity and cell-cell junction markers. Nucleus is stained with Hoecsht 33,258 (blue). **(A)** Immunostained images of  $\alpha$ 6-integrin (green) marks the basal polarity ( $N = 4$ ). **(B)** Immunostained images of LamininV (green) marks the basement membrane of the acini ( $N = 4$ ). **(C)** Immunostained images of GM130 (green) marks apical polarity ( $N = 3$ ). **(D)** Immunostained images of  $\beta$ -catenin (red) marks the cell-cell junctions. **(E)** Dissociated cells of control and PAF-treated acini immunostained with E-cadherin (green), a cell-cell junction marker and the image is a representative of the phenotype ( $N = 3$ ). **(F)** Dissociated cells of control and PAF treated acini immunostained with  $\beta$ -catenin (red), a cell-cell junction marker and the image is a representative of the diffused phenotype ( $N = 3$ ). **(G)** Median fluorescent intensity of E-cadherin line profile showing loss phenotype. **(H)** FWHM profile of  $\beta$ -catenin line profile showing diffused phenotype. The phenotypes are quantified from  $N > 3$  set independent experiments. Statistical analysis was performed for **(H)** using Mann Whitney U test; \*\*\*\* $p < 0.0001$ .

untreated dissociated cells (**Figure 2H**). This clearly indicated that PAF treatment altered epithelial polarity and also led to a loss and/or disruption of cell-cell junctions.

## PAF Treatment Induces Partial EMT-Like Phenotype

EMT is a process of transition of epithelial cells into mesenchymal cells. This program has been distinctively viewed as a two-stage program with two discrete cell populations of epithelial and mesenchymal cells expressing the cell-type specific proteins (Pastushenko and Blanpain, 2019). However, recent studies indicate that EMT is a gradual process that takes place through stages that are known as intermediate states. This state circumscribes the co-expression of epithelial and mesenchymal markers. It has also been shown in similar studies that this hybrid/incomplete state of EMT is more culpable to poor survival and higher chances of resistance to therapy (Lambert et al., 2017; Pastushenko and Blanpain, 2019).

Vimentin, a known mesenchymal marker, showed an upregulated phenotype in the acini grown in the presence of PAF (**Figures 3A,B**). The protein expression of the different EMT markers was also investigated as shown in (**Figure 3C**). Vimentin and N-cadherin protein levels showed an upregulation in the presence of PAF, and densitometric analysis showed a 2-fold and 1.76-fold increase in the respective protein levels. Fibronectin, which is also a mesenchymal marker, is also upregulated in the presence of PAF. E-cadherin, an epithelial and a cell-cell junction marker showed a 0.5-fold reduction in protein level, which further corroborated the loss that was observed earlier (**Figure 2E**).  $\beta$ -catenin protein levels did not show a significant change probably because there has not been a major loss of the protein but more of cellular redistribution from the junctions to the cytoplasm as granules. Hence, a clear difference in protein level was not observed. Slug, a transcription factor, showed a 1.47-fold increase at protein level.

Transcript levels of the various EMT markers were also investigated in the 20-day PAF-treated 3D cultures. Fibronectin, slug, and twist transcript levels were measured using semi-quantitative PCR. Fibronectin transcript level was more than 2-fold higher in the RNA lysates collected post 20 days of PAF treatment. The transcript levels of slug and twist also showed a 2-fold upregulation in the presence of PAF (**Figure 3D**). The quantifications of the transcript level were performed using densitometric analysis using ImageJ software. The role of tumor micro-environment (TM) is well-established in various cancers including breast cancer (Yu and Elble, 2016). TM is composed of different inflammatory and immune cells, apart from other components, which have been known to induce EMT-like phenotype (Yu and Elble, 2016). As mentioned before, PAF is a phospholipid mediator that is widely known to play a role in the activation of various immune cells. Hence, the above results are indicative of the formation of a link between hybrid state of EMT, TM and PAF; all leading to transformation.

**Figure 3E** shows the phase contrast images of control and PAF-treated dissociated cells grown as monolayer cultures. Control cells appear like MCF10A cells, epithelial-like, and cuboidal, while PAF-treated cells appear spindle-like,

large, and elongated. This appearance is retained when cells are both sparsely or densely seeded. This morphology strengthens the fact that PAF has the ability to transform MCF10A breast epithelial cells.

Since the data indicate induction of EMT, this was further supported by performing DQ collagen<sup>TM</sup> assay. PAF dissociated cells showed increased fluorescence when observed under SP8 confocal microscope (Leica, Germany; **Figure 3F**), which was quantified (**Figure 3G**). To strengthen the hypothesis that PAF induces invasion, gelatin zymography was performed using the conditioned media (CM) from the 3D breast acinar cultures. Increased activation of MMP-2 (1.42-fold) and MMP-9 (2.23-fold) were observed in the conditioned media collected from the PAF-treated samples (**Figure 3H**), thus indicating the ability of PAF stimulation to induce invasion, which is a known marker for transformation. Taken together, our data clearly indicate the induction of partial EMT and invasion in PAF-treated cells thereby leading to a transformation phenotype.

## Effect of PAF on Anchorage Independent Growth of MCF10A Cells and Activation of the PI3K/AKT Pathway

Anchorage independent growth is a key characteristic feature that cells attain when they have undergone transformation, and this ability is considered as a fundamental property of cancer cells. This capacity to grow on a semisolid substratum serves as a proxy for *in vivo* tumorigenicity (Horibata et al., 2015). In our study, soft agar assay was performed to investigate whether prolonged PAF-treatment could transform the cells, thus allowing them to grow in an anchorage-independent manner. Dissociated cells of both control and PAF-treated acini were grown on soft agar for 27 days and then stained with MTT, a tetrazolium dye, to visualize the colonies and to distinguish the dead cells from live ones. **Figures 4A,B** clearly show PAF dissociated cells to have gained the capability to form colonies in an anchorage-independent manner, which supports the hypothesis that PAF induces *in vitro* tumorigenesis.

Our data indicate PAF stimulation of non-tumorigenic breast epithelial cells to undergo transformation; however, the mechanism of this transformation process is not known. In the current study, PAF-R showed a 2-fold upregulation in transcript levels of the PAF-stimulated lysates (**Figure 4C**). Further, PAF-treated 3D culture lysates were immunoblotted and probed for pAKT and total AKT. pAKT showed close to 3-fold increase in activation with concomitant increase in AKT protein expression upon prolonged treatment with PAF (**Figure 4D**).

In support of the existing literature, our data also show MMP-2 and MMP-9 activation downstream of pAKT activation. Increased cellular proliferation observed in the presence of PAF is suggestive of the contribution of the AKT pathway in the PAF-mediated transformation of MCF10A cells grown as 3D cultures. Hence, we predict the following pathway (**Figure 4E**) using existing data and current literature; however, further research is required to delineate the mechanism of transformation through PAF. Since our data are preliminary,

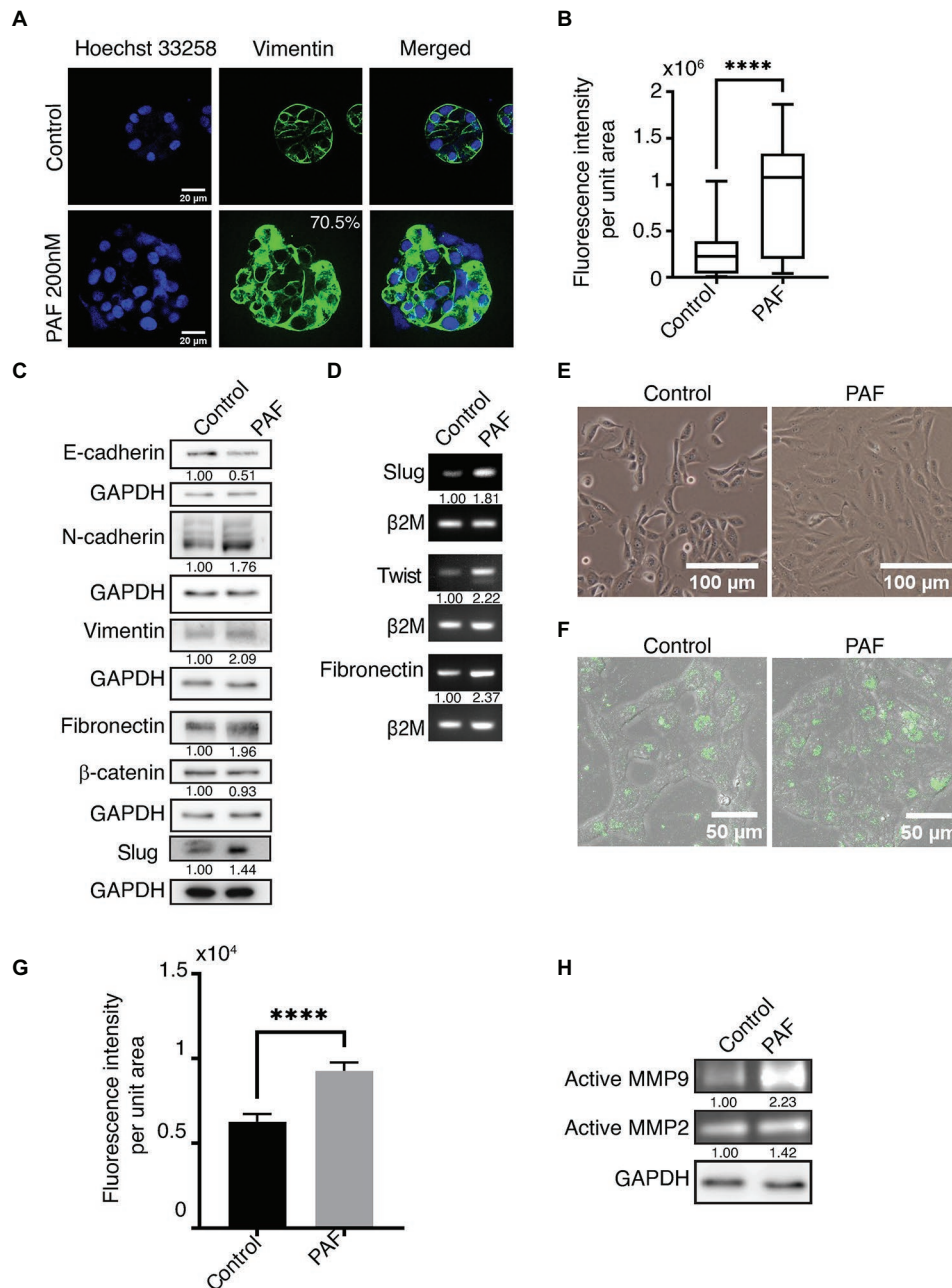
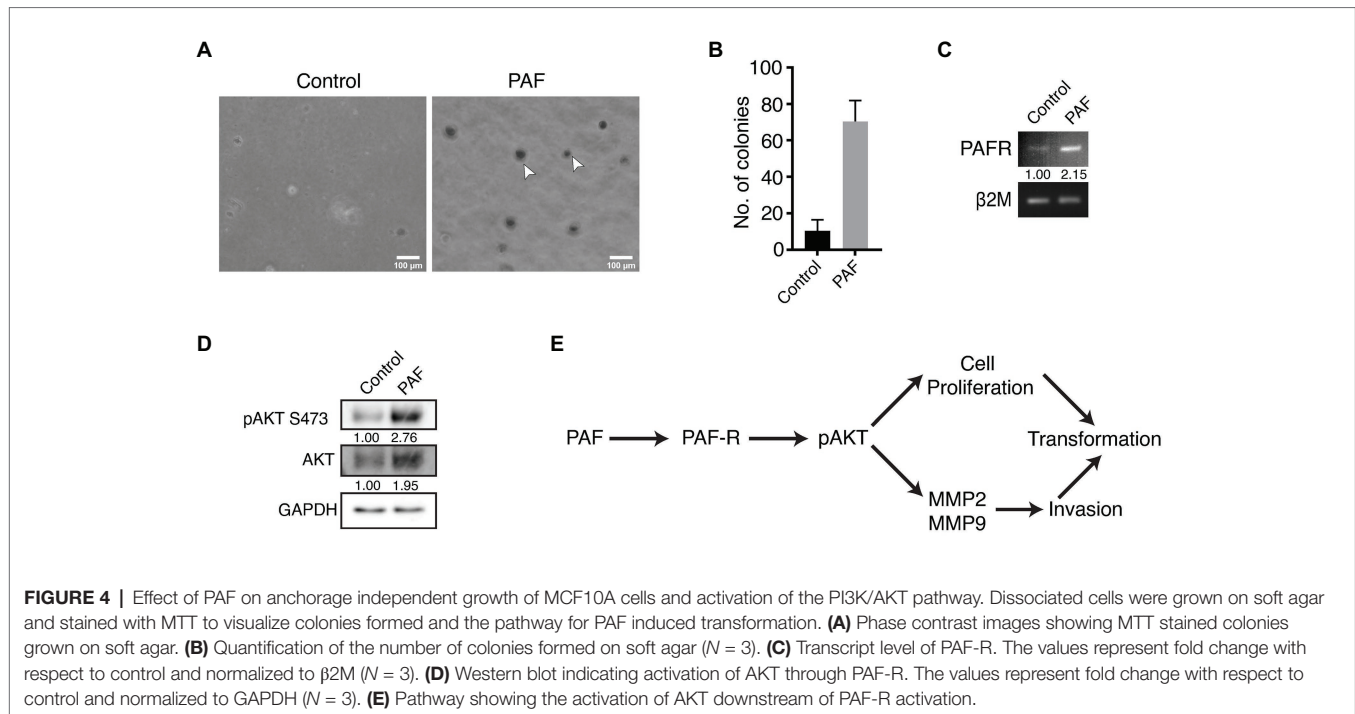


**FIGURE 3** | PAF treatment induces partial epithelial-mesenchymal transition (EMT)-like phenotype. MCF10A cells grown for 20 days on Matrigel™ treated with and without 200 nM PAF immunostained and immunoblotted with EMT markers. **(A)** PAF-treated acini showed upregulated vimentin expression (green). **(B)** Box plot depicts the acinar fluorescence (CTCF) of vimentin ( $N = 4$ ). **(C)** 20-day 3D culture lysates of control and PAF immunoblotted for various EMT markers. The values represent fold change with respect to control and normalized to GAPDH ( $N = 3$ ). **(D)** mRNA expression analysis done for various EMT markers using RNA lysates. The values represent fold change with respect to control and normalized to β2M ( $N = 3$ ). **(E)** Phase contrast images of dissociated cells of PAF treated acini grown as 2D cultures showed a mesenchymal phenotype. **(F)** Dissociated cells of control and PAF, seeded on rat tail collagen type1 containing DQ™ collagen type1 and fluorescence intensity captured on SP8 confocal microscope (Leica, Germany). **(G)** Quantification of the DQ fluorescence per cell ( $n = 150$ ). **(H)** Coomassie-stained gel showing gelatinase activity using conditioned media from 3D cultures. The values represent fold change with respect control and normalized to GAPDH. Statistical analysis was performed for **(A)** and **(F)** using Mann Whitney U test; \*\*\*\* $p < 0.0001$ .

further studies are called for using small molecule inhibitors to thoroughly dissect the signaling mechanism. Overall, PAF leads to phenotypic transformation of breast epithelial cells

when grown on ECM for 20 days and the activation of the oncogenic molecular players warrants deeper investigations for the mechanism.





## DISCUSSION

PAF is long known as a potent inflammatory bioactive molecule that is unequivocally proven to give rise to aberrant physiological effects (Lordan et al., 2019). Its role in various types of cancer is studied; however, the mechanism that leads to cancer is still understudied (Tsoupras et al., 2009). The current study will be instrumental in defining the mode of action of PAF in transforming non-tumorigenic breast epithelial cells. Health hazards of high levels of PAF in the system were studied earlier by Kispert et al., and although it is known to be naturally present in the living system, improper degradation leads to its accumulation and hence leads to cellular and molecular anomalies (Chen et al., 2007; Kispert et al., 2015, 2019). Bussolati et al. (2000) have shown that the stimulated secretion of PAF promotes migration, proliferation, and neo-angiogenesis in breast cancer cells, clearly indicating its role in carcinogenesis (Bussolati et al., 2000). Cell microenvironment perturbations by exogenous or endogenous sources lead to increased cellular proliferation that results in a loss of hollow lumen followed by the formation of multiple layers of cells in the lumen. Such a phenotype is predictive of transformation and can be a representative model for early stage mammary cancer *in vitro* (Vidi et al., 2013). Formation of a polarized, growth-arrested acinar structure with glandular epithelial cells surrounding a hollow lumen is archetypal of perfectly synchronized cellular and molecular events culminating into a normal breast acinus. When this tissue architecture is disturbed, cell survival, and differentiation processes get largely affected and eventually pave the way to tumor formation (Vidi et al., 2013). Transformation is the initial step to this process, wherein the normal cell signaling goes haywire, and

there is an aberrant expression of genes leading to malignant phenotypes, and this phenomenon is nearly recapitulated using the 3D breast acinar model system. Formation of disorganized acinar structures is characteristic of transformation and various phenotypic changes are categorized under lack of growth arrest, loss of cell polarity, disruption of BM and cell-cell junctions, EMT, and ability to grow in anchorage-independent conditions (Debnath et al., 2003). Our study encompasses all the above phenotypes in the zest to investigate the role of PAF in transformation of breast epithelial cells using the 3D breast acinar model.

Investigations revealed that continuous PAF treatment for 20 days leads to the disruption of polarity manifested by loss of apico-basal polarity. Generally, for apical polarity, *in vitro* studies as well as pathologists utilize Golgi marker as a strong identifying marker to understand polarity alteration leading to transformation or cancer (Debnath et al., 2003). Golgi is the hub for signal transduction for various pathways and alteration in its localization affects the polarized secretion of proteins from the ER to the plasma membrane and other compartments that in turn affects the signal transduction pathways (Millarte and Farhan, 2012). Hence, although the global secretory pattern does not change, but the directed trafficking of cargo is impaired. Alongside, breakage of BM is the key to loss of basal polarity. This phenomenon is significant because it provides a hallway to invading cells into the surrounding ECM and further into tissue stroma. The entirety of the BM is necessary to limit tumor growth and invasion and for this reason many solid tumors show discontinuous or a loss of BM (Ioachim et al., 2002). These investigations and the supporting literature revealed a structural loss of tissue architecture and loss of epithelial polarity in the presence of



PAF, indicating that such phenotypes are important components toward the maintenance of polarity and disruption of these leads to transformation and gives direct evidence in cancer development and progression (Lee and Vasioukhin, 2008).

E-cadherin, a cell-cell junction protein is known to maintain epithelial polarity by being a center for the intercommunicating signals between catenins and the cytoskeletal network and disruptions in this contact lead to various morphogenetic and developmental defects apart from loss of epithelial polarity (Olson et al., 2019). E-cadherin complexes with cytoplasmic  $\beta$ -catenin at the junctions and aberrations in this interaction leads to an increased flux of cytoplasmic  $\beta$ -catenin resulting in transformation and such an observation is commonly noted in solid tumors and epithelial cancers (Kourtidis et al., 2017). In our study, the loss of E-cadherin and diffused  $\beta$ -catenin at the junctions was observed in cells treated with PAF. Dissociation of the E-cadherin and  $\beta$ -catenin proteins from the complex leads to aberrant expression at the cell membrane and attributes to malignant progression, as well as has importance as a prognostic marker (Kaur et al., 2013).  $\beta$ -catenin expression leads to the transcription of various EMT inducing genes, thus identifying the various proteins that are under its transcriptional activity that lead to EMT is important (Solanas et al., 2008). EMT is a biological process that is employed during developmental stages; however, carcinoma cells hijack this program and herein the cells tend to lose their epithelial-like characteristics, both morphologically and functionally, and become mesenchymal or express such characteristics. Induction of EMT leads to the activation of various oncogenic programs including enhanced migration, invasion, metastasis, and the evasion of apoptotic stimuli (Kalluri and Weinberg, 2009; Scheel and Weinberg, 2011). Such complex programs are orchestrated by various EMT regulating transcription factors such as Snail, Slug, Twist, Zeb1, to name a few, to culminate into EMT. Apart from transcription factors, loss of cell-cell contacts and aberrant polarity also triggers EMT initiation. As cells fall loose in the cell matrix, they degrade it and attain mobility and this process is an attribute to EMT, which leads to the expression of mesenchymal proteins (Lamouille et al., 2014; Puisieux et al., 2014). Considering SNAIL1 and TWIST, the master regulators of EMT, they are classically known to repress E-cadherin and this opens the gate for tumor cells to migrate, either by mesenchymal movement or by amoeboid movement (Padmanaban et al., 2019). Concurrently, as E-cadherin levels decrease, N-cadherin levels increase and literature suggests that N-cadherin expression is TWIST-dependent (Alexander et al., 2006). Apart from the typical EMT markers, there are other molecules as well that play important roles in pathological EMT pathways. Fibronectin is an extracellular matrix protein, which gets enriched when EMT is induced, as well as various MMP's are expressed, which aid in the degradation of the matrix and enable tumor cells to invade deeper into tissues. Studies show that MMP-2 and MMP-9 deficient mice show impaired tumor cell growth and poor metastasis (Itoh et al., 1998). So, the conjoint efforts of BM disruption, mesenchymal expression, and MMP activation

hold key position in inducing EMT, and the study suggests the same. However, inherent heterogeneity that arises in carcinoma cells, the tissue-wise difference in signal that cells receive to drive the EMT program, the signaling pathways that get activated in response to the induction of EMT, and the original state of the normal differentiated cells are few of the factors that deter making a perfect molecular trait chart that describes EMT (Lambert et al., 2017).

Traditionally, anchorage independent growth is a key feature of a transformed cell, and this phenomenon is well studied in the limited scope of *in vitro* culture system through colony formation in low attachment conditions. In our study, we have shown that acinar cultures grown in the presence of PAF attain anchorage independent growth, when grown on soft agar. As a first attempt these investigations gave enough evidence to show that PAF leads to transformation and the molecular players involved in this process is probably pAKT (S473; Chen et al., 2015b). Further studies are necessary to delineate the pathways that are involved in transformation through PAF.

Until now several investigations have shown that PAF plays a leading role in inflammation, platelet aggregation, leukocyte migration, and many such inflammatory mechanisms (Chignard et al., 1979; Bussolati et al., 2000). Cigarette smoke exposure is shown to promote bladder cancer and motility leading to metastasis in breast cancer cells *via* PAF (Kispert et al., 2015, 2019). In our study, we show that continuous exposure of PAF to 3D breast acinar cultures for 20 days leads to the formation of aberrant acinar morphology as well as the functional disruption of acinar morphogenesis, which might be due to activation of the PI3K/AKT pathway.

## DATA AVAILABILITY STATEMENT

The original contributions presented in the study are included in the article/**Supplementary Material**, further inquiries can be directed to the corresponding author.

## AUTHOR CONTRIBUTIONS

LA, VC, and ML: study conceptualization, supervision, study design, and wrote the paper. LA, VC, KAA, KA, and RU: data collection. All authors contributed to the article and approved the submitted version.

## FUNDING

This study was supported by a grant from the Science and Engineering Research Board (SERB), Government of India (EMR/2016/001974) and partly by the IISER, Pune core funding. LA was supported by the INSPIRE fellowship. KAA was supported by the INSPIRE scholarship, Government of India. KA and RU were supported by the CSIR fellowship, Government of India.

## ACKNOWLEDGMENTS

We acknowledge the IISER Pune Microscopy Facility for access to equipment and infrastructure. We thank Lahiri lab members for their timely help with the experiments and comments.

## REFERENCES

- Alexander, N. R., Tran, N. L., Rekapally, H., Summers, C. E., Glackin, C., and Heimark, R. L. (2006). N-cadherin gene expression in prostate carcinoma is modulated by integrin-dependent nuclear translocation of Twist1. *Cancer Res.* 66, 3365–3369. doi: 10.1158/0008-5472.CAN-05-3401
- Anandi, V. L., Ashiq, K. A., Nitheesh, K., and Lahiri, M. (2016). Platelet-activating factor promotes motility in breast cancer cells and disrupts non-transformed breast acinar structures. *Oncol. Rep.* 35, 179–188. doi: 10.3892/or.2015.4387
- Anandi, L., Chakravarty, V., Ashiq, K. A., Bodakuntla, S., and Lahiri, M. (2017). DNA-dependent protein kinase plays a central role in transformation of breast epithelial cells following alkylation damage. *J. Cell Sci.* 130, 3749–3763. doi: 10.1242/jcs.203034
- Bennett, S. A., Leite, L. C., and Birnboim, H. C. (1993). Platelet activating factor, an endogenous mediator of inflammation, induces phenotypic transformation of rat embryo cells. *Carcinogenesis* 14, 1289–1296. doi: 10.1093/carcin/14.7.1289
- Bussolati, B., Biancone, L., Cassoni, P., Russo, S., Rola-Pleszczynski, M., Montrucchio, G., et al. (2000). PAF produced by human breast cancer cells promotes migration and proliferation of tumor cells and neo-angiogenesis. *Am. J. Pathol.* 157, 1713–1725. doi: 10.1016/S0002-9440(10)64808-0
- Chen, J., Lan, T., Zhang, W., Dong, L., Kang, N., Zhang, S., et al. (2015a). Feed-forward reciprocal activation of PAFR and STAT3 regulates epithelial-mesenchymal transition in non-small cell lung cancer. *Cancer Res.* 75, 4198–4210. doi: 10.1158/0008-5472.can-15-1062
- Chen, J., Lan, T., Zhang, W., Dong, L., Kang, N., Zhang, S., et al. (2015b). Platelet-activating factor receptor-mediated PI3K/AKT activation contributes to the malignant development of esophageal squamous cell carcinoma. *Oncogene* 34, 5114–5127. doi: 10.1038/ncr.2014.434
- Chen, J., Yang, L., Foulks, J. M., Weyrich, A. S., Marathe, G. K., and McIntyre, T. M. (2007). Intracellular PAF catabolism by PAF acetylhydrolase counteracts continual PAF synthesis. *J. Lipid Res.* 48, 2365–2376. doi: 10.1194/jlr.M700325-JLR200
- Chignard, M., Le Couedic, J. P., Tence, M., Vargaftig, B. B., and Benveniste, J. (1979). The role of platelet-activating factor in platelet aggregation. *Nature* 279, 799–800. doi: 10.1038/279799a0
- Debnath, J., and Brugge, J. S. (2005). Modelling glandular epithelial cancers in three-dimensional cultures. *Nat. Rev. Cancer* 5, 675–688. doi: 10.1038/nrc1695
- Debnath, J., Muthuswamy, S. K., and Brugge, J. S. (2003). Morphogenesis and oncogenesis of MCF-10A mammary epithelial acini grown in three-dimensional basement membrane cultures. *Methods* 30, 256–268. doi: 10.1016/S1046-2023(03)00032-X
- Foa, R., Bussolino, F., Ferrando, M. L., Guarini, A., Tetta, C., Mazzone, R., et al. (1985). Release of platelet-activating factor in human leukemia. *Cancer Res.* 45, 4483–4485.
- Fournier, M. V., Martin, K. J., Kenny, P. A., Xhaja, K., Bosch, I., Yaswen, P., et al. (2006). Gene expression signature in organized and growth-arrested mammary acini predicts good outcome in breast cancer. *Cancer Res.* 66, 7095–7102. doi: 10.1158/0008-5472.CAN-06-0515
- Hanahan, D., and Weinberg, R. A. (2011). Hallmarks of cancer: the next generation. *Cell* 144, 646–674. doi: 10.1016/j.cell.2011.02.013
- Horibata, S., Vo, T. V., Subramanian, V., Thompson, P. R., and Coonrod, S. A. (2015). Utilization of the soft agar colony formation assay to identify inhibitors of tumorigenicity in breast cancer cells. *J. Vis. Exp.* e52727. doi: 10.3791/52727
- Ioachim, E., Charchanti, A., Briasoulis, E., Karavasili, V., Tsanou, H., Arvanitis, D. L., et al. (2002). Immunohistochemical expression of extracellular matrix components tenascin, fibronectin, collagen type IV and laminin in breast cancer: their prognostic value and role in tumour invasion and progression. *Eur. J. Cancer* 38, 2362–2370. doi: 10.1016/S0959-8049(02)00210-1
- Ishii, S., and Shimizu, T. (2000). Platelet-activating factor (PAF) receptor and genetically engineered PAF receptor mutant mice. *Prog. Lipid Res.* 39, 41–82. doi: 10.1016/S0163-7827(99)00016-8
- Itoh, T., Tanioka, M., Yoshida, H., Yoshioka, T., Nishimoto, H., and Itohara, S. (1998). Reduced angiogenesis and tumor progression in gelatinase A-deficient mice. *Cancer Res.* 58, 1048–1051.
- Ivers, L.P., Cummings, B., Owlabi, F., Welzel, K., Klinger, R., and Saitoh, S., et al. (2014). Dynamic and influential interaction of cancer cells with normal epithelial cells in 3D culture. *Cancer Cell Int.* 14:108. doi: 10.1186/s12935-014-0108-6
- Jancar, S., and Chammas, R. (2014). PAF receptor and tumor growth. *Curr. Drug Targets* 15, 982–987. doi: 10.2174/1389450115666140903111812
- Kalluri, R., and Weinberg, R. A. (2009). The basics of epithelial-mesenchymal transition. *J. Clin. Invest.* 119, 1420–1428. doi: 10.1172/JCI39104
- Kaur, J., Sawhney, M., DattaGupta, S., Shukla, N. K., Srivastava, A., Walfish, P. G., et al. (2013). Clinical significance of altered expression of  $\beta$ -catenin and E-cadherin in oral dysplasia and cancer: potential link with ALCAM expression. *PLoS One* 8:e67361. doi: 10.1371/journal.pone.0067361
- Kispert, S., Marentette, J., and McHowat, J. (2015). Cigarette smoke induces cell motility via platelet-activating factor accumulation in breast cancer cells: a potential mechanism for metastatic disease. *Physiol. Rep.* 3:e12318. doi: 10.14814/phy2.12318
- Kispert, S., Marentette, J., and McHowat, J. (2019). Cigarette smoking promotes bladder cancer via increased platelet-activating factor. *Physiol. Rep.* 7:e13981. doi: 10.14814/phy2.13981
- Kourtidis, A., Lu, R., Pence, L. J., and Anastasiadis, P. Z. (2017). A central role for cadherin signaling in cancer. *Exp. Cell Res.* 358, 78–85. doi: 10.1016/j.yexcr.2017.04.006
- Lambert, A. W., Pattabiraman, D. R., and Weinberg, R. A. (2017). Emerging biological principles of metastasis. *Cell* 168, 670–691. doi: 10.1016/j.cell.2016.11.037
- Lamouille, S., Xu, J., and Derynck, R. (2014). Molecular mechanisms of epithelial-mesenchymal transition. *Nat. Rev. Mol. Cell Biol.* 15, 178–196. doi: 10.1038/nrm3758
- Lee, M., and Vasioukhin, V. (2008). Cell polarity and cancer—cell and tissue polarity as a non-canonical tumor suppressor. *J. Cell Sci.* 121, 1141–1150. doi: 10.1242/jcs.016634
- Lordan, R., Tsoupras, A., Zabetakis, I., and Demopoulos, C. A. (2019). Forty years since the structural elucidation of platelet-activating factor (PAF): historical, current, and future research perspectives. *Molecules* 24:4414. doi: 10.3390/molecules24234414
- Lv, X. X., Liu, S. S., Li, K., Cui, B., Liu, C., and Hu, Z. W. (2017). Cigarette smoke promotes COPD by activating platelet-activating factor receptor and inducing neutrophil autophagic death in mice. *Oncotarget* 8, 74720–74735. doi: 10.18632/oncotarget.20353
- Man, Y. G., Stojadinovic, A., Mason, J., Avital, I., Bilchik, A., Bruecher, B., et al. (2013). Tumor-infiltrating immune cells promoting tumor invasion and metastasis: existing theories. *J. Cancer* 4, 84–95. doi: 10.7150/jca.5482
- Millarte, V., and Farhan, H. (2012). The Golgi in cell migration: regulation by signal transduction and its implications for cancer cell metastasis. *ScientificWorldJournal* 2012:498278. doi: 10.1100/2012/498278
- Miyaura, S., Eguchi, H., and Johnston, J. M. (1992). Effect of a cigarette smoke extract on the metabolism of the proinflammatory autacoid, platelet-activating factor. *Circ. Res.* 70, 341–347. doi: 10.1161/01.RES.70.2.341
- Olson, A., Le, V., Aldahl, J., Yu, E. J., Hooker, E., He, Y., et al. (2019). The comprehensive role of E-cadherin in maintaining prostatic epithelial integrity during oncogenic transformation and tumor progression. *PLoS Genet.* 15:e1008451. doi: 10.1371/journal.pgen.1008451
- Padmanaban, V., Krol, I., Suhail, Y., Szczerba, B. M., Aceto, N., Bader, J. S., et al. (2019). E-cadherin is required for metastasis in multiple models of breast cancer. *Nature* 573, 439–444. doi: 10.1038/s41586-019-1526-3

## SUPPLEMENTARY MATERIAL

The Supplementary Material for this article can be found online at: <https://www.frontiersin.org/articles/10.3389/fgene.2021.634938/full#supplementary-material>

- Papakonstantinou, V. D., Lagopati, N., Tsilibary, E. C., Demopoulos, C. A., and Philippopoulos, A. I. (2017). A review on platelet activating factor inhibitors: could a new class of potent metal-based anti-inflammatory drugs induce anticancer properties? *Bioinorg. Chem. Appl.* 2017:6947034. doi: 10.1155/2017/6947034
- Pastushenko, I., and Blanpain, C. (2019). EMT transition states during tumor progression and metastasis. *Trends Cell Biol.* 29, 212–226. doi: 10.1016/j.tcb.2018.12.001
- Puisieux, A., Brabletz, T., and Caramel, J. (2014). Oncogenic roles of EMT-inducing transcription factors. *Nat. Cell Biol.* 16, 488–494. doi: 10.1038/ncb2976
- Scheel, C., and Weinberg, R. A. (2011). Phenotypic plasticity and epithelial-mesenchymal transitions in cancer and normal stem cells? *Int. J. Cancer* 129, 2310–2314. doi: 10.1002/ijc.26311
- Shaw, K. R., Wrobel, C. N., and Brugge, J. S. (2004). Use of three-dimensional basement membrane cultures to model oncogene-induced changes in mammary epithelial morphogenesis. *J. Mammary Gland Biol. Neoplasia* 9, 297–310. doi: 10.1007/s10911-004-1402-z
- Solanas, G., Porta-de-la-Riva, M., Agustí, C., Casagolda, D., Sánchez-Aguilera, F., Larriba, M. J., et al. (2008). E-cadherin controls beta-catenin and NF-kappaB transcriptional activity in mesenchymal gene expression. *J. Cell Sci.* 121, 2224–2234. doi: 10.1242/jcs.021667
- Tsoupras, A. B., Iatrou, C., Frangia, C., and Demopoulos, C. A. (2009). The implication of platelet activating factor in cancer growth and metastasis: potent beneficial role of PAF-inhibitors and antioxidants. *Infect. Disord. Drug Targets* 9, 390–399. doi: 10.2174/187152609788922555
- Vidi, P. A., Bissell, M. J., and Lelièvre, S. A. (2013). Three-dimensional culture of human breast epithelial cells: the how and the why. *Methods Mol. Biol.* 945, 193–219. doi: 10.1007/978-1-62703-125-7\_13
- Wu, X., and Gallo, K. A. (2013). The 18-kDa translocator protein (TSPO) disrupts mammary epithelial morphogenesis and promotes breast cancer cell migration. *PLoS One* 8:e71258. doi: 10.1371/journal.pone.0085166
- Yu, Y., and Elble, R. C. (2016). Homeostatic signaling by cell-cell junctions and its dysregulation during cancer progression. *J. Clin. Med.* 5:26. doi: 10.3390/jcm5020026

**Conflict of Interest:** The authors declare that the research was conducted in the absence of any commercial or financial relationships that could be construed as a potential conflict of interest.

Copyright © 2021 Chakravarty, Anandi, Ashiq, Abhijith, Umesh and Lahiri. This is an open-access article distributed under the terms of the Creative Commons Attribution License (CC BY). The use, distribution or reproduction in other forums is permitted, provided the original author(s) and the copyright owner(s) are credited and that the original publication in this journal is cited, in accordance with accepted academic practice. No use, distribution or reproduction is permitted which does not comply with these terms.

## **Supplementary Material**

### **Material and Methods**

#### **Chemicals and antibodies:**

Carbamyl PAF (Platelet Activating Factor) was procured from Cayman chemicals. Paraformaldehyde (16% w/v aqueous solution) used for immunostaining was bought from Alfa Aeser. DQ<sup>TM</sup> Collagen type1 was purchased from Invitrogen (D12060) while Collagen 1 Rat protein, tail was from Thermo Fisher Scientific (A1048301). Monoclonal antibodies used for immunofluorescence for laminin-5 (MAB19562) and  $\alpha$ 6-integrin (MAB1378) were bought from Millipore, GAPDH (G9545) antibody was bought from Sigma-Aldrich. Monoclonal antibodies for immunofluorescence for Ki67 (ab16667), vimentin (ab92547),  $\beta$ -catenin (ab32572), GM130 (EP8924) and E-cadherin (ab1416) were obtained from Abcam. For western blotting, monoclonal antibodies for Ki67 (ab16667), vimentin (ab8069) and N-cadherin (ab98952) was obtained from abcam. For western studies, fibronectin monoclonal antibody (610077), E-cadherin (610182),  $\beta$ -catenin (6101-53) were obtained from BD Biosciences. Polyclonal antibody for pAKT (S437) (9271S) was purchased from Bioresources. Slug (C19G7) (9585) monoclonal antibody was procured from Cell Signalling Technology. Peroxidase-conjugated AffiniPure goat anti-mouse and anti-rabbit as well as AffiniPure F(ab')<sub>2</sub> fragment goat anti-mouse IgG, F(ab')<sub>2</sub> fragment specific were obtained from Jackson Immuno Research. Hoechst 33258, Phalloidin 568 and 633, Alexa Fluor 488 and 568 were bought from Invitrogen.

#### **3D “on top” cultures:**

The 3D “on top” culture was set up in 8 well, 24 well and 12 well dishes using standard protocols (14,15,16). Cultures were maintained for 20 days at 37 °C and assay medium containing 2% Matrigel and 5 ng/mL EGF was supplemented every 4 days.

To dissociate cells from spheroids, cultures grown on 12 well dishes were treated with 187  $\mu$ l of Dispase<sup>TM</sup> and incubated at 37 °C for 30 minutes. The solution was collected in tubes and centrifuged at 900 rpm for 10 mins, supernatant discarded and further resuspended in growth medium. Centrifugation was repeated and the pellet was then resuspended in growth medium and replated on a 12 well dish. After 48 hours, depending on confluency (approximately 70%) cells were trypsinized and replated and finally the culture was expanded and cells were frozen down at every passage and later used for the experiments.

#### **Immunoblot analysis:**

MCF10A cells were grown on Matrigel<sup>®</sup> for 20 days in presence of PAF and the spheroids were extracted using sample buffer containing 0.06 mM Tris (pH 6.8), 6% glycerol, 2% sodium dodecyl sulphate (SDS), 0.1 M dithiothreitol (DTT) and 0.006% bromophenol blue and lysates were stored at - 40°C. These lysates were resolved on SDS-PAGE (sodium dodecyl sulphate polyacrylamide gel electrophoresis) and transferred to PVDF (P-polyvinylidene difluoride) membrane (Millipore). Blocking for non-phospho antibodies was performed in 5% (w/v) skimmed milk (SACO Foods, USA) and for phospho-specific

antibodies 4% (w/v) Block Ace (AbD Serotec) prepared in 1X Tris buffered saline containing 0.1% Tween 20 (1X TBS-T) for 1 hour at RT. Blots were incubated in primary antibody for 3 hours at RT (or for 16 hours at 4 °C) followed by washes with TBS-T, blots were then incubated with peroxidase-conjugated secondary antibody solution in the ratio 1:10,000 prepared in 5% (w/v) skimmed milk in 1X TBS-T for 1 hour at RT following which blots were developed using Immobilon Western Detection Reagent kit (Millipore) and visualised using ImageQuant LAS 4000 (GE Healthcare). Densitometric analysis using Image J software was performed in order to calculate the relative expression of proteins in the western blots.

### **RNA Extraction, cDNA preparation and semi-quantitative PCR:**

For extraction of RNA, MCF10A cells seeded on Matrigel<sup>®</sup> bed made in 12 well plates at a density of  $1.25 \times 10^5$  per well were harvested on day20 by scrapping cells following addition of TRIzol (Ambion). RNA extraction was done using standard protocol. 1µg of RNA was used for preparation of cDNA using 1 µl oligo dT (50 mM; Invitrogen) in RNase and DNase free water, dNTP (2.5 mM) and M-MLV-reverse transcriptase (Invitrogen). 1µl of the resultant reverse transcribed mix was PCR amplified with Taq DNA polymerase using 0.2µM of respective primers, and 0.125mM dNTP mix. Amplification was done using the following PCR cycle: 95 °C for 60 sec, 55 °C for 45 sec, 72 °C for 60 sec and final extension for 5 min; 40 cycles. Densitometric analysis of the gel images were performed using Image J software to determine the relative expression of the transcripts. Primer sequences used are as listed in Table 1:

Gene of interest	Forward	Reverse
TWIST	CGGAGACCTAGATGTCATTG	ACGCCCTGTTTGTGTTGAAT
SLUG	TGTTGCAGTGAGGGCAAGAA	GACCCTGGTTGCTTCAAGGA
PAFR	TACTGCTCTGTGGCCTTCCT	CTGCCCTTCTCGTAATGCTC
FN	CCCACCGTCTCAACATGCTTAG	CTCGGCTTCCTCCATAACAAGTAC
β <sub>2</sub> M(qRT)	TGTCTTTCAGCAAGGACTGGT	CTGCTTACATGTCTCGATCCCA

### **Soft Agar assay:**

$1.25 \times 10^5$  MCF10A cells were mixed with 0.3% (w/v) agar in DMEM and seeded onto a tissue culture dish coated with 0.6% (w/v) agar in DMEM. This culture was incubated at 37°C in 5% CO<sub>2</sub> incubator. Cells were supplemented with growth media 2-3 hrs post seeding and every 4<sup>th</sup> day (Anandi et al., 2017). The culture was maintained for 27 days and stained using MTT (5mg/ml). Images were acquired on Nikon Eclipse TS-100 under 4X objective and colonies were counted manually.

### **DQ collagen invasion assay**

The dissociated cells of MCF10A acinar cultures treated with and without PAF were seeded in 8-well chambers coated with ECM composed of Matrigel and Collagen in 1:1 ratio. ECM mix and DQ was used as per previously described protocol (Anandi et al., 2017). After the incubation period, cells were imaged at 40X magnification on SP8 confocal microscope (Leica, Germany). Fluorescence intensity from DQ cleavage was measured using Image J. Corrected total cellular fluorescence (CTCF) was calculated using the equation:

$CTCF = \text{Integrated fluorescence intensity of cell} - (\text{Area of cell} * \text{mean fluorescence intensity of background})$ .

### **Gelatin Zymography:**

After 20 days of culturing, the assay media from untreated MCF10A and 200 nM PAF-treated MCF10A cells were collected. The media was mixed with Gelatin Zymography (GZ) buffer and run on a 0.1% gelatin SDS-PAGE. The gel was developed using standard protocol (Hu and Beeton, 2010). The gel images were captured using ImageQuant LAS4000 gel documentation system (GE Healthcare) and densitometric analysis using Image J software was done on the gel images to ascertain relative increase in the secretion of MMPs.

### **Immunofluorescence Analysis:**

Fluorescence intensity for acinar structures was quantified using Image J software and analyzed by calculating the corrected total cellular fluorescence (CTCF) as described previously. Dissociated MCF10A cultures stained for  $\beta$ -catenin and E-cadherin was analyzed using plot profile function of Image J, for a line drawn perpendicular to the cell-cell junctions. The intensity profile for ~150 cell-cell junctions across 3 independent experiments was calculated and the mean was plotted to demonstrate the loss of E-cadherin at cell-cell junctions. For  $\beta$ -catenin, the full width half max for each plot profile was manually calculated (~100 cell-cell junctions) and represented as a box plot (Mikhaylova et al., 2015; Brandenburg et al., 2018).

Full Width Half Max =  $|X_2 - X_1|$ ; where  $X_2$ ,  $X_1$  are the values of X at  $f_{\max}/2$ .  $f_{\max}$  is the function of X.

### **Statistical analysis:**

Mann-Whitney U test, a non-parametric test, was used to analyse statistical significance of the difference in full width half max profile of  $\beta$ -catenin line profile to interpret the diffused phenotype. Mann-Whitney U test was also used to analyse the statistical significance of fluorescence intensity per unit area per acini for vimentin and fluorescence intensity per unit area per cell for DQ<sup>TM</sup> Collagen invasion assay.  $p < 0.05$  was considered statistically significant. \*\*\*\* indicates  $p < 0.0001$ . Graph Pad Prism software (Graph Pad Software, La Jolla, CA, USA) was used to plot the graphs and analyse data.

### **References:**

- Anandi, L., Chakravarty, V., Ashiq, K.A., Bodakuntla, S., and Lahiri, M. (2017). DNA-dependent protein kinase plays a central role in transformation of breast epithelial cells following alkylation damage. *J Cell Sci* 130(21), 3749-3763. doi: 10.1242/jcs.203034.
- Brandenburg, S., Pawlowitz, J., Fakuade, F.E., Kownatzki-Danger, D., Kohl, T., Mitronova, G.Y., et al. (2018). Axial Tubule Junctions Activate Atrial Ca(2+) Release Across Species. *Front Physiol* 9, 1227. doi: 10.3389/fphys.2018.01227.
- Hu, X., and Beeton, C. (2010). Detection of functional matrix metalloproteinases by zymography. *J Vis Exp* (45). doi: 10.3791/2445.
- Mikhaylova, M., Cloin, B.M., Finan, K., van den Berg, R., Teeuw, J., Kijanka, M.M., et al. (2015). Resolving bundled microtubules using anti-tubulin nanobodies. *Nat Commun* 6, 7933. doi: 10.1038/ncomms8933.